POLITECNICO DI TORINO

Collegio di Ingegneria Energetica

Corso di Laurea Magistrale
in Ingegneria Energetica e Nucleare

Tesi di Laurea Magistrale

Processes for the integration of supercapacitors and solar cells

Relatore

Dr. Federico Bella

Candidato

Matteo Sampò

Marzo 2021

Riassunto in lingua italiana

I. Introduzione

Il lavoro di Tesi qua presentato consta di due sezioni principali. Nella prima viene riportata una review riguardante l'avanzamento tecnologico negli ultimi dieci anni delle tecnologie di integrazione tra pannelli fotovoltaici e sistemi di accumulo, quali batterie o supercapacitori. Precede la review uno spaccato dello scenario energetico globale e delle tecnologie trattate. Nella seconda sezione viene esposta una simulazione, realizzata mediante il software MATLAB, riguardante l'analisi di un'utenza domestica dotata di pannelli fotovoltaici e sistema di accumulo ibrido (batterie e supercapacitori). Questa modellazione ha come obiettivo quello di simulare quanto riportato dagli articoli precedentemente analizzati integrandolo con alcune considerazioni relative a parametri non ancora presi in considerazione, quali la variazione dei cicli di carica e l'usura degli accumulatori ibridi. Lo scopo della simulazione è quello di ottimizzare il processo di gestione dell'accumulatore riducendone il numero di cicli ed aumentandone la durata di vita.

II. Scenario energetico globale

A partire dall'inizio del 2020 l'umanità ha dovuto affrontare uno degli eventi più tragici e dirompenti degli ultimi anni, la pandemia di COVID-19. La combinazione degli shock economici e sanitari derivanti da questa situazione è destinata a rimodellare il panorama economico, politico e sociale globale in cui siamo tutti immersi, sia nella sfera sociale che in quella lavorativa e privata. Questa crisi globale si è però dimostrata essere uno stimolo sostanziale per la crescita delle nuove tendenze energetiche, creando opportunità per lo spostamento del consenso sociale verso un percorso più sostenibile. In questo contesto alcuni elementi risultano fortemente positivi, in particolare la continua crescita delle energie rinnovabili. Tale incremento è guidato dall'energia solare ed eolica, che insieme hanno portato le rinnovabili ad una crescita record rappresentando oltre il 40% della crescita dell'energia primaria nell'ultimo anno. Allo stesso tempo, il consumo di carbone ha continuato la sua tendenza al ribasso, registrando sulla quota nel mix energetico globale il livello minimo degli ultimi 16 anni. Il carbone rappresenta però ancora più del 36% dell'energia globale, rispetto al solo 10% fornito dalle energie rinnovabili [1].

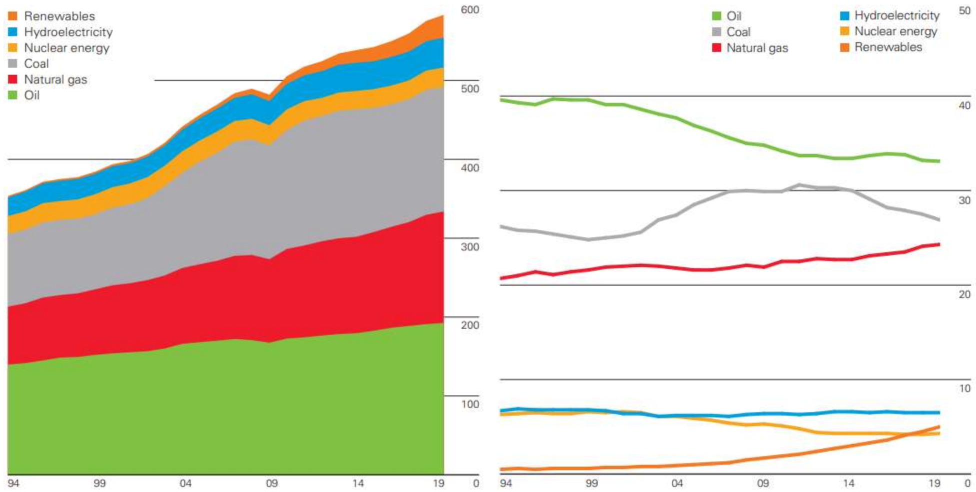

Figura 1 (a sinistra) Consumo mondiale di energia (in EJ); (a destra) cambiamento nelle quote mondiali di energia primaria. Adattato e ristampato con il permesso di [1].

III. Il fotovoltaico

Con l'espressione "fotovoltaico" si fa riferimento alla capacità di produrre energia elettrica attraverso la conversione dei fotoni provenienti dalla radiazione solare [2]. La conversione diretta dell'energia avviene attraverso un substrato semiconduttore che, esposto a fotoni di sufficiente energia, genera il rilascio di elettroni. Nello scenario globale, l'energia solare comprende sia il fotovoltaico che il solare a concentrazione. Quest'ultima si differenzia dalla prima per il fatto che la radiazione solare non viene convertita direttamente in energia elettrica ma, attraverso la generazione di energia termica, viene utilizzata per alimentare sistemi convenzionali di generazione a turbina. Tuttavia, il fotovoltaico rimane l'attore principale nella generazione globale di energia da fonti rinnovabili e sostenibili.

L'effetto fotovoltaico venne scoperto nel 1839 da A. E. Becquerel che ne dimostrò il principio di base. Le celle solari hanno visto numerosi miglioramenti tecnologici nel corso della loro storia che le hanno rese sempre più efficienti, economiche ed ecologiche [3]. Le celle fotovoltaiche possono attualmente essere classificate in tre diverse generazioni:

1) **Prima generazione:** celle composte da substrati a base di silicio monocristallino o policristallino;

2) **Seconda generazione:** celle in silicio amorfo a film sottile e celle a base di silicio addizionato ad altri semiconduttori come l'arseniuro di gallio e il tellururo di cadmio;

3) **Terza generazione:** i semiconduttori in silicio vengono sostituiti con materiali più economici, ibridi e multigiunzione.

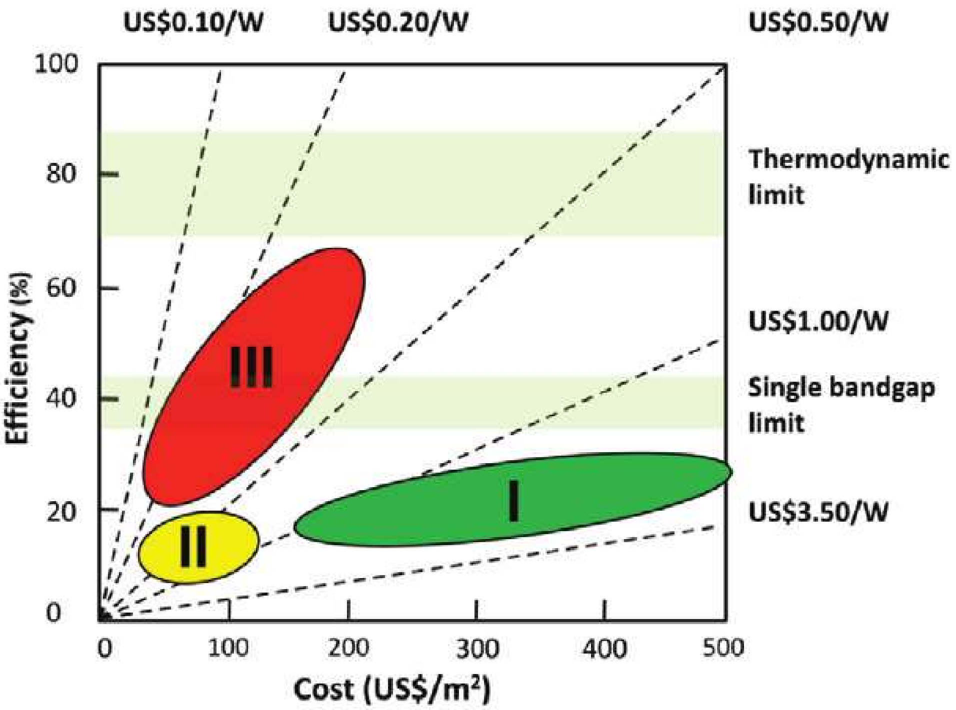

Figura 2 Efficienza e costi per tecnologie fotovoltaiche di prima, seconda e terza generazione. Adattato e ristampato con il permesso di [4].

IV. Sistemi di accumulo

Le batterie ricaricabili sono dispositivi di stoccaggio che, attraverso reazioni reversibili, permettono di eseguire cicli di carica e scarica. Al contrario, le batterie non reversibili possono essere utilizzate solo una volta, motivo per il quale non sono state menzionate in questo studio. Le batterie ricaricabili utilizzano generalmente lo stesso meccanismo delle batterie non ricaricabili, con la sola differenza che la reazione redox può essere invertita con un sufficiente apporto di energia nell'equazione. A seconda del tipo di utilizzo e dell'ambiente in cui deve operare, esistono diversi tipi di batterie.

Numerosi cicli operativi, lunghi periodi di inattività, uso in condizioni climatiche avverse, grandi densità di carica ed erogazione di elevate potenze sono solo alcune delle sfide attualmente in studio. Al momento non esistono tecnologie che possano eccellere in tutte le condizioni citate, pertanto, a seconda dell'applicazione richiesta si ha la necessità di determinare quale sia la più consona da adottare.

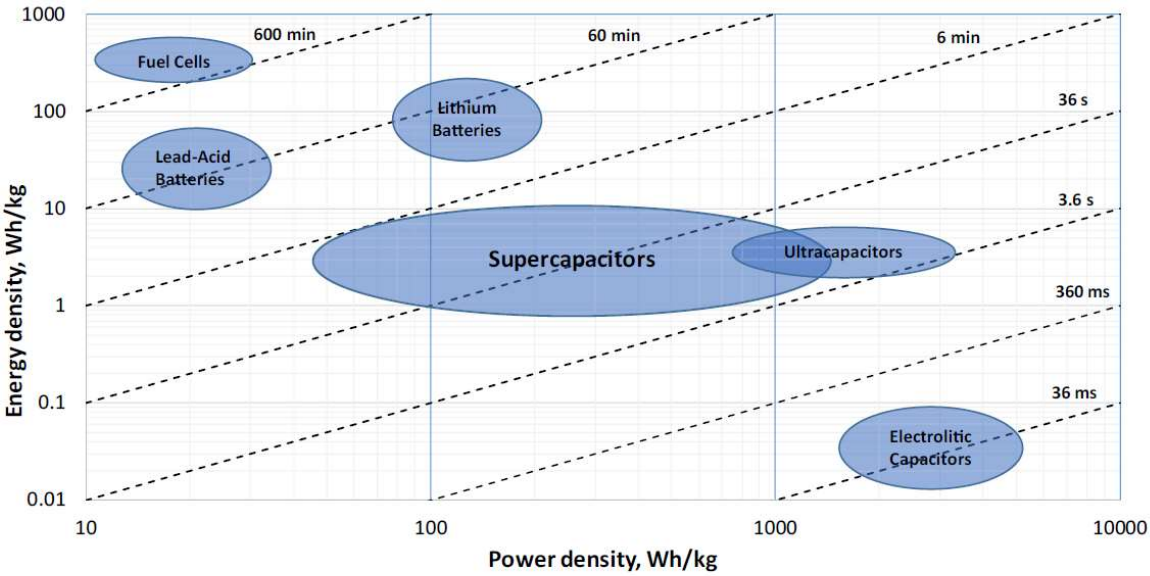

Figura 3 Potenza e densità di energia per diverse tecnologie di accumulatori. Adattato e ristampato con il permesso di [56].

Nel presente lavoro sono state prese in considerazione con particolare attenzione le seguenti tecnologie di accumulatori:

- **Batteria al piombo:** inventata nel 1859 dal fisico francese Gaston Planté, è la più antica tipologia di batteria ricaricabile ed è ancora largamente utilizzata. La sua popolarità non è dovuta principalmente alle prestazioni ma al costo molto basso dei componenti utilizzati, come il piombo e l'acido solforico.
- **Batteria ioni di litio:** le batterie agli ioni di litio sono ampiamente utilizzate in diversi scenari quali: l'elettronica portatile, la mobilità elettrica, applicazioni industriali, militari e aerospaziali. Utilizzano un composto di litio sul catodo e grafite o titanato di litio sull'anodo. Grazie alla loro alta densità energetica, al basso effetto memoria e alla bassa autoscarica, le batterie agli ioni di litio sono caratterizzate da un buon comportamento e da un'alta affidabilità.

- **Supercondensatore (SC):** a differenza dei condensatori tradizionali, con capacità nell'ordine di mF, sono in grado di immagazzinare una grande quantità di carica con valori di oltre 5000 F. Rispetto agli accumulatori chimici, i SC hanno il vantaggio di poter eseguire un grande numero di cicli di lavoro ed essere caricati e scaricati quasi istantaneamente, garantendo così una potenza specifica molto elevata. Lo svantaggio più significativo rispetto agli accumulatori tradizionali è legato alla bassa energia immagazzinabile ed al costo molto elevato.

Tabella 1 Confronto dei parametri chiave per le batterie agli ioni di litio e i supercapacitori. Adattato e ristampato con il permesso di [15].

	SUPERCONDENSATORE	***BATTERIA IONI DI LITIO***
TEMPO DI RICARICA	1-10 s	10-60 min
CICLI SOPPORTABILI	500,000-20,000,000	500-1,000
VOLTAGGIO DELLA CELLA (V)	2.7-3	3.6
ENERGIA GRAVIMETRICA (Wh kg^{-1})	4-10	100-265
AUTOSCARICA (% AL MESE)	40-50	2
TEMPERATURA DI CARICA (°C)	-40 to 65	0 to 45
TEMPERATURA DI SCARICA (°C)	-40 to 65	-20 to 60
VITA UTILE (ANNI)	10-15	5-10
PROCEDURE DI RICARICA:		
PER UNA CELLA	Facile	Complessa
PER CELLE IN SERIE	Complessa	Complessa
PERICOLOSITÀ:		
SCARICA PROFONDA	No	Sì
SOVRACCARICO	No	Sì
SURRISCALDAMENTO	No	Sì
ESPLOSIONE	No	Sì
VOLTAGGIO IN USCITA	Decrescente	Stabile
EFFICIENZA (%)	99	85-95
COSTO (€ kWh^{-1})	10,000	200-1,000

V. Integrazione tra fotovoltaico e accumulo

La ricerca, oltre a lavorare su pannelli fotovoltaici di nuova generazione e sistemi di accumulo con maggiori capacità e densità energetiche, sta cercando nuovi sistemi per integrare queste tecnologie tra di loro. Il metodo tradizionale di carica degli accumulatori, per mezzo di energia prodotta da impianti solari, consiste in un design discreto (o isolato). Tale design comporta un funzionamento indipendente delle componenti coinvolte, collegate tra loro per mezzo di cavi elettrici. Questi sistemi tendono ad essere costosi, ingombranti e poco flessibili, subendo anche perdite di energia attraverso i cavi di collegamento e l'elettronica di controllo.

Combinando il sistema di generazione con quello di immagazzinamento si ottiene un design integrato. Tale design ha la capacità di funzionare da fonte di energia autosufficiente con immagazzinamento integrato per l'energia in eccesso. I sistemi fotovoltaico-batteria integrati sono in grado di offrire una versione compatta ed efficiente dal punto di vista energetico rispetto ai tradizionali. La flessibilità di tale design è offerta dalla necessità di adottare un minor numero di cablaggi, mentre il minore ingombro è significativamente importante soprattutto per l'elettronica di piccola scala e la sensoristica ambientale.

Pur essendo ancora nelle fasi iniziali, la ricerca sta compiendo passi significativi concentrandosi sui materiali che saranno necessari per superare le future sfide. I sistemi integrati possono essere classificati in due differenti configurazioni: a tre elettrodi ed a due elettrodi. Nella prima configurazione l'elettrodo centrale viene utilizzato come elettrodo comune tra le componenti, funzionando da catodo o da anodo sia per il dispositivo fotovoltaico che per la batteria. Nella seconda configurazione, invece, l'elettrodo positivo viene usato con la funzione di fotoconversione, l'elettrodo negativo sarà invece connesso al sistema di immagazzinamento. Queste due possibilità sono rappresentate schematicamente in Figura 4.

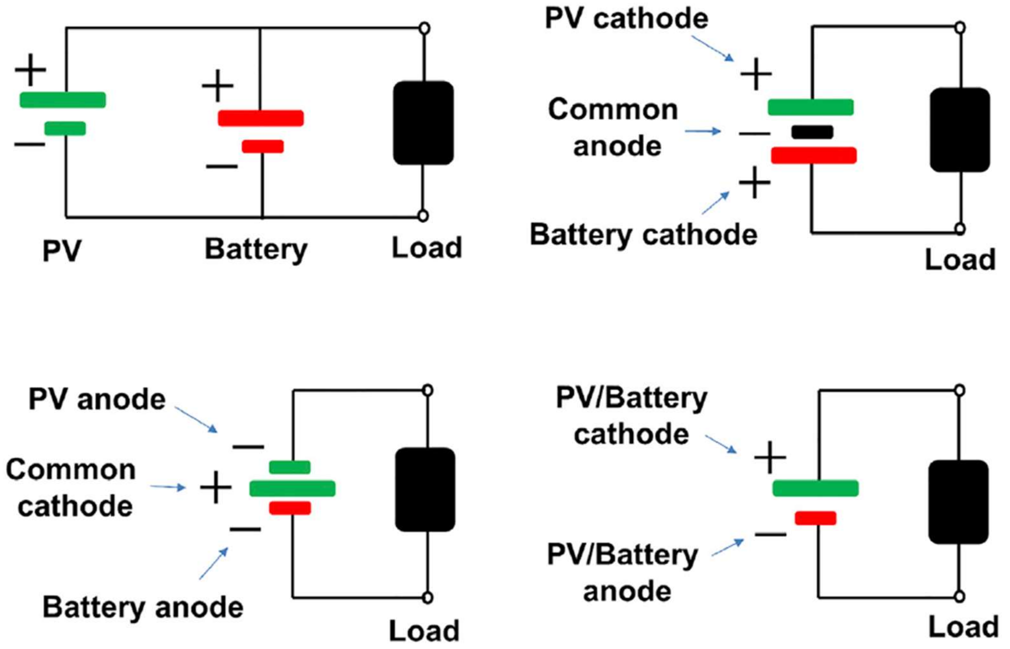

Figura 4 (in alto a sinistra) Design discreto, la netta separazione tra generatore e accumulatore è ben visibile; (in alto a destra) design integrato con configurazione a tre elettrodi, anodo comune; (in basso a sinistra) design integrato con configurazione a tre elettrodi, catodo comune; (in basso a destra) design integrato con configurazione a due elettrodi. Adattato e ristampato con il permesso di [17].

VI. Sezione di review

L'elaborato si divide in due corpi principali, quello di review qui presentato e quello di simulazione esposto nel capitolo seguente. Gli articoli analizzati vertono sulle due tipologie di integrazione viste precedentemente (integrato o discreto) e per un'esposizione più chiara sono esaminate separatamente. In entrambe le sezioni sono raccolti gli elaborati disponibili in letteratura dal 2010 al 2020. Questi articoli forniscono la base per la simulazione MATLAB seguente.

VI.1. Review sistemi integrati

Al fine di migliorare le efficienze in gioco, in particolare quella di stoccaggio energetico e del sistema di integrazione, le indagini relative ai dispositivi sono incentrate sulla ricerca di materiali innovativi e di nuove metodologie per l'assemblaggio.

Tabella 2 Raccolta delle efficienze raggiunte in alcuni articoli analizzati; la terza colonna riporta la tipologia di tecnologie integrate durante i singoli test. Le sigle usate identificano: PV (pannello fotovoltaico al silicio), DSSC (celle solari sensibilizzate con coloranti), PSC (cella solare a base di perovskite), LIB (batteria ioni di litio), SC (supercapacitore).

Articolo	ANNO	Tipo di integrazione	$\eta_{FOTOVOLTAICO}$	$\eta_{ACCUMULATORE}$	$\eta_{GLOBALE}$
Guo *et al.*	2012	DSSC-LIB	-	41.00%	0.82%
Bagheri *et al.*	2014	DSSC-SC	4.90%	54.00%	0.60%
Zhang *et al.*	2014	PV-SC	-	65.60%	0.82%
Westover *et al.*	2014	PV-SC	14.80%	84.00%	6.00%
Xu *et al.*	2015	PSC-LIB	-	12.65%	7.80%
Xu *et al.*	2015	PSC-SC	-	-	10.00%
Agbo *et al.*	2016	PV-LIB	-	-	8.80%
Xia *et al.*	2016	PSC-LIB	12.00%	97.20%	-
Xu *et al.*	2016	PSC-SC	7.10%	73.77%	4.70%
Wen *et al.*	2016	DSSC-SC	-	-	5.64%
Kim *et al.*	2017	PV-SC	-	80.31%	10.97%
Scalia *et al.*	2017	DSSC-SC	-	70.00%	1.46%
Muralee *et al.*	2017	DSSC-SC	-	90.80%	6.41%
Liu *et al.*	2017	PSC-SC	7.79%	76.00%	5.26%
Liu *et al.*	2017	PV-SC	13.00%	-	10.50%
Ng *et al.*	2018	PSC-SC	13.37%	-	2.92%
Yuan *et al.*	2019	PV-LIB	10.91%	74.24%	8.10%
Yuan *et al.*	2019	PV-SC	10.90%	74.42%	8.10%
Weng *et al.*	2020	PSC-LIB	16.80%	77.00%	9.30%
Di *et al.*	2020	PV-LIB	7.15%	88.00%	6.29%
Qin *et al.*	2020	PV-SC	13.60%	88.00%	2.20%
Liu *et al.*	2020	PV-SC	-	-	6.00%

Come mostrato nella Tabella 2 si possono osservare le differenti tecnologie adottate e implementate negli ultimi anni, ciò ha portato ad un graduale incremento delle efficienze in gioco con il raggiungimento di un rendimento globale del quasi 11%.

I dispositivi integrati si possono suddividere a loro volta in due tipologie. La prima atta alla realizzazione di un sistema autonomo sviluppato per alimentare in modo continuativo piccoli sensori o dispositivi indossabili. La seconda consiste invece in pannelli fotovoltaici da adottare nei sistemi di accumulo domestici. Questi ultimi sono sviluppati per portare un notevole miglioramento nella stabilità degli impianti di generazione fotovoltaica, in quanto grazie alla presenza di un accumulatore interno che funziona da filtro, sono caratterizzati da curve di produzione più lineari quando si verificano repentine variazioni di irraggiamento solare.

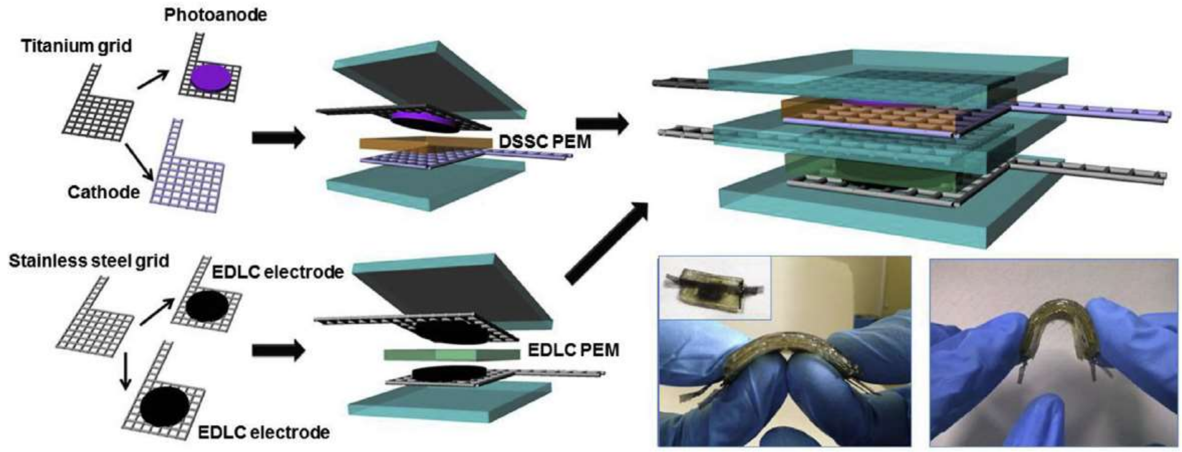

Figura 5 Illustrazione di un dispositivo integrato realizzato su di una matrice flessibile. Adattato e ristampato con il permesso di [68].

In Figura 5 è riportato un dispositivo della prima tipologia realizzato per essere autosufficiente e fabbricato su di una matrice flessibile. Tale sistema è in grado di funzionare sia da dispositivo di produzione elettrica, mediante la DSSC, sia da accumulatore grazie all'utilizzo del supercapacitore. Il design a tre elettrodi, con il mediano comune tra la cella fotovoltaica e l'accumulatore, risulta ben visibile.

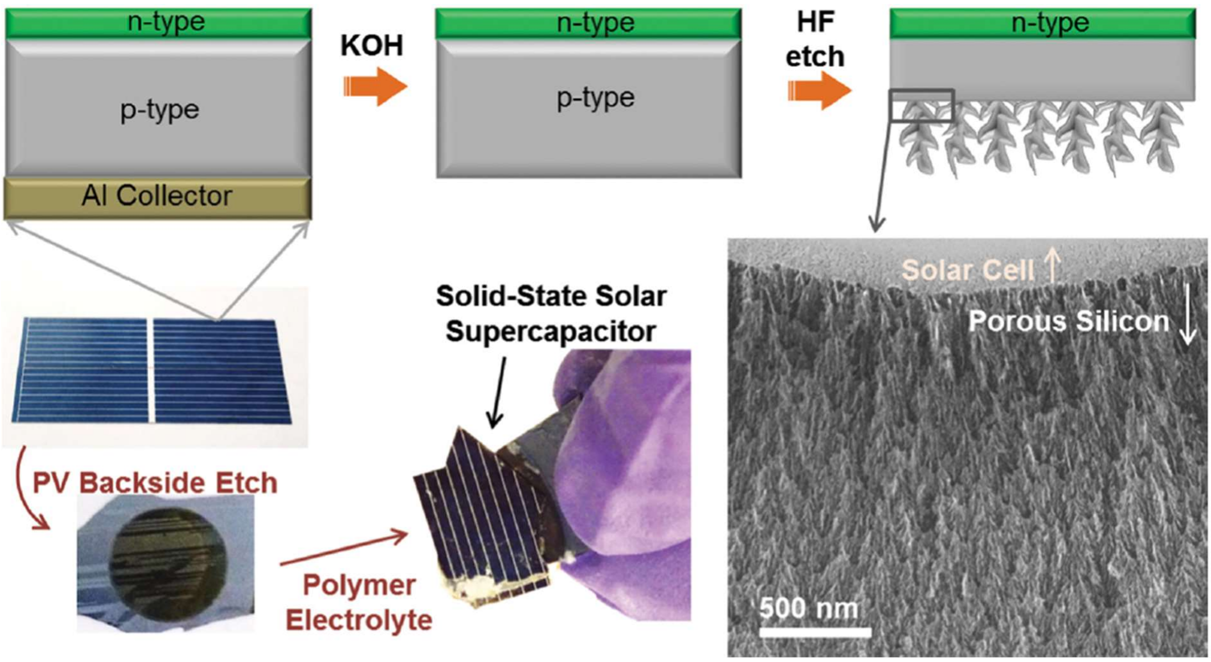

Figura 6 Dispositivo integrato realizzato mediante l'incisione di un SC sul retro di un pannello fotovoltaico. Adattato e ristampato con il permesso di [62].

Il dispositivo in Figura 6 rientra nella seconda tipologia di dispositivi integrati, ovvero sviluppati per livellare la curva di produzione fotovoltaica mediante la presenza del supercapacitore posto al loro interno. In questo caso il supercapacitore venne direttamente realizzato sulla superficie posteriore in silicio del pannello fotovoltaico. Dopo aver rimosso la precedente copertura in alluminio avente funzioni di elettrodo, mediante un bagno in soluzione basica, l'accumulatore venne realizzato con un'incisione elettrochimica direttamente sullo strato in silicio del pannello. La porosità così generata (visibile nell'ingrandimento al microscopio in Figura 6) funziona da supercapacitore, ponendosi come filtro tra la produzione fotovoltaica e l'utilizzatore.

VI.2. Review sistemi discreti

Per i sistemi discreti non è possibile fare un confronto diretto tra tutti gli studi analizzati, a differenza degli articoli riguardanti i sistemi integrati. Ogni articolo differisce dal precedente per tematica indagata e obbiettivi preposti. Come filo conduttore, in ogni articolo presente in questa sezione della review, si è ricercato quale tecnologia fosse la migliore per un determinato scopo, quali fossero le migliori logiche di funzionamento per impianti fotovoltaici dotati di accumulo e come far lavorare tra di loro diversi sistemi di generazione elettrica e di accumulo. Sono quindi riportati soltanto alcuni tra gli articoli più innovativi e rilevanti.

Nel 2011, Thounthong *et al.*, proposero di utilizzare dei supercapacitori come fonte di accumulo elettrico di breve durata, da inserire all'interno di un impianto composto da pannelli fotovoltaici e fuel cell. I supercapacitori hanno quindi il compito di sopperire alle repentine variazioni di potenza richiesta, dando così il tempo alla fuel cell di intervenire e coprire la richiesta elettrica. In Figura 7 si possono osservare le componenti del sistema e un grafico riportante i differenti tempi di intervento dei moduli presenti all'interno dell'impianto.

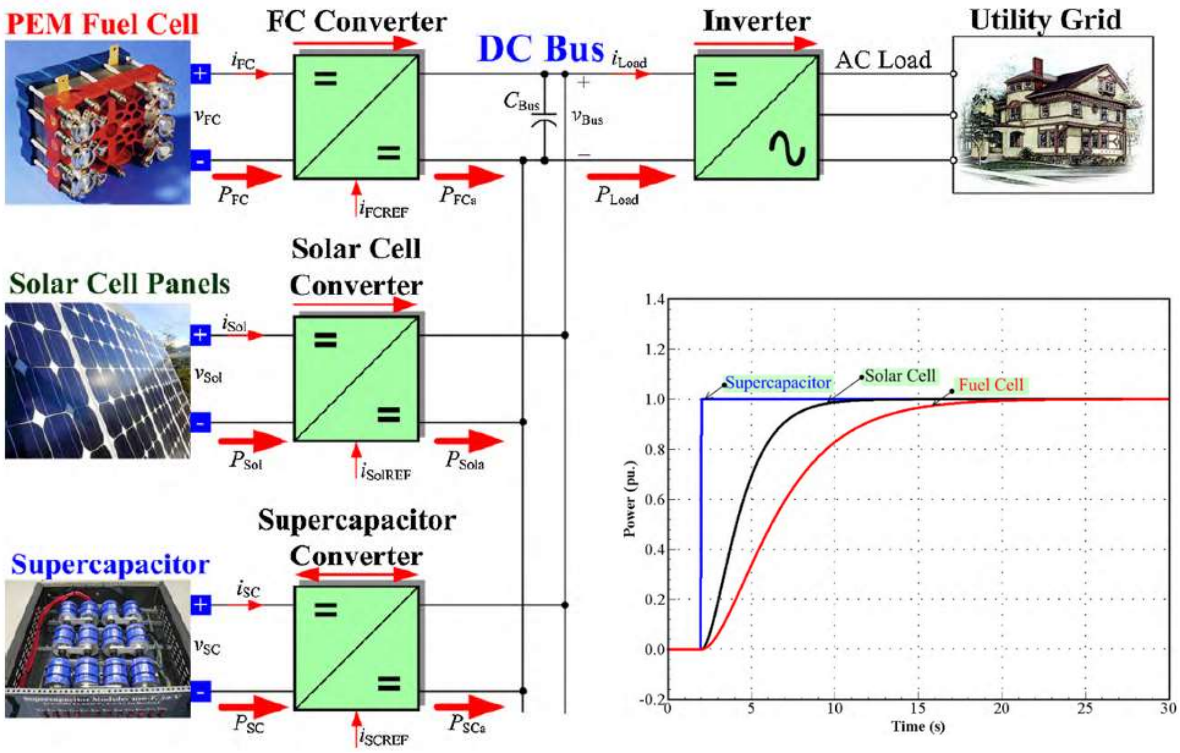

Figura 7 Schema dell'impianto proposto composto da un generatore fotovoltaico e da una fuel cell; i supercapacitori servono da accumulo di breve durata per i transitori. Il grafico riporta i differenti tempi di intervento dei moduli utilizzati. Adattato e ristampato con il permesso di [32].

In Figura 8 è riportato il grafico di intervento del sistema dove sono chiaramente osservabili le differenti tempistiche di risposta dei sottosistemi impiegati.

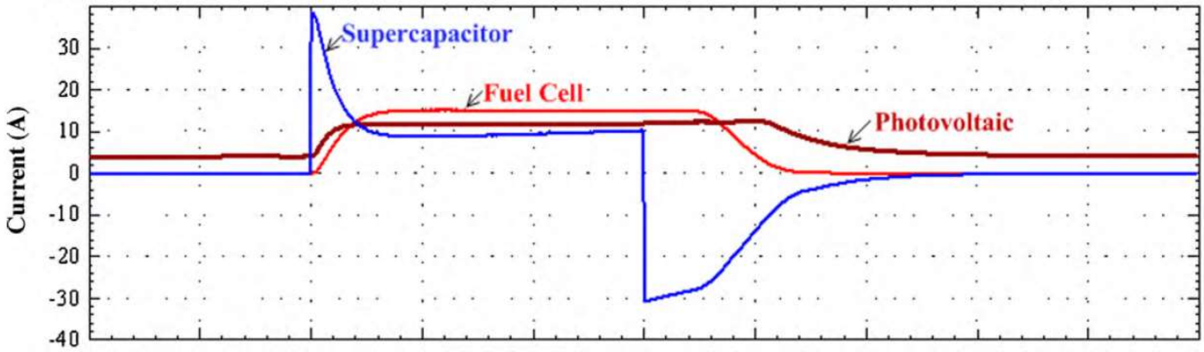

Figura 8 Grafico di intervento del sistema: sono osservabili le tempistiche di intervento delle differenti componenti presenti. Adattato e ristampato con il permesso di [32].

Nel 2017, Cabrane et al., indagarono sulla possibilità di realizzare un accumulatore ibrido (composto sia da batterie che supercapacitori) per operare al meglio in combinata con un impianto fotovoltaico. Tale accumulatore, realizzato sfruttando i punti di forza di ambedue le tecnologie, permette di migliorare il funzionamento della batteria riducendone l'usura.

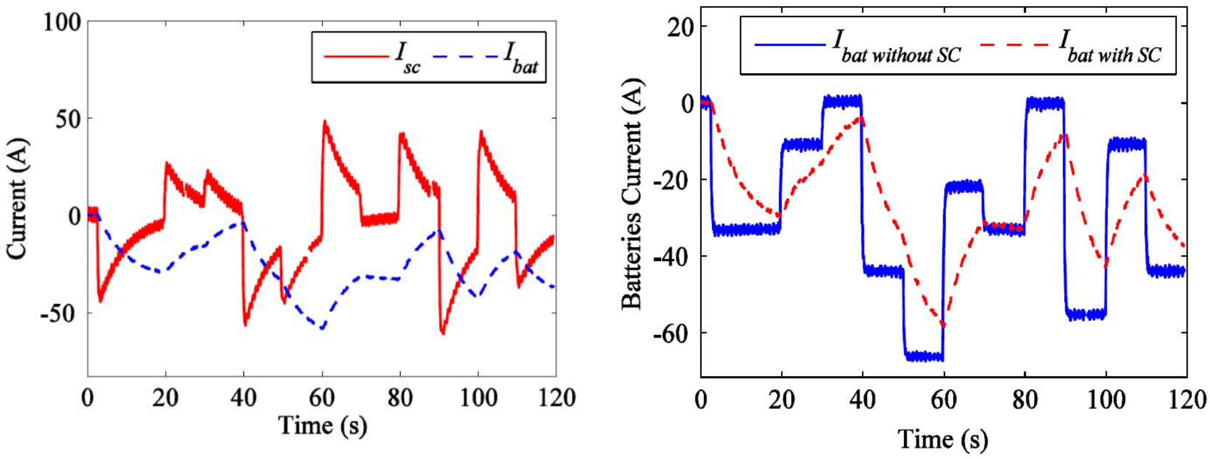

Figura 9 Andamenti delle correnti in un accumulatore ibrido (sinistra) in cui sono riportate le correnti erogate dal SC e dalla batteria; confronto tra un accumulatore ibrido ed un accumulatore a batterie (destra) posti nelle medesime condizioni. Adattato e ristampato con il permesso di [45].

Il grafico di sinistra (Figura 9) evidenzia i diversi comportamenti delle componenti presenti nell'accumulatore ibrido. Sono ben visibili i repentini interventi del SC. Nel grafico di destra è invece riportato il confronto, sviluppato nelle medesime condizioni, della corrente erogata da una batteria inserita all'interno di un accumulatore ibrido e di quella erogata da una batteria da sola. È osservabile il netto vantaggio portato dall'accumulatore ibrido e della riduzione di stress causato alla batteria ad esso connessa.

VII. Simulazione MATLAB

Dalle precedenti pubblicazioni è emerso un crescente interesse della comunità scientifica nei confronti dell'integrazione di diverse fonti di accumulo all'interno di un dispositivo ibrido, in modo tale da ottimizzarne le prestazioni globali sfruttando i punti di forza delle singole componenti. Gli studi presi in esame si sono concentrati principalmente sulla possibilità di sfruttare i SC nella gestione dei picchi di potenza riducendo il carico normalmente gestito dalle sole batterie. L'accumulatore ibrido ha così mostrato di essere una valida variante ai tradizionali sistemi di stoccaggio energetico, portando ad una maggiore stabilità della rete e riducendo le caratteristiche fluttuazioni legate agli impianti fotovoltaici.

L'attenzione negli studi è sempre stata focalizzata sulla sola gestione dei picchi di potenza e non sulle variazioni di usura riscontrabili nelle componenti di un sistema d'accumulo ibrido posto a confronto con un accumulatore tradizionale usati nelle medesime condizioni. A tale fine è stata implementata la seguente simulazione realizzata per indagare il numero di cicli subiti dalle singole componenti, la durata di ogni ciclo, la variazione delle prestazioni in relazione al rapporto capacità SC/capacità totale e le influenze portate dalle diverse efficienze in gioco. L'analisi è stata gestita mediante una simulazione MATLAB, prendendo come sistema in esame un'abitazione unifamiliare nel Nord Italia. Sui consumi di questa abitazione è stato dimensionato il sistema di produzione fotovoltaica e il relativo sistema di accumulo ibrido.

VII.1. Definizione dei consumi

In modo da poter dimensionare correttamente le varie componenti del sistema occorre studiare i carichi a cui esso è sottoposto. Per definire il carico occorre quindi studiare le potenze istantanee coinvolte e la loro distribuzione durante l'arco temporale di riferimento. Le caratteristiche e variabili del sistema in analisi sono:

- **Tipologia di utenza:** il profilo dei consumi di un'utenza è intrinsecamente legato alla tipologia di utenza stessa e agli orari di attività. Il carico in esame fa riferimento a quello generato da un'utenza domestica e quindi sarà caratterizzato da grosse differenze di consumi tra giorno e notte.
- **Time steps:** al fine di approcciare correttamente il sistema occorre analizzarlo con la dovuta precisione e utilizzare la scala temporale più adatta al tipo di analisi voluto. Il time steps preso in considerazione per questo studio è di 10 min; questo valore è ritenuto un giusto compromesso tra precisione e affidabilità per l'analisi delle energie scambiate.
- **Variabilità dei consumi:** a causa della molteplicità di azioni compiute quotidianamente nella propria abitazione è necessario simulare diversi scenari di consumo energetico giornaliero assegnando ad ognuno di essi una differente probabilità di verificarsi. Sono state realizzate per questo motivo quattro curve di carico per i giorni lavorativi e due per quelli festivi. Le curve di carico differiscono tra loro per l'intensità dei picchi e la distribuzione dei consumi nel corso della giornata. Ad ogni curva di carico è assegnata una differente probabilità di verificarsi e mediante questo valore la simulazione assegna giorno per giorno un diverso profilo dei consumi.
- **Sistema di condizionamento:** una delle principali fonti di assorbimento elettrico nelle utenze domestiche è il sistema di condizionamento estivo ed invernale. L'abitazione presa in considerazione dispone di una pompa di calore come sistema di condizionamento estivo. L'energia termica per il riscaldamento invernale viene invece

gestita da una fonte esterna (teleriscaldamento, riscaldamento centralizzato condominiale, caldaia a gas, *etc.*). Occorrerà quindi maggiorare i consumi durante i mesi estivi al fine di rappresentare al meglio questa condizione. Questo scenario è il migliore al fine di ottimizzare l'autoconsumo elettrico, in quanto l'andamento dei consumi segue quello della produzione solare.

Al fine di garantire la non ripetitività delle curve di carico è stata introdotta una componente di incertezza atta a simulare l'alta variabilità dei carichi domestici. Sono riportate di seguito due curve con e senza la componente di incertezza.

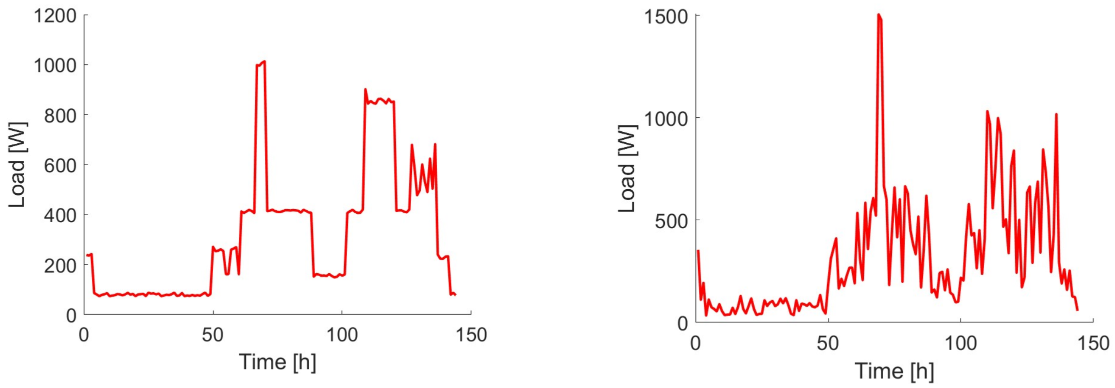

Figura 10 Curva di carico giornaliera (sinistra) pura, (destra) con il fattore di incertezza.

VII.2. Dimensionamento dell'impianto fotovoltaico

Per analizzare la producibilità del sistema fotovoltaico sono prese in considerazione le condizioni meteorologiche e di irraggiamento relative all'anno 2016 per la città di Torino. Lo studio è effettuato mediante l'applicativo "Photovoltaic Geographical Information System (PVGIS)" fornito dal JRC EU Science Hub. Il sistema produttivo considerato è composto da pannelli monocristallini al silicio, con delle perdite di sistema stimate al 14%. I parametri geometrici scelti sono quelli di massima producibilità quindi slope di 35° e azimuth di 0°. I pannelli non dispongono di inseguimento solare e sono montati free-standing.

La producibilità così ottenuta si riferisce ad un impianto avente un kWp installato ed il grado di precisione temporale dei dati forniti dal software è di un'ora. Si vede quindi necessario interpolare linearmente i dati durante la simulazione MATLAB in modo tale da ottenere la stessa scala temporale del carico domestico. I valori di producibilità così ottenuti necessitano di essere moltiplicati per la reale dimensione dell'impianto installato nel sistema.

Al fine di poter correttamente dimensionare l'impianto, per poter sopperire alla richiesta energetica e garantire la giusta ricarica del sistema di accumulo, occorre considerare i consumi elettrici definiti nella precedente analisi. Il dimensionamento è stato effettuato seguendo questa procedura:

1. Sono state elaborate tre differenti curve di carico medio mensile riferite ai mesi di: marzo, luglio e dicembre. Gli ultimi due rappresentano le condizioni estreme del sistema mentre il primo rappresenta il valor medio (valore di riferimento per il dimensionamento).

2. Le curve dei consumi medi precedentemente ricavate sono state sovrapposte alle curve di produzione media relative ai mesi in analisi. È stata quindi simulata la potenza da installare che meglio coprisse la curva dei consumi per i mesi in analisi. Le potenze sono riportate di seguito e rappresentano la quota di impianto fotovoltaico dedicata all'autoconsumo istantaneo.

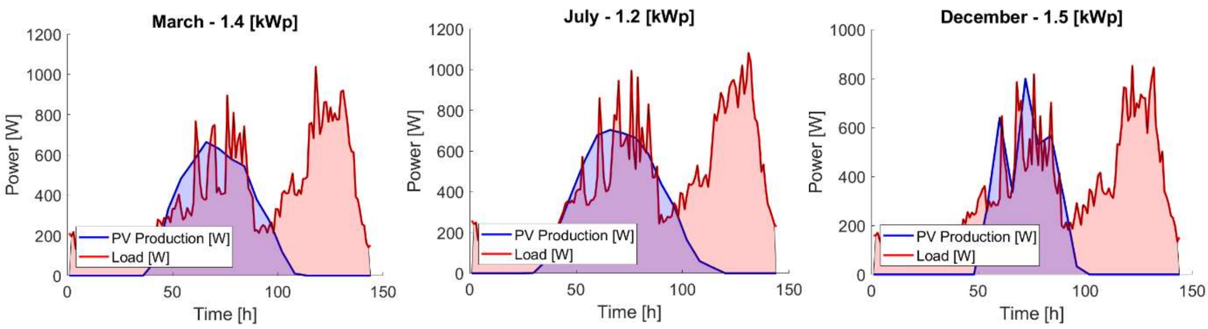

Figura 11 Sovrapposizione delle curve di produzione solare, in blu, con quelle del carico domestico, in rosso, per i mesi di: (sinistra) marzo 1.4 kWp; (centro) luglio 1.2 kWp; (destra) dicembre 1.5 kWp.

3. Occorre ora considerare i valori delle aree totali sottese ai grafici. Si può così trovare la quota di energia mancante per i singoli mesi ed utilizzare tali valori come punto di partenza per il dimensionamento dell'accumulatore. Come potenza fotovoltaica installata è stato adottato il valore di 1.4 kWp, derivato dal mese di riferimento (marzo).

Tabella 3 Dati ricavati dalla simulazione dei tre mesi in esame con un impianto fotovoltaico di 1.4 kWp

[kWh]	Marzo	Luglio	Dicembre
Carico domestico	9.187	10.307	8.138
Produzione fotovoltaica	4.659	6.510	3.251
Energia mancante	4.528	3.797	4.887

I possibili valori di capacità dell'accumulatore vanno quindi da 3.797 kWh (calcolati a luglio) a 4.887 kWh (calcolati a dicembre). Un accumulatore con una capacità totale netta di 4.5 kW, come evidenziato nel mese di marzo, risulta essere il miglior compromesso tra le diverse stagioni.

4. Dopo aver fissato la capacità netta dell'accumulatore è stato dimensionato l'impianto fotovoltaico, in modo da garantire la completa ricarica durante la maggior parte delle giornate. Per fare ciò ci si avvale delle seguenti equazioni:

$$Self - sufficiency\ (autosufficienza) = {(consumo\ annuo - energia\ comprata\ dalla\ rete)}/{consumo\ annuo}$$

$$Self - consumption\ (autoconsumo) = {(consumo\ annuo - energia\ comprata\ dalla\ rete)}/{produzione\ totale}$$

Dall'analisi del grafico sottostante si può osservare come i precedenti valori risultino ottimizzati per un impianto fotovoltaico avente una potenza installata di 4 kWp. Al fine di non sovradimensionare l'impianto è stato quindi considerato accettabile un valore di self-sufficiency pari all'80%.

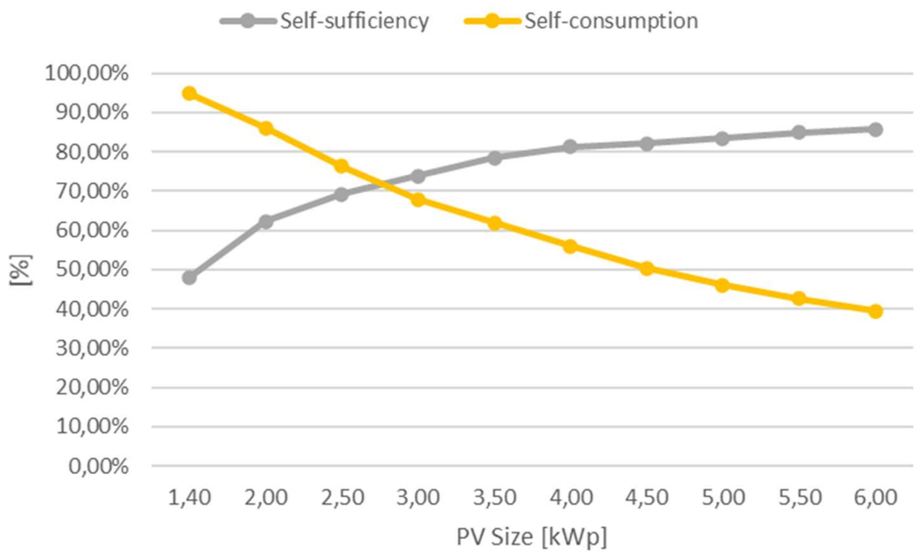

Figura 12 Andamento della self-sufficiency e self-consumption in relazione al dimensionamento dell'impianto fotovoltaico.

VII.3. Dimensionamento dell'accumulatore ibrido

Lo studio adottato per il dimensionamento dell'array di SC da adottare è basato sulla correlazione tra la sua dimensione e la riduzione del numero di cicli compiuti dalla batteria in un anno. Questa riduzione avviene perché l'uso prioritario del SC permette di soddisfare i piccoli picchi di potenza senza interrompere il ciclo della batteria. Ciò significa che, oltre alla riduzione del numero di cicli annuali, è possibile avere anche ricariche più profonde e complete, garantendo così un minor deterioramento del sistema.

Di seguito sono riportate le capacità totali dei supercapacitori assunti nelle varie simulazioni e i relativi cicli di carica/scarica effettuati dalla batteria. Per ottimizzare il sistema anche dal punto di vista economico è necessario tenere in considerazione l'aumento del prezzo causato dall'introduzione delle nuove componenti.

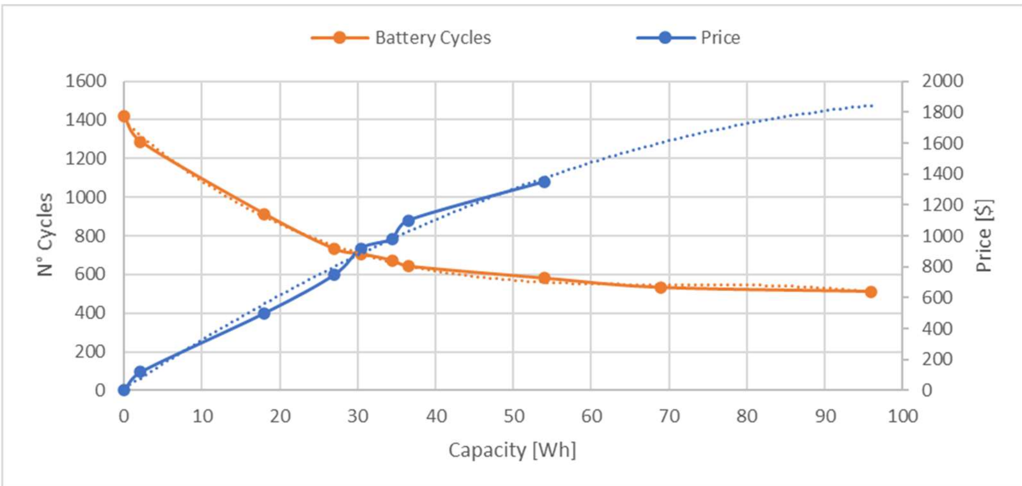

Figura 13 Risultati delle simulazioni, sono evidenziati il numero di cicli compiuto dalla batteria e il prezzo dei SC adottati. Il costo si riferisce ai SC prodotti della "MAXWELL TECHNOLOGIES" [86].

Considerando la riduzione dell'usura della batteria e l'incremento economico derivatone, è accettabile l'inserimento di un SC con una capacità di 36.5 Wh.

VII.4. Logica di utilizzo dell'accumulatore ibrido

Ottenuta la potenza assorbita dal carico domestico e quella generata dall'impianto fotovoltaico è possibile ricavare la potenza netta per la fascia temporale in esame e la relativa energia in kWh. L'energia così ricavata può essere positiva o negativa, segno rispettivamente di un eccesso o di un difetto nella produzione. Nel primo caso si procede allo stoccaggio e nel secondo alla scarica dell'accumulatore. Il processo logico seguito è quello di dare priorità di intervento al SC sfruttandone così i punti di forza.

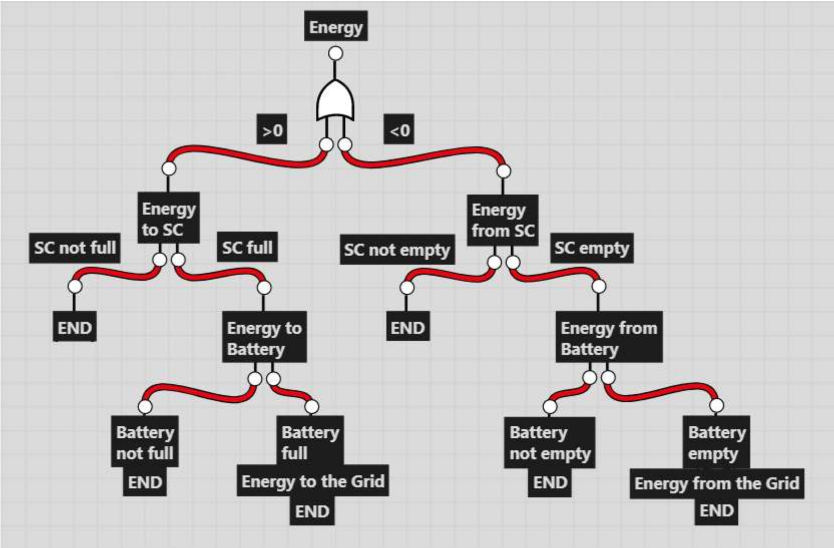

Figura 14 Schema logico del processo decisionale per l'utilizzo dell'accumulatore ibrido.

VII.5. Risultati

1. Il **numero di cicli annui** subiti dalla batteria tradizionale è di 1417, quelli compiuti dalla batteria nell'accumulatore ibrido risultano essere 649, meno della metà.
2. **Distribuzione della percentuale di carica:** data la piccola capacità del SC e la medesima capacità netta dei due accumulatori non vi sono variazioni significative.
3. **Durata dei cicli:** con ciclo si intende il tempo trascorso tra l'inizio di una fase di carica e l'inizio della successiva, al netto delle fasi di compravendita di corrente dalla rete.

   Tabella 4 Durata dei cicli di funzionamento delle diverse componenti

Sistema analizzato	Durata [ore]
Accumulatore tradizionale *(sola batteria)*	3.18
Accumulatore ibrido *(batteria)*	6.25
Accumulatore ibrido *(supercapacitore)*	0.50

   Anche in questo caso la batteria posta all'interno dell'accumulatore ibrido presenta un netto miglioramento delle proprie condizioni di utilizzo.
4. **Energie perse:** a causa delle differenti efficienze si ha un lieve miglioramento globale ma tale aumento di efficienza (1.69%) è molto ridotto a causa delle basse energie trattate dal SC.

VIII. Conclusioni

Nello studio sono state esaminate le principali tecnologie attualmente sotto analisi per quanto riguarda le dinamiche di integrazione tra pannelli fotovoltaici e accumulatori. Particolare interesse è stato posto al futuro dei SC in questo ambito e al ruolo che potranno ricoprire. Le aree di interesse individuate per i SC sono principalmente due: all'interno di piccoli dispositivi direttamente integrati con le celle fotovoltaiche o inseriti all'interno di un accumulatore ibrido per servire da filtri e sopperire a repentine variazioni di potenza. Nel primo caso la grande versatilità e resistenza dei SC li ha resi una valida alternativa alle batterie per alimentare piccoli dispositivi portatili o moduli di analisi *in situ,* sviluppati per resistere ad intemperie e numerosi cicli di carica/scarica. Nel secondo caso invece, a causa dei costi ancora elevati, risulta non conveniente utilizzare un sistema di accumulo interamente composto da SC, ciò risulterebbe anche non motivato dalle modeste potenze normalmente in gioco in un impianto fotovoltaico. La funzione dei SC è quindi quella di un filtro a supporto di un accumulatore a batteria principale.

Il secondo campo di applicabilità è anche stato analizzato mediante una simulazione MATLAB atta ad indagare il processo di deterioramento subito da una batteria con e senza la presenza di un SC di supporto. Dai risultati ottenuti si può affermare la loro consistenza con quanto appreso dall'analisi delle precedenti pubblicazioni. L'inserimento dei SC, se correttamente dimensionati, permette di garantire un miglioramento delle condizioni di funzionamento del sistema. L'appiattimento dei picchi di carico e la riduzione del numero di cicli sono una valida motivazione per investire in un sistema di accumulo ibrido. I risultati ottenuti hanno dimostrato che un accumulatore ibrido permette di allungare la vita utile delle batterie e riduce possibili costi futuri di manutenzione e sostituzione. Dall'analisi del dimensionamento del SC è emerso che la sua capacità deve essere circa un 1/120 di quella totale. Nel caso in analisi l'incremento totale di costo dell'impianto è di 1000 €, a fronte di un prezzo di partenza di 5800 € per l'accumulatore a batterie (prezzo riferito ad un pacco batterie 'Soltaro AIO2 5 kW / 5 kWh' con energia netta utilizzabile di 4.5 kWh [87]). Tale pacco batterie è garantito per una durata di almeno dieci anni. Si può quindi considerare l'adozione di un sistema di accumulo ibrido qualora l'incremento di vita utile dell'impianto fosse di almeno 1/6 di quella iniziale, incremento proporzionale all'aumento dei costi.

Al fine di validare quanto emerso da questa analisi, misurando il reale aumento di vita utile delle batterie, si rende opportuno eseguire delle prove con un impianto pilota confrontando ed implementando i risultati ottenuti con quelli sperimentali. L'impianto di test dovrebbe verificare sia l'effettivo funzionamento dell'accumulatore ibrido che le variazioni portate alle dinamiche delle potenze gestite dallo stesso e l'entità della diminuzione di usura registrata.

Summary

I. Introduzione I

II. Scenario energetico globale I

III. Il fotovoltaico II

IV. Sistemi di accumulo III

V. Integrazione tra fotovoltaico e accumulo V

VI. Sezione di review VI

VII. Simulazione MATLAB X

VIII. Conclusioni XV

Acronyms and symbols 1

1 Introduction 2

2 Global energy scenario 4

3 Photovoltaics 7

3.1 First generation solar cells 8

3.2 Second generation solar cells - thin film 9

3.3 Third generation solar cells 10

4 Energy storage 12

4.1 Lead–acid battery 13

4.2 Nickel–cadmium battery 13

4.3 Lithium-ion battery 13

4.4 Vanadium redox battery 14

4.5 Supercapacitor 15

5 Traditional versus advanced PV-accumulator systems 17

5.1 Traditional systems 18

5.2 Advanced PV-accumulator systems 18

6 Photovoltaics and batteries 20

6.1 Discrete charging 20

6.1.1 Gibson et al.: PV charging of Li-ion batteries (2010) 20

6.1.2 Kelly et al.: Nickel metal hydride battery (2012) 21

6.1.3 Gurung et al.: PSC for photo-charging of LIBs using DC–DC booster (2017) 22

6.1.4 Khataee et al.: DSSC and organic-inorganic redox flow battery (2019) 23

6.2 Integrated charging 24

6.2.1 Guo et al.: DSSC and Li-ion battery (2012) 24

6.2.2 Chakrapani et al.: PV-LIB on single Si substrate (2012) 24

6.2.3 Xu et al.: LIB and perovskite solar cell (2015) 25

6.2.4 *Nagai et al.: PV – LIB fabricated by molecular precursor method (2016)* 26
6.2.5 *Agbo et al.: Thin-film silicon triple-junction solar cell and batteries (2016)*.................. 28
6.2.6 *Ogaryov et al.: Metal nanoparticles and quantum dots as photosensitizers (2016)* 29
6.2.7 *Xia et al.: Integrated charging PSC for smart windows (2016)* 29
6.2.8 *Vega-Garita et al.: Suitable battery technology for integrated module (2019)*............ 30
6.2.9 *Yuan et al.: Integrated $NiCo_2O_4$ battery-supercapacitor hybrid device (2019)*............. 31
6.2.10 *Weng et al.: PSC- aqueous Li/Na-ion battery system (2020)* 32
6.2.11 *Di et al.: Photo-charging integrated device with DSSC and LIB (2020)* 33
7 Photovoltaics and Supercapacitors 36
7.1 *Discrete charging* 36
7.1.1 *Thounthong et al.: Fuel cell/solar cell/supercapacitor hybrid power source (2011)*..... 36
7.1.2 *Meekhun et al.: Buck converter and MPPT algorithms (2011)*.................................... 38
7.1.3 *Yuan et al.: Hybrid storage system (2011)* 38
7.1.4 *Thounthong et al.: Standalone PV/PEMFC/SC (2013)* 38
7.1.5 *Benyahia et al.: Characterization and control of SC bank (2013)*................................. 39
7.1.6 *Guerrero et al.: PV/SC connected to the grid (2013)* 40
7.1.7 *Worku et al.: Mitigation of power fluctuations for grid connected PV plant (2016)* 40
7.1.8 *Sikkabut et al.: PV/PEMFC/SC/LIB hybrid power plant (2016)* 42
7.1.9 *Fahmi et al.: Battery/SC hybrid PV system (2016)*.. 43
7.1.10 *Cabrane et al.: Hybrid energy storage system for PV (2016)* 45
7.1.11 *Yin et al.: Off-grid PV, diesel generator and supercapacitor energy system (2017)*...... 47
7.1.12 *Cabrane et al.: Fuzzy logic management (2017)* 47
7.1.13 *Miñambres et al.: Grid connected hybrid energy storage (2017)* 47
7.1.14 *Cabrane et al.: Hybrid vs. non-hybrid PV systems (2017)*... 47
7.1.15 *Wang et al.: Hybrid wind and PV system with SC (2018)* 48
7.1.16 *Barbosa et al.: MPPT and optimal charging for a PV/LIB/SC system (2018)*................ 50
7.1.17 *Ciccarelli et al.: Hybrid PV and SC system in the railway sector (2018)*........................ 50
7.1.18 *Shchur et al.: Distributed MPPT and energy storage (2018)* 50
7.1.19 *Vargas et al.: Harmonic modelling and simulation of a hybrid system (2019)* 51
7.1.20 *Perdana et al.: Direct connection of the hybrid storage system to the grid (2019)* 51
7.1.21 *Kong et al.: Electric storage with SC and alkaline electrolyser (2019)* 52
7.1.22 *Kamel et al.: Optimisation of a PV/PEMFC hybrid system (2020)* 53
7.1.23 *Guo et al.: Analysis of SC charging (2020)*.. 54
7.1.24 *Jaszczur et al.: PV system with pure SC storage (2020)*.. 55
7.2 *Integrated charging*.. 56
7.2.1 *Kim et al.: MPPT for Integrated Device (2010)*... 56

7.2.2 Li et al.: PV and SC (2012) ... 56
7.2.3 Ongaro et al.: Long lifetime PV wireless sensor network (2012) ... 56
7.2.4 Liu et al.: Losses and performance of SCs (2013) ... 58
7.2.5 Bagheri et al.: Integrated PV/SC system (2014) ... 58
7.2.6 Zhang et al.: Energy fibre (2014) ... 59
7.2.7 Westover et al.: Commercial PV panel and porous silicon SC (2014) ... 60
7.2.8 Xu et al.: Perovskite cell and polypyrrole-based SC (2015) ... 61
7.2.9 Selvam et al.: Common electrode for high temperatures device (2015) ... 61
7.2.10 Xu et al.: Integrated photo-supercapacitor based on PEDOT (2016) ... 62
7.2.11 Wen et al.: PV energy textile (2016) ... 63
7.2.12 Kim et al.: Self-charging monolithic power packs (2017) ... 64
7.2.13 Scalia et al.: Flexible and portable powerpack (2017) ... 64
7.2.14 Sun et al.: Review of existing PS technologies (2017) ... 66
7.2.15 Muralee et al.: Metal sulphides and carbon nanotube support (2017) ... 66
7.2.16 Liu et al.: PSC-SC integrated device (2017) ... 67
7.2.17 Liu et al.: Silicon Nanowire/Polymer Hybrid PV-SC (2017) ... 67
7.2.18 Dong et al.: Integrated PV device (2017) ... 68
7.2.19 Ng et al.: Perovskite-DSSC for high humidity conditions (2018) ... 69
7.2.20 Liu et al.: Laser engraved SC and Si nanowires/PEDOT PV panel (2018) ... 69
7.2.21 Yun et al.: Wearable solar device (2018) ... 70
7.2.22 Kalasina et al.: PV and SC in Ionic Liquid Electrolyte (2018) ... 71
7.2.23 Yuan et al.: Integrated system with hybrid battery-SC devices (2019) ... 71
7.2.24 Chuang et al.: SC based on graphene-doped activated carbon (2020) ... 72
7.2.25 Orozco-Messana et al.: Realization of a SC based on a ceramic tile (2020) ... 73
7.2.26 Yue et al.: Estimation of the charge of a SC (2020) ... 74
7.2.27 Qin et al.: PS semi-transparent and flexible $Ti_3C_2T_x$ MXene-based (2020) ... 74
7.2.28 Liu et al.: Ultra-flexible PS system (2020) ... 75
8 MATLAB simulation 77
8.1 Load definition ... 78
8.1.1 Working day ... 80
8.1.2 Holiday ... 82
8.1.3 Average daily electricity use ... 83
8.1.4 Consumption ranges ... 85
8.2 Plant dimensioning ... 87
8.3 SC sizing ... 94
8.4 Analysis of MATLAB code ... 96

8.4.1 Data initialisation 96
8.4.2 Energy management 97
8.4.3 Leakage analysis 98
8.5 Results 99
8.5.1 Comparison of cycle numbers and SOC 99
8.5.2 Comparison of cycle lengths 101
8.5.3 Comparison of lost energies 102
8.5.4 Analysis of daily trends 103
9 Conclusions **106**
10 Appendix A **108**

Acronyms and symbols

Acronyms & Symbols	Meaning
µC-SI:H	Microcrystalline Si
AE	Alkaline electrolyser
AQDS	Anthraquinone-2,7-disulfonate disodium
A-SI:H	Amorphous Si
BSH	Battery-supercapacitor hybrids
CdTe	Cadmium telluride
DAQ	Data acquisition system
DSSC	Dye-sensitized solar cell
EL	Electrolyser
EREV	Extended-range electric vehicles
EROEI	Energy returned on energy invested
ESR	Equivalent series resistance
FCEV	Fuel-cell electric vehicles
FEHD	Flexible extended harmonic domain
GaAs	Gallium arsenide
IOT	Internet of things
Jsc	Short-circuit current density
LAB	Lead-acid battery
LFP	Lithium iron phosphate
LIB	Lithium-ion battery
LI-ION	Lithium-ion
LTO	Lithium titanate
MPM	Molecular precursor method
MPP	Maximum power point
MPPT	Maximum power point tracking
NiCd	Nickel-cadmium battery
NT	Nanotube
PA	Photo-assisted
PEMFC	Polymer electrolyte membrane fuel cell
PS	Photo-supercapacitor
PSC	Perovskite solar cell
PV	Photovoltaic
RFB	Redox flow battery
RGO	Reduced graphene
RTDS	Real time digital simulator
SC	Supercapacitor
SEM	Scanning electron microscope
SOC	State of charge
SRFC	Solar redox flow cell
ss-DSSC	Solid-state dye-sensitized solar cell
STC	Standard test conditions
TF	Thin film
Voc	Open-circuit potential
η	Efficiency

1 Introduction

Until the 18^{th} century, the energy needs of human society were limited to the utilization of animal and thermal energy. Wood burning was mainly used for cooking and heating houses. However, thanks to the invention of the steam engine in the 18^{th} century, the Industrial Revolution began. The exploitation of fossil fuels (coal, oil and gas) enabled the mechanisation and automation of industrial processes. Since then, with industrialisation and the ever-increasing demand for energy, human impact on the environment has increased dramatically, both in terms of environmental degradation and emission of pollutants.

It is clear, however, that this increase in energy demand cannot be satisfied by increasing the consumption of fossil fuels. A significant focus is placed on the development of renewable technologies, which greatly limit the emission of pollutants. The main renewable sources include solar, hydroelectric, wind, geothermal and biomass energy.

Solar energy is currently the most popular of these, and to reduce the problems and costs associated to the construction and recycling/disposal of these devices, many research groups are working to produce greener and more sustainable photovoltaic technologies. The substitution of noble elements, together with the research for an energy-efficient manufacturing process, is the focus of the research.

In conjunction with the problem of energy production, there is the problem of the intermittency of renewable energy sources and the necessity to accumulate and store part of the production. Energy storage systems, varying in the technology on which they are based, bring with them different issues. These problems may be related to the toxicity of the chemical elements used or to intrinsic characteristics which compromise their lifetime or use under certain conditions.

In the first part of this thesis, the current energy scenario is briefly presented with its critical issues and future developments. Then, the main photovoltaic technologies based on crystalline silicon (first generation), thin films (second generation) and hybrid materials (third generation) are presented. Subsequently, the different electrical storage technologies and possible integration designs between photovoltaic panels and batteries or supercapacitors are described in detail. These technologies are then analysed separately in the review, examining their different strengths and applications. The articles have been subdivided according to the type of storage (battery or supercapacitor) and then according to the type of integration between the production system and the storage one, in order to facilitate the reading. At the end of the review section, a MATLAB simulation is carried out to analyse the behaviour of a hybrid accumulator (consisting of batteries and supercapacitors) to validate its possible use in a domestic scenario. The analysis focuses on comparing the degradation of a hybrid battery compared to a conventional one.

2 Global energy scenario

Recently, humanity has been confronted with one of the most tragic and disruptive events of the century, *i.e.* the COVID-19 pandemic [1]. The combination of the economic and health shocks resulting from this situation is bound to reshape the global economic, political and social landscape in which we are all immersed in both social and working spheres.

This global crisis has shown its potential to accelerate emerging trends, creating opportunities to move the world towards a more sustainable path. In contrast, the emerging economic crisis could lead to a shift in current energy investments to other areas.

In this context, some elements are positive, in particular the continuous strong growth of renewable energy. Growth is led by wind and solar power, which has led to record growth in renewable energy, resulting in an increase of over 40% in primary energy growth over the past year. At the same time, coal consumption has continued its downward trend, with its share in the global energy mix declining to its lowest level in 16 years. Despite this, coal still accounts for more than 36% of global energy, compared to the only 10% provided by renewables [1].

However, this decrease has not resulted in a decrease in carbon dioxide (CO_2) emissions. The average value of its annual growth in 2018 and 2019 was higher than its 10-year average growth.

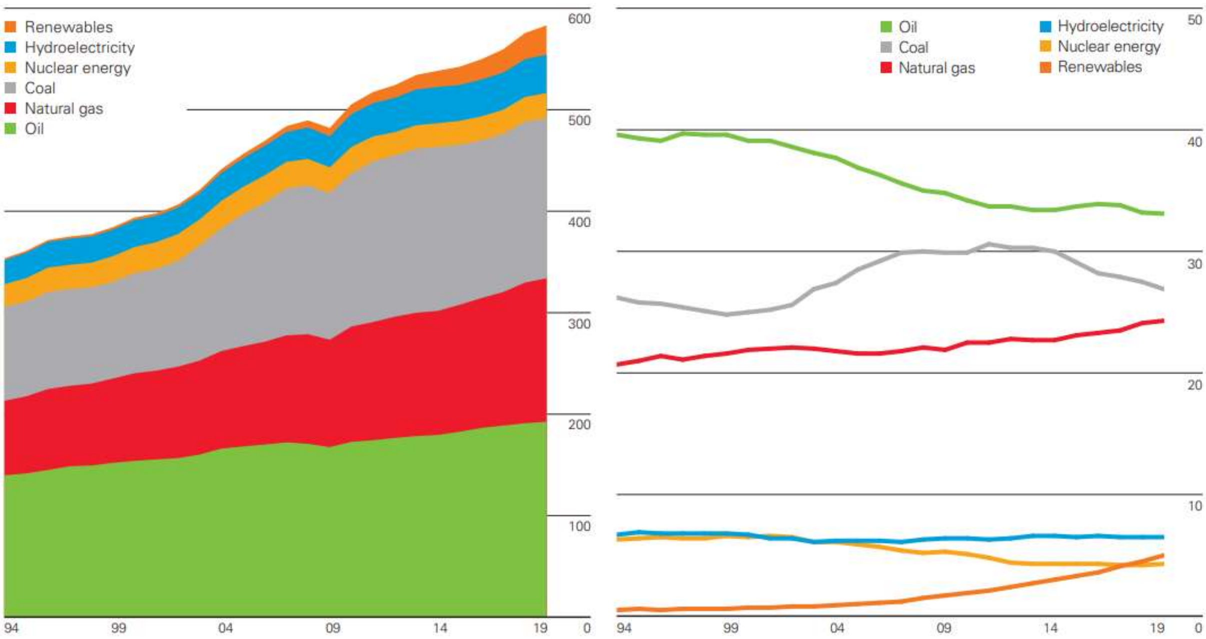

Figure 1 (left) World energy consumption (in EJ) over the last 25 years; (right) change in world primary energy shares over the last 25 years. Adapted and reprinted with permission from [1].

During 2019, primary energy demand increased by 1.3%, as shown in Figure 1 (left), less than half of the growth rate seen in 2018 (it was equal to 2.8%). Renewable energy and natural gas are the sources that drove this trend, their increase is shown in Figure 1 (right). The largest share of the energy mix (33.1%) is still held by oil, followed by coal. As mentioned above, however, in 2019 and despite accounting for 27.0% of the total, coal has lost share compared to previous years.

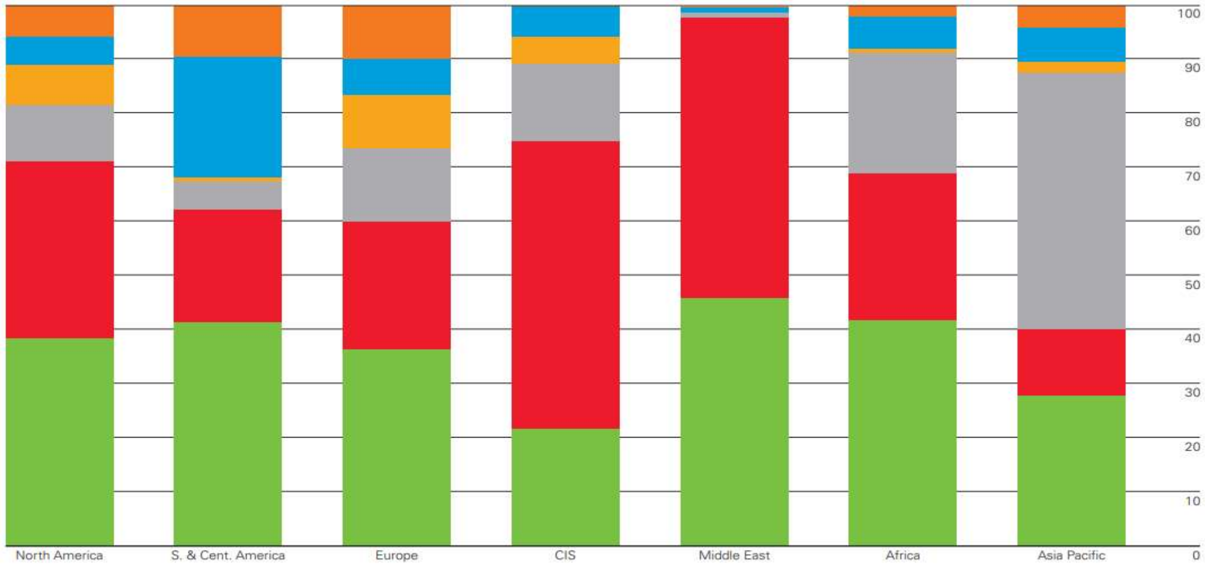

Figure 2 World energy consumption by region of use and type of production. Adapted and reprinted with permission from [1].

As shown in Figure 2, oil remains the dominant fuel in the Middle East, Africa, Europe and the Americas. Natural gas remains dominant in the CIS and the Middle East, accounting for more than half of the energy mix in both regions. Coal, on the other hand, is the dominant fuel in the Asia-Pacific region, due in part to its large underground resources.

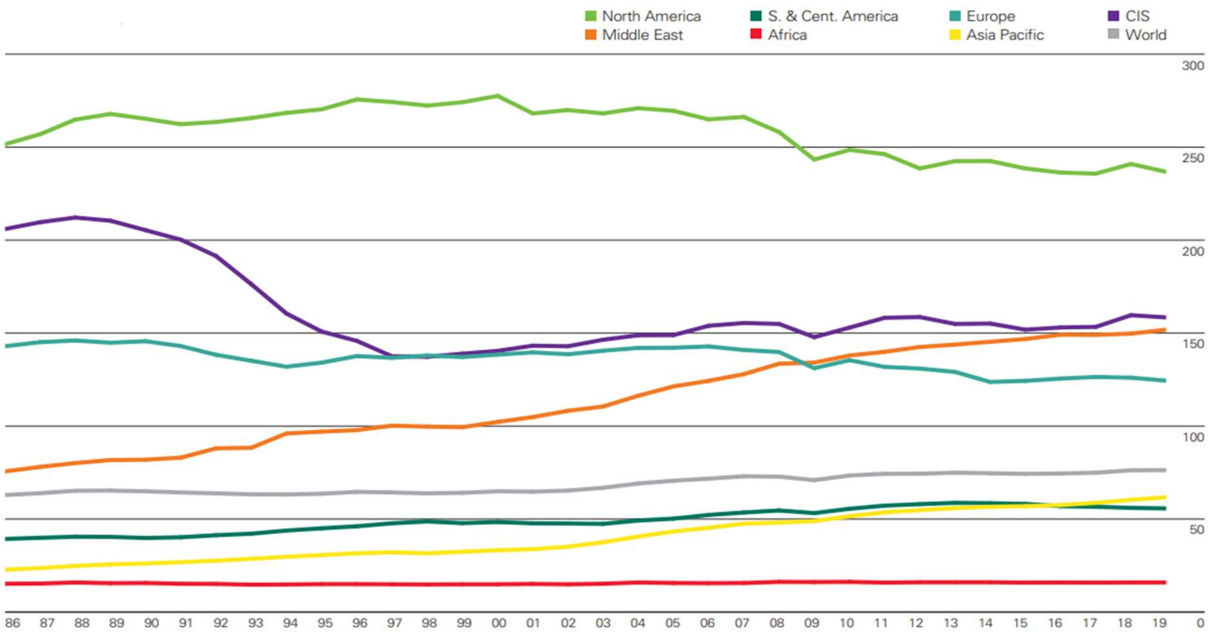

Figure 3 Energy consumption per capita by region of origin. Adapted and reprinted with permission from [1].

The increase in global average energy consumption *per capita*, shown in Figure 3, increased by only 0.2% in 2019 to 75.7 GJ *per capita*. Growth is led by increases in the Middle East (1.4%) and Asia Pacific (2.4%). However, all other regions saw a reduction in consumption. North America is still the region with the highest *per capita* consumption (236 GJ capita^{-1}), despite a declining trend in recent years. Africa remains the region with the lowest average consumption (15 GJ capita^{-1}).

3 Photovoltaics

The expression "photovoltaics" (PV) refers to the capacity to produce electrical energy through the conversion of photons from solar radiation [2]. The direct conversion of energy takes place through a semiconductor substrate which, on exposure to photons of sufficient energy, generates the release of electrons. In the global scenario, solar energy includes both PV and concentrated solar power. The latter differs from the former in the fact that solar radiation is not directly converted, but – through the generation of thermal energy – is used to power conventional turbine generation systems. However, PV remains the main player in global power generation from renewable and sustainable sources.

The PV effect was discovered in 1839 by A. E. Becquerel, who demonstrated the basic principle of a PV cell [3]. Solar cells have seen numerous technological improvements over decades, making them more and more efficient, economical and environmentally friendly. Solar cells can currently be classified into three different generations:

1) First generation: cells composed of monocrystalline or polycrystalline silicon-based substrates;
2) Second generation: use of silicon together with other semiconductors such as gallium arsenide (GaAs) and cadmium telluride (CdTe);
3) Third generation: semiconductors are replaced with cheaper, hybrid and multijunction materials.

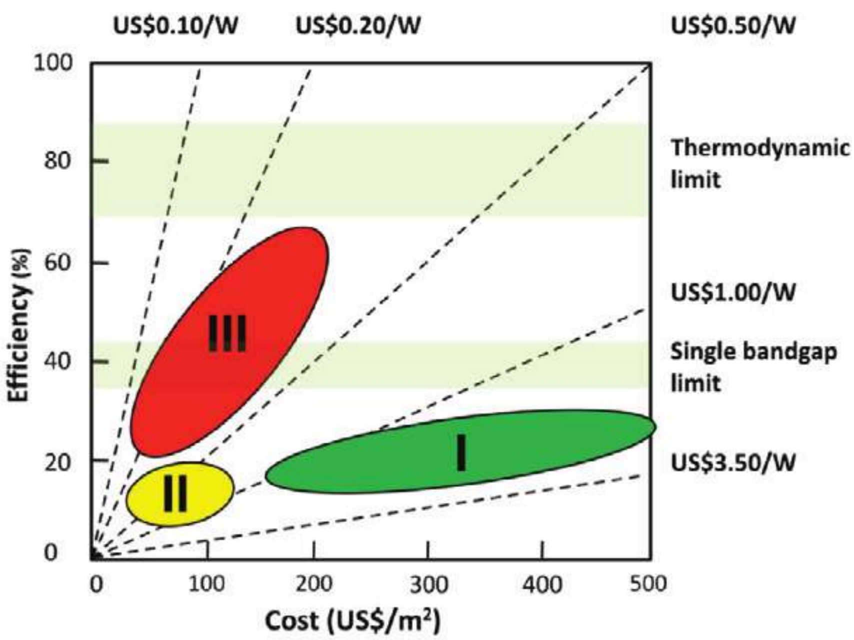

Figure 4 Efficiency and cost for first, second and third generation PV technologies. Adapted and reprinted with permission from [4].

3.1 First generation solar cells

The first generation of PV cells saw the focus of research on the structure of the silicon used as the basis of the cell and its crystalline composition. The possible alternatives were amorphous, polycrystalline and monocrystalline silicon in order of appearance. The structure of monocrystalline silicon enables higher performance, as the presence of less defects makes it difficult for electrons to recombine, thus increasing electricity production. The band gap generated is approximately 1.12 eV. This value allows the absorption of radiation with wavelengths between 0.35 and 1.2 μm, which corresponds to around 40% of the total energy coming from the sun. Under certain circumstances, in cases of low solar incidence angles, polycrystalline panels are sometimes preferred as they optimise the radiation utilisation. The first generation PV systems is now characterised by a high efficiency, even above 20%, making silicon cells the most popular on the PV market. However, the production of these cells is characterised by numerous wastes and costs resulting from the need for solar grade silicon (silicon for solar use with impurities between 10^{-7} and 10^{-9}) and the manufacturing processes involved. The cost of producing the silicon substrate amounts to 20/25% of the total cost, and because of its fragility it is also necessary to use thicknesses of more than 100 μm, which increases costs [5]. The cell structure contains two silicon-based sections. The first, with a thickness ranging from 180 to 300 μm, is doped with boron and forms the p-type junction. The second, which is much thinner (about 1 μm) to prevent electronic recombination, is doped with phosphorus compounds and forms the n-junction. The combination of the two junctions, the electrodes and the protective glass forms the sandwich structure of the PV cell [6].

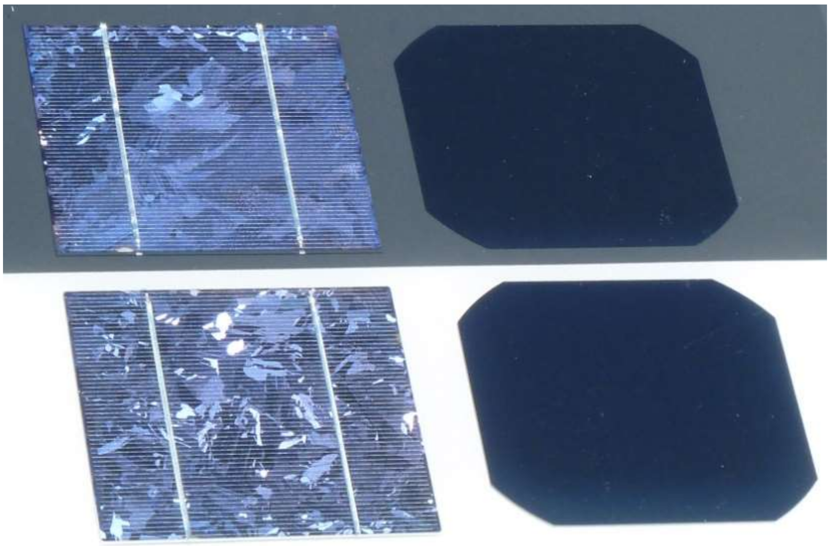

Figure 5 Visual comparison of first-generation solar cells. Those on the left are made of multicrystalline silicon (multi-Si), while those on the right are made of monocrystalline silicon (mono-Si). Adapted and reprinted with permission from [7].

- **Polycrystalline silicon**
  - Polycrystalline silicon has an efficiency of 15 to 17%;
  - Lower production and material costs;
  - Better diffuse light conversion;
  - Better thermal coefficient, the percentage of loss due to the increase in cell temperature is lower.
- **Monocrystalline silicon**
  - Monocrystalline silicon has an efficiency of 18 to 21%;
  - Higher material waste during processing;
  - Very energy-intensive production process.

3.2 Second generation solar cells - thin film

Second-generation cells were developed because of the need to reduce the use of raw materials and energy during the production of PV panels. They are also known as thin film (TF) cells.

TF PV modules are manufactured by depositing semiconductor materials onto a substrate. This substrate can be rigid, normally glass for outdoor use, or flexible, plastic is used to make flexible panels for less conventional uses. The deposited materials consist mainly of silicon, indium, tellurium and cadmium. This technology forms a *p-i-n* junction diode. The *p-i-n* layers are doped and are very thin. The intrinsic layer *i* absorbs light, transfers energy to the charge carriers and is used for current generation. In this case, the semiconductor materials are amorphous, doped and show poor electrical properties due to the presence of defects acting as recombination centres. In this type of cell, diffusion cannot guarantee electron transport, so an electric field generated by the *p-i-n* junction is required, which allows the separation of electrons from the generated interstices and improves charge transfer to the *n* and *p* layers [8].

TF modules are divided into various categories depending on the semiconductor materials deposited on it, the most common of which are:

- **Amorphous silicon**

  Amorphous silicon PV panels are characterised by silicon atoms deposited by chemical processes in an amorphous phase, *i.e.* deliberately disorganised, formed onto the supporting substrate (Figure 6). One of the advantages of this technology is the small amount of silicon used (thickness in the order of μm). The main disadvantage of amorphous silicon modules is their lower and less constant efficiency compared to other PV technologies. The most interesting data, however, concerns the energy savings associated with their production, measured by the "energy returned on energy invested" (EROEI). From a mathematical point of view, it represents the ratio between the energy obtained and all the energy spent to obtain it. The result is that an energy source with an EROEI of less than 1 is at a loss from an energy point of view. Energy sources with an EROEI of less than 1 cannot be considered a primary source of energy, as their exploitation requires more energy than is obtained. The EROEI proves to be a fundamental parameter for making strategic energy policy choices, evaluating and comparing supply between different energy sources. In this case, this coefficient shows very high values (in some cases up to 9), demonstrating the high cost-effectiveness of this technology [9].

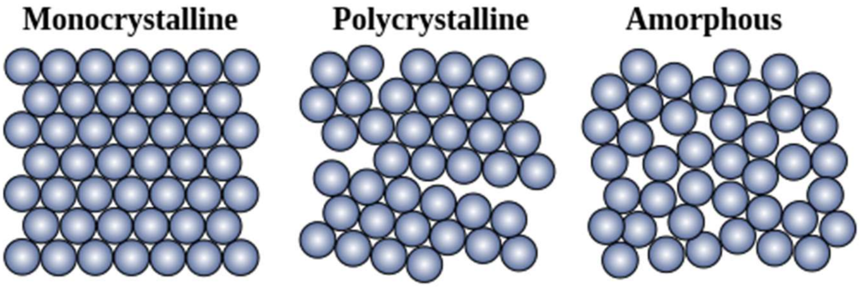

Figure 6 Schematisation of the allotropic forms of the distribution of silicon atoms. Adapted and reprinted with permission from [10].

- **Cadmium telluride**
  This is a semiconductor with characteristics similar to those of gallium arsenide or silicon, but less expensive, as both cadmium and tellurium are considered waste materials in non-ferrous mining processes. The efficiency claimed by manufacturers is in the order of 6% and 9% [9]. Due to the toxicity of cadmium, its use is not widespread.

- **Copper diselenide indium biselenide, copper indium and gallium diselenide**
  These compounds are semi-crystalline semiconductors with a high absorption coefficient. As an advantage, they have no degradation problems, but are unstable in humid and hot environments, which considerably reduces their field of application. Indium is also a very rare material with a very variable price on the market [11].

3.3 Third generation solar cells

Third-generation cells were born out of the need to move away from silicon technology and introduce cheaper and more environmentally friendly materials. In recent years, research has shifted towards materials that are abundant and whose processing does not require large amounts of energy and purity. Third-generation PV have experienced a period of considerable growth in recent years, but efficiency has not yet reached that of previous categories.

- **Dye-sensitized cells and quantum dots**
  Dye-sensitised solar cells (DSSC) mostly employ semiconductors such as TiO_2 and use a thin layer of Pt as a cathode. Polymers are being developed to replace Pt, PEDOT being one example as it is cheaper and more environmentally friendly. Quantum dots solar cells have optical characteristics that allow the size of the particles that make up the photoactive species to be varied. Quantum dots are semiconductors with a low forbidden band (InP, CdSe, CdS) [2]. They can be adsorbed by the semiconductor through treatments and, when irradiated, can generate multiple excitations with the absorption of a single photon.

- **Perovskite solar cells (PSC)**
  The term "perovskite" refers to any material that adopts the same crystal structure as calcium titanate: ABX_3 [12]. This chemical structure is very popular as it allows the creation of materials with a huge variety of properties including thermoelectric, piezoelectric, insulating, semiconducting, conductive and superconductive capacity. By using perovskite, it is possible to make solar cells with improved absorption of sunlight.

4 Energy storage

Rechargeable batteries are storage devices which, through reversible reactions, can perform charge and discharge cycles. In contrast, non-reversible batteries can only be used once, which is why they are not included in this study. Rechargeable batteries generally use the same mechanism as non-rechargeable batteries, the only difference being that the redox reaction can be reversed with sufficient energy input into the equation.

Depending on the type of use and the environment in which it has to operate, there are different types of batteries.

Numerous operating cycles, long periods of inactivity, use in harsh climatic conditions, large charge densities and high-power output are just some of the challenges currently being studied. At present, there are no technologies that can excel in all the above functions. Therefore, depending on the application required, a decision must be made as to which of the following technologies is best suited.

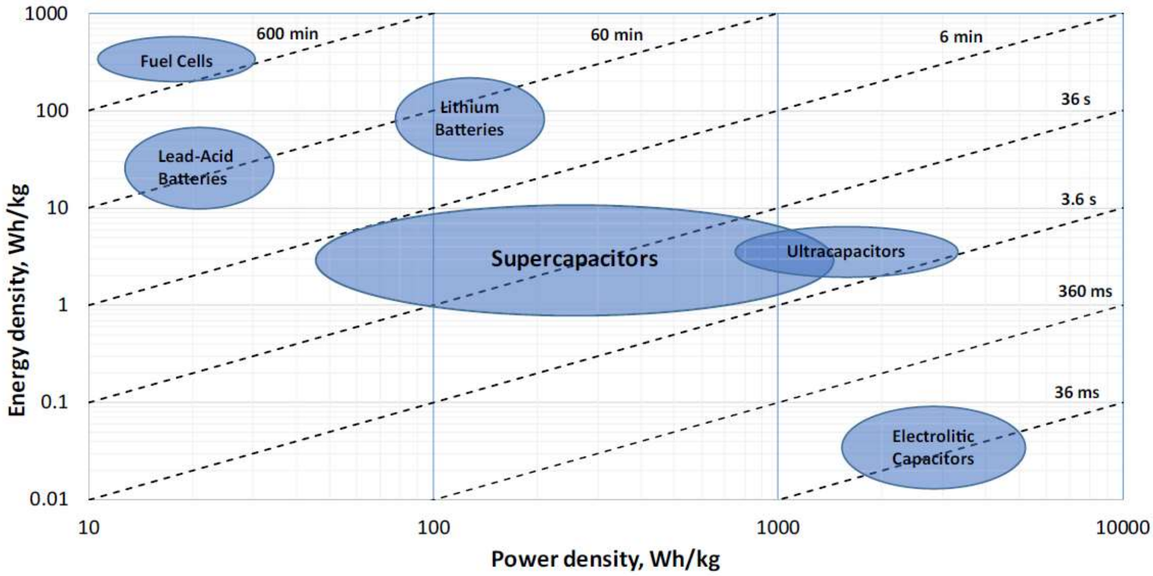

Figure 7 Power and energy density for different technologies. Adapted and reprinted with permission from [55].

In Figure 7 it is clearly visible how each technology is related to different energy and power density values. Depending on the use required, the space available and the masses involved, it is necessary to evaluate which technology is the most efficient in that scenario. The main technologies currently under development are analysed below.

4.1 Lead–acid battery

Invented in 1859 by French physicist Gaston Planté, the lead-acid battery (LAB) is the oldest type of rechargeable battery and is still largely used in automotive endothermic engine vehicles. Its main use is for starting the internal combustion engine and for powering on-board electronics. Its popularity is not due primarily to its characteristics as an accumulator, but to the very low cost of the components used, such as lead and sulphuric acid. In the land transport sector, the standard has imposed a configuration of 6 cells arranged in series, capable of providing a total potential difference, when fully charged, of 12.30-12.90 V at open-circuit (2.05-2.15 V for the single cell) and about 12 V under operation (2 V for the single cell), at a reference temperature of 25 °C.

The main weaknesses are related to the rather low energy/weight and energy/volume ratios, whereas sulphation of the plates/cells is a natural chemical process which occurs during discharge. This process leads to self-discharge, which reduces the energy available in the battery.

4.2 Nickel–cadmium battery

Nickel-cadmium (NiCd) batteries are a popular type of battery, often used in portable consumer electronics devices and toys. They base their operation on metals such as nickel and cadmium as chemical reagents.

It is suitable for low-temperature conditions with a low self-discharge. However, NiCd batteries are more expensive and their capacity in terms of watt-hours per kilogram is lower than other rechargeable batteries.

4.3 Lithium-ion battery

Lithium-ion batteries (LIB) are a type of rechargeable battery that is widely used in different scenarios. Commonly used for portable electronics, they are also used in electric vehicles, industrial, military and aerospace applications. LIBs use a lithium compound on the cathode and graphite or lithium titanate on the anode. Due to their high energy density, low memory effect and low self-discharge, LIBs are characterised by good behaviour and high reliability [13]. However, since they contain a flammable electrolyte and materials considered hazardous, they can be a source of fire and explosion leading to safety hazards. The basis of these accidents can be an incorrect or excessive recharge, incorrect use or physical damage resulting in the generation of an internal short circuit.

The widespread use of LIBs is also due to the wide range of shapes and sizes they can take during manufacture, which allows them to efficiently use and fill the space available in the devices that they power. A further advantage is their low weight, which is due to the fact that lithium-ion (Li-ion) has a higher charge density than other storage technologies. LIBs have a nominal voltage of 3.6~3.7 V, which is the average value between the voltage at full charge (4.2 V) and the voltage beyond which it should not fall (3.0~3.2 V) to avoid damage to the device. Charging is done at constant voltage with current limitation. This means that charging takes place at constant current until the element almost reaches the voltage of 4.2 V (to be safe, it is usually a few tens of millivolts below this value), after which it continues at constant voltage until the current becomes zero or almost zero (typically, charging is completed at 3% of the initial charging current) [13].

4.4 Vanadium redox battery

Vanadium redox batteries are based on the interactions resulting from the combination of electrochemical cells in which the electrolytes are separated by a proton exchange membrane. The battery thus consists of two half-cells, the positive semi-cells contain VO_2^+ and VO^{2+} ions, while the negative ones contain V^{3+} and V^{2+} ions. There are different technologies for preparing the electrodes, the most common consists in the electrolytic dissolution of vanadium pentoxide (V_2O_5) in a solution of sulphuric acid (H_2SO_4). The resulting solution has strongly acidic characteristics. In this type of battery, the storage capacity is linked to the amount of solution available. The two half-cells are therefore connected to storage tanks containing a large volume of electrolyte. This electrolyte is circulated in the cell using special pumps when it is necessary to produce electricity. This technology, based on the circulation of liquid electrolytes, takes up a considerable amount of space, but limits the capacity of the accumulator to the tanks available. The use of this device is limited to fixed installations, as the characteristics listed above limit its small-scale use and dynamism. However, one company has become interested in electric vehicle applications, replacing the electrolyte solution for rapid battery charging [14].

The reaction that originates during the charging phases is the oxidation of vanadium in the positive half-cell, with its change from VO^{2+} to VO_2^+. As a result of the oxidation, electrons are released and inserted into the negative half-cell, where the vanadium is reduced from V^{3+} to V^{2+}. During battery use, the process takes place in reverse order, leading to the generation of an open-circuit potential difference of 1.41 V at 25 °C.

Currently produced vanadium redox batteries generate an energy density of about 25 Wh kg^{-1} of electrolyte. This energy density is rather low compared to that of other rechargeable batteries such as lead-acid (30-50 Wh kg^{-1}) and Li-ion (110-160 Wh kg^{-1}).

4.5 Supercapacitor

A supercapacitor (SC) is a special capacitor which has the characteristic of storing an exceptionally large amount of electrical charge compared to conventional capacitors. While conventional capacitors have capacitance values of the order of mF, SCs can have capacitance values of over 5000 F. SCs are mainly used as electrical energy accumulators. Compared with chemical accumulators, SCs have the advantage that they can be charged or discharged almost instantaneously, thus guaranteeing a very high specific power. They also have a much higher number of charge/discharge cycles than conventional accumulators. The most significant disadvantage compared with chemical accumulators is the low energy that can be stored.

Table 1 Comparison of key parameters for Li-ion batteries and supercapacitors. Adapted and reprinted with permission from [15].

FUNCTION	***SUPERCAPACITOR***	***LITHIUM-ION (GENERAL)***
CHARGE TIME	1-10 s	10-60 min
CYCLE LIFE	500,000-20,000,000	500-1,000
CELL VOLTAGE (V)	2.7-3	3.6
GRAVIMETRIC ENERGY (Wh kg^{-1})	4-10	100-265
SELF-DISCHARGE (% PER MONTH)	40-50	2
CHARGE TEMPERATURE (°C)	−40 to 65	0 to 45
DISCHARGE TEMPERATURE (°C)	−40 to 65	−20 to 60
LIFETIME (YEARS)	10-15	5-10
CHARGING PROCEDURE:		
FOR 1 CELL	Easy	Complex
CELLS IN SERIES	Complex	Complex
RISK OF:		
DEEP DISCHARGE	No	Yes
OVERLOAD	No	Yes
THERMAL RUNWAY	No	Yes
EXPLOSION	No	Yes
VOLTAGE OUTPUT	Decreasing	Stable
EFFICIENCY (%)	99	85-95
COST (€ kWh^{-1})	10,000	200-1,000

5 Traditional versus advanced PV-accumulator systems

The research, in addition to working on new generation PV panels and storage systems with higher capacities and energy densities, is looking for new ways to integrate these technologies with each other. The traditional method of recharging accumulators, using energy produced by solar installations, consists of a discrete or isolated design [16]. Such designs involve independent operations of the two main components involved, PV generation and storage, which are electrically connected by electrical cables. Such systems tend to be expensive, bulky and inflexible, also suffering energy loss through the connecting cables and control electronics.

Combining the generation system with the storage system results in an integrated design. This design has the potential to function as a sufficient energy source with internal storage for surplus energy. Integrated PV-accumulator systems can offer a compact and energy efficient alternative to conventional PV-accumulator systems. The flexibility of this design is offered by the need to adopt less wiring, while the smaller footprint is significantly important especially for small scale consumer electronics.

Despite the merits of this innovative integrated approach, there are significant efficiency, capacity and stability challenges. They are not yet high enough to make this approach successful on a commercial scale. While still in the early stages, research is taking significant steps to focus on the materials that will be needed to overcome these challenges. Integrated PV-accumulator systems can be classified into two different configurations: three-electrode and two-electrode. In the three-electrode configuration the central one is used as common between the two systems, acting as cathode or anode for both, the PV and battery device. In the second configuration, the positive electrode is used for the photoconversion, while the negative electrode is connected to the storage system. These two possibilities are shown schematically in Figure 8.

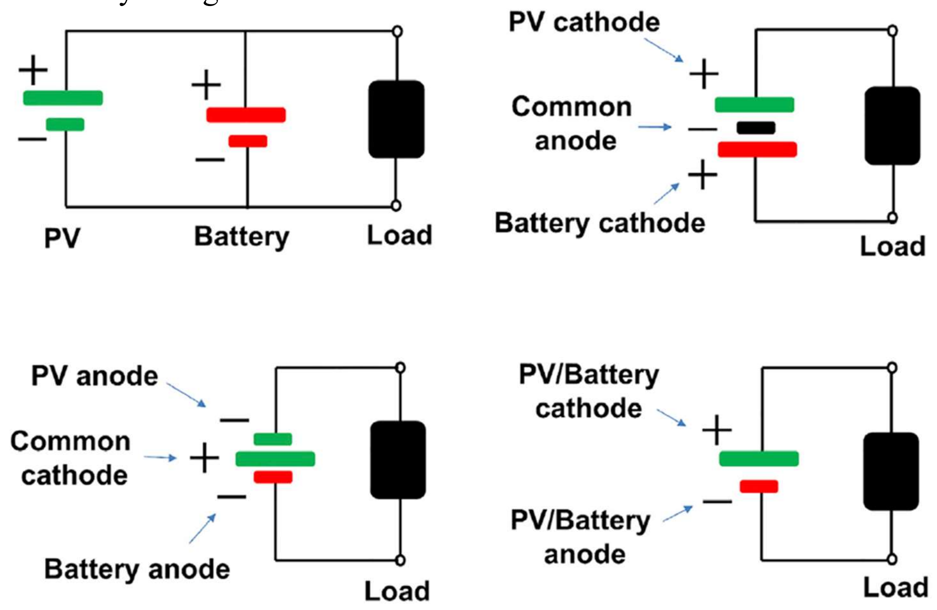

Figure 8 Diagram of the different circuits that differentiate the types of integration: (top left) discrete design, the clear separation between generator and accumulator is well visible; (top right) integrated design with three-electrode configuration, common anode; (bottom left) integrated design with three-electrode configuration, common cathode; (bottom right) integrated design with two-electrode configuration. Adapted and reprinted with permission from [16].

5.1 Traditional systems

The management of storage systems in conventional PV systems considers the production component separately from the storage. This management often leads to installing the different components at considerable distances, increasing transmission losses or maximising production without taking into account the huge losses due to the high power sent to the accumulator. In many cases, attention must be given to these issues by improving the plant layout or improving the MPPT software of the solar charge controller.

However, the extensive experience gained over the years with this type of system still makes it significantly cheaper and more efficient than the integrated variant. In the review part, it will be analysed how this type of system can be improved by inserting a SC in order to act as a filter to reduce the stress on the main accumulator. The presence of an SC, at the side of the batteries, does not create an improvement in the electrical transport losses but helps in the management of power peaks and reduces the stress suffered by the accumulator.

5.2 Advanced PV-accumulator systems

Integrated PV-accumulator systems can again be divided into two types based on the kind of charging, which can be direct or photo-assisted (PA).

With direct integration, the aim is to create a monolithic structure containing both the photovoltaic cell and the accumulator, making the system autonomous and self-sufficient. PA integration is based on photo-charging for the first part of the charging process before completing the process with an external source.

- **Direct integration**
  Monolithic integrated devices contain both the solar cell and the accumulator. The charge is directly transferred by means of a common electrode, which drastically reduces transmission and auxiliary losses. The most critical aspect of the system is the charging voltage of the battery or the SC, which cannot be regulated externally. In order to regulate the recharging of the accumulator, a PV module is generally chosen to deliver a maximum voltage lower than the limit voltage of the battery.
- **Photo-assisted integration**
  In this type of charging, the PV system is not seen as the only electrical supply. The primary purpose of PA charging is to charge the battery in the best way without completing the charging process. This process requires an external source to be completed.
  Although these systems are highly efficient, they require an external charging source and are therefore not suitable for a wide variety of scenarios. For this reason, they cannot be considered as a self-sufficient integrated design from an energy point of view.

6 Photovoltaics and batteries

The following section provides a literature review of research carried out over the last 10 years on the integration of photovoltaic cells with different types of batteries.

The analysis is divided into two groups according to the type of integration adopted. The first group studied concerns discrete charging, where it is possible to find analyses concerning the optimal production ratio and battery sizing analyses, as well as studies concerning the best battery operating conditions. This is followed by the analysis of innovative charging systems through direct or monolithic integration of the storage system with the production one. In this second group, there is also research into innovative materials for increasingly high-performance, small-scale devices.

6.1 *Discrete charging*

6.1.1 Gibson et al.: PV charging of Li-ion batteries (2010)

Gibson *et al.* combined the PV maximum power point (MPP) with the operating voltage of the electrolyser to study and optimize the solar charge of LIB [17]. This experimental system seeks to design a new home-scale solar charging station for extended range electric vehicles (EREV), eliminating losses due to inverter efficiency, transmission efficiency and charge regulator efficiency. LIB modules (produced by A123 Systems) were grouped in strings composed by series of 10 to 16 cells and the terminals were connected directly to the output cables of the PV system. A data acquisition system (DAQ) was added to measure voltage and current. The battery composed of 15 cells allowed to reach the maximum charging efficiency of 14.5% once connected to the 50.2 V PV module (15% PV conversion efficiency). The change in efficiency, which occurs between the different battery modules, is due to the sudden drop in power delivered by the PV module that occurs when the PV MPP voltage (approx. 50 V for test conditions) is exceeded by the battery charge voltage. Figure 9 shows the performance of the different battery packs in relation to the $V_{mpp}/V_{battery}$ charging ratio.

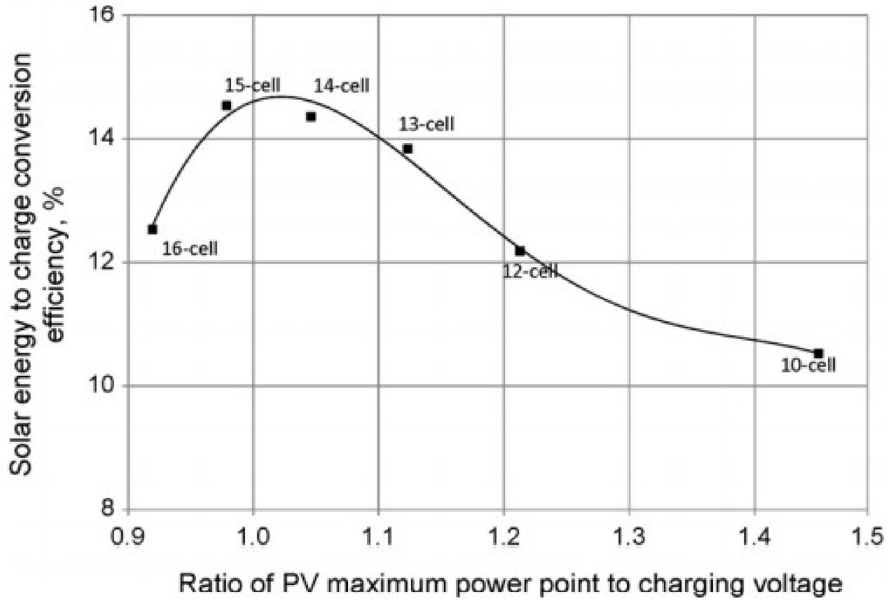

Figure 9 Relation between battery packs and $V_{mpp}/V_{battery}$ charging ratio. Adapted and reprinted with permission from [17].

Thus, to design a solar PV charging system of this type it is needed to slightly set the PV MPP voltage below the desired maximum battery charge voltage, so that the battery pack can be fully charged without overcharging problems.

6.1.2 Kelly et al.: Nickel metal hydride battery (2012)

Kelly *et al.* used a high voltage solar system capable of emitting a wide range of voltages needed to charge the nickel metal hydride (NiMH) battery [18]. The PV system in question consists of five to eight modules (50 V) that, connected in series, could deliver about 250-400 V by 50 V increments. Maximum efficiency as high as 15% was achieved using seven PV modules in series, the value is due to the simplicity of the system and its ability to maintain solar energy coupling and battery charge close to the unit throughout the curve, as shown in Figure 10.

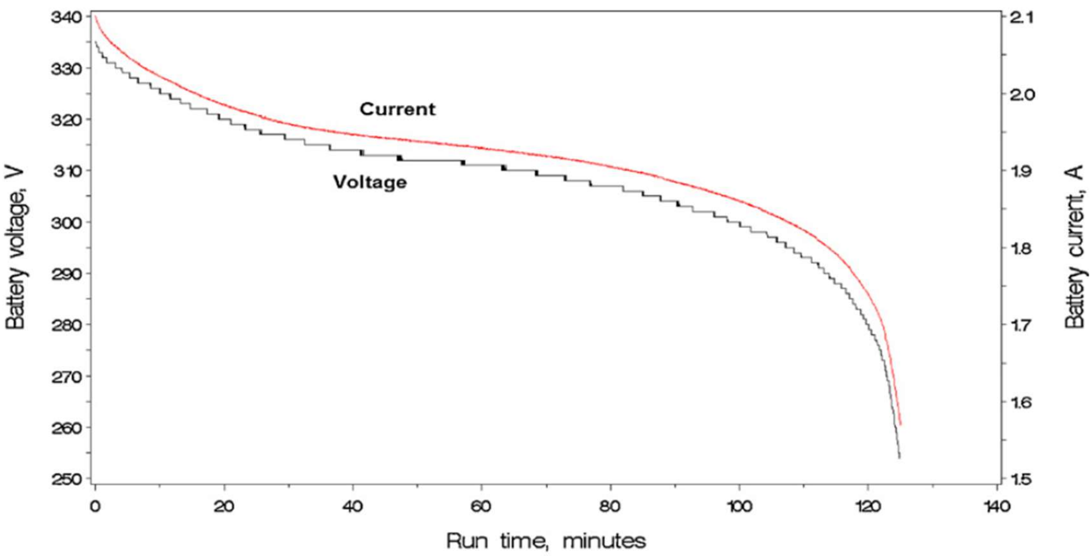

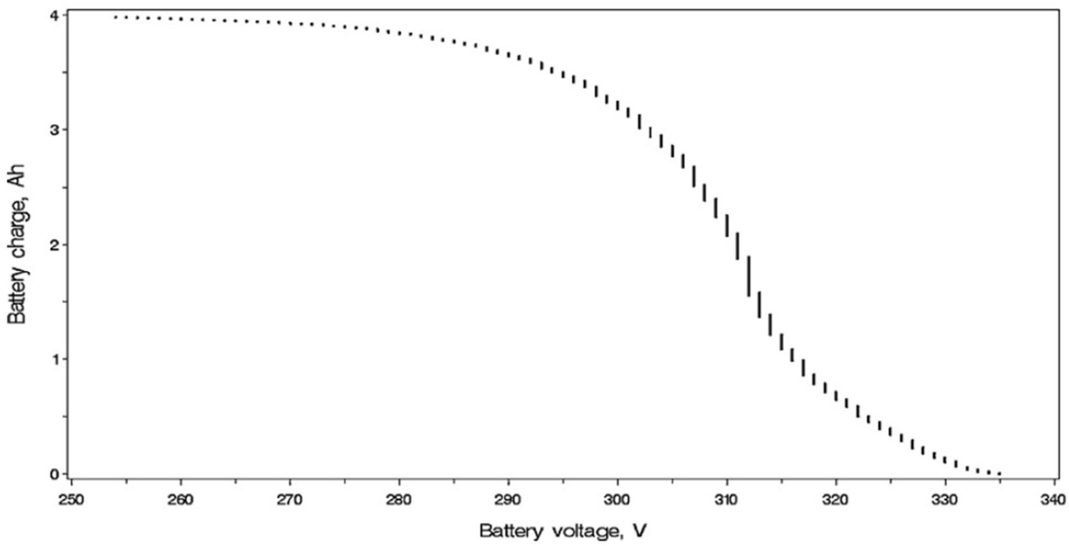

Figure 10 Diagrams showing the results of a discharge test of the battery under analysis, the battery starts with a SOC of 100% (fully charged). (top) Graph showing battery voltage and current as a function of time; (bottom) battery charge as a function of battery voltage. Adapted and reprinted with permission from [18].

To compare this result with a basic one, the system was compared with an old study. In that case, the PV system was in low voltage mode (PV modules in parallel with 50 V output) and the voltage was increased by a DC-DC regulator. In this old scenario, the overall efficiency was close to 13.5%.

6.1.3 Gurung et al.: PSC for photo-charging of LIBs using DC–DC booster (2017)

Gurung *et al.* integrated a DC-DC boost converter to regulate the battery charging voltage and to track the MPPT point of the PV cell [19]. The DC-DC boost converter was chosen to be a viable system for charging a LIB based on $Li_4Ti_5O_{12}$-$LiCoO_2$. The operation of this component consists of boosting the low voltage of the PV cell to a satisfactory level for charging the LIB, achieving an overall efficiency of 9.36% and an average storage efficiency of 77.2% at 0.5C discharge rate for the PSC-LIB system. The DSSC-LIB coupling achieved an overall efficiency of 5.62% and storage efficiency of 81.2% due to a voltage, at the output of the DSSC, that was too low to fully charge the battery. The following overview of the two systems shows the equipment involved and the internal structure of the two different PV modules used.

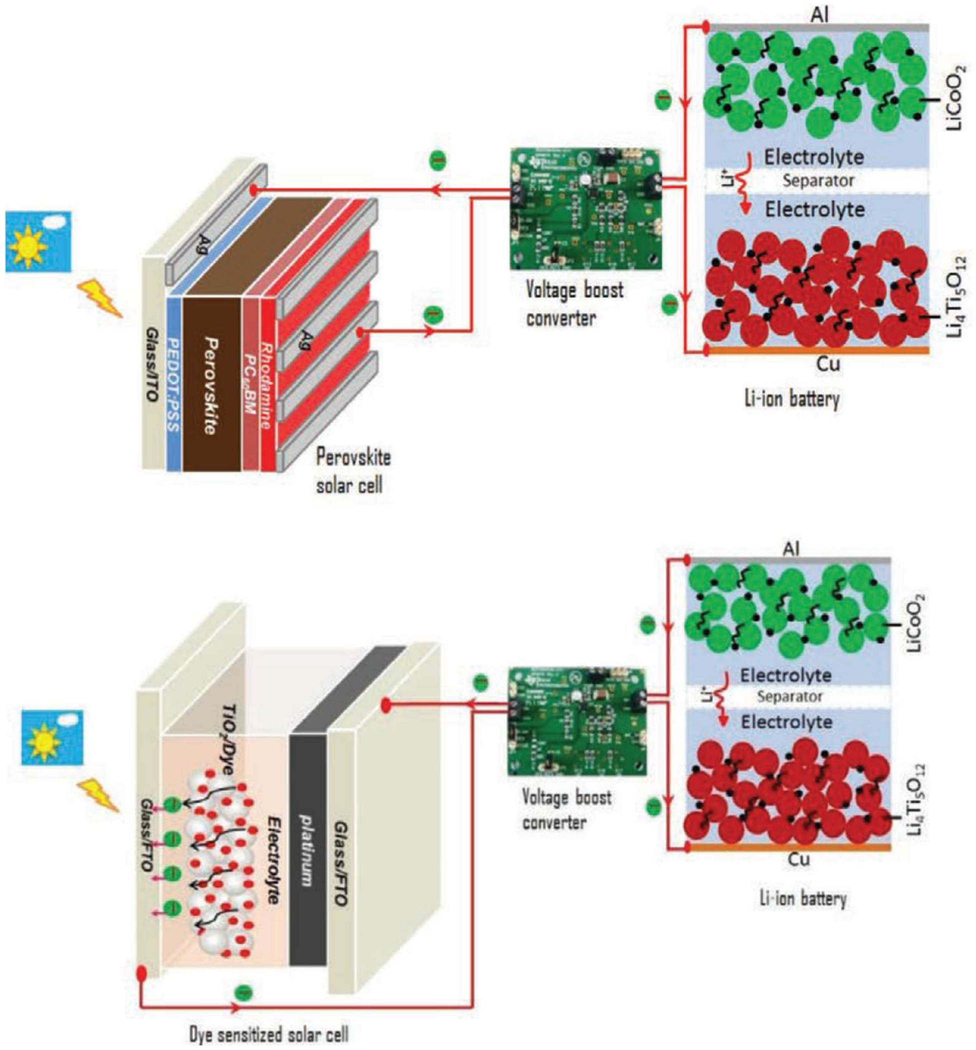

Figure 11 (top) Scheme of the solar charging device based on a PSC cell, PSC-LIB system; (bottom) Scheme of the solar charging device based on a DSSC cell, DSSC-LIB system. Adapted and reprinted with permission from [19].

6.1.4 Khataee et al.: DSSC and organic-inorganic redox flow battery (2019)

Khataee *et al.* integrated a photo-electrochemical cell with a redox flow battery into a solar redox flow cell (SRFC) [20]. RFBs are a source of multiple challenges related to the use of metal-based redox species. This involves high costs, use of rare elements, low solubility and environmental risks related to their toxicity (*e.g.*, vanadium and chromium). To address these issues, research has focused on organic redox couples so that an environmentally friendly SRFC can be developed. Anthraquinone-2,7-disulfonate disodium (AQDS) was chosen as an organic redox active material. A tandem DSSC device was chosen to produce 1.6 V, sufficient to achieve 100% charge, for testing the SRFC. The system analysed in the charge and discharge tests showed very stable cycles with a coulombic efficiency of over 99% with a power density of 0.15 W cm^{-2}.

6.2 Integrated charging

6.2.1 Guo et al.: DSSC and Li-ion battery (2012)

Guo *et al.* integrated the technology of the DSSC with the LIB one through double-sided TiO_2 nanotubes (NTs) grown on the same substrate [21]. Compared to other integrated solar energy/storage systems, the NTs-based structure of TiO_2 on both sides allowed to obtain a larger electrode area for DSSC and LIB units. This led to an improvement in the electron transport properties of the DSSC and simplified its preparation, making it more economical and controllable. The core of the cell consisted of a Ti foil covered with TiO_2 NTs on both sides. The upper part was the DSSC anode and the lower one was the LIB anode, as shown in Figure 12.

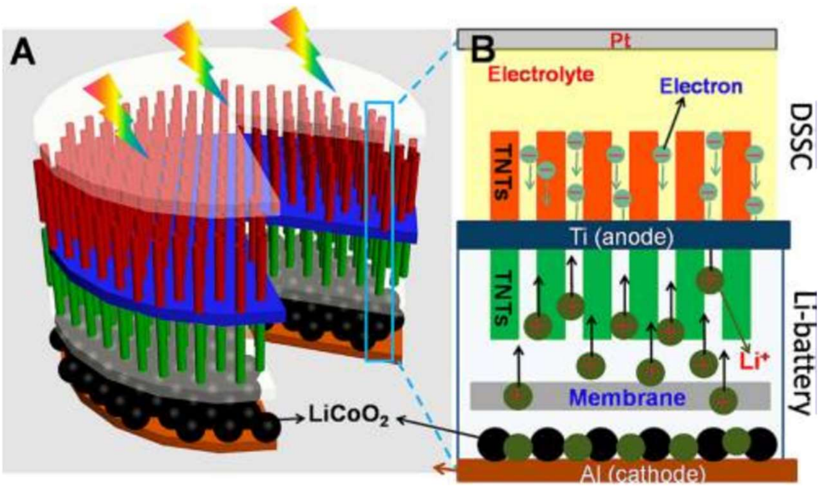

Figure 12 Design and general scheme of operation of an integrated charging system based on double-sided TiO_2 NTs. Adapted and reprinted with permission from [21].

To absorb the full spectrum of the wavelength of solar radiation, the two parts of the DSSC were sensitised by different dyes (N-719 for the upper part and N-749 for the lower part). As a first result, the total V_{OC} value of the DSSC tandem was 1.36 V, very close to the sum of the individual V_{OC} of the two cells. This technique not only allows to collect a wider light spectrum, but also can improve the V_{OC} without increasing the active area. As a final result, the conversion efficiency (η) of the entire cell was ~0.82%, with an efficiency for energy storage equal to 41%.

6.2.2 Chakrapani et al.: PV-LIB on single Si substrate (2012)

Chakrapani *et al.* studied several problems related to the performance of an integrated PV-LIB built on a single Si substrate with a shared negative electrode [22]. The configuration combined a nanowire-based LIB anode with a nanowire-based PV device. With this configuration, the user could benefit from the great knowledge in planar PV technology, while maintaining a high nanometric surface area at the battery anode. Figure 13 shows the different device components and the structure of the multi-junction PV cell. It was decided to use a multi-junction cell as it allowed to increase the voltage without using a DC-to-DC energy converter, which would have brought further losses.

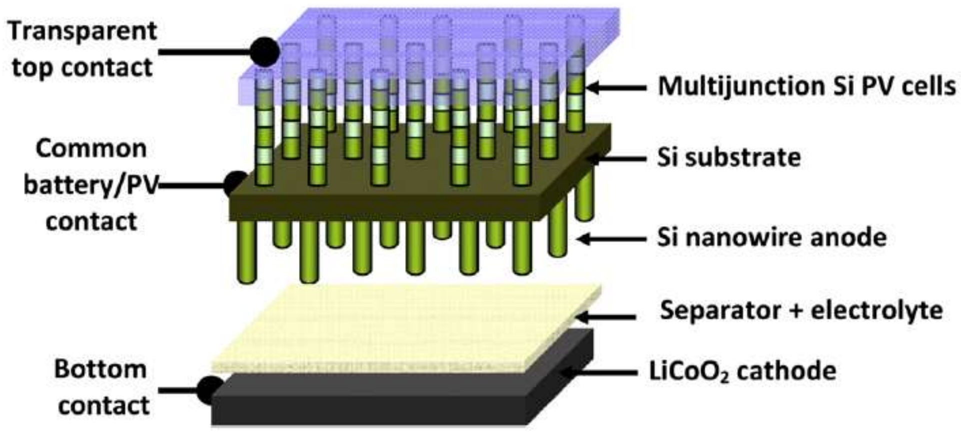

Figure 13 System illustration with Si substrate as common anode. Adapted and reprinted with permission from [22].

Li^+ can spread within many metals and semiconductors because of its small atomic radius. TiN was found as the best material to be use as barrier against Li^+ transmission. This membrane prevents the diffusion of Li^+ into the PV substrate, protecting it from physical damage and preventing the loss of Li^+ from the battery by deteriorating it. The TiN membrane achieved a blockage efficiency of 78% in laboratory.

6.2.3 Xu et al.: LIB and perovskite solar cell (2015)

Xu *et al.* demonstrated for the first time the use of PSC modules for direct photo-charging of LIBs [23]. The PV system consisted of four single $CH_3NH_3PbI_3$ PSCs connected in series with a total conversion efficiency of 12.65% (15.67% for the single cell). The complete system, shown in Figure 14, demonstrated a high specific capacity and reactivity. The overall efficiency of the system, including photoelectric conversion and storage, was 7.80% with excellent stability during repetition of charge and discharge cycles.

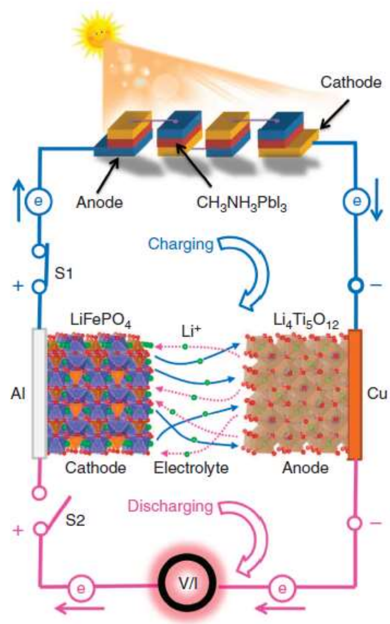

Figure 14 Schematic diagram of PSC–LIB system in study. Adapted and reprinted with permission from [23].

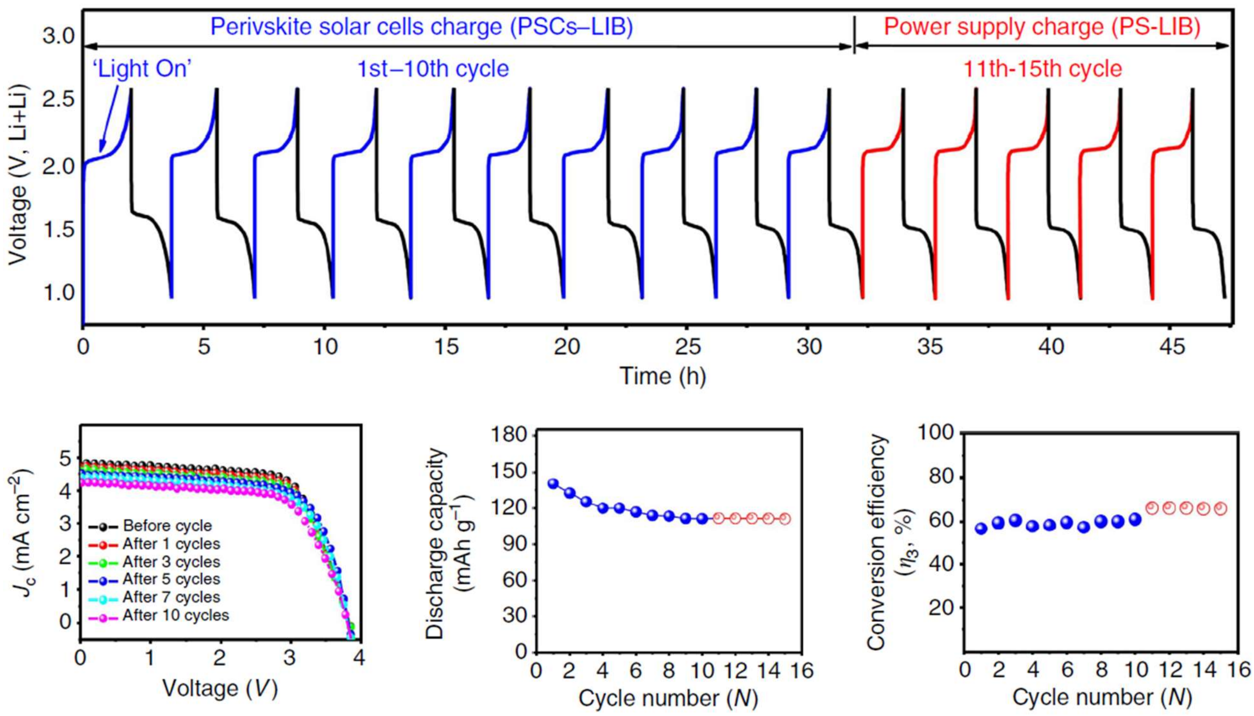

Figure 15 Comparison between solar charging with perovskite solar cell and power supply charge. (top) The blue lines represent the cycles loaded with PSC and galvanically discharged at 0.5C. The red lines represent the comparison cycles loaded and galvanically discharged at 0.5C using the power supply;(bottom left) J-V curves after different numbers of cycles; (bottom centre) discharge capacity as a function of the number of cycles; (bottom right) energy storage efficiency such as function of the cycle number. In the last two graphs, the blue values indicate measurements made with solar charging, the red values with an external source. Adapted and reprinted with permission from [23].

6.2.4 Nagai et al.: PV – LIB fabricated by molecular precursor method (2016)

Nagai *et al.* studied translucent thin-film LIBs manufactured using the molecular precursor method (MPM) [24]. Titania for the anode and $LiCoO_2$ for the cathode were deposited on a fluorine-doped tin oxide pre-coated glass substrate. TiO_2 is considered a good substitute for graphite anodes for LIB, due to the discharge potential difference of 1.50-1.75 V against Li^+/Li, Li ions are also a cause of decomposition for organic electrolytes. The layered structure of $LiCoO_2$ is chemically and electrochemically stable and it is characterised by a high capacity of about 140 mAh and a discharge potential difference of 3.8 V against Li^+/Li. Based on these plateau values, the potential difference between TiO_2 and $LiCoO_2$ can theoretically be estimated in 2.0-2.3 V. X-ray diffraction was used to study the transmittance of the battery and reported an average value of 50% (Figure 16), detected at 700 nm (the lowest value in the visible region) and the device appeared translucent.

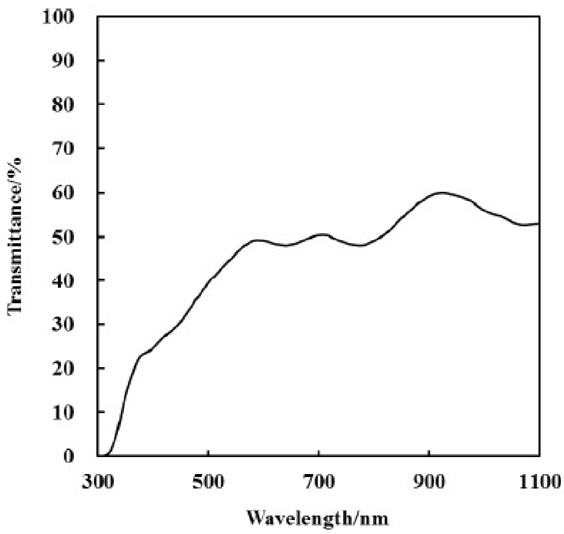

Figure 16 Analysis of the optical transmittance spectrum of the LIB realised with the molecular precursor method. The graph represents the transmittance as a function of the incident wavelength. In the visible range 400-700 nm, it shows a transmittance value of approximately 50%, resulting translucent to the viewer. Adapted and reprinted with permission from [24].

For the study, a charge and discharge cycle repeated 30 times in a time interval of 60 s at room temperature was considered. The analysis was divided in the three cases shown in Figure 17: (a) providing the constant current of 0.2 mA using a DC charger, (b) using 1 sun irradiation, (c) repeating experiment "b" providing 1.0 mA current before the first light irradiation.

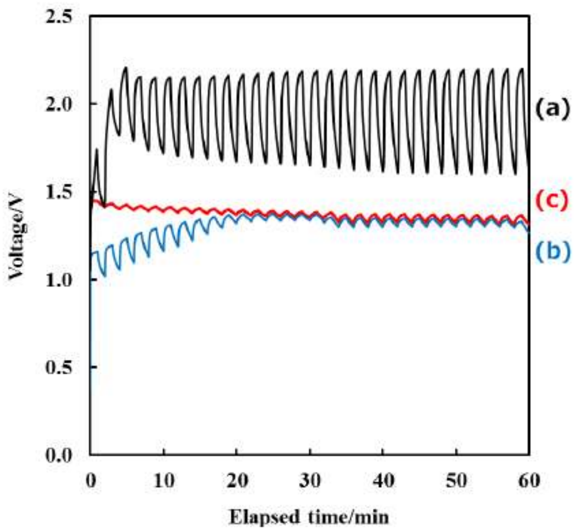

Figure 17 Different cyclic charge/discharge tests with the following boundary conditions: (a) constant charging current of 0.2 mA, externally provided by a DC charger; (b) solar charging at 1 sun irradiation; (c) solar charging at 1 sun irradiation, providing a pre-current of 1.0 mA. Adapted and reprinted with permission from [24].

The effectiveness of PV charging is visible from the fact that the self-discharge voltage is almost identical to the charge voltage under light irradiation.

6.2.5 Agbo et al.: Thin-film silicon triple-junction solar cell and batteries (2016)

Agbo *et al.* studied triple junction solar cells based on amorphous and microcrystalline silicon used to charge LIB in a monolithic integrated solar cell to battery device [25]. The multijunction cells under examination are based on amorphous Si (a-Si:H) and microcrystalline Si (μc-Si:H). The voltage supplied varies from 1.3 V in the tandem device to about 3 V in quadruple multijunction cells. The output voltage of the solar cells and their flexibility make them particularly suitable for integration with batteries and accumulators. Starting from a common Asahi VU substrate (Figure 18), two different prototypes were developed. The first, referred as Triple A, has one a-Si:H upper and two μc-Si:H lower. The second, referred as Triple B, has the two upper cells composed of a-Si:H and a μc-Si:H below.

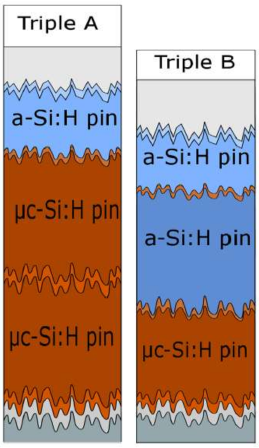

Figure 18 Schematic structure of two different triple-junction solar cell prototypes. Adapted and reprinted with permission from [25].

The single cell battery used consisted of a lithium iron phosphate (LFP) cathode and a lithium titanate (LTO) anode. The separator membrane was made of a glass fibre soaked in the electrolyte. The properties of the battery can be summarised as follows: 1.93 V voltage, potential difference at the cathode 3.43 V *vs.* Li^+/Li, at the anode 1.5 V *vs.* Li^+/Li and capacity of about 0.15 mAh. Analysing the current density-voltage plot, shown in Figure 19, it emerged that Triple A had too high values of short-circuit current density for direct connection with the LIB, while Triple B had too high current density, but acceptable voltage. They decided to reduce the current by decreasing the active area of the solar cell and used neutral density filters to attenuate the lighting. The maximum conversion and storage efficiency of the integrated device was equal to the efficiency of the solar cells (8.8%), demonstrating the absence of losses due to energy transfer to the battery.

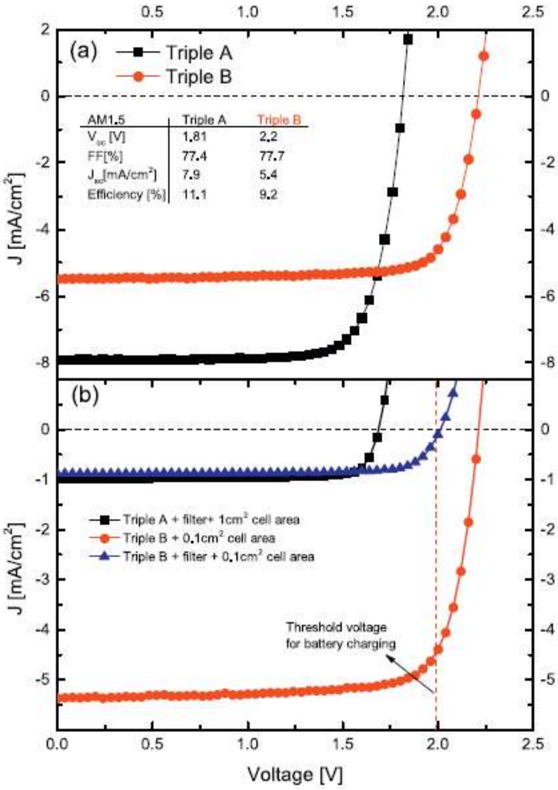

Figure 19 Data on the two cell types and their integration with neutral density filters and area cropping. Adapted and reprinted with permission from [25].

6.2.6 Ogaryov et al.: Metal nanoparticles and quantum dots as photosensitizers (2016)

Ogaryov *et al.* analysed the use of photosensitization for solar cells with metal nanoparticles and quantum dots [26]. The effect of metal nanoparticles varied with the nature and size of the grain used, thus affecting electron transitions in semiconductors by varying the bandgap. This can significantly improve the efficiency of PV cells. With the contact between the metal nanoparticles and the semiconductor, the electrons generated by the PV reactions were distributed between the TiO_2 and the Au nanoparticles. The excited electrons passed from TiO_2 to Au, shifting the gold Fermi level towards negative potentials and bringing it closer to the conductivity band of the semiconductor. The shift in the Fermi level indicated better charge separation and therefore better composite reactivity.

6.2.7 Xia et al.: Integrated charging PSC for smart windows (2016)

Xia *et al.* investigated solid-state electrochromic batteries with a bilayer cathode consisting of NiO nanoflake arrays and an anode based on WO_3 nanowire arrays made from reduced graphene (rGO) [27]. This technology can function as an accumulator by changing colour according to its state of charge (from transparent to blue). The study of this intelligent window was conducted by assuming a system consisting by a PV window frame placed around the electrochromic glass. Due to the optimisation of the electrodes by using arrays consisting of WO_3 nanowires for the anode and multilayer NiO nanowires for the cathode, remarkable efficiencies were achieved. The storage system demonstrated a significant optical modulation of 43% when subjected to a visible wavelength of 750 nm and 62% at a near-IR wavelength of 2000 nm. Figure 20 shows the dependence of the charge/discharge state with the transmittance of the glass.

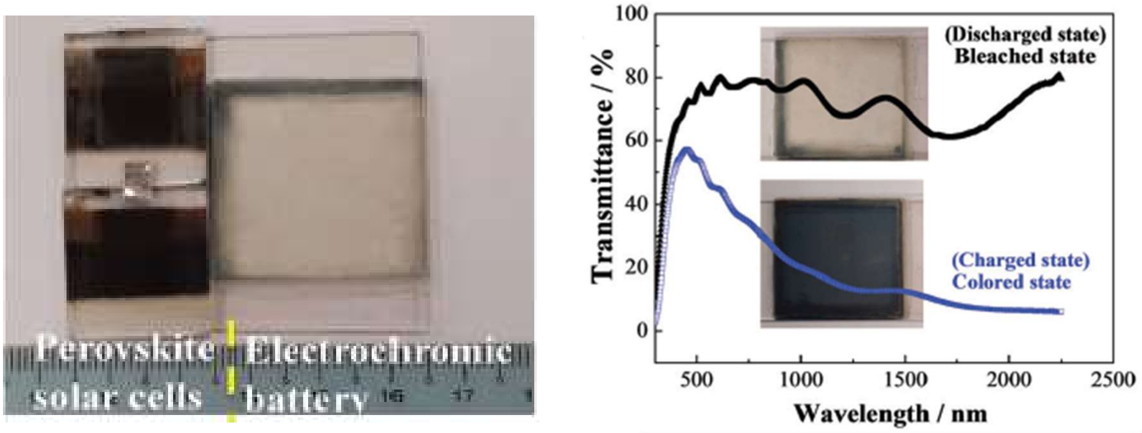

Figure 20 (left) Structural diagram of the device consisting of PSC and solid-state electrochromic batteries; (right) variation of colour and transmittance of the battery as the incident light radiation changes and the state of charge. Adapted and reprinted with permission from [27].

In addition to the result obtained in the attenuation of the IR wavelength, which is very relevant when regulating the flow of heat/light through the windows, the batteries showed great efficiency during charge and discharge cycles, with an average value of 97.2%.

6.2.8 Vega-Garita et al.: Suitable battery technology for integrated module (2019)

Vega-Garita *et al.* tried to find the best battery technology available on the market in the 2019 [28]. Existing technologies differ on many features, so the analysis was carried out by investigating the main issues related to integrated systems. Table 2 shows the different criteria and technologies considered.

Table 2 Comparison between different types of batteries. Adapted and reprinted with permission from [28].

		LA	NiCd	NiMH	Li-ion	NaS	VRB
Energy density	Wh/kg	25-50	50-60	60-120	75-200	150-240	10-30
Power density	W/kg	75-300	>200	250-1000	500-2000	150-230	80-150
Cycle life	100% DOD	200-1k	>1.5k	180-2k	1k-10k	2.5k-4k	>12k
Capital cost	$/kWh	100-300	300-600	900-3500	300-2500	300-500	150-1000
Round-trip efficiency	-	75-85	70-75	65-80	85-97	75-90	75-90
Self discharge	-	Low	High	High	Medium	-	Negligible

Given the advantages associated with LIBs, they can be considered as the best batteries currently on the market for the development of integrated PV devices. The main types of LIBs currently existing at commercial level are based on $LiFePO_4$ and $LiCoO_2$. Through cyclic stress tests conducted in laboratory, even at high temperatures to recreate the real conditions of use, $LiFePO_4$ showed lower capacity fading rates. This made it the best commercially available technology for this purpose.

6.2.9 Yuan et al.: Integrated $NiCo_2O_4$ battery-supercapacitor hybrid device (2019)

Yuan *et al.* designed a faradic electrode made with three-dimensional hierarchical $NiCo_2O_4$ arrays, with capacitive electrode based on active carbon [29]. Battery-supercapacitor hybrids (BSH) make it possible to combine the advantages of batteries with those of supercapacitors. The hybrid technology combined with the use of the 3D hierarchical $NiCo_2O_4$ structure for the electrodes made it possible to achieve the storage characteristics shown in Table 3, while the volumetric energy density and power density are provided in Figure 21.

Table 3 Experimental performance of BSH accumulators. Adapted and reprinted with permission from [29].

Cell voltage	1.6	V
Cycle performance After 15k cycles	100	%
Specific capacity	130	mAh g^{-1}
Energy density	16.6	Wh kg^{-1}
Power density	7,285	W kg^{-1}
self-discharge	Low	-

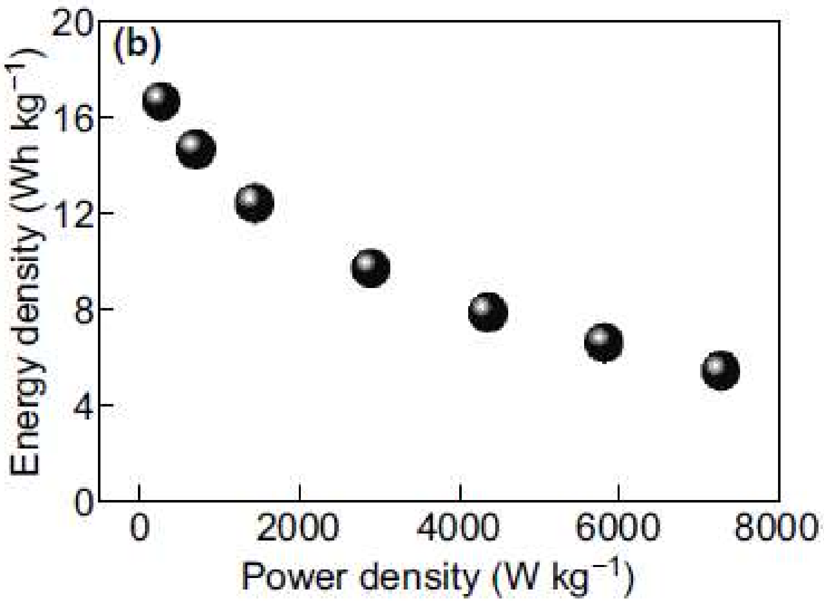

Figure 21 Volumetric energy density and power density for BSH. Adapted and reprinted with permission from [29].

The BSH was powered with two a-Si:H PV cells, the performances of which are shown in Figure 22, to achieve the desired voltage and the system was tested at an irradiance of AM1.5G. Analysing the charge/discharge profiles, the shape of the curves is repeated in all five cycles. This demonstrates the stability and reliability of the technology in question, reporting excellent resistance to stress cycles due to charging and discharging the device.

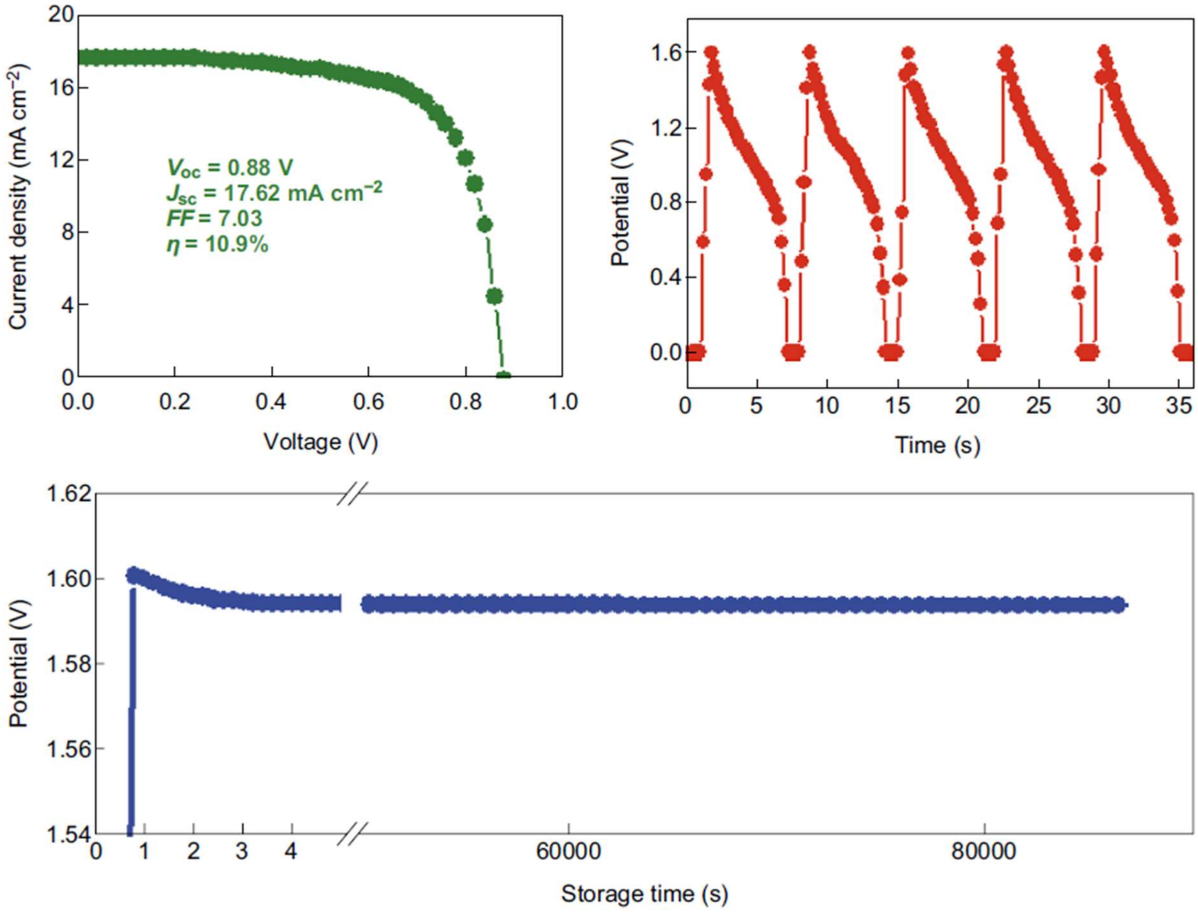

Figure 22 Characteristic diagrams of the system under consideration: (top left) development of current density as the voltage changes; (top right) change in voltage during 5 charge and discharge cycles; (bottom) change in open circuit voltage as the number of cycles increases. Adapted and reprinted with permission from [29].

In terms of overall performance, the integrated system demonstrated an efficiency of 8.1% with a storage efficiency of 74.24%.

6.2.10 Weng et al.: PSC- aqueous Li/Na-ion battery system (2020)

Weng *et al.* developed a series of aqueous Li/Na-ion batteries using carbon-coated $LiTi_2(PO_4)_3$ (named ALIB) and $NaTi_2(PO_4)_3$ (called ANIB) [30]. The electrochemical performance of these batteries is shown in Figure 23, the main feature being the innovative carbon-coated electrodes, derived from low-cost asphalt, which have shown high performance.

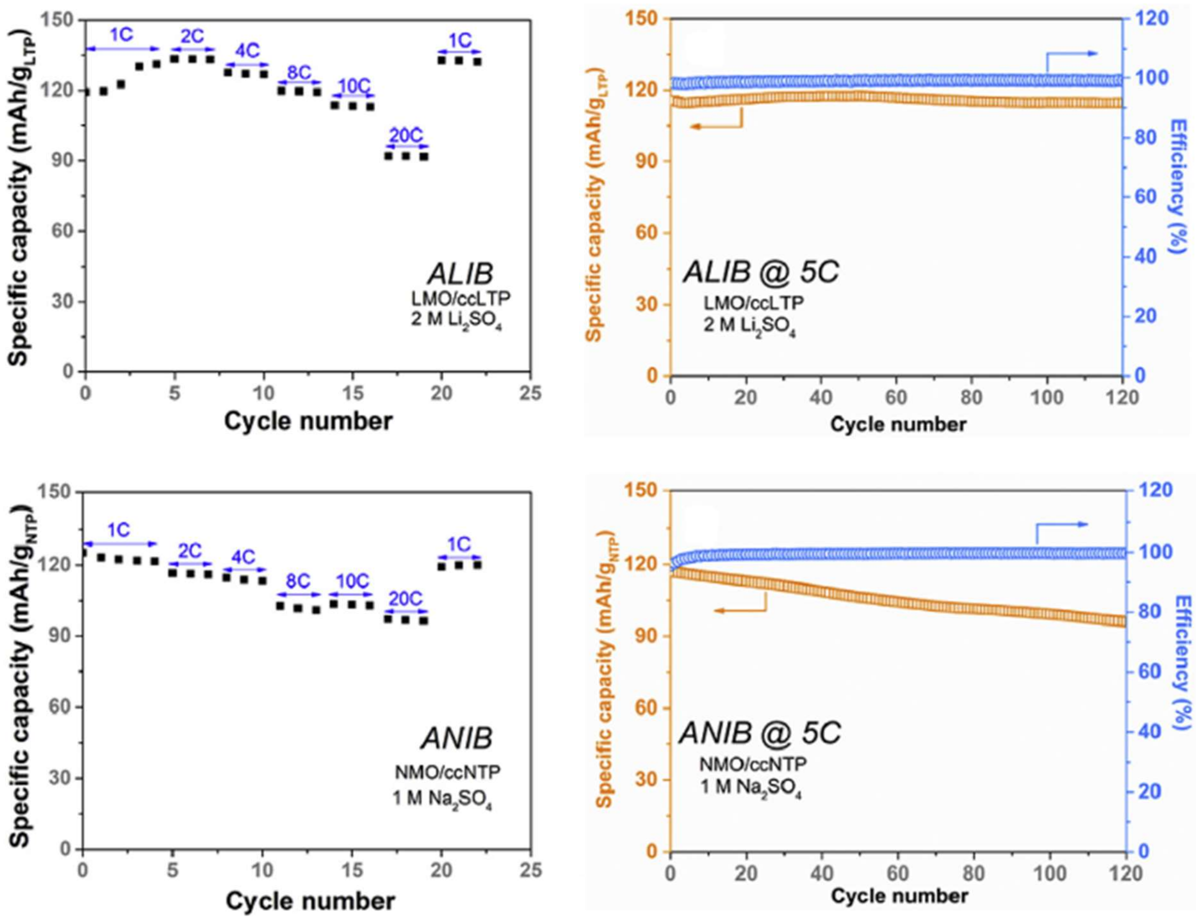

Figure 23 Operating characteristics of ALIB and ANIB systems. (left) Trend of specific capacity in relation to discharge rate; (right) cyclic stress test at a predefined discharge rate, specific capacity and efficiency are shown for each cycle. Adapted and reprinted with permission from [30].

The combination of these batteries with high-efficiency PSC showed excellent durability in cyclic tests and very high overall efficiency of 9.3% at a discharge rate of 2C.

6.2.11 Di et al.: Photo-charging integrated device with DSSC and LIB (2020)

Di *et al.* investigated an integrated three-electrode DSSC-LIB system based on $LiFePO_4$ as intermediate electrode material [31]. In this type of device, the central electrode played a key role as it is common between the two systems. The electrode must be able to function as a reversible redox agent to regenerate the dye in the DSSC and must act as a cathode in the battery without degrading the organic electrolyte. The conversion of $LiFePO_4$ into $FePO_4$ thus enabled the device to function. To properly integrate the two systems, the output voltage from the DSSC had to be increased, since the theoretical charge voltage of LIBs can generally be determined by comparing the difference of the Li^+/Li redox potential and the quasi-fermi level of electrons in the TiO_2 photoelectrode. For this reason, four DSSCs were used in series, as shown in Figure 24.

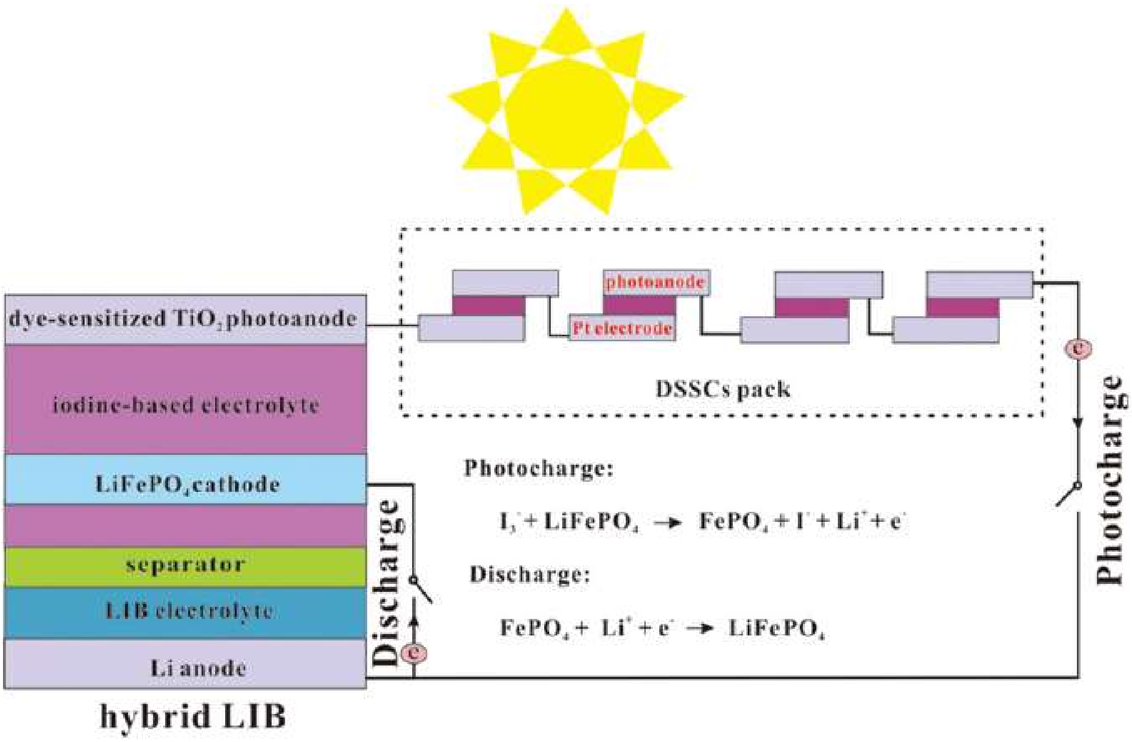

Figure 24 Constructional diagram of the monolithic device, the principal equations of solar charging and discharging are also shown. Adapted and reprinted with permission from [31].

By increasing the voltage of the PV system, it was possible to charge the hybrid LIB to a voltage of 2.85 V, which is lower than the classic operating values, but sufficient for the integration. However, the hybrid LIB demonstrated poor cyclic resistance, maintaining 73.6% of initial capacity after only 7 cycles as shown in the Figure 25.

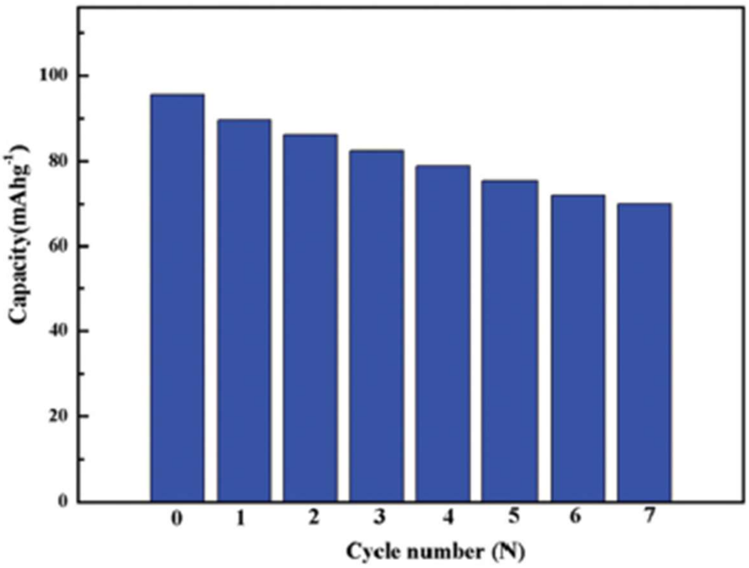

Figure 25 Variation in maximum capacity due to work cycles. Adapted and reprinted with permission from [31].

7 Photovoltaics and Supercapacitors

As in the previous chapter, here follows an analysis of the publications of the last 10 years concerning the use of SCs in association with PV cells. The analysis focused on the two possible types of integration already analysed above.

The division adopted results in two distinct groups of devices; the devices thus grouped also present a considerable disparity in terms of the scale of the systems under study. For discrete-charge devices, the focus is often on domestic or industrial applications. In the case of integrated devices, the scale of the investigated installations is typically smaller and mainly concerns prototypes of wearable devices or environmental sensors.

7.1 Discrete charging

7.1.1 Thounthong et al.: Fuel cell/solar cell/supercapacitor hybrid power source (2011)

Thounthong *et al.* investigated a new control algorithm for hybrid energy system based on renewable energy sources such as polymer electrolyte membrane fuel cell (PEMFC) and PV system [32]. The algorithm was implemented on a small-scale test system consisting of a PEMFC (1200 W,46 A), a PV array (800 W, 31 A) and a SC module (100 F, 32 V). These three elements were selected for their different dynamics of intervention, thus ensuring the greatest possible stability of the system, shown in Figure 26.

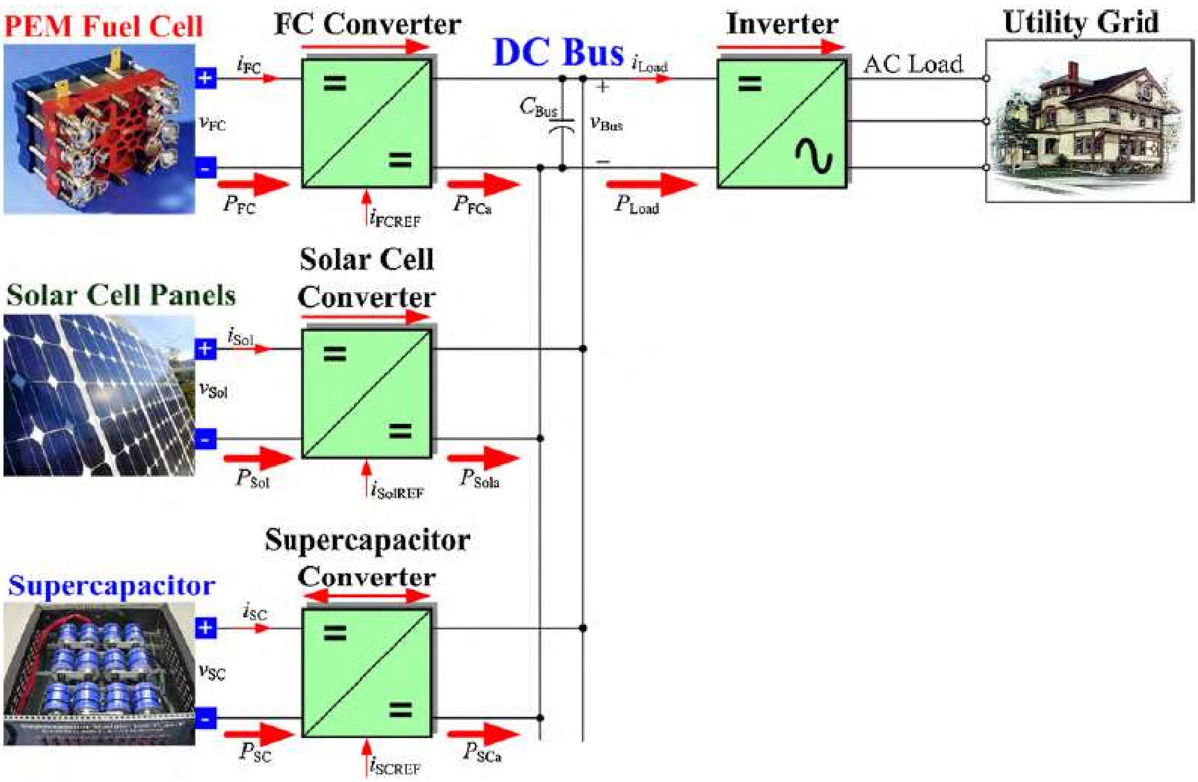

Figure 26 Logical diagram of the system and the necessary equipment. Adapted and reprinted with permission from [32].

In the graph shown in Figure 27, it is possible to see that the intervention time of the supercapacitors is almost zero, which makes it possible to instantly cover power gaps due to the start-up times of the other two systems. During the peaks and troughs of the generators, the SC provides the necessary power. Increasing the capacity of the accumulator improves energy quality and efficiency. Priority is given to the PV system, for its dependence on climatic conditions and its intermittency, the PEMFC is essential in order to guarantee coverage at other periods.

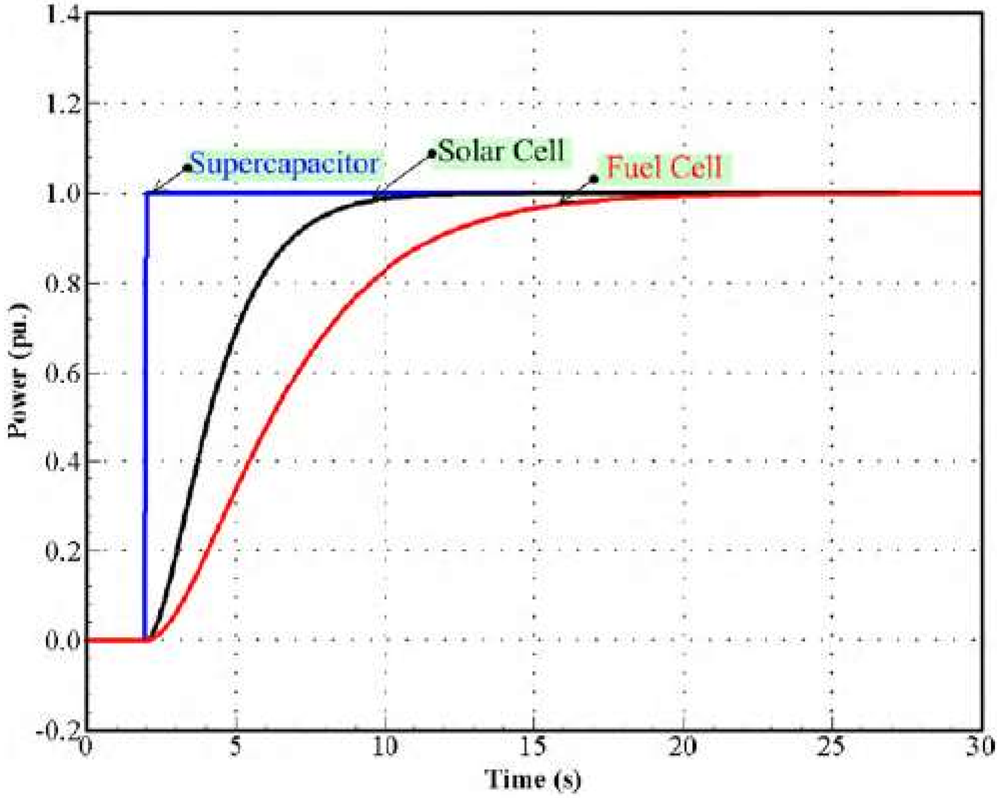

Figure 27 Speed of intervention of the three energy sources. Adapted and reprinted with permission from [32].

The intersection of the three operating curves, during load tracking, gives rise to the following graph (Figure 28).

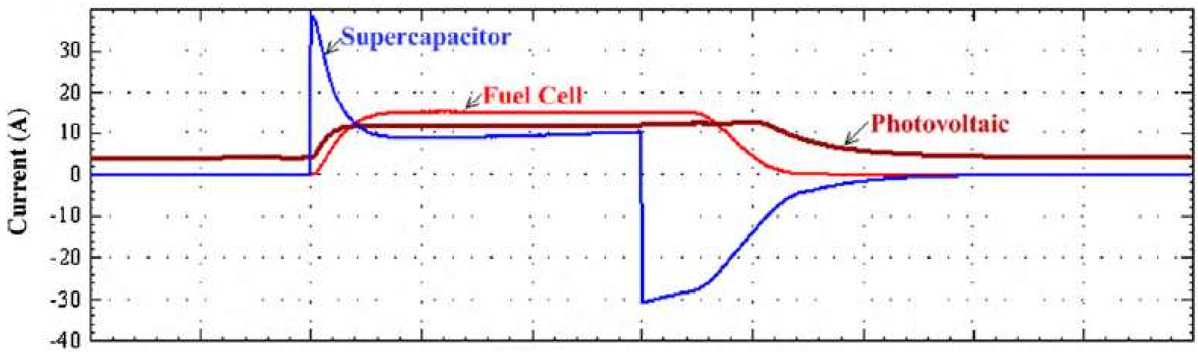

Figure 28 Possible distribution of the current supplied by the different components in the event of a sudden intervention to compensate for a load peak. Adapted and reprinted with permission from [32].

7.1.2 Meekhun et al.: Buck converter and MPPT algorithms (2011)

Meekhun *et al.* analysed the operation of buck converters and compared two different operating algorithms for MPPT hill-climbing and fractional-V_{OC} [33]. The two different algorithms considered in this paper are hill-climbing (characterised by high accuracy, but requiring two sensors: voltage and current) and fractional-V_{OC} (easier to implements as it relies only on voltage at the expense of accuracy). Testing these codes produced the values shown in Table 4. To get a valid reading of V_{OC}, for the fractional-V_{OC} algorithm the microprocessor opened the circuit to measure the no-load voltage every 10 s.

Table 4 Comparison of the efficiency of the two algorithms under analysis with varying input power. Adapted and reprinted with permission from [33].

	FRACTIONAL-V_{OC}			**HILL-CLIMBING**		
	% η_{MPPT}	% η_{CONV}	% η_{TOTAL}	% η_{MPPT}	% η_{CONV}	% η_{TOTAL}
P_{IN}=1.32 W	92.80	65.75	62.83	95.23	67.55	64.33
P_{IN}=1.76 W	93.64	74.66	69.93	94.14	75.14	70.74
P_{IN}=4.7 W	97.02	74.93	72.70	96.72	74.46	72.03
P_{IN}=5.27 W	97.12	75.16	72.99	96.85	73.77	71.46

7.1.3 Yuan et al.: Hybrid storage system (2011)

Yuan *et al.* devised a control strategy for integrating PV systems with SC and batteries, extending their service life [34]. In PV systems, mainly stand-alone systems, there is need for storage system so that the energy produced can be stored and used continuously. Using MATLAB and Simulink, a hybrid storage system was implemented, combining the advantages of the two storage elements mentioned above. The advantages of a hybrid system are based on the four main problems that reduce the life of conventional batteries:

- The decrease in the state of charge below a certain level;
- The excessive power supply to the battery;
- Very high-power demand on the battery;
- Small charge/discharge currents.

The simulations showed two positive results from the addition of a SC, not only the reduction in battery size, but also its life is prolonged.

7.1.4 Thounthong et al.: Standalone PV/PEMFC/SC (2013)

Thounthong *et al.* worked out the implementation of the control system based on the special features of the PV/PEMFC/SC hybrid plant components for stand-alone applications [35]. The prototype under consideration consisted of a PEMFC system (1200 W), a PV system (800 W) and an SC module (100 F). The PV system is the main component, as it is independent of the other components. The PEMFC cell plays the role of a back-up source to compensate for reductions in production from the solar source. SCs ensure continuity and stability during transients. Using the intelligent fuzzy logic control for DC connection stabilization based on the flatness property, it was possible to find a simple construction solution to the problems arising from the stabilisation of non-linear electrical power systems.

7.1.5 Benyahia et al.: Characterization and control of SC bank (2013)

Benyahia *et al.* devoted their work mainly to the characterisation of SCs using the RC model, the simplest circuit to test a capacitor [36]. The aim of this paper was to characterise a hybrid PV/SC system. The analysed equivalent circuit, shown in Figure 29, has the following fictitious components: the non-linear capacitance C(vsc), the equivalent series resistance (ESR) and the nominal capacitance Ccd.

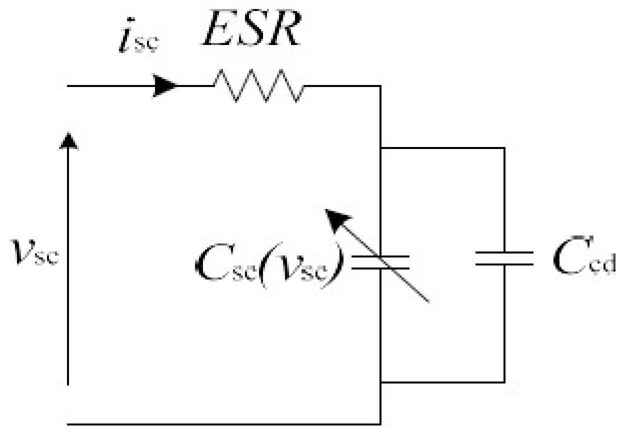

Figure 29 Simplified diagram of an RC circuit, used to study SC behaviour. Adapted and reprinted with permission from [36].

Once implemented the circuit was subjected to a succession of cycles, each consisting of a constant current charge, from (Vd) to (Vc). Each cycle was separated by a rest period (td-tc = 5 s) during which the no-load voltage (Vo) was measured. The average nominal capacitance (Ccd) and ESR can thus be measured. The parameters are shown in Figure 30.

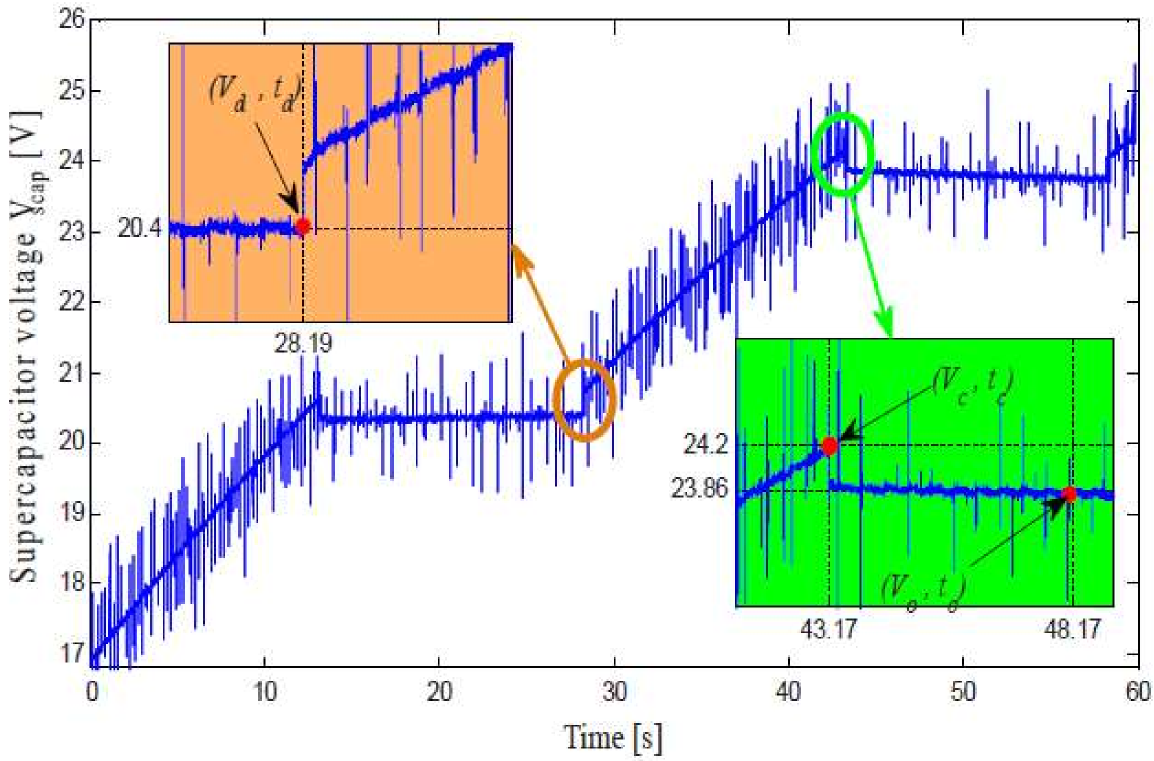

Figure 30 Variations reported by the voltage at the ends of the SC during the test to investigate its characteristics. Adapted and reprinted with permission from [36].

Thanks to the developed model of the SC, the dynamic characteristics of the SC can be reproduced. Its high-power density and resistance to charge/discharge cycles make the SC a valuable auxiliary source in PV systems.

7.1.6 Guerrero et al.: PV/SC connected to the grid (2013)

Guerrero *et al.* implemented a bidirectional DC-DC converter to mitigate power fluctuations inserted between the PV cells and the inverter [37]. The benefits of using an energy storage system to dampen fluctuations and to keep the power injected into the grid constant over time allows steady and dynamic performance to be maintained.

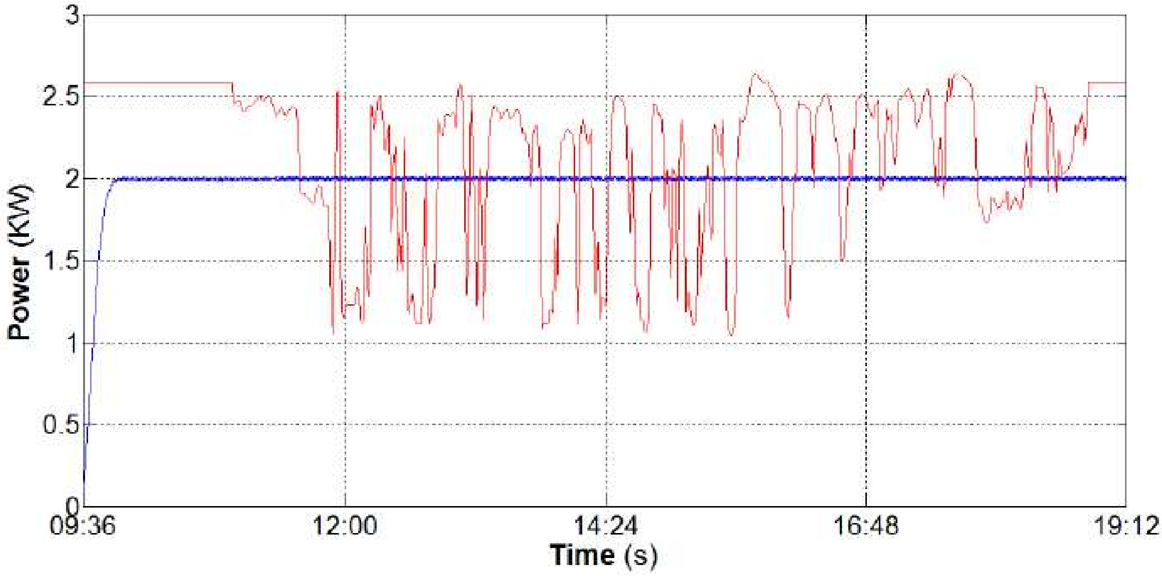

Figure 31 Power diagram for a grid-connected PV-SC system. The red line represents the power instantaneously produced by the PV system; the blue line represents the power injected into the grid. The peaks are flattened due to the presence of the SCs. Adapted and reprinted with permission from [37].

The sudden change in the SC operation, from charging to discharging, made it possible to fully exploit its characteristics and its great resistance to cycling. Figure 31 shows the curve representing the power output from the panels (in red) and the power input to the transformer (in blue), downstream of PV/SC system.

7.1.7 Worku et al.: Mitigation of power fluctuations for grid connected PV plant (2016)

Worku *et al.* implemented a system to mitigate oscillations due to radiation and temperature variations by integrating a SC and specially developed hardware [38]. The operation of the controllers was examined through the hardware in the loop setup using the real time digital simulator (RTDS). The implemented scheme is reported in Figure 32.

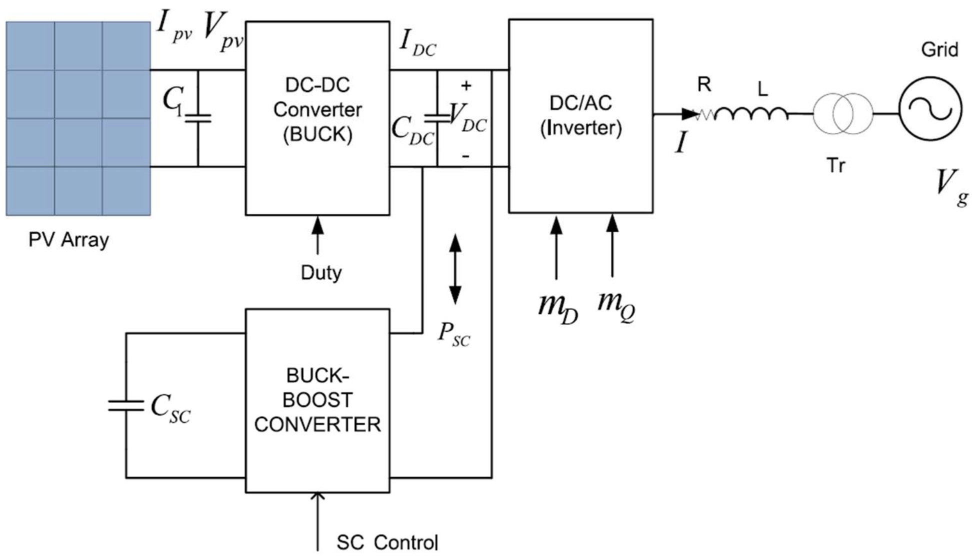

Figure 32 System diagram, the following components can be observed: PV array for electricity production, the two converters for regulating the PV production and managing the SCs, DC-AC converter for correctly feeding the power into the domestic grid or the national grid. Adapted and reprinted with permission from [38].

Analysing the response to variations in PV production, it can be noted that the SC provides the necessary continuity to avoid fluctuations in power output from the system. In Figure 33 (top), an increase in PV production leads to a decrease in the discharge power of the SC, while Figure 33 (bottom) shows how the SC is able to compensate for a reduction in the energy produced by the primary system.

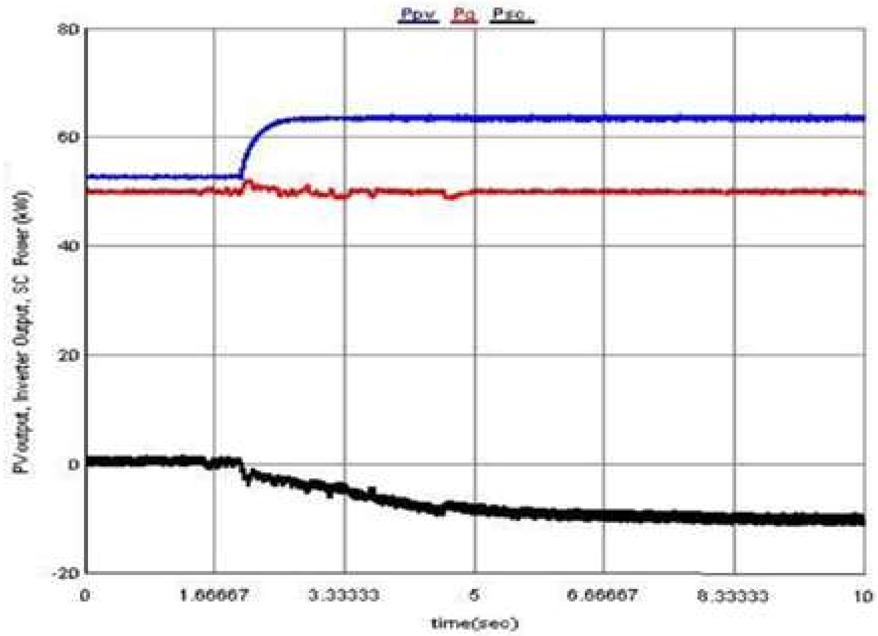

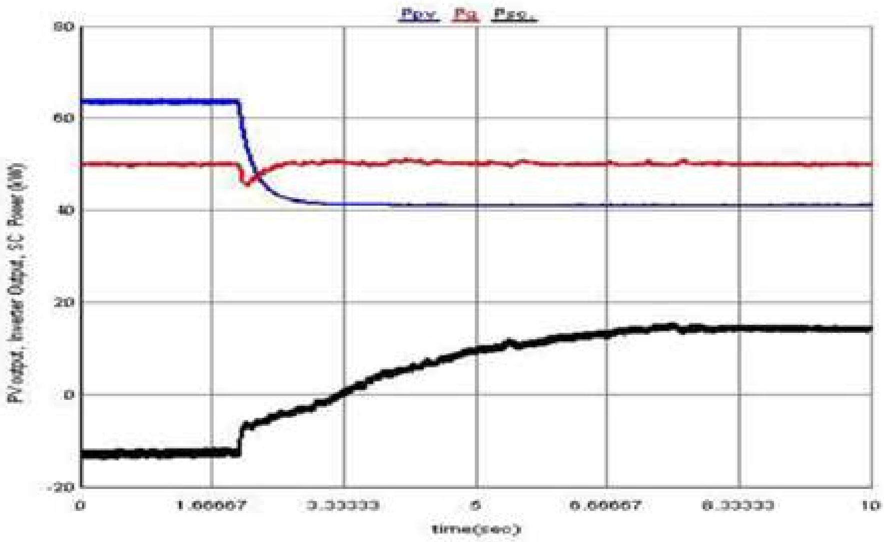

Figure 33 (top) System response to an increase in PV production; (bottom) System response to a decrease of production. Adapted and reprinted with permission from [38].

The proposed scheme substantially reduced the oscillations characteristic of PV sources, providing greater stability and reliability.

7.1.8 Sikkabut et al.: PV/PEMFC/SC/LIB hybrid power plant (2016)

Sikkabut *et al.* worked on a system for electrical generation based on hybrid management of two different generation modules (PV array and PEMFC) and two storage systems (LIB and SC bank) [39]. To validate the approach used in the control system, a pilot plant was set up and the results were compared with those obtained from the numerical calculator (dSPACE). By estimating the differential flatness of the system, a logic controller (T-S fuzzy logic) has been implemented to keep the DC bus voltage constant. The pilot plant, built on a small-scale test bench, was constructed with a PEMFC (1.2 kW, 46 A), a PV (800 W, 31 A), a SC bench (100 F, 32 V) and a LIB module (11.6 Ah, 24 V).

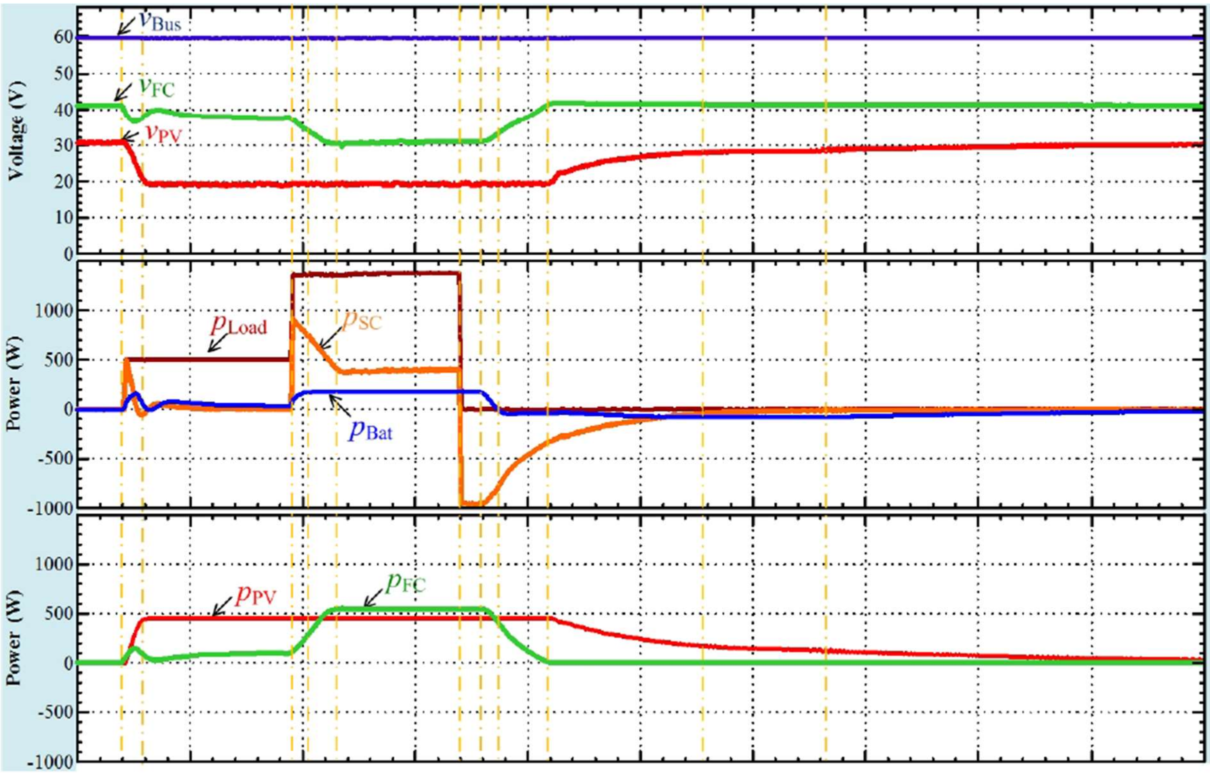

Figure 34 Pilot system response during load variation. Adapted and reprinted with permission from [39].

Figure 34 shows the response of the prototype and the respective waveforms obtained when the system is stressed by a variation of the required load. The graph above shows the DC bus voltage (with PEMFC and PV system voltage, respectively). As the required power increases, there is instantaneous intervention of the SC and subsequently of the LIB. It can be seen that the SC is able to fully cover the increase in power demand waiting for the increase of production by the PEMFC.

7.1.9 Fahmi et al.: Battery/SC hybrid PV system (2016)

Fahmi *et al.* developed a prototype PV system for large-scale use in Semenyih Malaysia with the aim of increasing battery lifetime and reducing maintenance costs [40]. The direct charging of a battery using the current produced by the PV system is not ideal because of fluctuations in the intensity of the current supplied. The inclusion of a SC makes it possible to improve the performance of the battery and extend its lifetime. In order to demonstrate the advantages of a hybrid battery, simulations were performed and the results compared with experimental data (the system is shown in Figure 35).

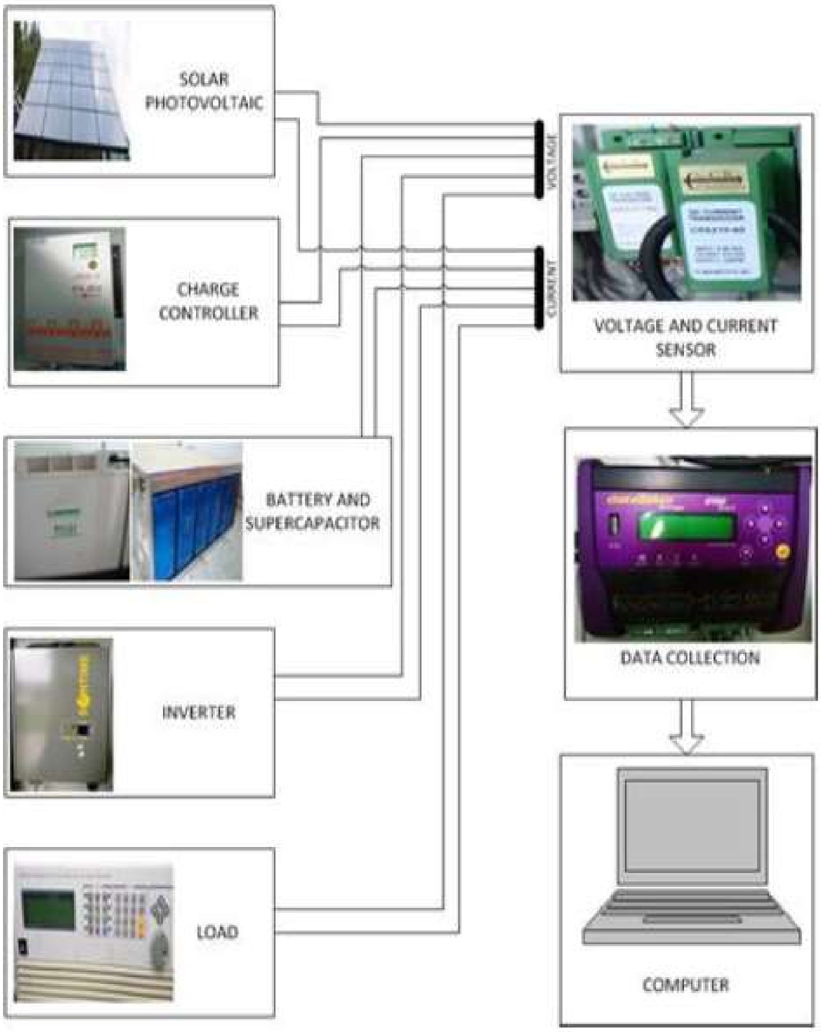

Figure 35 Hybrid system block diagram. Adapted and reprinted with permission from [40].

With this system it is possible to maintain high battery voltage and charge levels during the day, using the SCs as a filter between them and the PV panels. The graphs shown in Figure 36 compare a conventional storage system with the one under consideration in a normal daylight cycle. The SCs are also able to flatten the daily load peaks, greatly reducing the strain on the main battery pack, thereby increasing its lifetime.

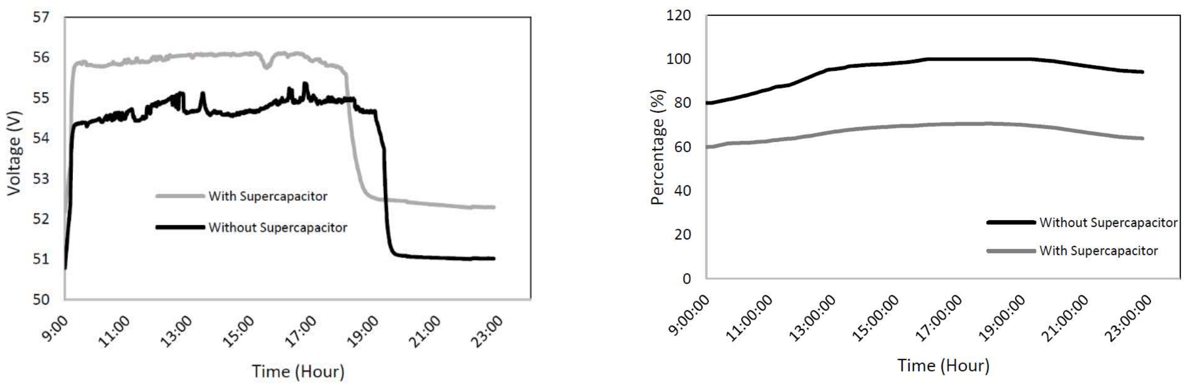

Figure 36 (left) Battery voltage with presence or absence of SC; (right) State of charge with presence or absence of SC (SOC). Adapted and reprinted with permission from [40].

It is therefore possible to summarise the results obtained in the following Table 5. The results to be highlighted concern the decrease in the average current delivered by the battery (reduced from 2.75 A to 0.23 A), the decrease in the average power delivered (reduced from 147.95 W to 12.1 W) and the peak current of the battery (reduced from 20.8 A to 16.4 A). It is also visible how the experimental results agree with the theoretical ones.

Table 5 Average and peak results for hybrid system simulations and tests. Adapted and reprinted with permission from [40].

		SIMULATION		**EXPERIMENT**	
		With supercapacitor	Without supercapacitor	With supercapacitor	Without supercapacitor
AVERAGE BATTERY VOLTAGE	V	54.75	53.52	52.59	53.08
AVERAGE BATTERY CURRENT	A	0.88	3.83	0.23	2.75
AVERAGE BATTERY POWER	W	54.67	247.08	12.10	147.95
AVERAGE SUPERCAPACITOR CURRENT	A	0.0051	-	0.29	-
PEAK BATTERY CURRENT	A	12.21	21.82	16.41	20.84
PEAK SUPERCAPACITOR CURRENT	A	1.01	-	7.24	-

7.1.10 Cabrane et al.: Hybrid energy storage system for PV (2016)

Cabrane *et al*. investigated variations related to the number of SCs used and their location in hybrid storage systems [41]. In order to obtain the best performance from the matching of batteries and SCs, the correct configuration must be chosen. The most used topologies are listed below. The easiest configuration is shown in Figure 37, the SC and the batteries are connected directly to the load. The SC operates essentially as a low-pass filter. The main advantage is the ease of implementation, the disadvantage is the complete absence of a controller to make the best use of the existing components.

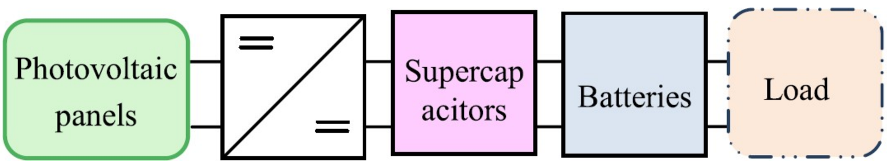

Figure 37 Basic passive hybrid configuration. Adapted and reprinted with permission from [41].

The following two configurations allow for greater system manageability (Figure 38). In the first one, the bidirectional buck-boost converter has to be oversized in order to allow the correct operation of the SC. However, it is not possible to modify the battery operating values. The second design, on the other hand, allows more gain from the hybrid system by adjusting the battery pack voltage and using the SCs as a filter for peak management.

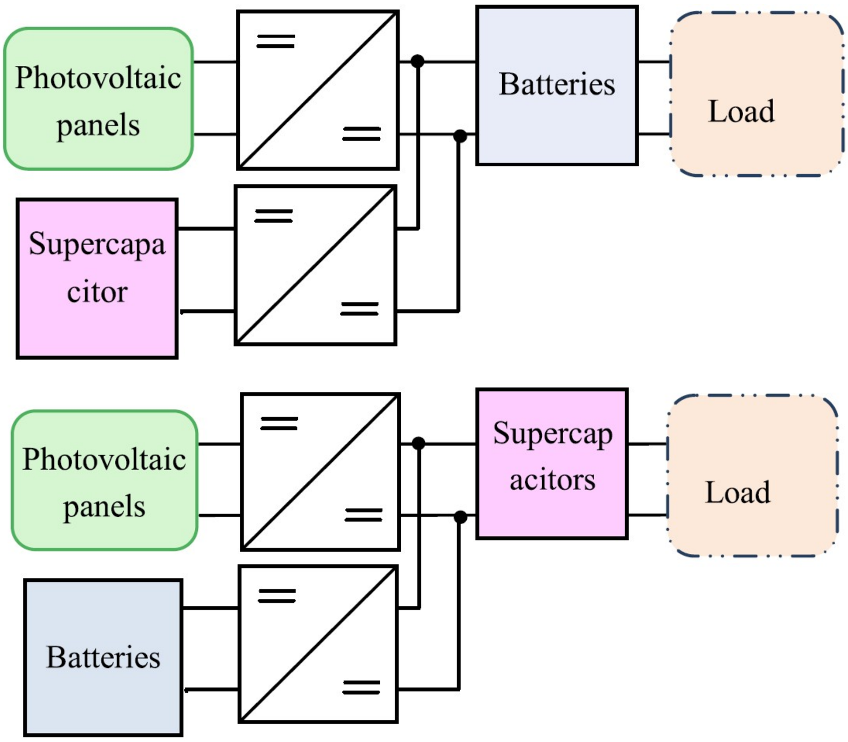

Figure 38 (top) Supercapacitor/battery parallel configuration; (bottom) battery/supercapacitor parallel configuration. Adapted and reprinted with permission from [41].

The SC/battery independent configuration shown in Figure 39 is the best one, as it allows accurate control of the system, but the higher number of components causes increased costs and complications in energy management.

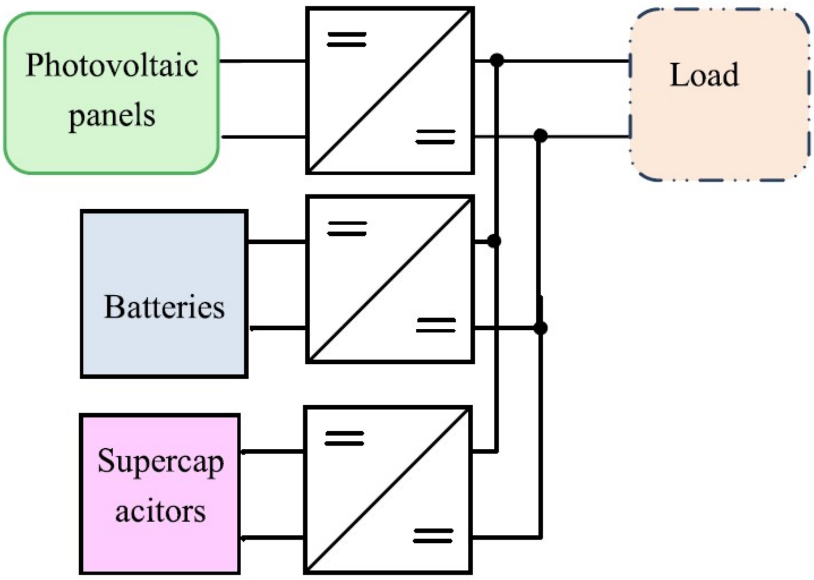

Figure 39 Multiple active hybrid configuration. Adapted and reprinted with permission from [41].

7.1.11 Yin et al.: Off-grid PV, diesel generator and supercapacitor energy system (2017)

Yin *et al.* proposed an intervention algorithm for the energy control of a DC network fed by a multi-source hybrid system [42]. The plant was based on a PV system, with lead-acid battery storage, providing continuity to the system by a diesel generator. In order to mitigate peaks, to better manage the charge/discharge cycles of the batteries and to compensate for the non-instantaneous intervention of the auxiliary generator, SCs were also inserted.

7.1.12 Cabrane et al.: Fuzzy logic management (2017)

Cabrane *et al.* introduce a fuzzy logic control system, which can manage a hybrid storage PV system based on batteries and SCs [43]. The energy management strategy is based on the need to adopt the optimal operating mode to ensure the correct supply of the battery pack and the stability of the DC grid. The control logic adopted made it possible to gain from the simplicity of fuzzy logic in solving energy management problems. The programming logic was optimised to keep the batteries and SCs within their optimum operating levels, in order to extend their service life.

7.1.13 Miñambres et al.: Grid connected hybrid energy storage (2017)

Miñambres *et al.* worked on the improvement of the limited lifetime through the collaboration of batteries and SCs [44]. The system under study was a grid-connected device capable of adapting to sudden changes in power requirements. The proposed scheme demonstrated, through simulations and laboratory tests, the reduction of battery charge/discharge cycles and the production of an almost perfectly sinusoidal wave to be fed into the grid. Using the algorithm developed, the capacity of the battery is calculated by setting the nominal power and the time range wanted.

7.1.14 Cabrane et al.: Hybrid vs. non-hybrid PV systems (2017)

Cabrane *et al.* compared the operation of a PV storage system composed of only batteries with a hybrid battery/SC system [45]. The main stresses on a battery pack in a PV system are due to fluctuations in the charging system caused by environmental variations, sudden power demands and low charge levels. By including an SC on the DC bus, it is possible to mitigate the stresses suffered by the chemical accumulator. Figure 40 shows the reaction of the hybrid storage system when subjected to sudden external stresses due to variations in PV production. Figure 40 (left) shows the production graph of the solar system and the load level to which the system is connected. The current output of the two modules of the hybrid system must therefore be modulated in such a way as to be able to cover the electrical energy demand, as it can be seen in Figure 40 (right), the battery/SC coupling manages to exploit the peculiarities of the individual devices, not overloading the traditional battery, thus reducing its deterioration.

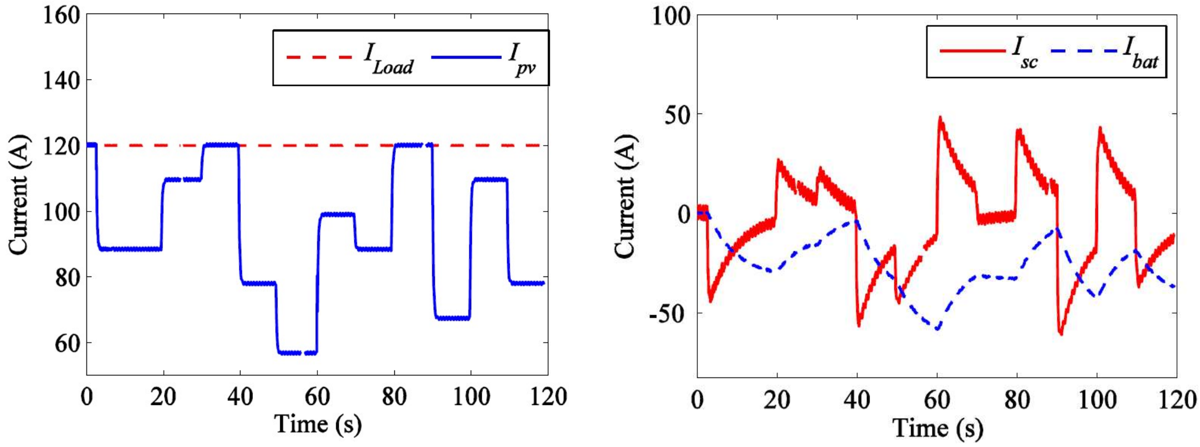

Figure 40 (left) PV production and load level; (right) Battery/SC power supply. Adapted and reprinted with permission from [45].

In order to compare the stresses experienced by a battery when it is included (or not) in a hybrid system, a comparison was implemented and the results are reported in Figure 41.

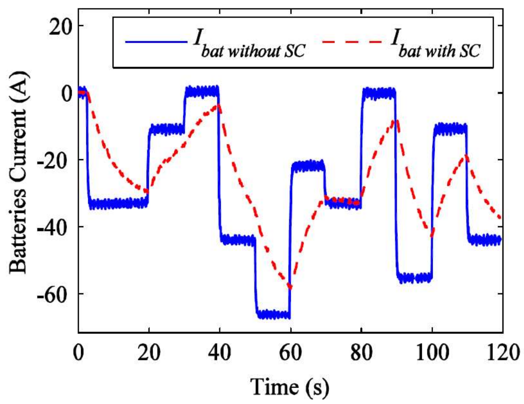

Figure 41 Comparison of the current delivered by a battery in a hybrid vs. a non-hybrid system. Adapted and reprinted with permission from [45].

A drastic reduction in the peaks and a small decrease in the maximum current delivered by the battery occurred, which made it possible to extend its life by reducing its degradation.

7.1.15 Wang et al.: Hybrid wind and PV system with SC (2018)

Wang *et al.* worked on a multi-machine power system based on a wind turbine and a PV plant by stabilizing the produced current with SCs [46]. The power plant, sketched in Figure 42, consisted of a 300 MW wind-turbine and 75 MW PV array. The turbine was connected to a voltage-source converter, while the PV array to a MPPT DC/DC boost converter; the produced current was driven through a DC bus to the voltage-source inverter and the SC stack.

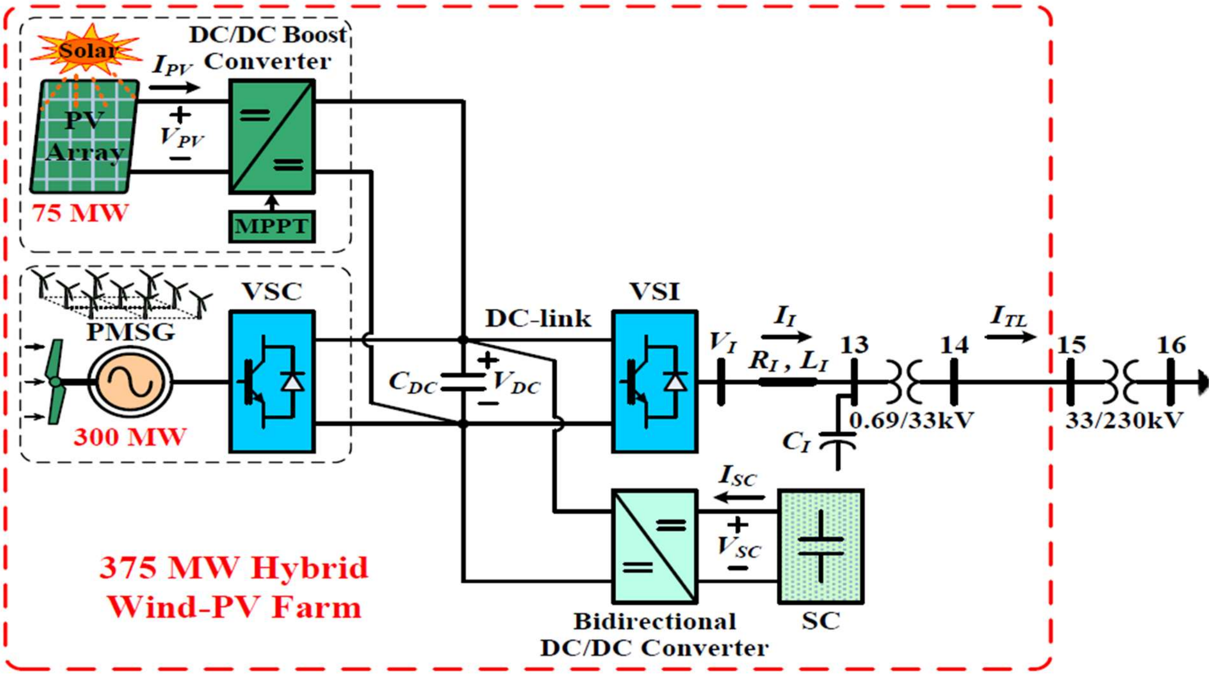

Figure 42 Schematic diagram of the system and electrical components. Adapted and reprinted with permission from [46].

SCs served for a dual purpose, *i.e.* to stabilise production to dampen fluctuations due to variations in light intensity or wind and to attenuate low-frequency oscillations, increasing system stability. From the results obtained, which can also be seen in the graph in Figure 43, the system reported an excellent ability to suppress power fluctuations, improving system performance. This made production less susceptible to variations in wind speed and solar radiation.

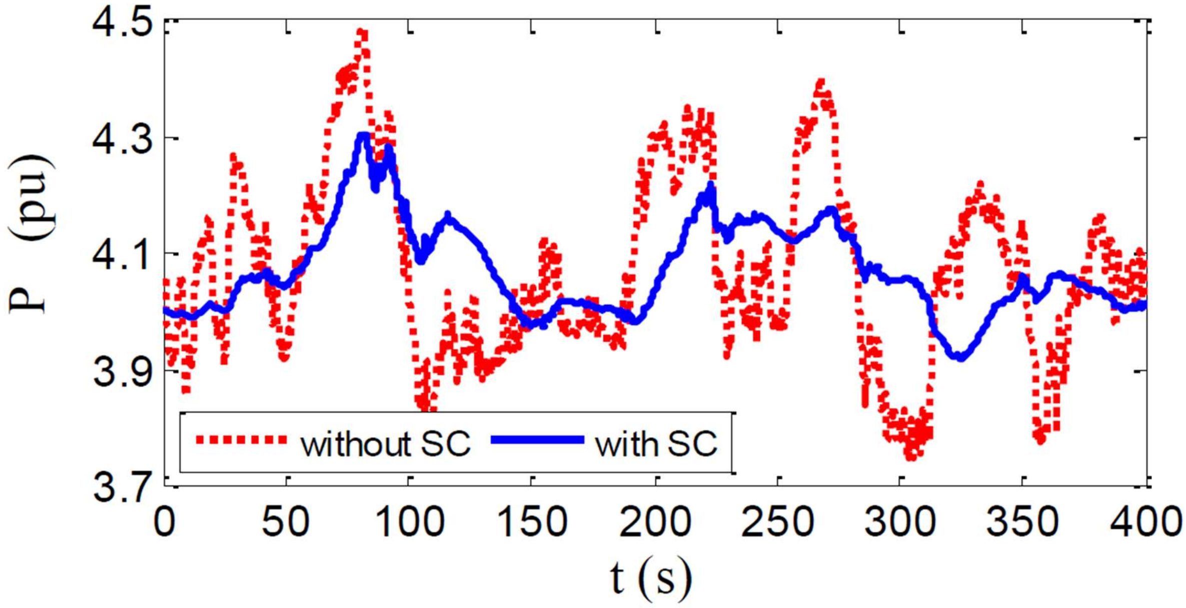

Figure 43 Comparison of the system with and without fluctuation damping given by SCs. Adapted and reprinted with permission from [46].

7.1.16 Barbosa et al.: MPPT and optimal charging for a PV/LIB/SC system (2018)

Barbosa *et al.* analysed a collaborative operation between batteries and SCs to ensure the best operation of the first one by recharging it with a PV system [47]. Figure 44 (left) shows the graph of the trend of the power supplied by a panel using the MPPT, while Figure 44 (right) shows the optimal trend of the power required to recharge a LIB. The problem with the inhomogeneity between the two trends was that the LIB needed two stages, the first at constant current and the second at constant voltage. In order to be able to use the PV system with the MPPT and recharge the battery optimally without waste, a SC was inserted into the system to manage the charging current.

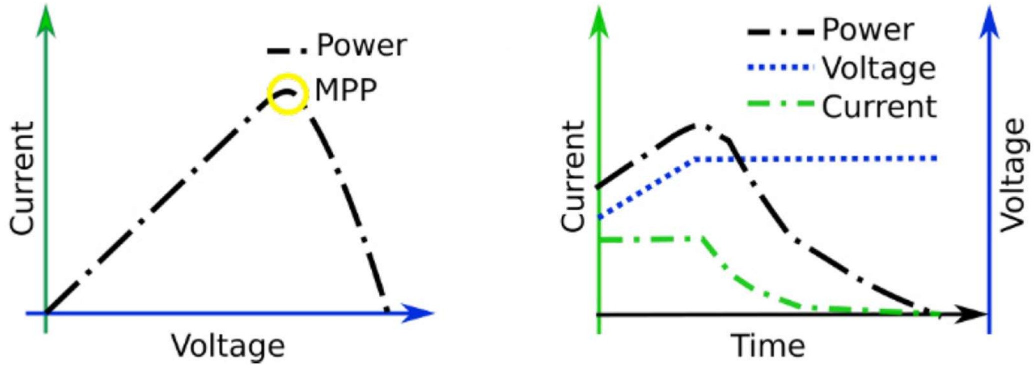

Figure 44 (left) PV panel power curve; (right) Battery charge curve. Adapted and reprinted with permission from [47].

Through this implementation, it was possible to correctly use maximum power output from the PV system, using the SCs as an auxiliary storage system to manage peak demand and to charge the LIB. The SC was able to maintain the charge of the LIB or complete it even during periods of temporary absence of PV production due to external atmospheric conditions.

7.1.17 Ciccarelli et al.: Hybrid PV and SC system in the railway sector (2018)

Ciccarelli *et al.* proposed a procedure for the integration of PV systems, rail brake recovery systems and SC [48]. During the braking phase it is possible to recover energy useful for the restart of the train itself or other vehicles. The modules are therefore designed to be installed on yards, so that they can serve the line and not the single vehicle. The modules consist of an array of PV panels and a stack of SCs. The use of these systems could guarantee a significant energy reduction and a decrease in peak demand caused by the energy demand of departing trains. The presence of accumulators in stations would benefit from the large amount of space available and the possibility of reduction in the size of power lines without substantial changes.

7.1.18 Shchur et al.: Distributed MPPT and energy storage (2018)

Shchur *et al.* developed a new architecture for a stand-alone/grid-connected installation based on a cascaded half-bridge DC-DC converter array [49]. The system combines distributed MPPT management by connecting cascaded DC-DC converters to SCs. The combination of different devices made it possible to better manage the system and the interactions between them. The studies were carried out using MATLAB/Simulink simulations showing the feasibility and effectiveness of the proposed solution. The use of this cascaded structure allows both the charging and discharging phase of the SCs to be managed, while maintaining a stable voltage in the DC bus.

7.1.19 Vargas et al.: Harmonic modelling and simulation of a hybrid system (2019)

Vargas *et al.* analysed the transmission of harmonic waves and their generation within a hybrid generation plant [50]. By using a battery/SC storage system and implementing control software, they aimed to monitor the stability of the generated current. The research was based on the flexible extended harmonic domain (FEHD) algorithm, an innovative technique for modelling and studying the harmonic domain. This technique was able to decrease the computational load due to system simulation, while still maintaining good resolution and analysis. The proposed model aimed to cope with load variations, while maintaining system control during transients. The analysis implemented in the study made it possible not only to represent a reliable model that accurately reproduced harmonic dynamics, but also to accurately analyse the real performance of individual components. The main feature of the FEHD model was that of being able to divide the entire system, based on the dynamic performance of the individual parts, into subsystems using distinct integration time steps.

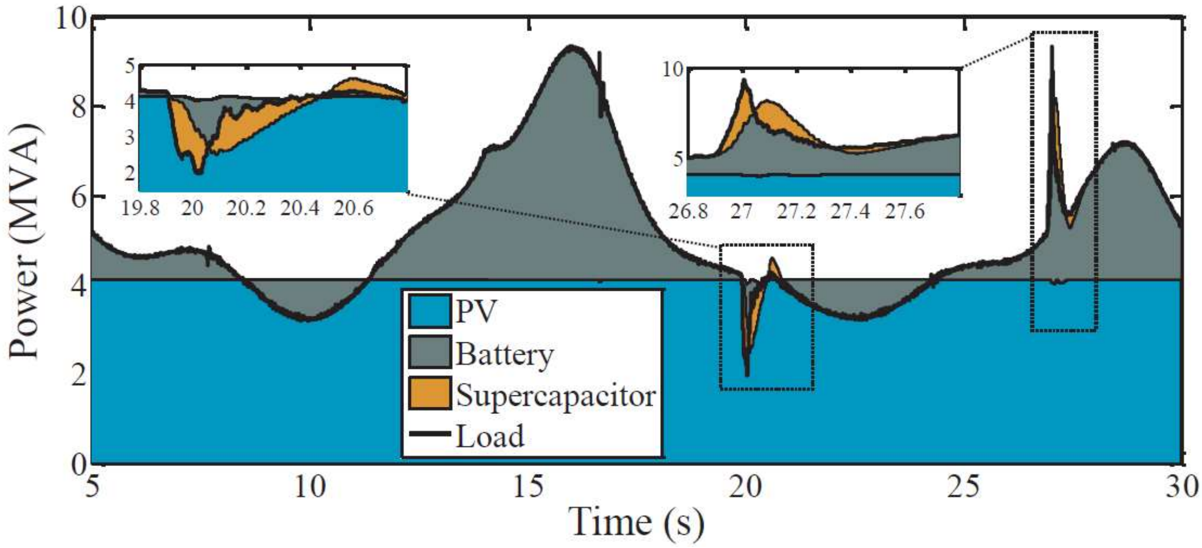

Figure 45 Graph representing the different power contributions during a simulation. Adapted and reprinted with permission from [50].

7.1.20 Perdana et al.: Direct connection of the hybrid storage system to the grid (2019)

Perdana *et al.* worked on reducing the instability of electricity grids based on PV systems [51]. This control was carried out by directly inserting a SC into the system, thus decreasing the instabilities and cycles experienced by the primary battery storage. The direct connection had the function of decreasing the components number, and thus the losses that lead to a decrease in overall efficiency. The proposed connection is shown in Figure 46; the hierarchical control strategy also allowed the bus voltage to be maintained unaltered.

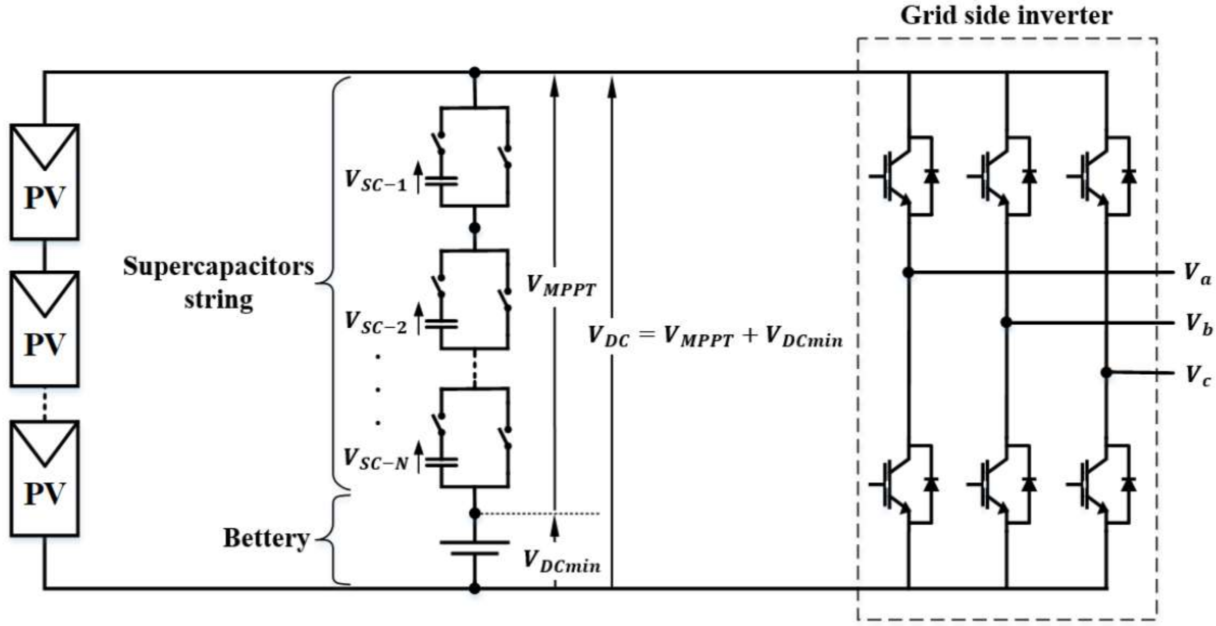

Figure 46 Diagram representing the direct connection implemented in the hybrid storage PV system. Adapted and reprinted with permission from [51].

The analysis was focused on the ability of the system to follow the speed ramp of the power output from the PV system by applying an MPPT algorithm. The ability to manage the voltage of the panels and therefore the MPPT was ensured by connecting/disconnecting the SC unit, varying the circuit specifications.

7.1.21 Kong et al.: Electric storage with SC and alkaline electrolyser (2019)

Kong *et al.* studied a hybrid storage system based on a SC module and an alkaline electrolyser (AE) [52]. A system based on PV cells and a PEMFC cell, connected to the common DC grid, was chosen for the electrical generation. The schematic structure of the grid-connected hybrid generator is shown in Figure 47.

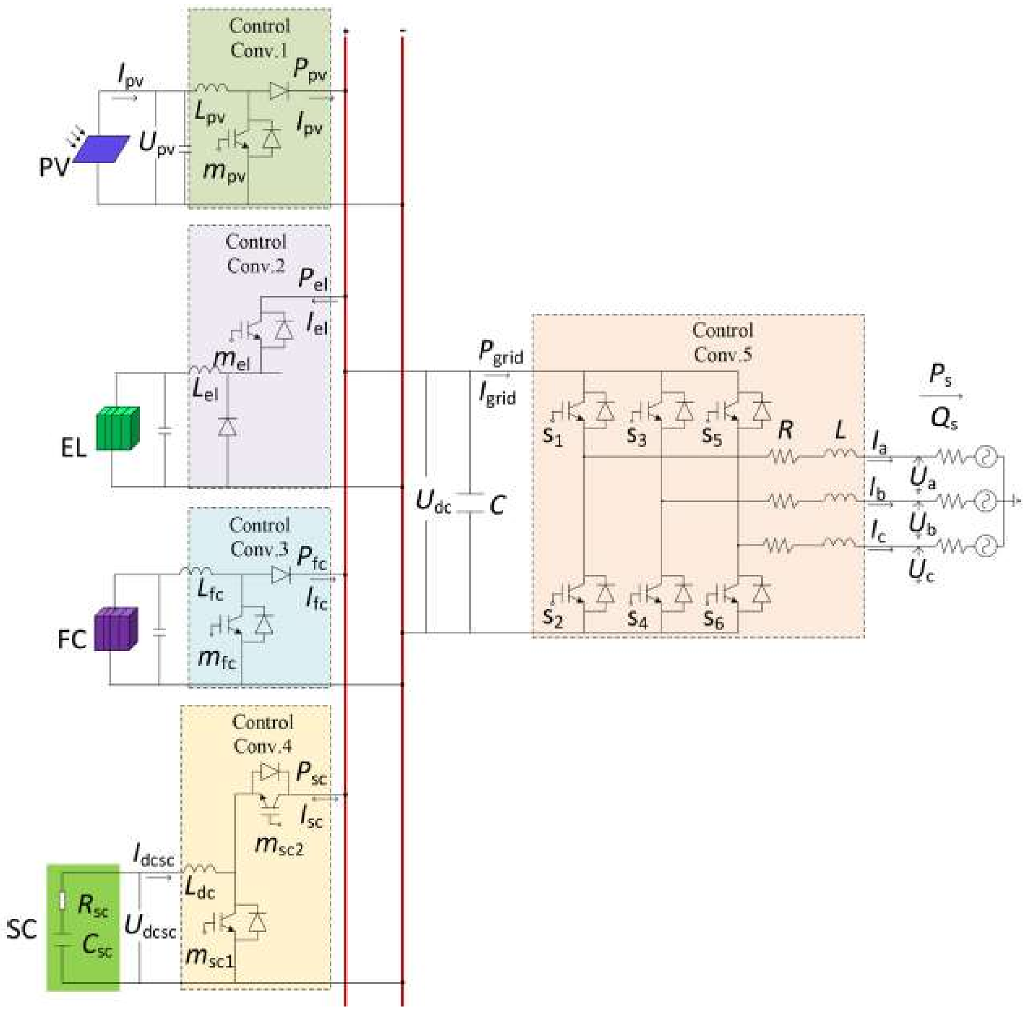

Figure 47 Structure of the hybrid power generation system. Adapted and reprinted with permission from [52].

The PV system, in MPPT operation, generated the basis for electricity production. Excesses are stored by the electrolyser (EL) in the form of hydrogen, to be reused during peak demand by the PEMFC. The SCs have the function of mitigating the peaks and compensating for the intervention issues of the individual components. The presence of SCs and connection to the network are crucial due to the slow response times of the EL and PEMFC system. Without the grid connection, SCs would be required, which would be too large and costly.

7.1.22 Kamel et al.: Optimisation of a PV/PEMFC hybrid system (2020)

Kamel *et al.* implemented a control strategy for a hybrid PV and PEMFC generation system with a storage system based on SCs and batteries [53]. Priority was given to saving hydrogen and trying to keep the SOC of the battery as high as possible. The SC bank was inserted and used to control the peaks and transients due to the intervention times of the individual components. Reducing power consumption and optimising battery use are key parameters for achieving maximum efficiency and ensuring the highest sustainability of the device under study. It also reduces operation and maintenance costs. Fuzzy logic and component decoupling were used to achieve this goal, so that their operation could be regulated as precisely as possible. The operating rules found are shown in the following Table 6 and are based on adjusting the system according to the SOC of the battery.

Table 6 Battery SOC and system reaction. Adapted and reprinted with permission from [53].

SATE	SOC	POWER	OUTPUT
STATE = 1	High	$P_{LOAD} < Pfc_{MIN}$	$Pfc = Pfc_{MIN}$
STATE = 2	High	P_{LOAD} & $[Pfc_{MIN}, Pfc_{MAX}]$	Pfc =Pload
STATE = 3	High	$P_{LOAD} \geq Pfc_{MAX}$	$Pfc = Pfc_{MAX}$
STATE = 4	Normal	$P_{LOAD} < Pfc_{OPTIMAL}$	$Pfc = Pfc_{OPTIMAL}$
STATE = 5	Normal	P_{LOAD} & $[Pfc_{OPT}, Pfc_{MAX}]$	Pfc =Pload
STATE = 6	Normal	$P_{LOAD} \geq Pfc_{MAX}$	$Pfc = Pfc_{MAX}$
STATE = 7	Low	$P_{LOAD} < Pfc_{MAX}$	Pfc =Pload + Pcharge
STATE = 8	Low	$P_{LOAD} \geq Pfc_{MAX}$	$Pfc = Pfc_{MAX}$

The proposed regulation allows to follow the load and to manage the variations related to the non-continuity of the solar source, the results obtained showed a saving of 19.6% of hydrogen consumption and an increase of 5.4% of the SOC value. The production trend can be seen in the graph below (Figure 48), which shows a classic PV production trend of a typical day and a fluctuating external load.

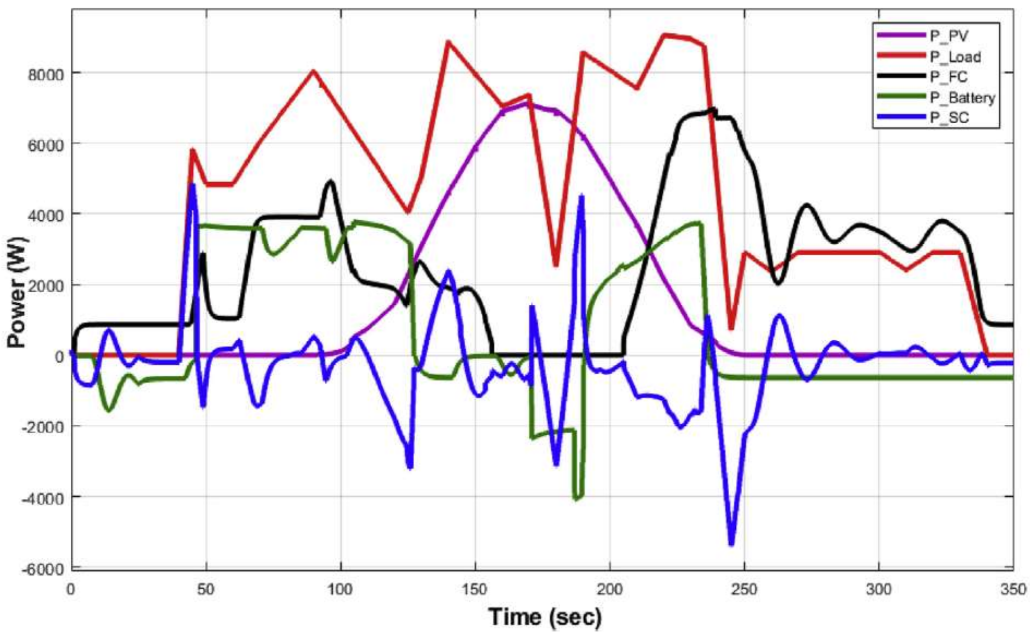

Figure 48 System performance when subjected to alternating load. Adapted and reprinted with permission from [53].

7.1.23 Guo et al.: Analysis of SC charging (2020)

Guo *et al.* analysed the behaviour of SCs with different charging methodology and used an RC model to validate their study [54]. Two converters were used to charge the accumulator with the PV system, the first connected to the generation system in MPPT mode and the second connected to the SC array. The control system studied was analysed by subjecting the PV system to different lighting conditions. Different types of charging were tested, including the soft start, for which low current intensities are used at the beginning of the charging process. This strategy provides a significant improvement in the efficiency of the storage system.

7.1.24 Jaszczur et al.: PV system with pure SC storage (2020)

Jaszczur *et al.* worked on the study of a PV system with a storage system consisting only of SCs [55]. These systems are rarely analysed, but the positive aspects associated with them are the increase in self-consumption and the considerable stabilisation of the grid.

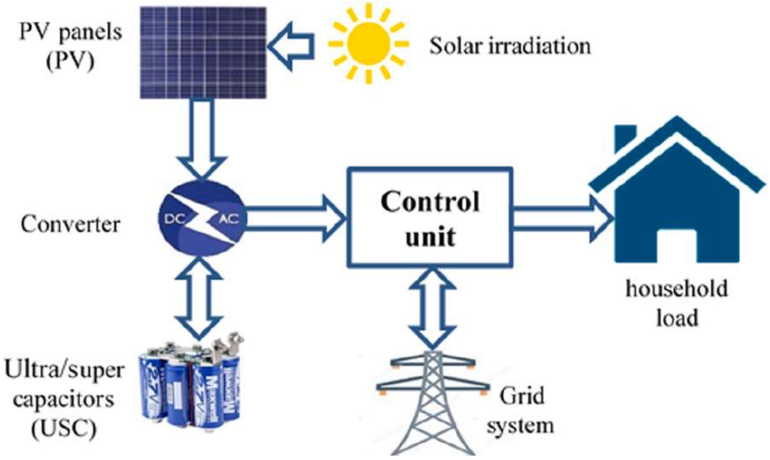

Figure 49 Schematic diagram of the solar system with SC storage. Adapted and reprinted with permission from [55].

To accurately capture the system variations brought about by SCs, different time scales of analysis were analysed (Figure 50). The management of the system was based on fuzzy logic in order to maximise self-consumption. The studies showed that, by adding a small SC to a PV generation system, it was possible to increase the share of self-consumption from 83% to 114% on a partly cloudy sunny day. Compared to a system without an accumulator, the increase in self-consumption was certainly greater than 100%. By adding an SC, it was also possible to feed a higher quality current into the grid without rapid fluctuations.

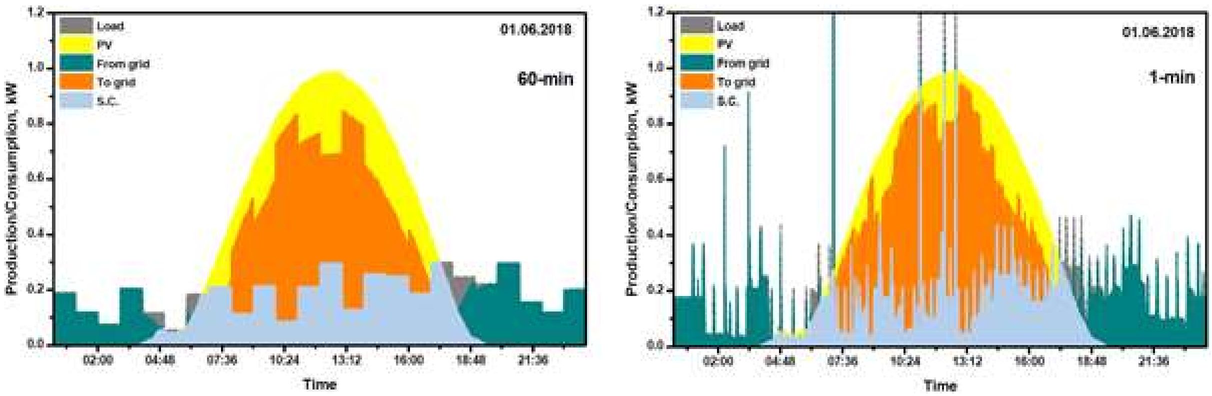

Figure 50 Two graphs showing simulations carried out with different time scales. Adapted and reprinted with permission from [55].

7.2 Integrated charging

7.2.1 Kim et al.: MPPT for Integrated Device (2010)

Kim *et al.* carried out the first optimisation study for the efficiency of SC charging processes using PV systems [56]. The technique employed was to modulate the MPPT, not to maximise the output power of the PV cell, but to ensure maximum efficiency of the energy storage system. The charging system, depending on how high the input voltage is, can have efficiencies ranging from 10% to 80%. This has a direct impact on the overall charging efficiency of the SC. The charging performance was found to be 6 times better than the one obtained from a low cost MPPT and the improvement was 5.7% when compared to a high performance MPPT.

7.2.2 Li et al.: PV and SC (2012)

Li *et al.* tested SCs as an energy storage device, basing their research on probabilistic analysis and operational models of the individual components [57]. The advantages of using SCs include their strong ability to withstand large power fluctuations, long cycle life, high charge and discharge efficiency and high-power density. The charge regulation system of SCs is also more flexible than those of conventional LIBs and can be more precisely and efficiently adjusted. However, their low specific energy and high initial costs must also be considered.

7.2.3 Ongaro et al.: Long lifetime PV wireless sensor network (2012)

Ongaro *et al.* analysed a strategy for statistical sizing of hybrid batteries to ensure continuity of operation for remote sensors [58]. Four different types of rechargeable batteries (NiCd, nickel-metal hydride, LIB and sealed lead-acid) were considered. Due to their low energy density and shallow discharge cycles, SLA and NiCd batteries were discarded. The choice between NiMH and Li^+ fell on the second technology because it is more efficient, has a longer life cycle, has a lower self-discharge rate and does not suffer from residual memory. First, the two main factors leading to a decrease in the number of useful charge cycles for LIBs were considered, so that the system could be sized in the most appropriate way. Figure 51 (top) shows the dependence of the charge cycles on the intensity of the charge: with currents higher than 1C, the useful life is drastically reduced. In Figure 51 (bottom), the number of charging cycles is linked to the voltage applied to the LIB; in this case too, the problem of overvoltage is very detrimental.

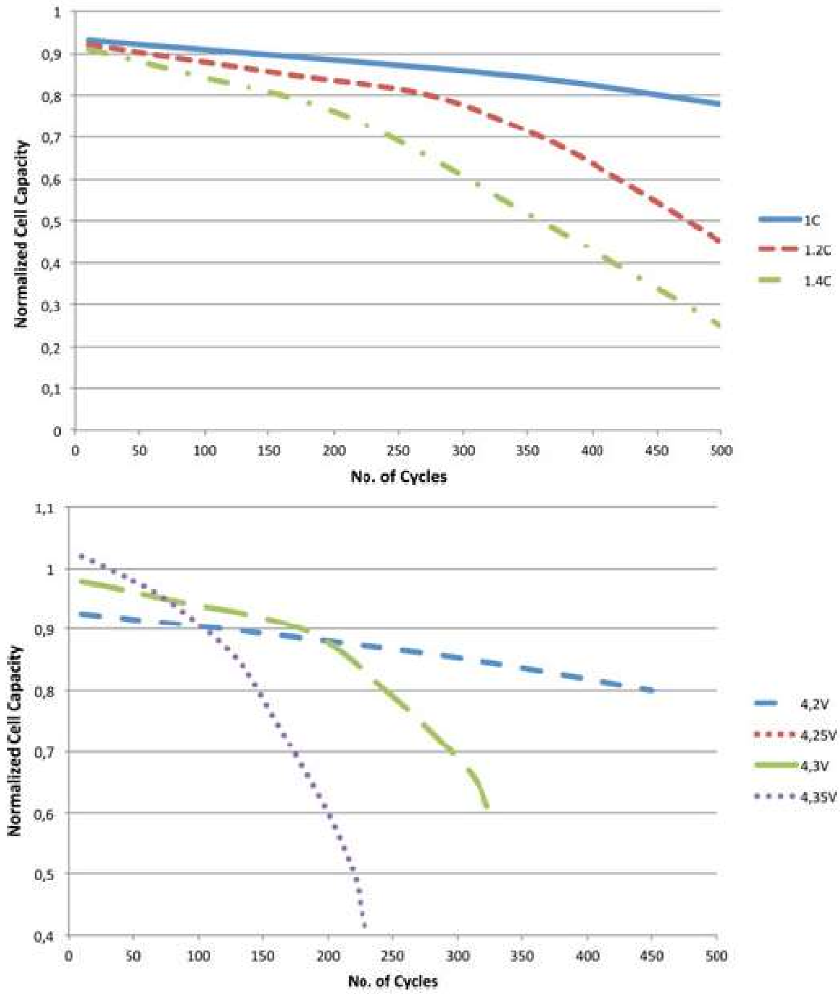

Figure 51 Analysis of storage system wear due to: (top) charging speed; (bottom) charging voltage. Adapted and reprinted with permission from [58].

As a result of the data collected, a block diagram, shown in the Figure 52, was developed, including the procedures to be implemented to ensure the greatest autonomy and to extend the life of the storage system.

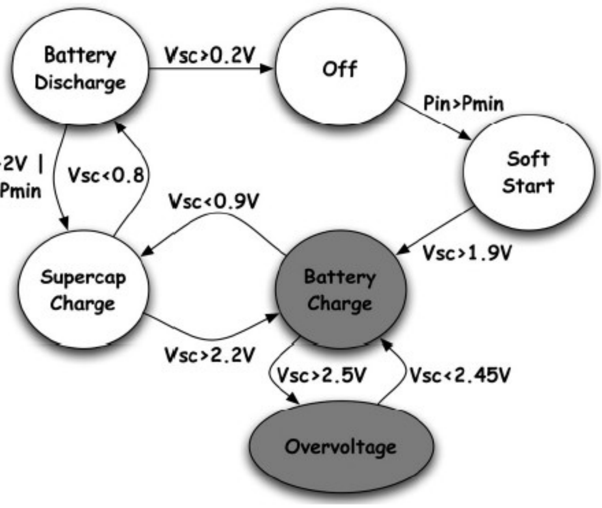

Figure 52 Power management logic system diagram. Adapted and reprinted with permission from [58].

Using a MATALB-Simulink model of this diagram, the algorithm for calculating the exact size of the accumulator was developed. The theoretical and experimental results were very satisfactory, demonstrating a reduction in battery charge/discharge cycles by a factor of 4. The main problem was the high consumption of the control system, compared to the one of the sensors to be powered by the system itself.

7.2.4 Liu et al.: Losses and performance of SCs (2013)

Liu *et al.* analysed the energy losses in PV/SC energy systems coming not only from the inefficient charging process, but also from discharge process and energy leakage [59]. Based on a realistic power model of each hardware component, the different processes of electrical energy conversion (charging, discharging and losses) were examined. The problem was analysed in a non-linear way by examining the performance through numerical simulations and laboratory tests. The results led to an increase of the active time of use of a SC by 56/60% compared to a fixed cycle. Leakage losses were reduced by modulating the voltage of the SCs correctly; as it can be seen in Figure 53, the losses depend on the applied voltage.

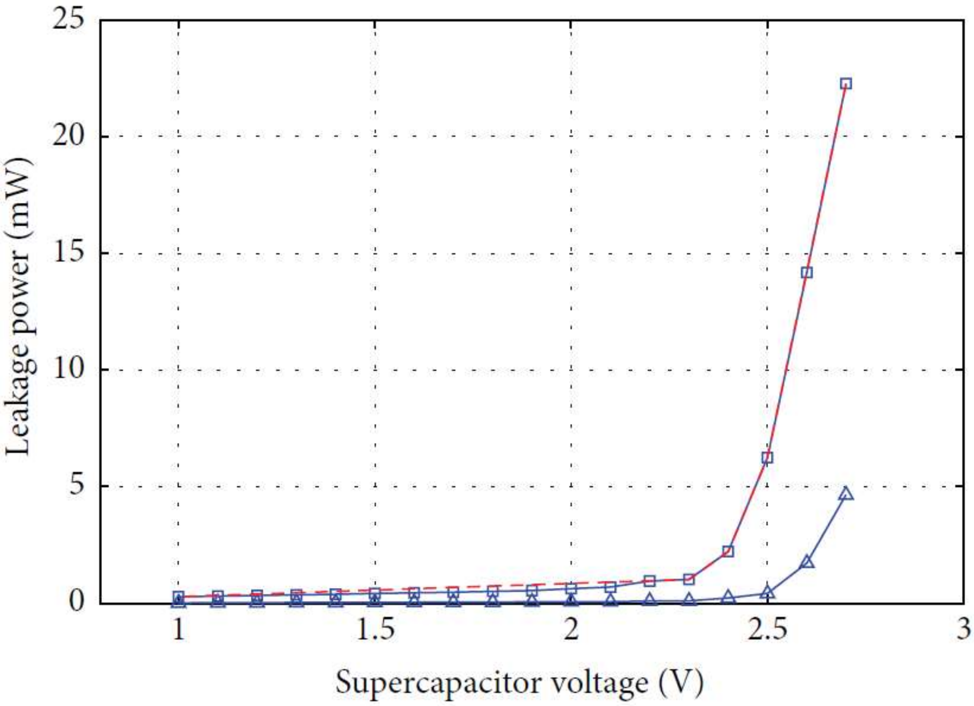

Figure 53 Relationship curve between leakage losses and SC voltage. Adapted and reprinted with permission from [59].

7.2.5 Bagheri et al.: Integrated PV/SC system (2014)

Bagheri *et al.* focused their research on the development of an integrated system capable of producing electrical current using a DSSC and storing it with an SC [60]. The DSSC used was based on a metal-free organic sensitizer and cobalt (II,III) redox shuttle. A three-electrode design was used to integrate the PV cell with the SC, as shown in Figure 54. The intermediate electrode was realized from a low-cost nickel foil. It allows regeneration of the electrolyte on the DSSC side and charge storage on the SC side, thanks to cobalt doping.

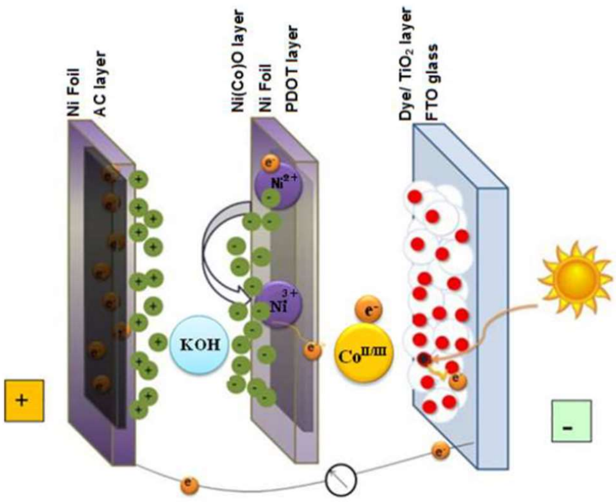

Figure 54 Schematic structure of the cell under analysis. Adapted and reprinted with permission from [60].

The cell was tested with an irradiation of 100 mW cm^{-2}, generating an open circuit voltage of 0.8 V and a short circuit current density 8 mA cm^{-2}. The electrical energy thus produced was directly stored within the SC, resulting in a specific capacity of 32 F g^{-1} and an energy density of 2.3 Wh kg^{-1}. The overall efficiency achieved was 0.6% compared to an energy production efficiency of 4.9% and a storage efficiency of 54%.

7.2.6 Zhang et al.: Energy fibre (2014)

Zhang *et al.* introduced solid-state polymeric photovoltaic cells consisting of a PV cell and an SC, which are flexible and capable of producing and storing electricity [61]. The use of coaxial structures provided advantages during both the production and storage phases. In the first one, the charges generated were quickly separated and transported. In the second, the SC benefitted from the large effective contact area. The "energy fibre" demonstrated good flexibility and resistance to charge and discharge cycles, as shown in Figure 55.

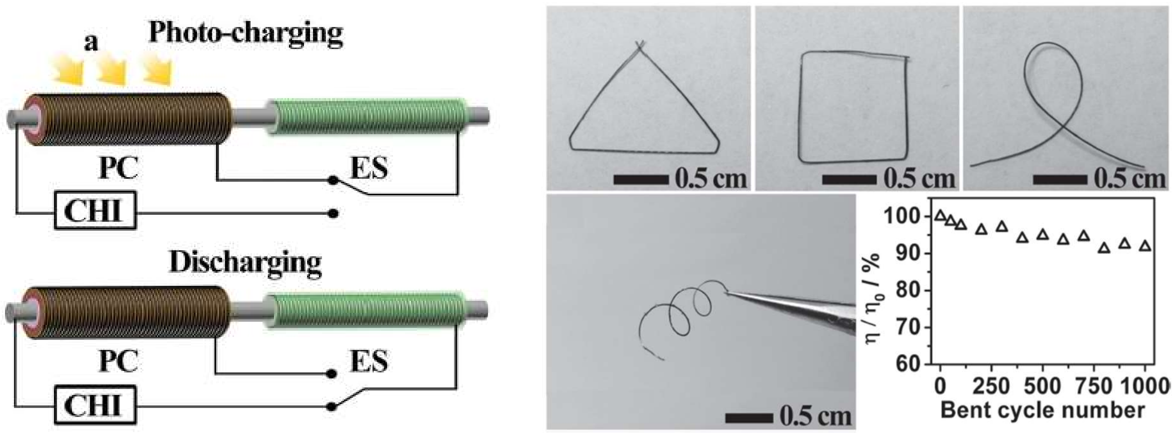

Figure 55 Schematic structure of the 'energy fibre' and photographs showing the flexibility tests carried out. Adapted and reprinted with permission from [61].

The efficiency of the SC was 65.6%, while that of the PV panel depended on the thickness of the multi-walled carbon nanotubes. As shown in Figure 56, as the thickness of this layer increased, the efficiency of the system increased too, up to a constant efficiency of 0.82% with a thickness of 20 μm.

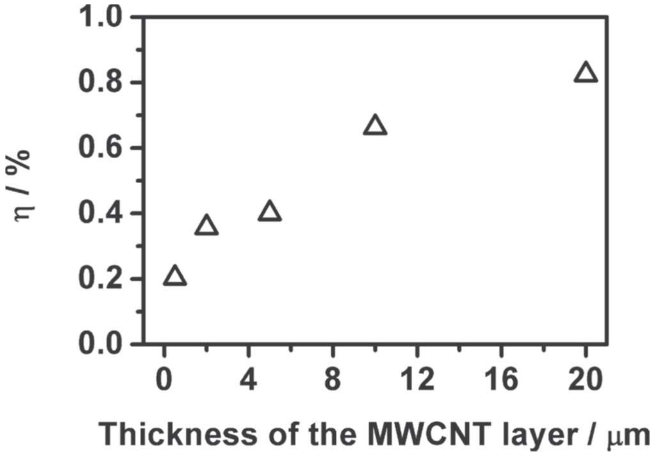

Figure 56 Variation in electrical production efficiency as cell thickness varies. Adapted and reprinted with permission from [61].

With only a 10% decrease in storage capacity after undergoing 1000 bending cycles, the fibre proved that it could simultaneously meet the need to produce electricity and store it inside.

7.2.7 Westover et al.: Commercial PV panel and porous silicon SC (2014)

Westover *et al.* retrofitted a commercial PV panel by engraving a porous Si SC to the bottom of the collector [62]. Porous Si SCs, which have a Coulombic efficiency of 84%, can be directly engraved on the existing Si layer. The procedure, as illustrated in Figure 57, started with the removal of the aluminium collector normally used in PV panels with a basic 1 M KOH solution. The excess Si was then removed by electrochemical etching and the SC was fabricated.

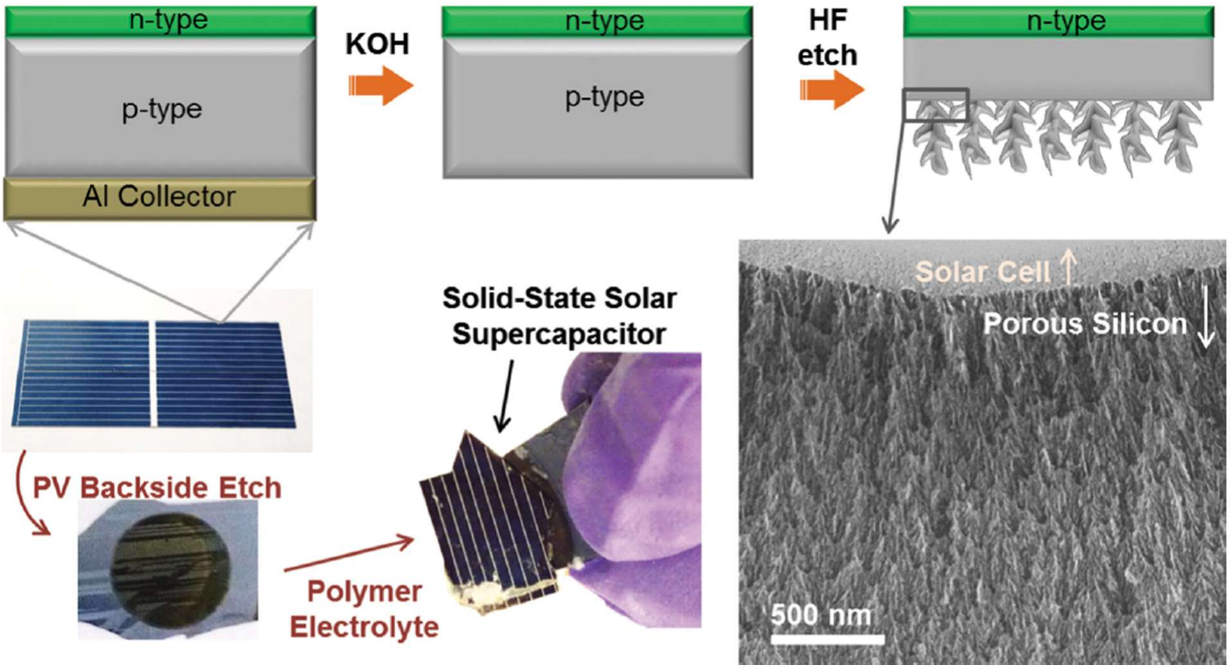

Figure 57 Steps for preparing the SC layer on the panel: (top) schematic diagram of a commercial PV cell; (bottom left) removal of the aluminium foil; (bottom right) microscopic analysis of the porous silicon SC. Adapted and reprinted with permission from [62].

The presence of the SC created a phase shift between the PV output and the cell power output, which made it possible to mitigate variations due to external agents. Figure 58 shows how the output current intensity was kept almost constant.

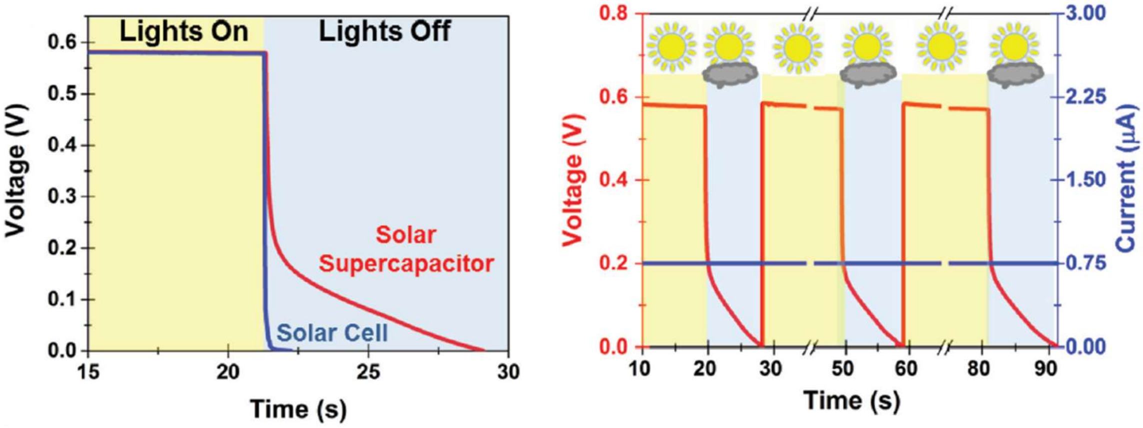

Figure 58 System response to variation of PV output. Adapted and reprinted with permission from [62].

SC resistance to cycling also does not affect the panel service life, ensuring a long lifetime. A higher efficiency could be achieved by using graphene-based surface passivation, which allowed 7 Wh kg^{-1} with a 4 µm thick active layer.

7.2.8 Xu et al.: Perovskite cell and polypyrrole-based SC (2015)

Xu *et al.* worked on the construction of an integrated device based on a perovskite solar cell and a polypyrrole-based SC [63]. An overall efficiency of 10% was achieved, making the device not only capable of producing and storing solar energy, but also able to avoid energy waste and maintain a stable power output. The open circuit voltage was 1.45 V, developed by the PV cell and the SC in tandem. The introduction of these systems acted as a buffer mitigating the typical PV unbalance between power output and demand.

7.2.9 Selvam et al.: Common electrode for high temperatures device (2015)

Selvam *et al.* demonstrated how the sulphated ß-cyclodextrin/PVP/$MnCO_3$ composite was able to serve as a common electrode for the integration of a SC into a DSSC [64]. This material was chosen due to its high performance at high temperatures and its environmentally friendly composition. This ensures clean energy even in high temperature environments. The typical counter electrode material is platinum (Pt), but this limits its wide application due to its corrosiveness and high cost. A further problem that was addressed was the instability of liquid electrodes in a hot environment. The DSSC demonstrated a fill factor of 68.2% and an efficiency of 5.57%. By comparison, a DSSC with a Pt counter electrode had an efficiency of 6.71%. The maximum specific capacity of the SC was 202 F g^{-1} over a temperature range of 25 to 75 ºC. In the case of higher temperatures (up to 200 ºC), this electrode maintained a capacity of 152 F g^{-1} with 3.9% efficiency at DSSC. The results are shown in Figure 59.

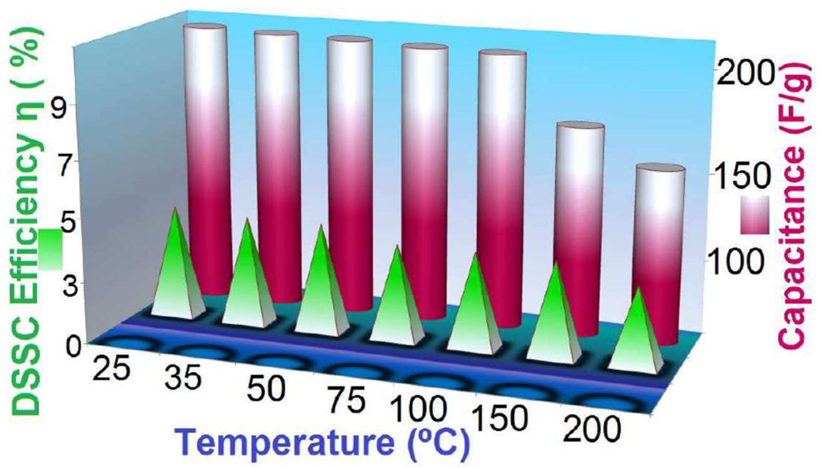

Figure 59 DSSC cell efficiency and SC capacity at different temperatures. Adapted and reprinted with permission from [64].

Due to its high stability to thermal stress, this composite electrode could be considered a good material for components to be used in hot environments.

7.2.10 Xu et al.: Integrated photo-supercapacitor based on PEDOT (2016)

Xu *et al.* integrated a printable perovskite-based PV cell with a SC [65]. The electrons produced by solar radiation are transferred to the storage system based on a PEDOT-carbon matrix. The overall efficiency achieved was 4.70%, with a maximum storage performance of 73.77%. The internal composition of the photo-supercapacitor (PS) device is shown in Figure 60.

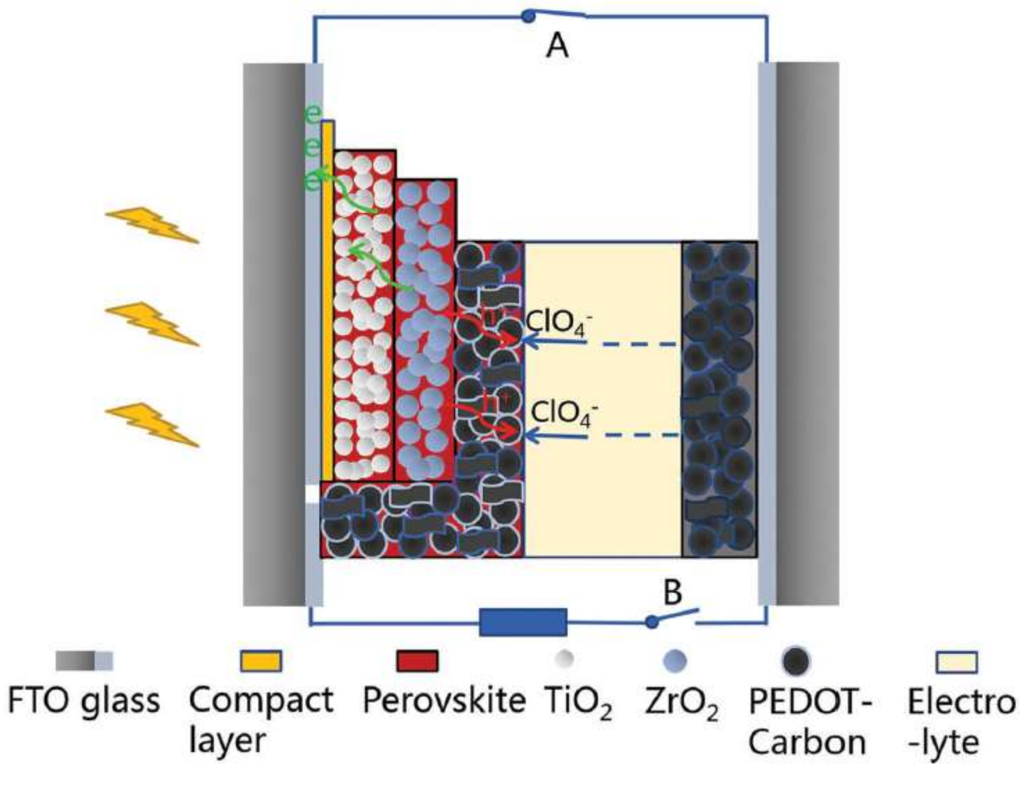

Figure 60 Internal composition of the PS device. Adapted and reprinted with permission from [65].

The perovskite-based PV cell is shown in the left side of the device shown in Figure 60; it is directly connected to the PEDOT-carbon based SC, shown on the right side of the scheme. The design adopted allowed good performance to be guaranteed even when the required current varied, ensuring excellent stability in the operating cycles. After 2000 charge/discharge cycles, the charge capacity remained at 95% of the initial capacity, as shown in Figure 61.

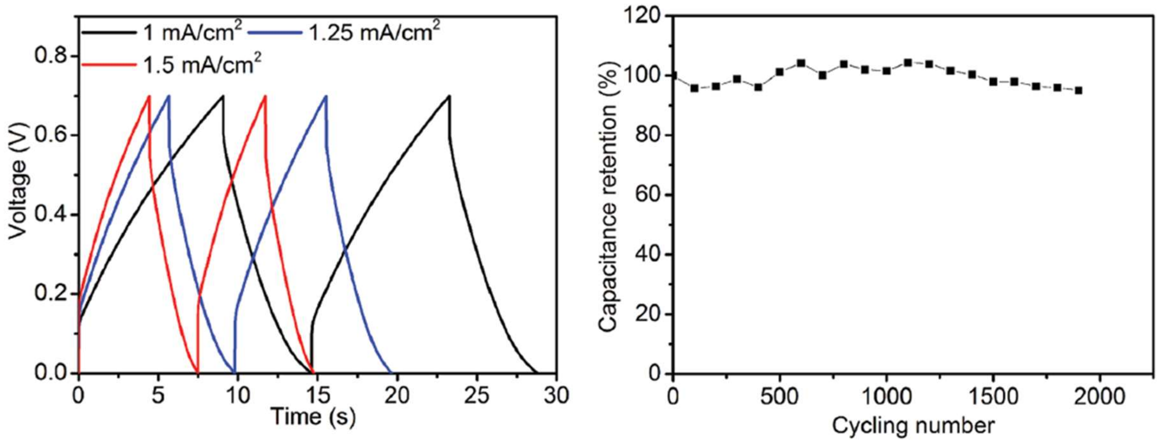

Figure 61 (left) Galvanostatic curves examined at different current densities; (right) stability of SC capacity after 2000 cycles. Adapted and reprinted with permission from [65].

7.2.11 Wen et al.: PV energy textile (2016)

Wen *et al.* proposed a hybrid fibre developed to produce current by PV system and random body movement storing it inside via SC [66]. A DSSC was used to convert solar radiation into electricity and fibre-shaped triboelectric nanogenerators were implemented to produce energy from body movement. The device consisted of two main parts, as shown in Figure 62, the upper part was formed by the fibres containing the DSSCs and the lower part by those with the SCs. The tensions formed between them are used to produce energy from movement.

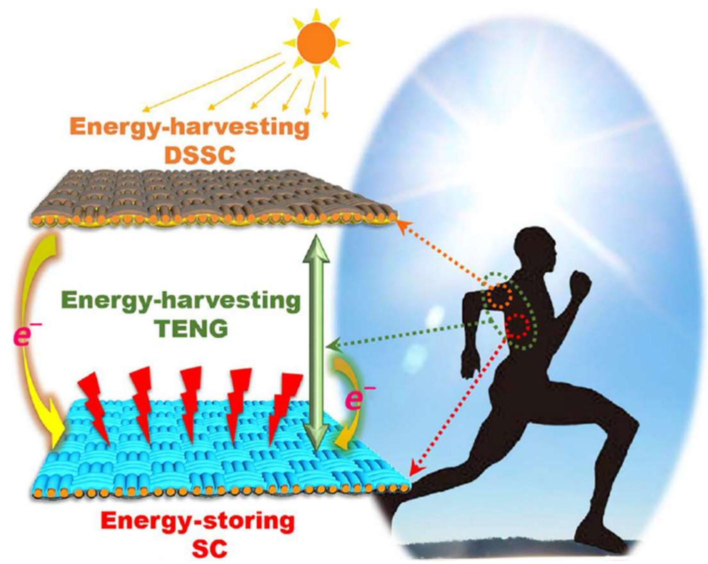

Figure 62 Diagram of the application of self-loading fibres. Adapted and reprinted with permission from [66].

The system achieved an overall efficiency of 5.64%, showing a DSSC V_{OC} of 0.74 V cm^{-2} and a SC J_{SC} of 11.92 mA cm^{-2}.

7.2.12 *Kim et al.: Self-charging monolithic power packs (2017)*

Kim *et al.* worked on a self-charging monolithic power packs based on the integration of a PVA/H_3PO_4 based SC and perovskite/polymer-based PV cells [67]. The connection between the production component (PV panel) and the storage one (SC module) was not made (as previously experienced) by wires or using liquid electrolyte technology, but with a highly conductive glue. With the introduction of this element, the production process of the different components was simplified and the connection between them guaranteed a high mechanical adhesion as well as a large contact area, reducing the overall electrical resistance.

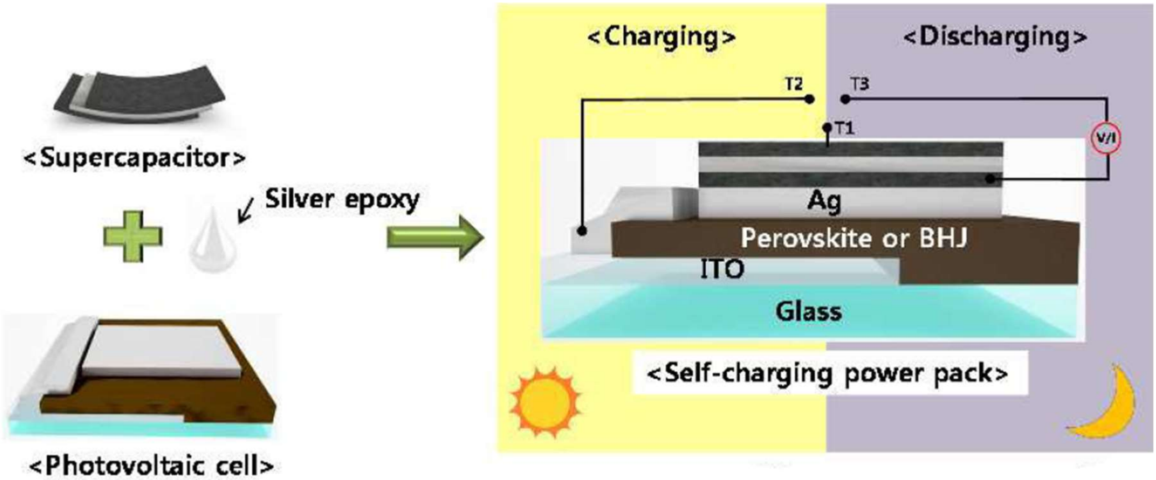

Figure 63 Device architecture. Adapted and reprinted with permission from [67].

The analysis of the cells in discussion resulted in an overall efficiency of 10.97% and storage efficiency of 80.31% for the polymer-based PV cells. For the perovskite-based cells, the values were 5.07% and 64.59%, respectively.

7.2.13 *Scalia et al.: Flexible and portable powerpack (2017)*

Scalia *et al.* developed a flexible integrated device based on TiO_2 nanotubes structure for the DSSC and a graphene-based bilayer SC integrated in a flexible architecture [68]. A structure of vertically aligned dye-sensitised TiO_2 nanotubes was used as photoanode in order to benefit from the large contact surface area. In both DSSC and SC, methacrylate-based polymer electrolyte membranes (PEMs) were used. After being immersed in the respective electrolytes, they ensured good flexibility of the system and also reduced the evaporation of the electrolyte itself. Thanks to the materials used, the non-wired flexible integrated device guaranteed good flexibility without leading to material degradation. Figure 64 shows an illustration of the structure produced in laboratory.

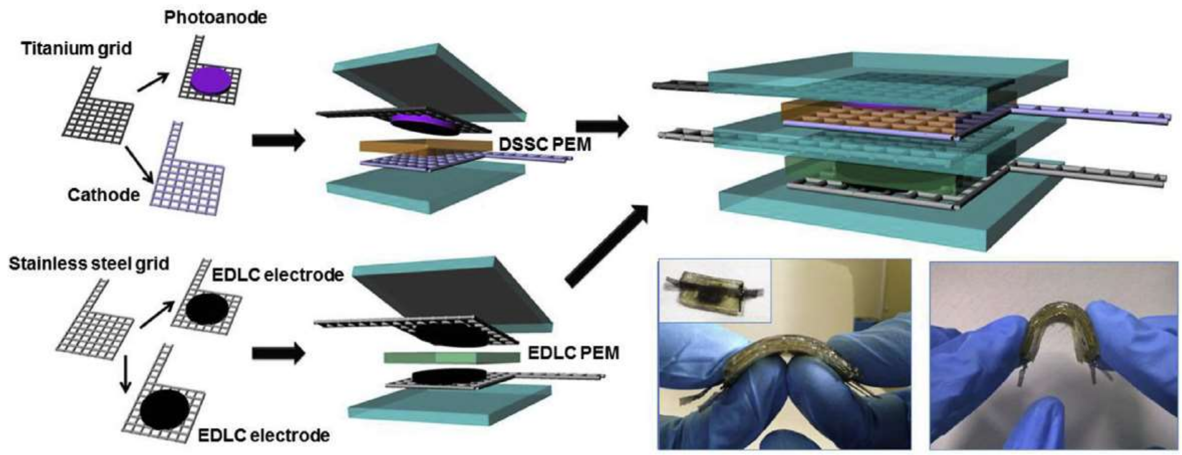

Figure 64 Diagram of the components and assembly of the flexible integrated system. Two photos of the realised cell are shown, the great flexibility can be seen. Adapted and reprinted with permission from [68].

The mitigation of the production peak, given by the coupling of the solar cell with the SC, can be seen in Figure 65 (top left). The great versatility and efficiency even under a bending stress of the DSSC is shown in Figure 65 (top right), where the potential difference generated by the cell under different bending stresses is visible. Figure 65 (bottom) analyse the current density of the DSSC in relation to the irradiated light intensity and the SC ability to maintain its capacity after repetition of work cycles, respectively.

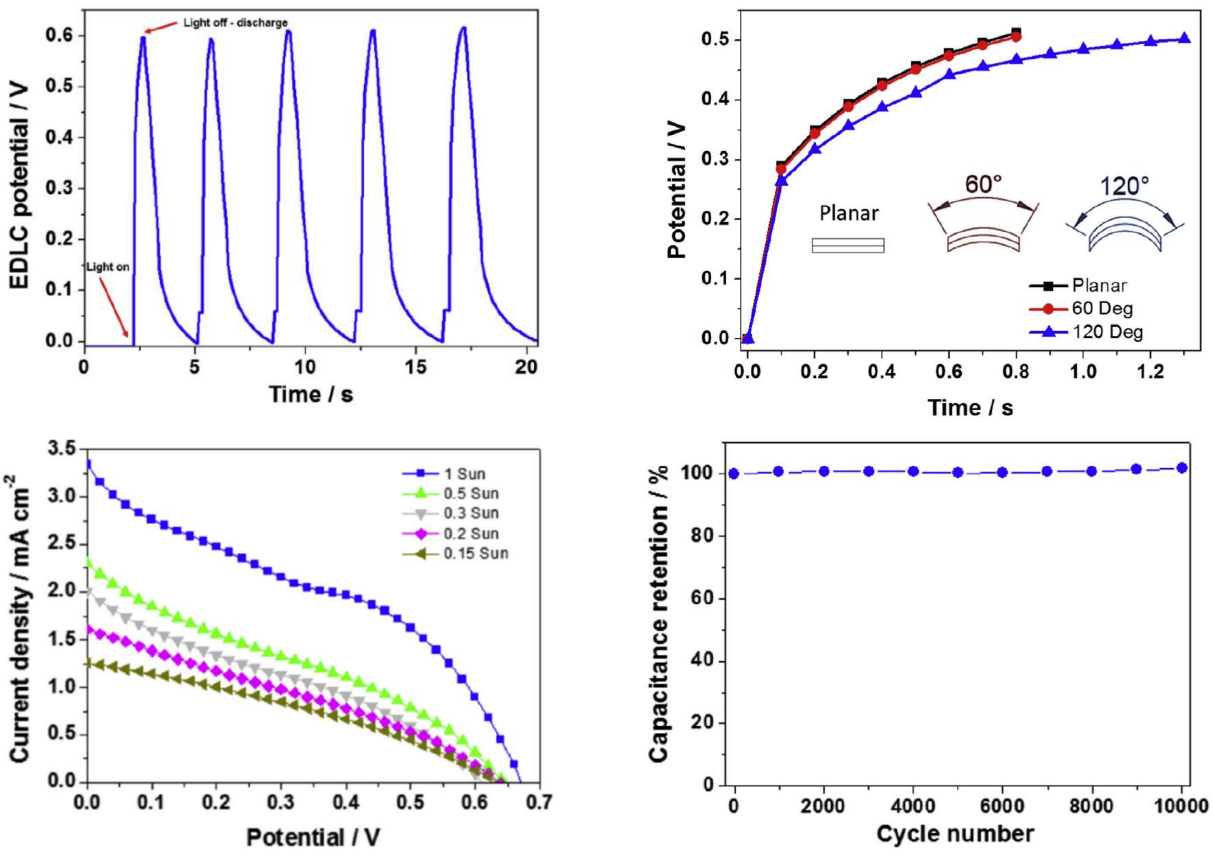

Figure 65 (top left) First five photo-charges and imposed constant current discharge cycles; (top right) Photo-charging curves for different bending angles conditions; (bottom left) Short circuit current at different illumination conditions; (bottom right) Capacitance retention of the SC. Adapted and reprinted with permission from [68].

The SC showed coulombic efficiency of 70%, in line with the performance of flexible SCs, with excellent capacity retention (no losses after 10,000 consecutive cycles). The maximum overall efficiency of the device was achieved at 0.3 sun and was 1.4%. At 1 sun, it was equal to 1.01%. The device was able to perform at its best not in optimal conditions, but in real conditions with diffuse radiation and clouds.

7.2.14 Sun et al.: Review of existing PS technologies (2017)

Sun *et al.* reviewed the currently existing technologies and the history regarding the integration of PV cells with SCs [69]. They started with the introduction and possible benefits of PS research and then described the main challenges and issues encountered over the years (Figure 66). The publication concludes with an analysis of possible future opportunities and possibilities for development in this area.

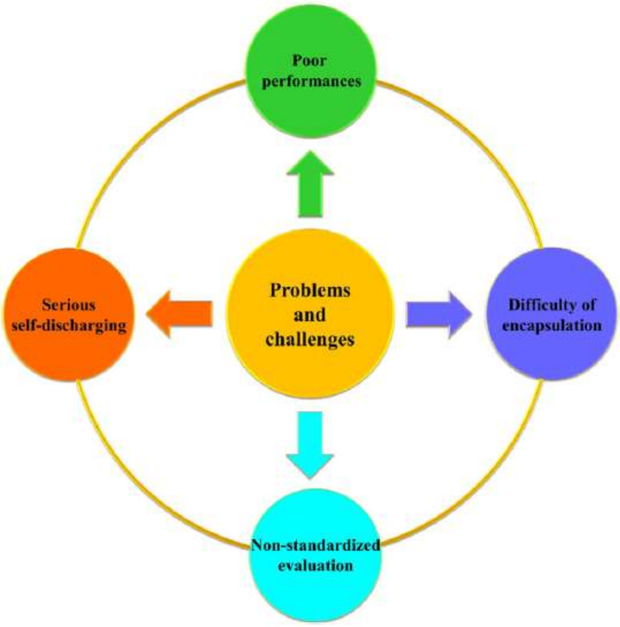

Figure 66 Main challenges and issues of PS over the last few years. Adapted and reprinted with permission from [69].

7.2.15 Muralee et al.: Metal sulphides and carbon nanotube support (2017)

Muralee *et al.* focused on the development of composite materials based on metal sulphides over carbon nanotube supports for electrodes [70]. Due to the high electrical conductivity of the nanotubes and the electrochemical performance of the metal sulphides (PbS, CuS, CoS and NiS), these cathodes can benefit from electrocatalytic behaviour. The electrodes under investigation were tested within DSSC and SC. The role of the metal sulphides was to provide active sites for polysulphide redox pair reduction, exploiting the carbon nanotube substrate for electron transport. CNT/NiS-based electrodes for DSSCs showed the best conversion efficiency, reaching 6.41%, *i.e.* a 90.8% increase over that with carbon nanotube electrodes. NiS-based SCs also showed the best results, achieving a high specific capacity and energy density of 398.16 F g^{-1} and 35.39 Wh kg^{-1} at 1 mA cm^{-2}.

7.2.16 Liu et al.: PSC-SC integrated device (2017)

Liu *et al.* developed an integrated monolithic cell based on perovskite deposited on a carbon electrode in common with the SC [71]. The proposed innovative integration method consisted of spin-coating a perovskite layer on the PSC side of the carbon electrode and MnO_2 on the other side for the SC. With the integration of the two components connected in series, the instantaneous power of the PV cell raised significantly. The construction diagram of the prototype is shown in Figure 67.

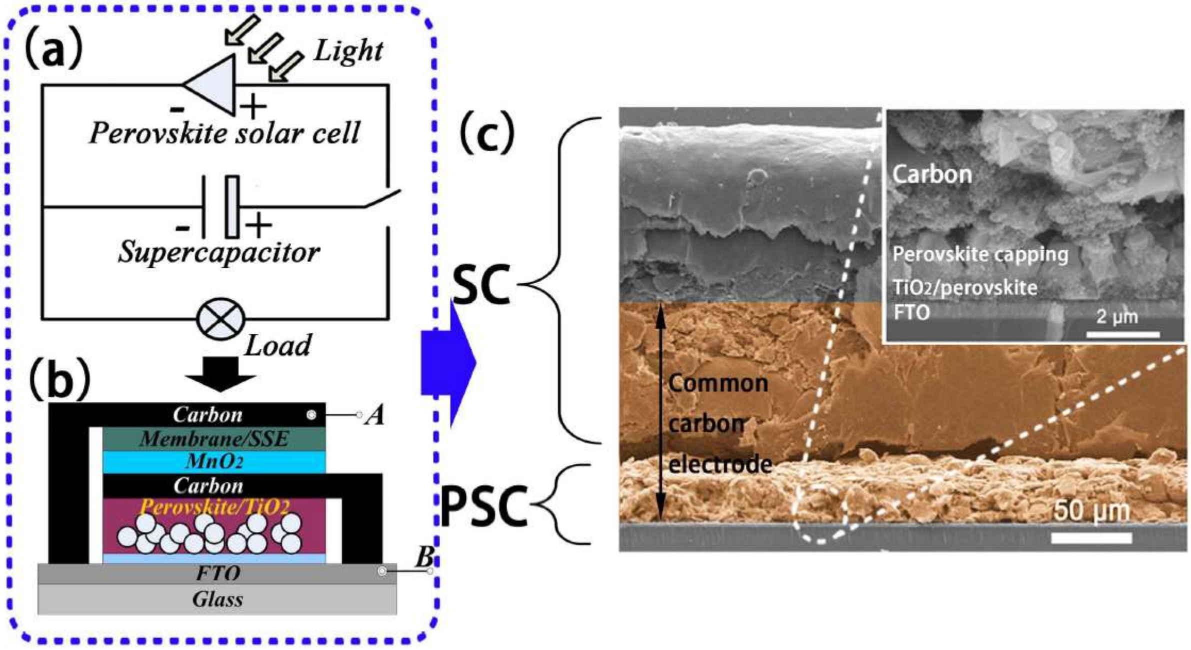

Figure 67 Schematic illustration of the integrated device. Adapted and reprinted with permission from [71].

With an active area of 0.071 cm^2 and a white light illumination of AM1.5G, the achieved voltage was 0.84 V with a storage efficiency of 76% and an overall conversion performance of 5.26%. However, by pre-charging the SC to 1 V, an overall efficiency of 22.9% was achieved.

7.2.17 Liu et al.: Silicon Nanowire/Polymer Hybrid PV-SC (2017)

Liu *et al.* integrated a high-efficiency SiNWs/PEDOT PV cell with a polypyrrole SC [72]. The hybrid PV cell developed in this study demonstrated a 13% efficiency due to the technique of metal-assisted chemical etching with nanospheric lithography, which allowed precise control of the doping of the electrode substrate. The electrode surface was also modified using a surface passivation process based on chemical solvents. A titanium film was used as the common electrode between the two parts of the system. Thus, the device achieved a total efficiency of 10.5%. Figure 68 shows the schematic configuration of the two units of the system, with the upper part representing the solar cell and the lower part the supercapacitor. PEDOT was deposited by spin-coating on the SiNWs, while the polypyrrole film was electrochemically deposited on Ti.

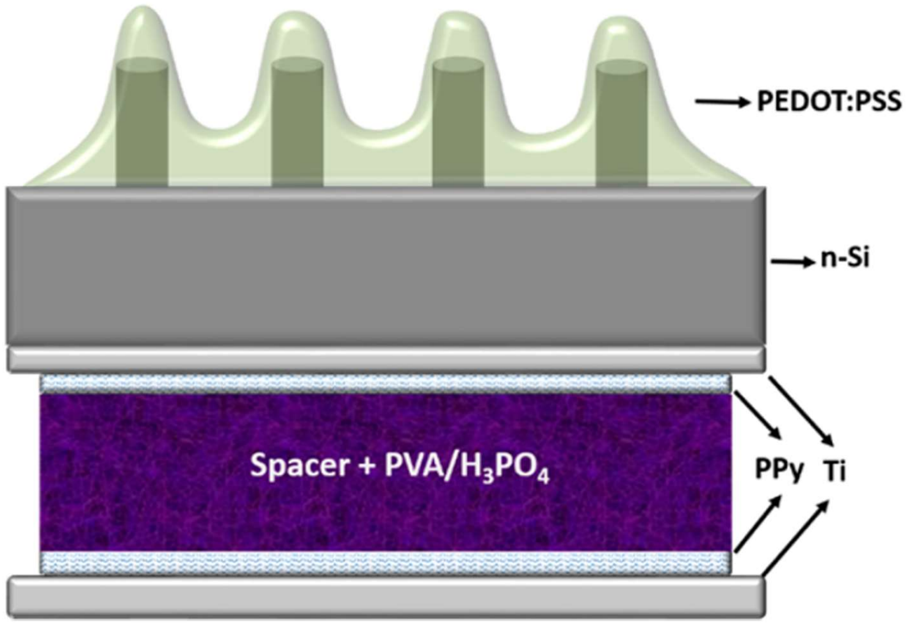

Figure 68 Schematic illustration of the integrated device. Adapted and reprinted with permission from [72].

By exposing the solar cell to an illumination of AM1.5G and connecting it to the SC, the voltage of the accumulator increased rapidly to about 0.55 V after 20 s of photo-charging, following the trend in Figure 69. At the same time, the photocurrent in the system decreased rapidly, meaning that most of the energy is correctly stored.

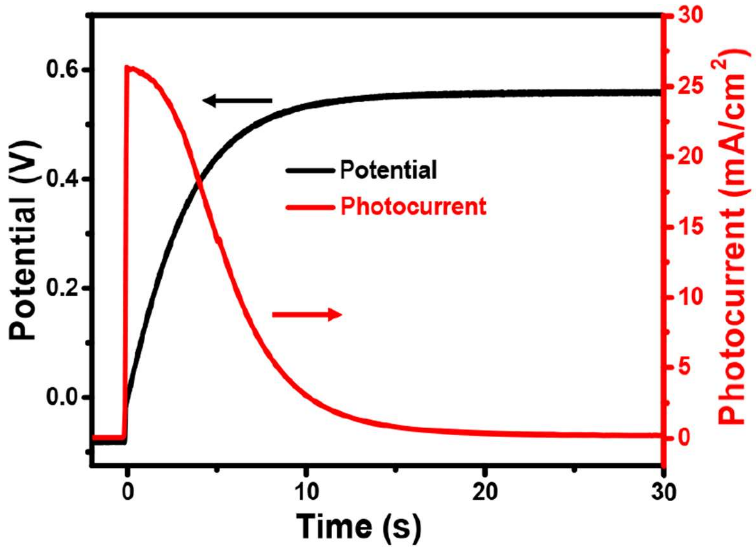

Figure 69 Voltage-time and the corresponding photocurrent-time profile for the hybrid solar cell. Adapted and reprinted with permission from [72].

7.2.18 Dong et al.: Integrated PV device (2017)

Dong *et al.* worked on an integrated flexible and printable system based on DSSC and SC [73]. This device was able to deliver up to 1.8 V and demonstrated very stable performance under a variety of operating, environmental and load conditions. The efficiency achieved by the DSSC was 2.8%, with a FF of 0.59. The highest current density delivered was 6.7 mA cm^{-2}, with a V_{OC} of 0.71 V.

7.2.19 *Ng et al.: Perovskite-DSSC for high humidity conditions (2018)*

Ng *et al.* realised a caesium-based perovskite-sensitised solar cell integrated with an asymmetric SC for application under high humidity conditions [74]. The cell was manufactured in an environment with humidity above 80% and tested in high humidity and under UV exposure. The cell showed a V_{OC} of 0.67 V, FF of 31% and J_{SC} of 2.2 mA cm^{-2}, with a conversion efficiency of 0.46%. The cell maintained 70% of its starting efficiency after one week in a dark dryer and 33% after 24 h under UV exposure and with a relative humidity above 80%.

7.2.20 *Liu et al.: Laser engraved SC and Si nanowires/PEDOT PV panel (2018)*

Liu *et al.* developed a PS based on Si nanowires array/PEDOT for solar radiation conversion structurally connected to a graphene SC made with laser engraving [75]. Through the use of surface passivation, photoelectric conversion efficiencies of 13.37% were achieved for a cell with 1 µm long SiNWs. The cell was then combined with a SC by a common gold electrode. The storage system showed a remarkable resistance to charge/discharge cycles, as shown in Figure 70 (bottom left) and proved to be very reliable. The overall efficiency of the system was 2.92%.

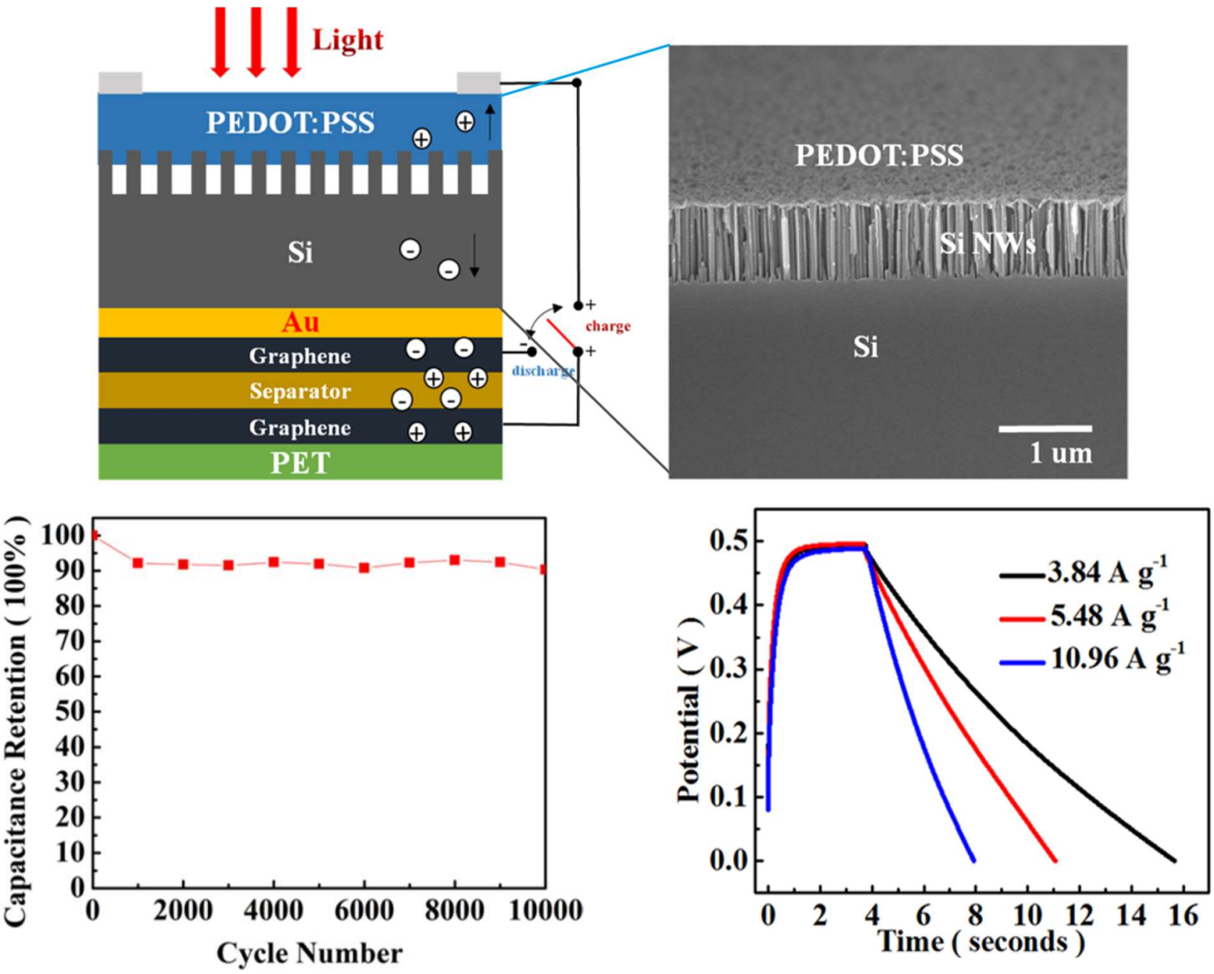

Figure 70 (top) Schematic illustration of the monolithic cell and microscopic cross-sectional scanning (SEM) of Si nanowires with PEDOT coating film; (bottom left) conservation of nominal capacitance evaluated by cyclic stress; (bottom right) charging curves at AM1.5G illumination and discharge in the dark at fixed current densities of 3.84, 5.48 and 10.96 A g^{-1}. Adapted and reprinted with permission from [75].

7.2.21 Yun et al.: Wearable solar device (2018)

Yun *et al.* worked on an innovative wearable and deformable electronic device [76]. The device consisted of several modules as shown in Figure 71, divided into three different types: Si-based PV solar cells, solid-state microSCs and a strain sensor. The interconnection of the modules was achieved by an extensible coil, which is able to guarantee the deformations of the substrate.

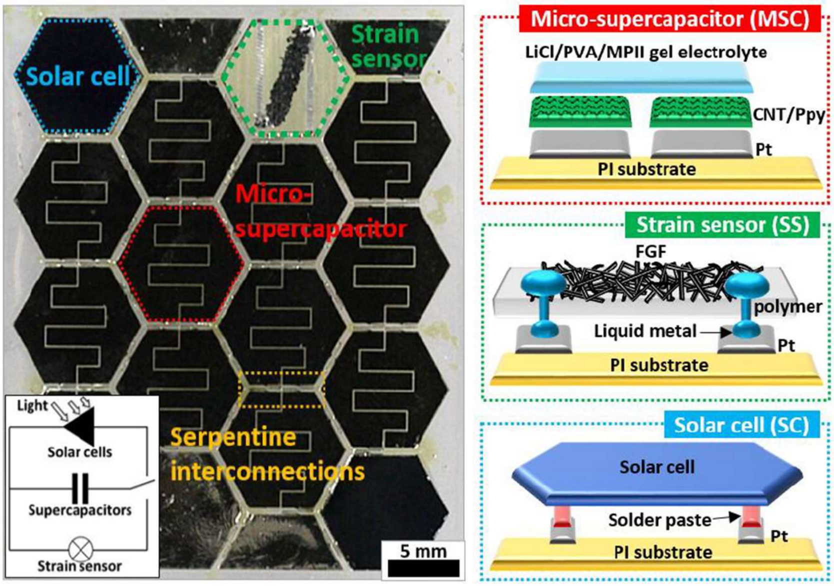

Figure 71 Optical image of the biaxially extendable device with the three different types of integrated modules. The circuit diagram and the components of the device are schematised on the side. Adapted and reprinted with permission from [76].

The device, developed to interact with the human body, was able to monitor signals created by external stresses. Its flexibility and extensibility ensured good adaptability, and reliability was provided by the fact that after 1,000 repetitive biaxial stretch/release cycles of 30%, no change in the charge/discharge capacity of the device was detected.

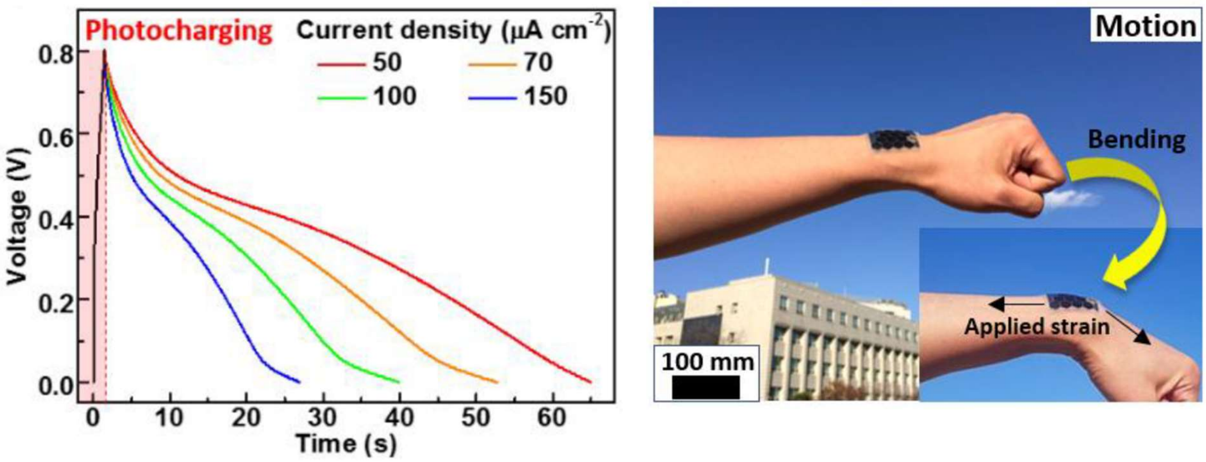

Figure 72 A) Charge-discharge curves of the PS device, charged by solar radiation, discharged at different current intensities and in dark conditions; B) Photographing the device during testing. Adapted and reprinted with permission from [76].

7.2.22 *Kalasina et al.: PV and SC in Ionic Liquid Electrolyte (2018)*

Kalasina *et al.* developed a monolithic cell for the conversion and storage of solar radiation based on alpha-cobalt hydroxide (α-$Co(OH)_2$) in ionic liquid [77]. This semiconductor material shows an optical band gap of 2.85 eV, generating a photoelectric effect; research has always been focused on its stabilisation in liquid electrolytes. Instead, the authors used a solution of 1-butyl-1-methylpyrrolidinium dicyanamide (BMpyr)(DCA) to replace KOH electrolyte. The accumulation showed 100% coulombic efficiency and 99.99% retention capacity after 2000 cycles.

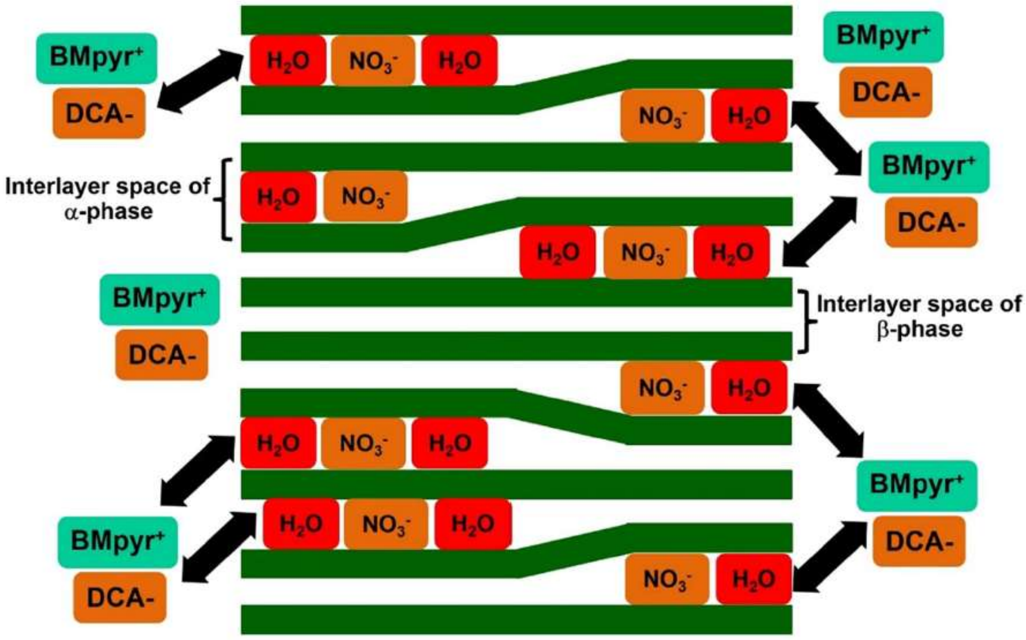

Figure 73 Schematic of the $Co(OH)_2$ layer; α-phase contains solvent nitrate anions in its interlayer, while the β-phase contains no anions in its interlayer. Without polarisation, the ionic liquid electrolyte mainly adsorbs on the outer surface of $Co(OH)_2$. Adapted and reprinted with permission from [77].

7.2.23 *Yuan et al.: Integrated system with hybrid battery-SC devices (2019)*

Yuan *et al.* fabricated a device for PV energy production and storage based on the use of a hybrid battery with three-dimensional hierarchical $NiCo_2O_4$ array technology as a faradic electrode, with a capacitive activated carbon electrode [78]. The PV cell used was a-Si/H solar cell, assembled with the storage system having energy density of 16.6 Wh kg^{-1}, power density of 7285 W kg^{-1} and resistance to 100% charge/discharge cycles after 15,000 cycles (Figure 74).

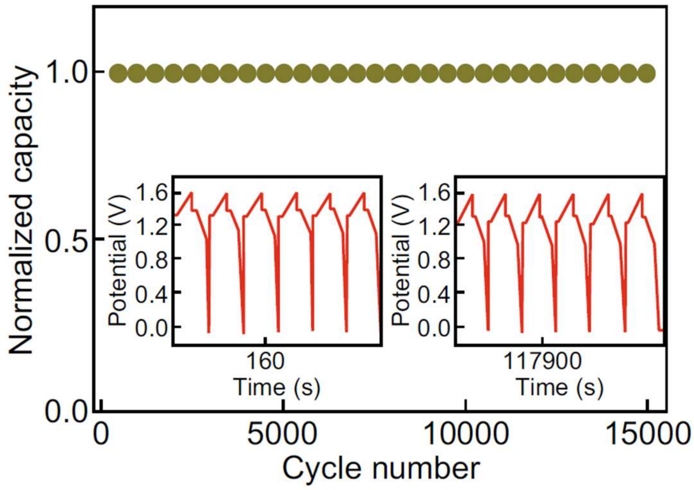

Figure 74 Graph of charge cyclic stability for a current of 20 mA cm^{-2}. Adapted and reprinted with permission from [62].

The system was tested to be capable of autonomously and reliably powering a LED light, demonstrating an overall efficiency of 8.1%, with a storage efficiency of 74.42%. To achieve these results, a structure consisting of a $NiCo_2O_4$ nanowire core covered by a shell of different $NiCo_2O_4$ nanowires, was implemented. Each nanoflake was parallel to a nanowire, as visible in Figure 75, obtained by a scanning electron microscope (SEM). This layout made it possible to create channels that were highly permeable to the electrolyte.

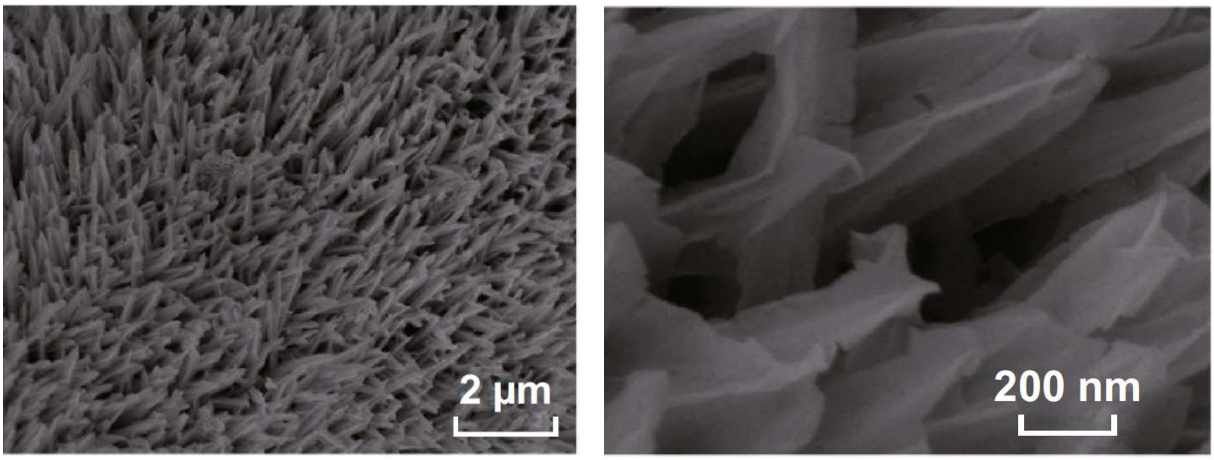

Figure 75 Low and high magnification scan of the 3D structure of the accumulator. Adapted and reprinted with permission from [78].

7.2.24 Chuang et al.: SC based on graphene-doped activated carbon (2020)

Chuang *et al.* prepared a flexible SC using graphene-doped activated carbon and integrated it with a DSSC to make a flexible monolithic device [79]. The device was then tested in a dedicated circuit to power a LED. A special firing technique was used to produce the basic material for the SC, activated carbon treated with a graphene powder additive. This paste was deposited by spin-coating to form the electrodes of the storage device. The resulting SC, with a graphene content of 0.05 wt%, showed a remarkable charge capacity of 218 F g^{-1} with a working efficiency of 85.29%. The flexibility of the device did not affect its characteristics, having high performance even under bending.

Figure 76 Photograph of the SC during a bending test. Adapted and reprinted with permission from [63].

7.2.25 Orozco-Messana et al.: Realization of a SC based on a ceramic tile (2020)

Orozco-Messana *et al.* investigated the possibility of using ceramic substrates for the realisation of a monolithic device for electricity generation and storage [80]. The study focused on the use of a Cu_2O/ZnO heterojunction PV cell coupled with a SC based on a ceramic tile. Starting from a porous stoneware tile, an electroless conductive Ni-Mo-P layer was deposited by exploiting its infiltration into the porosity of the substrate. A p-Cu_2O/n-ZnO heterojunction was deposited on the open conductive surface.

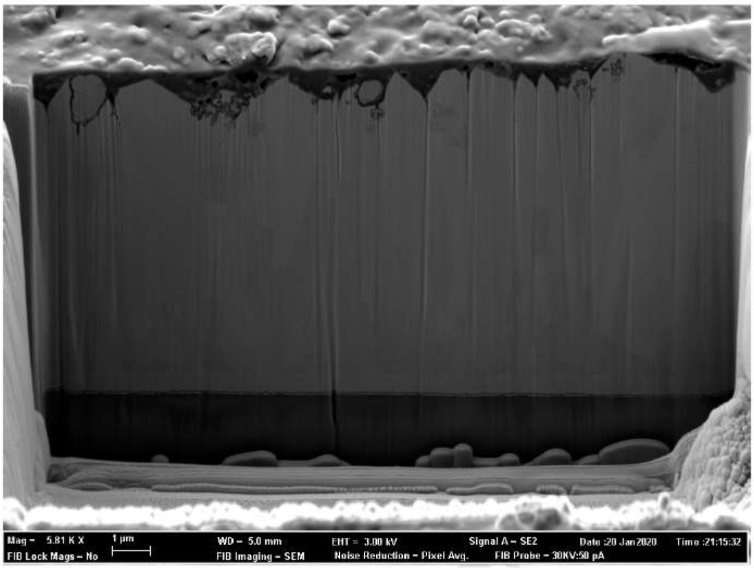

Figure 77 Cross-section of the joint made on the ceramic tile. Adapted and reprinted with permission from [64].

The resulting ceramic tiles proved to be able to perform as a SC and store electrical energy with an excellent energy density of 26.3 Wh kg^{-1} and a power density of 2.92 kW kg^{-1}. The resulting SC was connected to a low-cost PV cell, but the greatest achievement remained the fabrication of a self-sustainable device from a commercial facade tile.

7.2.26 Yue et al.: Estimation of the charge of a SC (2020)

Yue *et al.* worked on a new methodology to measure the state of charge of a SC so that its operation could be optimised [81]. A methodology was developed and, by analysing the leakage discharge current, it made it possible to assess the charge of the SC even after a long time elapsed since it was recharged. The study was pursued because of the growing interest in SCs in Internet of things (IoT) applications. Due to the difficulty in assessing the charge of a SC-based device, it is critical to define new analysis methodologies. The proposed method provided a new point of view, useful for the implementation of these devices and the future of IOT.

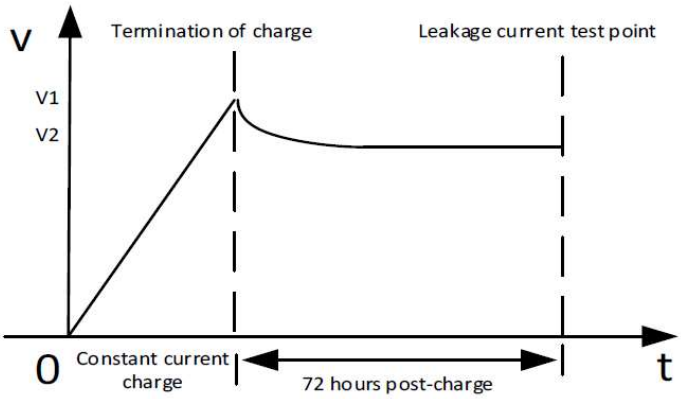

Figure 78 Self-discharge pattern of a SC. Adapted and reprinted with permission from [81].

7.2.27 Qin et al.: PS semi-transparent and flexible $Ti_3C_2T_x$ MXene-based (2020)

Qin *et al.* took advantage of the properties of MXenes and developed a monolithic integrated PS device based on semi-transparent and flexible $Ti_3C_2T_x$ MXene [82]. Using the spin-casting technique, films of $Ti_3C_2T_x$ nanoflakes aligned parallel to the substrates were produced. With the help of the transfer-printing method, the previously obtained transparent films were used as electrodes for the transparent device under development. The device achieved a conversion efficiency of 13.6% and a storage capacity of 502 F cm^{-3} with excellent cyclic stability and a storage efficiency of 88%.

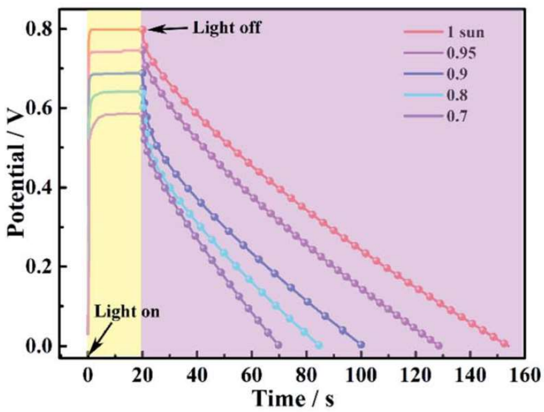

Figure 79 Photographic charge of device subjected to different levels of light irradiation and galvanostatic discharge at 2 A cm^{-3}. Adapted and reprinted with permission from [82].

7.2.28 Liu et al.: Ultra-flexible PS system (2020)

Liu *et al.* developed flexible, biocompatible PS devices designed to provide the energy needed to operate possible next-generation biomedical devices or wearable electronics [83]. With a thickness of just 50 µm, this device achieved a total efficiency of almost 6%. The SC, made of carbon nanotubes/polymers, was 40 µm thick. The stability of the device showed an efficiency retention after 100 cycles of over 96% and 94.66% after 5000 bending cycles.

8 MATLAB simulation

From the publications reviewed above, it has emerged that there is a growing interest in the scientific community in integrating different storage technologies to optimise their overall performance by exploiting the strengths of the individual devices. These studies have mainly focused on the possibility of using SCs to manage power peaks by reducing the load normally handled by batteries alone. The hybrid storage derived from them has thus proved to be a valid alternative to traditional energy storage systems, leading to greater grid stability and reducing the characteristic fluctuations associated with PV systems.

The studies have always been focused on managing power peaks and reducing currents inside the batteries. In literature articles, an analysis aimed at considering the different deterioration due to the charge/discharge cycles suffered by the components of a hybrid battery has never been offered. To this end, the following simulation was implemented to simulate and study the cyclical deterioration of the components of a hybrid storage system, comparing it with the degradation of a conventional battery under the same conditions. Other parameters were also considered during the simulation, such as the duration of each cycle, the variation in performance as the SC capacity/total capacity ratio varies and the influences of the different efficiencies involved.

The analysis was managed by a MATLAB simulation, taking as a system the typical consumption of a single-family house in Northern Italy with a household of 2-3 people. The PV production system and the related hybrid storage system were sized on the consumption of this typical house.

8.1 Load definition

To properly size the various components of the system, it is necessary to study the loads to which it will be subjected. In order to define the load, it is therefore necessary to study the instantaneous powers involved and their distribution over the reference time frame.

It is therefore essential to define the main characteristics of the system in question so as to be able to predict and reproduce the annual electricity consumption as faithfully as possible. The characteristics analysed are:

- **Type of user:** the consumption profile of a user is intrinsically linked to the type of consumer and the operating time. The load in question refers to that generated by a domestic user and will therefore be characterised by large differences in consumption between day and night.
- **Time steps:** in order to approach the system correctly, it is necessary to analyse it with the appropriate precision and using the most suitable time step for the type of analysis required. To analyse the powers involved, the length of the time steps should be reduced to the minimum, in that case the optimal time interval would be of seconds or fractions of a second. If, on the other side, it is necessary to analyse the energies exchanged in the system, as in this simulation, the time steps can be extended. The time step taken into account for this study is equal to 10 min, this value was considered as a good compromise between accuracy and reliability for the analysis of the energies exchanged.
- **Consumption variability:** due to the various actions performed daily in the home, it was necessary to simulate different scenarios of daily energy consumption, assigning to each of them a different probability of occurrence. For this reason, four load curves were created for working days and two for holidays. The load curves differ from each other in peak intensity and distribution of consumption over the day. A different probability of occurrence has been assigned to each load curve. Using this value, the simulation will assign a different consumption profile day by day.
- **Air-conditioning system:** one of the main sources of electricity consumption in households is the summer and winter air-conditioning system. The dwelling under consideration has a heat pump as a summer air conditioning system. The thermal energy for winter heating is managed by an external source (district heating, central heating, gas boiler, ...). It will therefore be necessary to increase consumption during the summer months in order to best represent this condition. This scenario is the best in order to optimise self-consumption, as the pattern of electricity consumption follows that of solar production.

The values at the base of the analysis were measured directly by the electric meter placed in a house with consumption similar to that under examination. In this way it was possible to identify three different basic levels of consumption, which can be defined as: night-time, daytime with lights off and home with lights on. These values were taken with their uncertainties and form the baseline values for the different load curves.

Table 7 Basic consumption levels, derived from the analysis of consumption in a real house, divided by the moment of the day.

	[W]	[ΔW]
NIGHT-TIME	120	20
DAYTIME WITH LIGHTS OFF	215	40
LIGHTS ON	280	50

Possible consumptions derived from the use of household appliances and equipment at different times of the day are added to the values thus obtained. The load curves differ for different types of devices used during each day and for the relative time and duration of operation.

Table 8 Consumption values of the electrical equipment and devices considered with relative ranges of variance.

	[W]	[ΔW]
WASHING MACHINE	1100	300
VACUUM CLEANER	900	200
OVEN	800	200
MICROWAVE	500	200
TV	300	100
COMPUTER	50	20

The load curves, which are essential for the actual simulation, can be developed on the basis of the previous assumptions, the sampled values and the considerations made.

8.1.1 *Working day*

- *Working day 1*

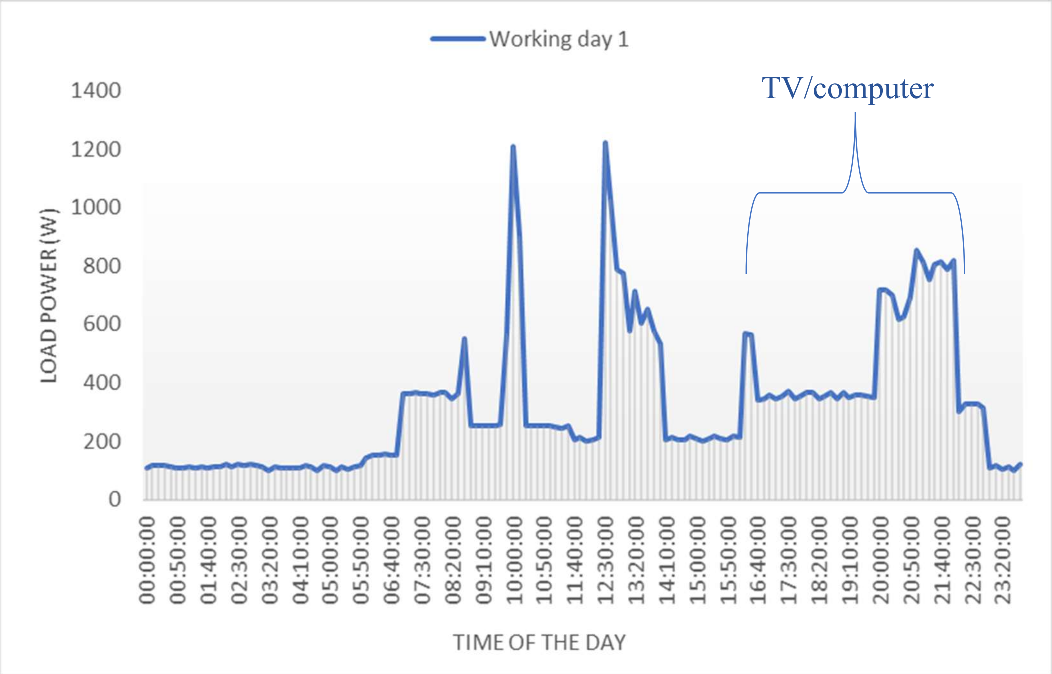

Figure 80 Working day 1.
(h 10:30) Use of vacuum cleaner and household cleaning.
(from h 12:30 to h 14:00) Preparing lunch with microwave oven and TV on.

- *Working day 2*

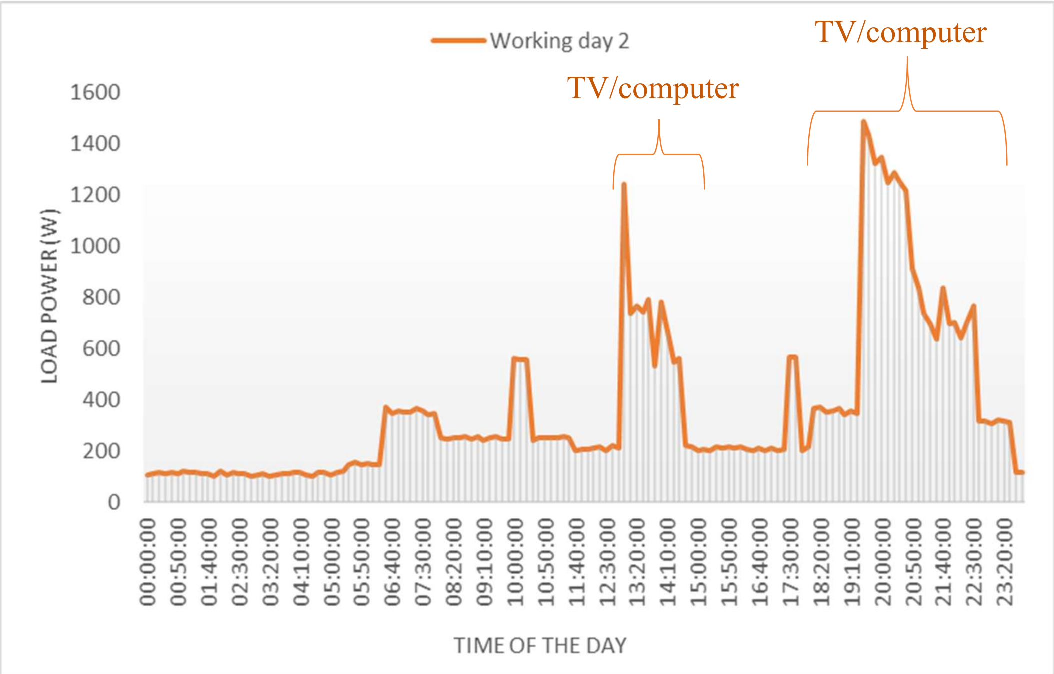

Figure 81 Working day 2.
(from h 13:00 to h 14:30) House cleaning.
(from h 19:30 to h 20:30) Oven on.

- *Working day 3*

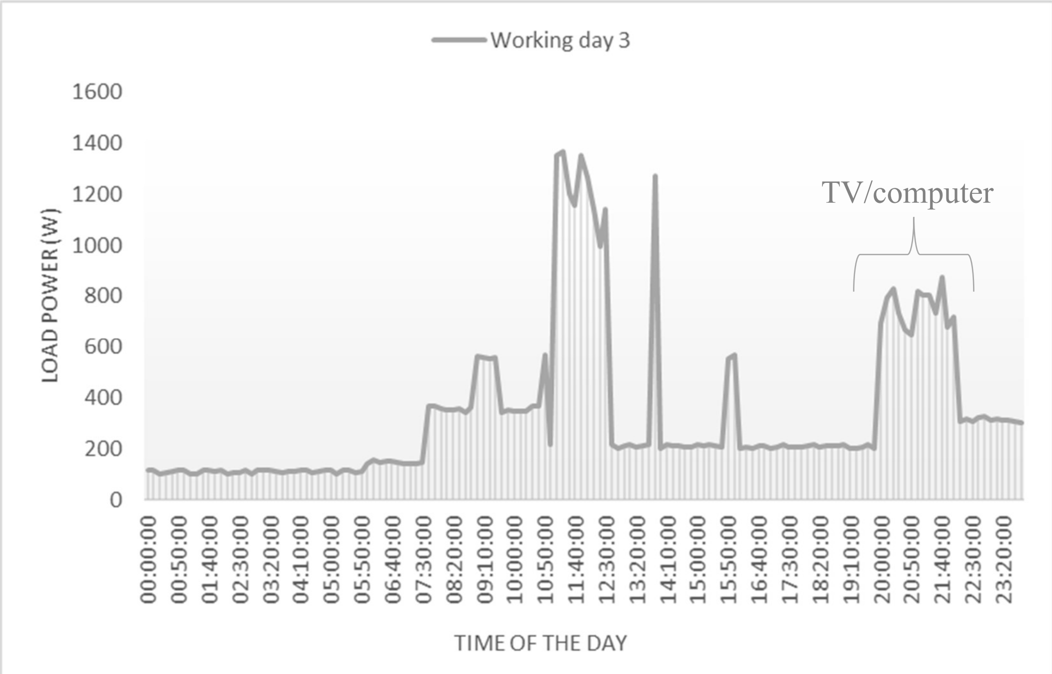

Figure 82 Working day 3.
(from h 11:10 to h 12:20) Washing machine.
(h 13:50) Use of vacuum cleaner and household cleaning.

- *Working day 4*

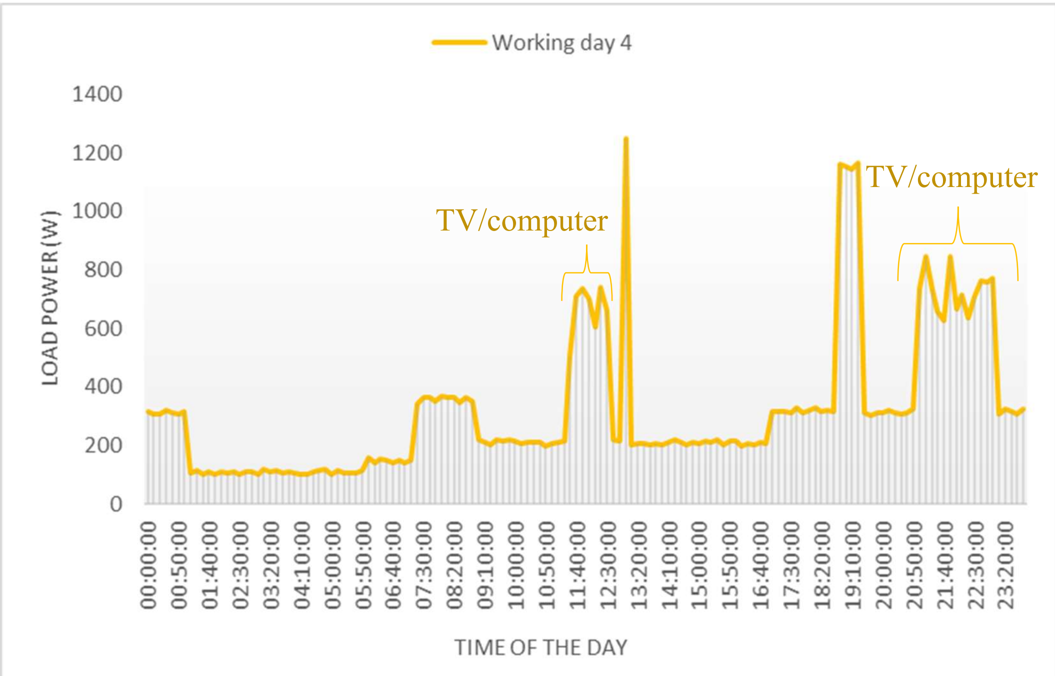

Figure 83 Working day 4.
(h 13:00) Use of vacuum cleaner and household cleaning.
(from h 18:50 to h 19:00) Oven on.

8.1.2 Holiday

- *Holiday 1*

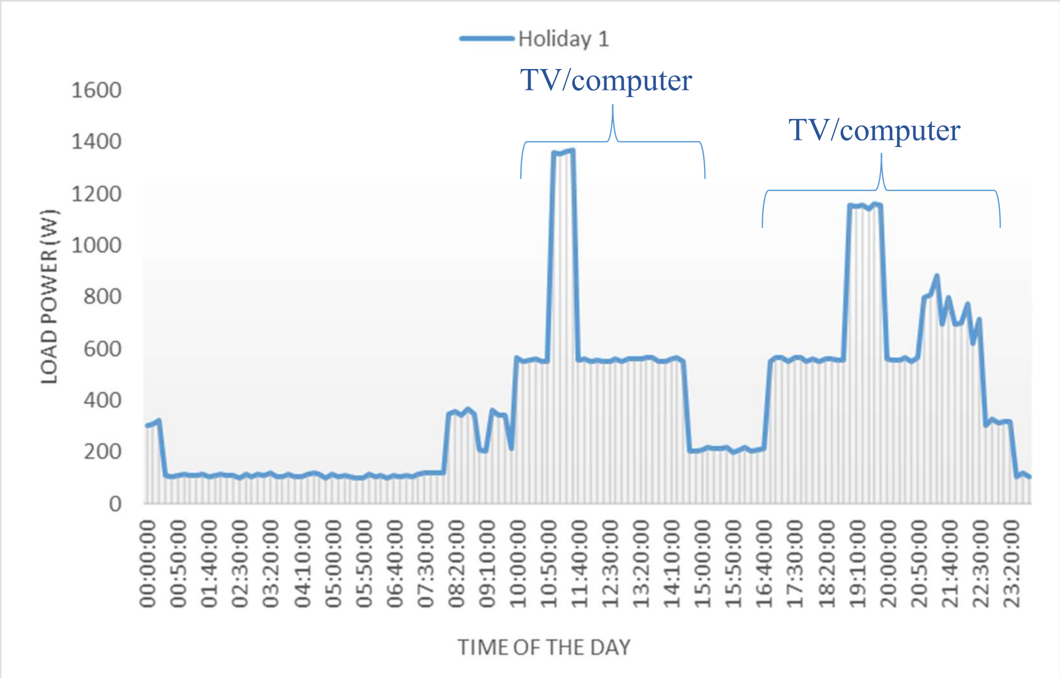

Figure 84 Holiday 1.
(from h 11:00 to h 11:30) Washing machine.
(from h 19:00 to h 20:00) Oven on.

- *Holiday 2 (day off, no one at home before h 20:00)*

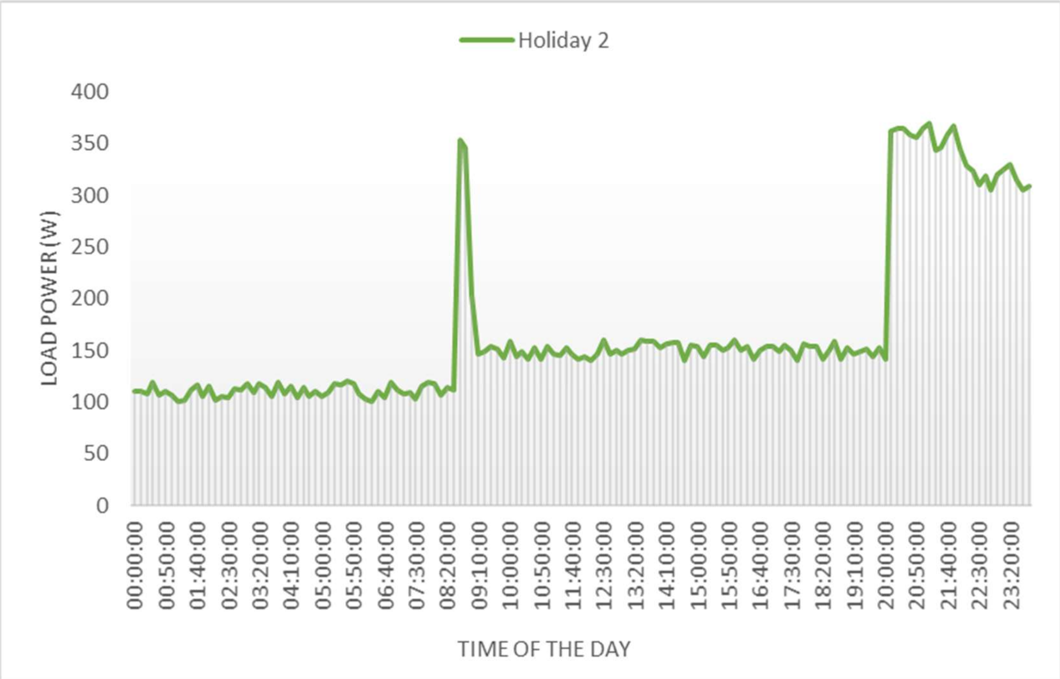

Figure 85 Holiday 2 (day off, no one at home before h 20:00).

8.1.3 Average daily electricity use

To ensure non-repetitiveness of the load curves, the following equation was introduced into the program:

$$Load = Load + Load \times \left(rand - \frac{1}{2}\right)$$

"Load" means the power value extracted from the Excel document containing the different load curves, to which is subtracted or added a variable quantity between zero and half its value. Using this equation, it is possible to reproduce the non-linearity and high variability of domestic loads, variations caused by the numerous electrical appliances present in a normal home (refrigerator, freezer, water pumps, lighting, ...).

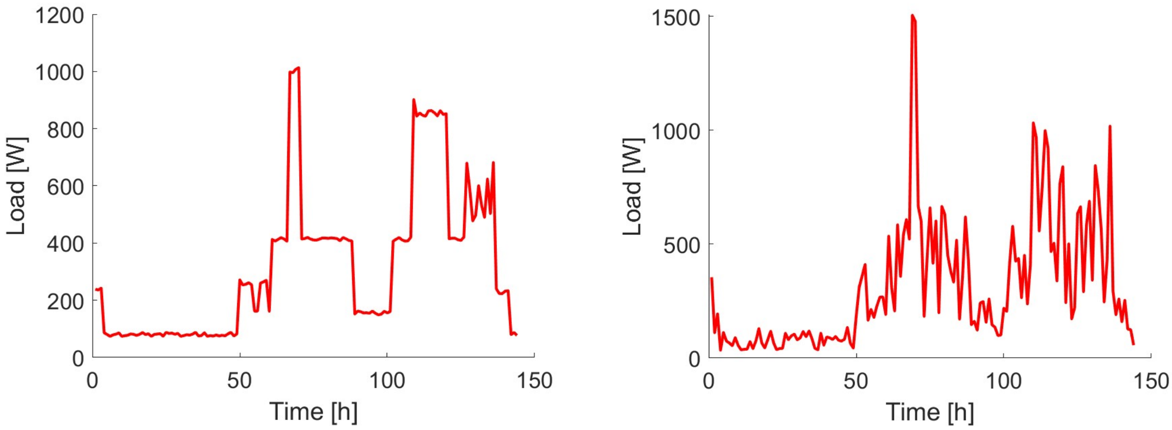

Figure 86 Comparison of the same load curve with and without uncertainty.

The average daily load profile obtained from the MATLAB analysis is shown below; the resulting graph takes into account the average of the values obtained during the simulation.

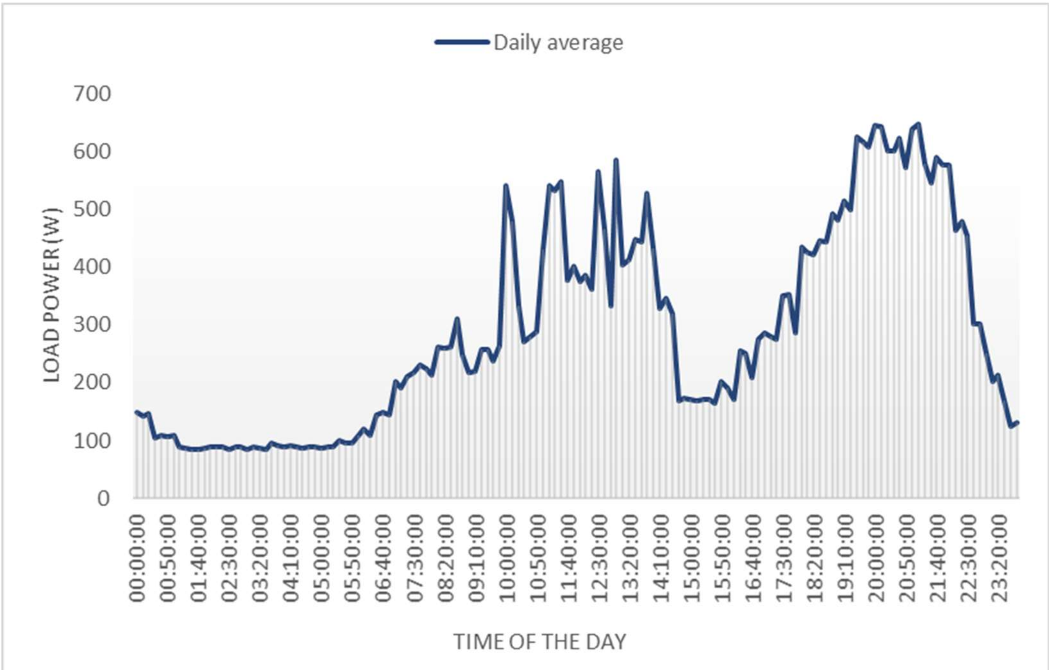

Figure 87 Average daily load curve of the house under investigation analysed over the whole year.

The validity of the values obtained can be seen by a visual comparison between the experimental load curve and the statistical mean value shown in the graph below. This graph shows the annual average consumption of a house with similar characteristics to those taken into consideration in this analysis.

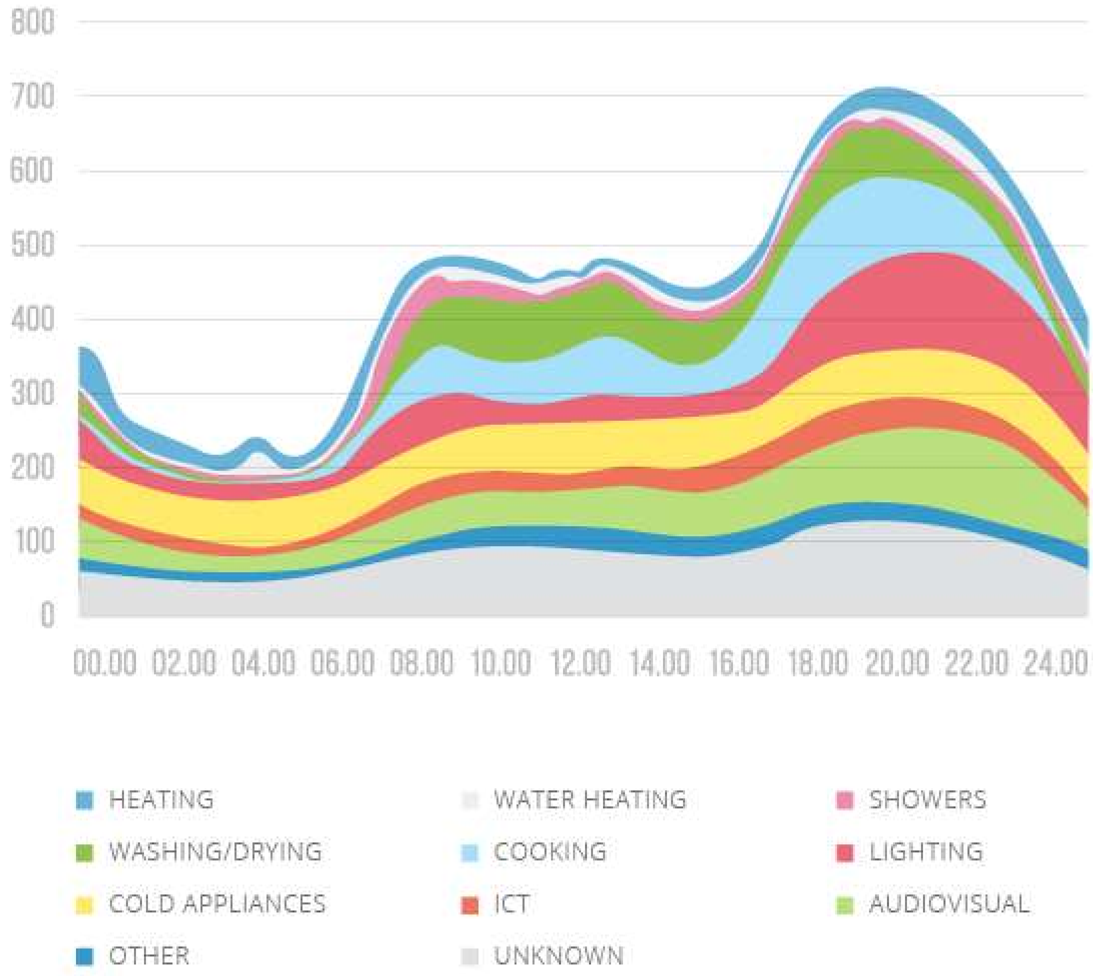

Figure 88 Estimation of the average daily load curve of a typical house. Adapted and reprinted with permission from [84].

8.1.4 Consumption ranges

The curves defined above make it possible to assess the annual consumption of the home. Dividing this consumption into time slots makes it possible to better define energy consumption and its distribution over time:

- **F1:** Monday to Friday, 8 a.m. to 7 p.m.
- **F2:** Monday to Friday, 7:00 to 8:00 a.m. and 7:00 to 11:00 p.m.
  Saturdays from 7 a.m. to 11 p.m.
- **F3:** Monday to Saturday, 11 p.m. to 7 a.m.
  Sundays and public holidays all hours of the day.

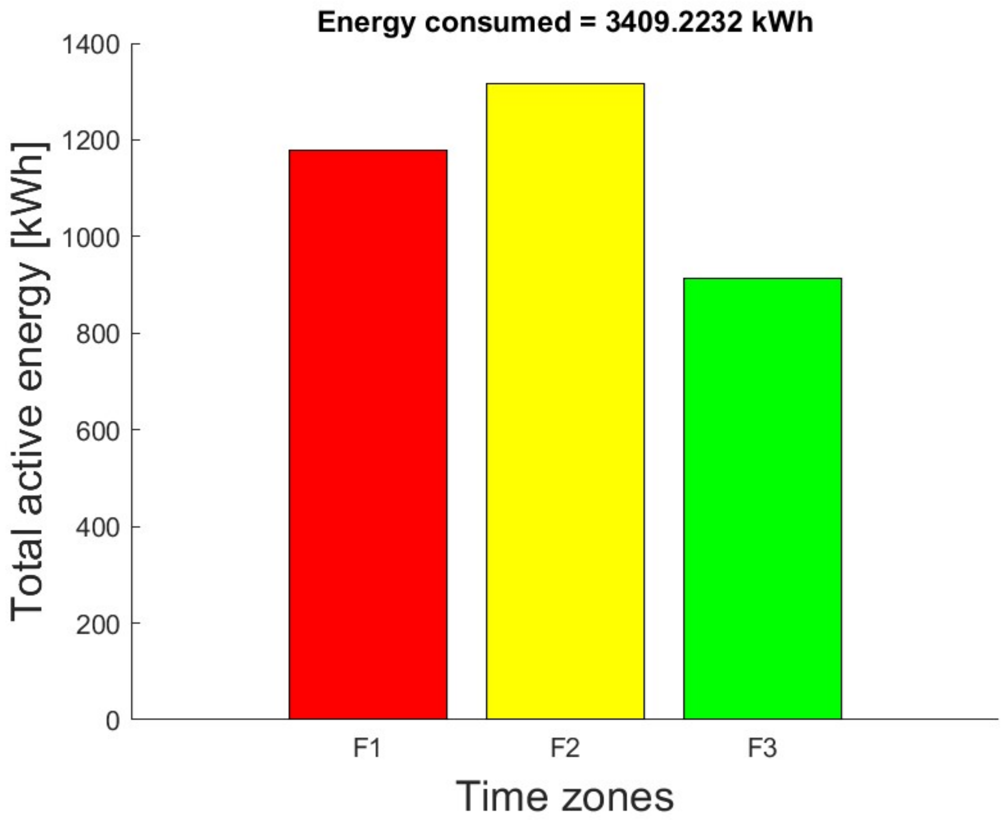

Figure 89 Analysis of the annual consumption of the building according to time zones F1, F2 and F3.

In the following graph it is possible to analyse the monthly distribution of the three different consumption bands, in accordance with the assumptions made previously the peak of consumption occurs in the summer months.

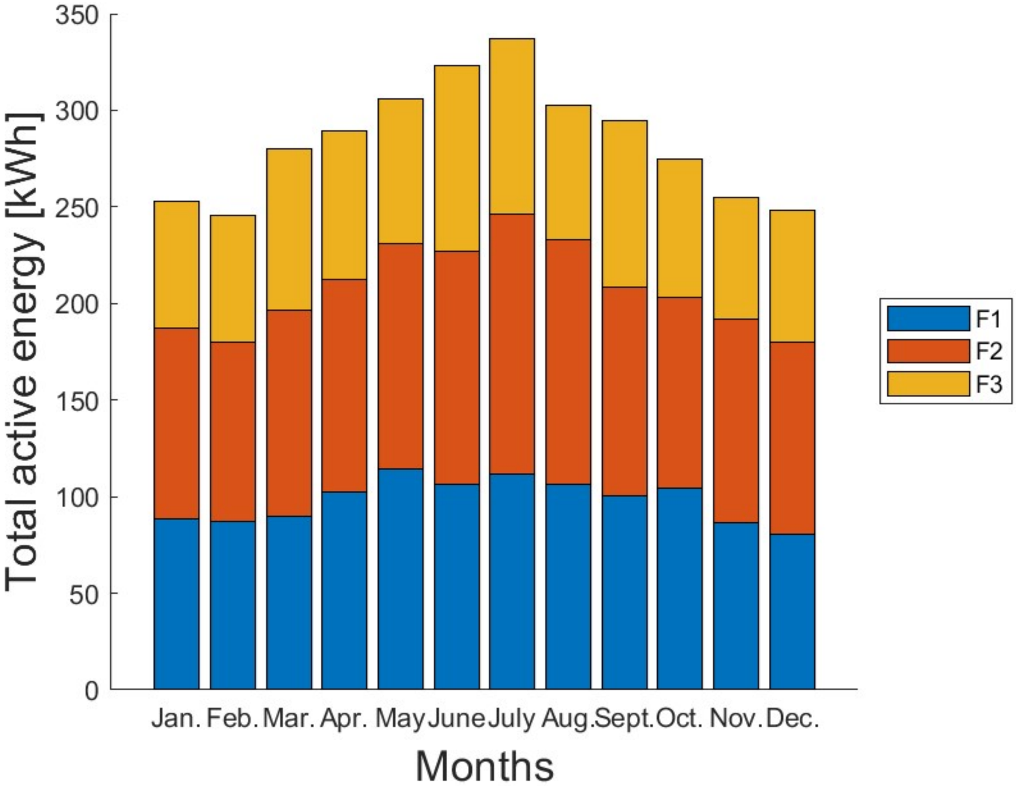

Figure 90 Analysis of the consumption of the building, grouped per month, divided into F1, F2 and F3 time zones.

8.2 Plant dimensioning

In order to analyse the producibility of the PV system, the meteorological and irradiation conditions in 2016 for the city of Turin were taken into account. The study was carried out using the "Photovoltaic Geographical Information System (PVGIS)" application provided by the JRC EU Science Hub.

The system considered is composed of monocrystalline silicon panels, with system losses estimated at 14%. The geometric parameters chosen are those of maximum producibility, *i.e.* slope of 35° and azimuth of 0°. The panels have no solar tracking and are mounted free-standing.

The yield obtained in this way refers to a system with one kWp installed, the level of time accuracy of the data provided by the application is 1 h. It is therefore necessary to linearly interpolate the data during the MATLAB simulation in order to obtain the same time scale as the domestic load. The producibility values obtained in this way need to be multiplied by the actual size of the system installed.

In order to correctly size the system to be able to meet the energy demand and guarantee the correct recharge of the storage system, it is necessary to consider the electrical consumption defined in the previous analysis. The dimensioning was carried out following this procedure:

1. The average monthly load curve has been constructed for three reference months: March, July and December. The choice of months is not random. July and December represent the maximum PV production and the minimum, respectively. The month of March, on the other hand, allows us to study an intermediate condition, as it is absent of high PV production and high consumption.

2. The following graphs have been made, containing the overlapping of the average monthly production curves (referring to a 1 kWp PV system) and the average monthly load curve.

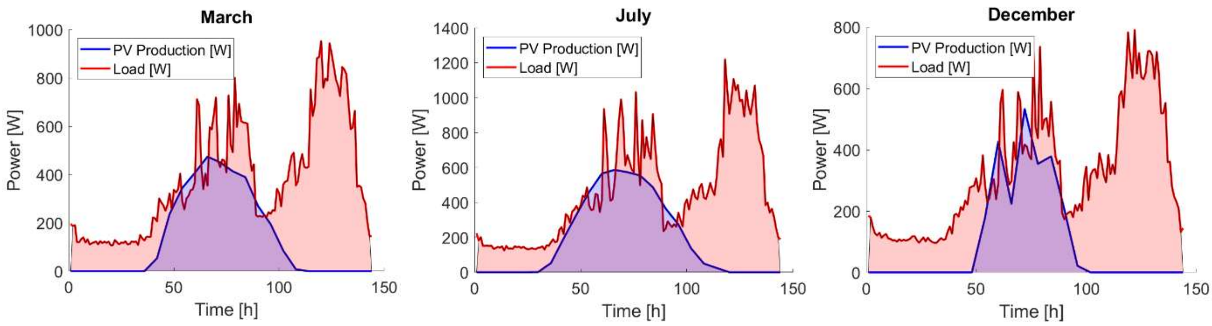

Figure 91 These graphs represent the average monthly production curves (referring to a 1 kWp PV system) and the average monthly load curve for the months of: (left) March; (middle) July; (right) December.

3. By varying the sizing of the solar plant, the power to be installed that best covered the average monthly consumption curve was determined. The analysis was carried out considering the areas under the curves. The installed peak powers obtained in this way are shown below and represent the share of the PV system dedicated to instantaneous self-consumption.

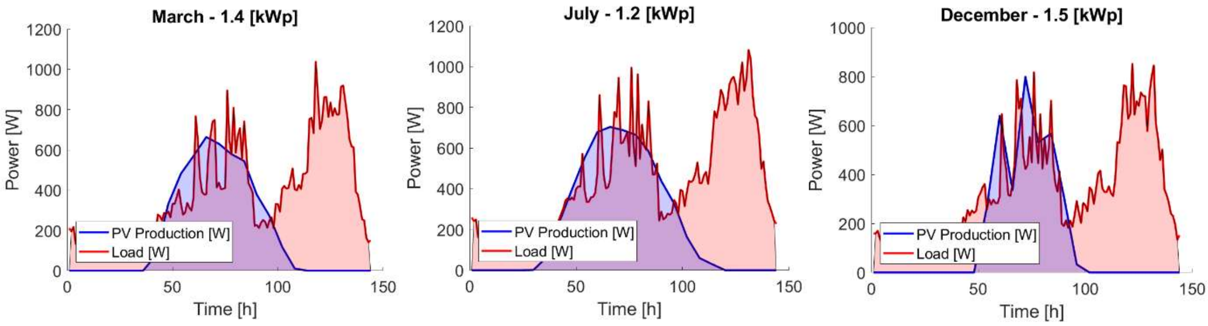

Figure 92 Graphs showing the average monthly PV production and electrical load situation for the different sizes of the chosen PV system. (left) March, 1.4 kWp; (centre) July, 1.2 kWp; (right) December, 1.5 kWp.

In order to optimise self-consumption over the whole year, it is a good idea to use the month of March as the optimal time. This first phase of the study does not take into account accumulation, but only direct consumption.

4. It is now necessary to consider the values of the total areas underlying the graphs. In order to find the missing energy share so that we have a value on which to base the dimensioning of the accumulator. A value of 1.4 kWp was kept as the PV system size for the following simulations.

Table 9 Data from preliminary simulation with 1.4 kWp PV power installed.

[kWh]	March	July	December
Load	9.187	10.307	8.138
PV Production	4.659	6.510	3.251
Missing Energy	4.528	3.797	4.887

The difference between the average load and the energy produced represents the missing energy, *i.e.* the size of the storage tank. The possible storage capacity values range from 3.8 kWh (calculated in July) to 4.9 kWh (calculated in December). The first value would be optimal for the summer months, but would be significantly undersized in the winter months, while the second value would be oversized in the summer period. It is necessary to find an intermediate value in order to optimise the system in both situations, as done above, the value of the missing energy of March can provide considerable help. An accumulator with a total net capacity of 4.5 kWh could be a good compromise.

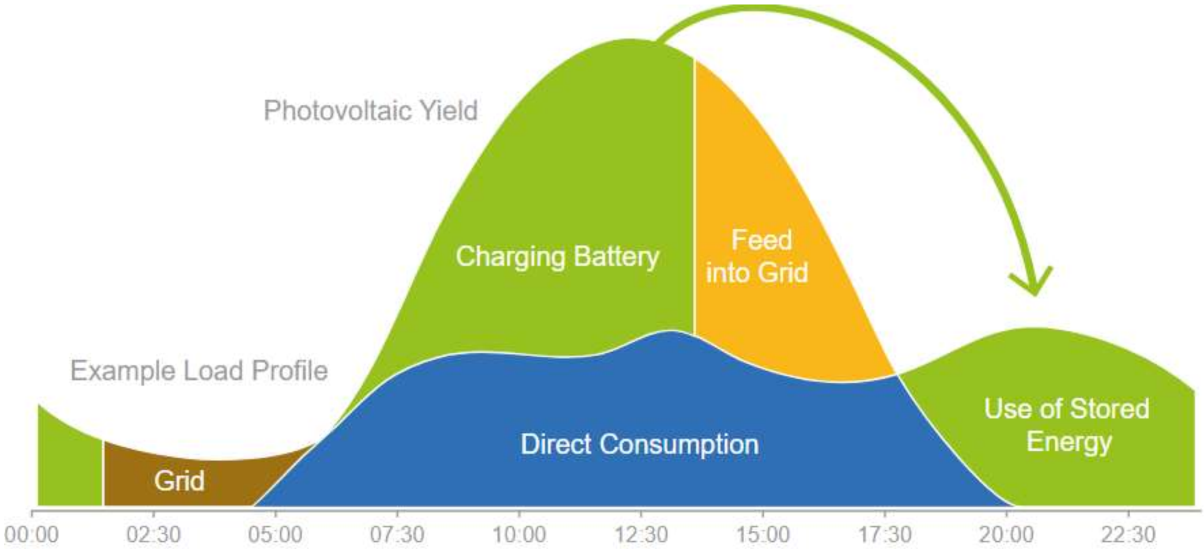

Figure 93 Illustrative diagram concerning the use of accumulators to manage the evening and night-time electrical load. Adapted and reprinted with permission from [85].

By inserting the accumulator, the excess current produced by the PV system during the day will be stored in the batteries for future use. The dimensioning has not been designed in such a way as to guarantee the self-sufficiency of the system. The grid will therefore be used to sell the electricity in excess of the storage capacity and to make up for production shortfalls.

5. Depending on the size of the storage tank decided upon, the PV system must be sized accordingly, so that it is able to fully utilise the storage tank without being oversized. This is done using the following equations:

$$Self - sufficiency = {(annual\ load - energy\ purchased\ from\ the\ grid)}/{annual\ load}$$

$$Self - consumption = {(annual\ load - energy\ purchased\ from\ the\ grid)}/{total\ production}$$

The following values of average energy sold and bought from the grid during an average day in March emerged from the plant simulation.

Table 10 Energy produced and energy purchased according to the size of the proposed PV system. The values refer to a typical day in March.

PV SIZE	SOLD	PURCHASED
kWh	kWh	kWh
1,40	0.00	4.77
2,00	0.23	3.46
2,50	0.99	2.83
3,00	2.08	2.41
3,50	3.36	1.97
4,00	4.88	1.73
4,50	6.19	1.65
5,00	7.89	1.52
5,50	9.51	1.39
6,00	10.96	1.32

From these values, self-sufficiency and self-consumption can be calculated, the aim of the analysis is to maximise both.

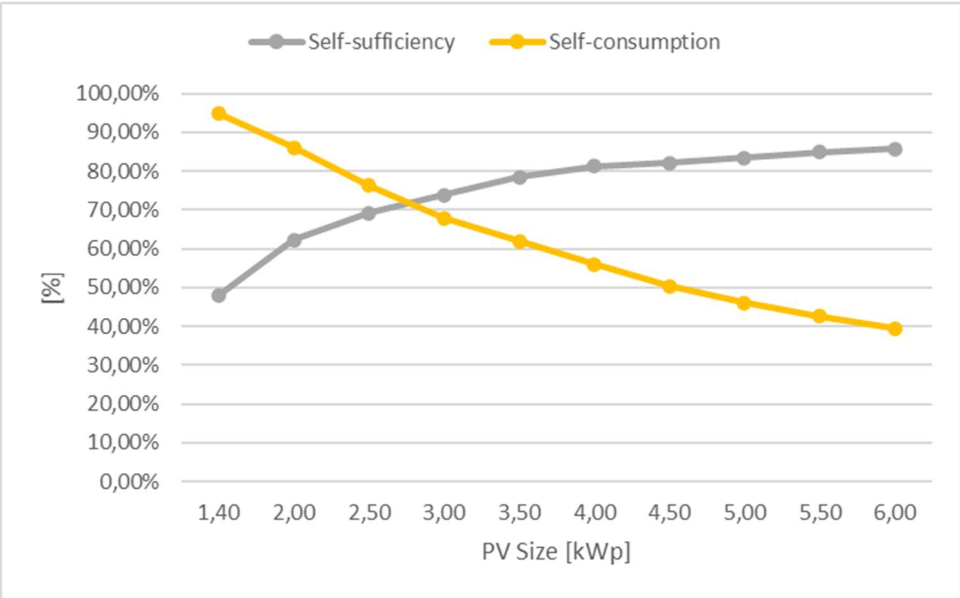

Figure 94 Trend of self-sufficiency and self-consumption values as the size of the PV system changes.

From the graph, it can be seen that the battery is slightly undersized as self-sufficiency tends asymptotically to 90% as the size of the PV system increases, but never reaches 100%. This was to be expected due to the assumptions made and the decision to adopt a total storage capacity of 4.5 kWh, which is slightly lower than what emerged from the previous analysis.

In order not to oversize the production plant, an acceptable self-sufficiency value of 80% can be considered. The installed PV power will be 4 kWp. A graph representing the average production, average consumption and average energy stored on an ideal March day is shown below.

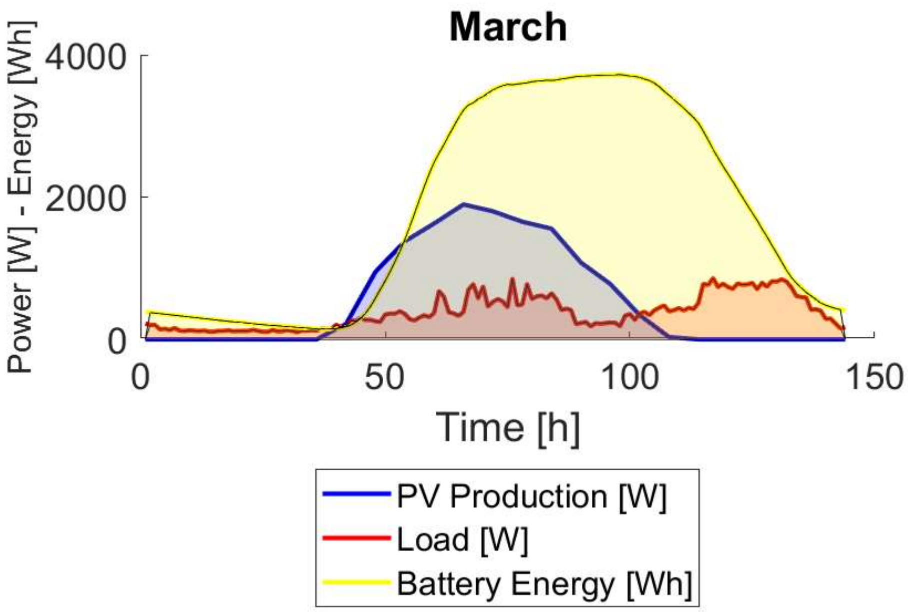

Figure 95 Diagram of the average power produced and consumed in one day in March. The energy stored in the battery during the same simulation is overlaid.

Statistically, the storage system is able to guarantee continuity of supply throughout most of the day.

In July and December the situation is also acceptable, with a good amount of residual charge in the accumulator even in the early hours of the day for the winter period.

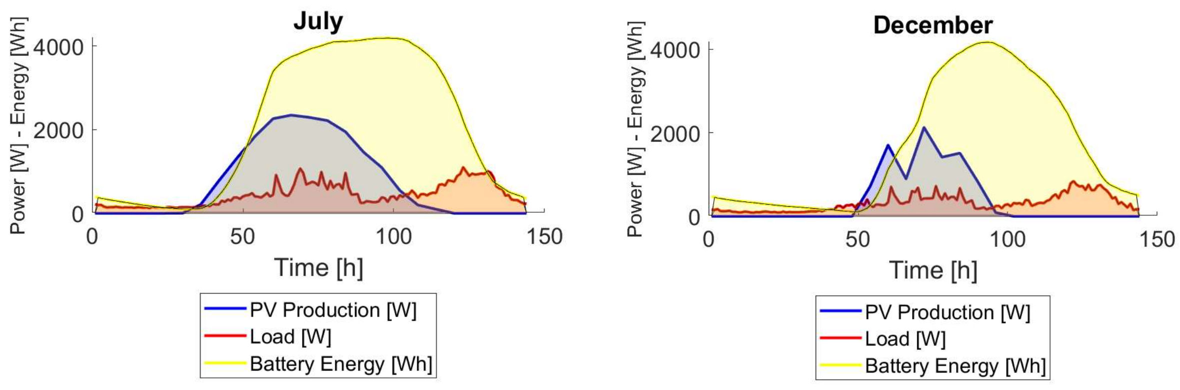

Figure 96 Diagrams of the average power produced and consumed on a day in (left) July and (right) December. The energy stored in the battery during the same simulations is overlaid.

An analysis of the annual graph showing the interaction of the generation system with the national grid reveals that the data are in line with expectations, with a production surplus in the summer months and a deficit in the winter ones.

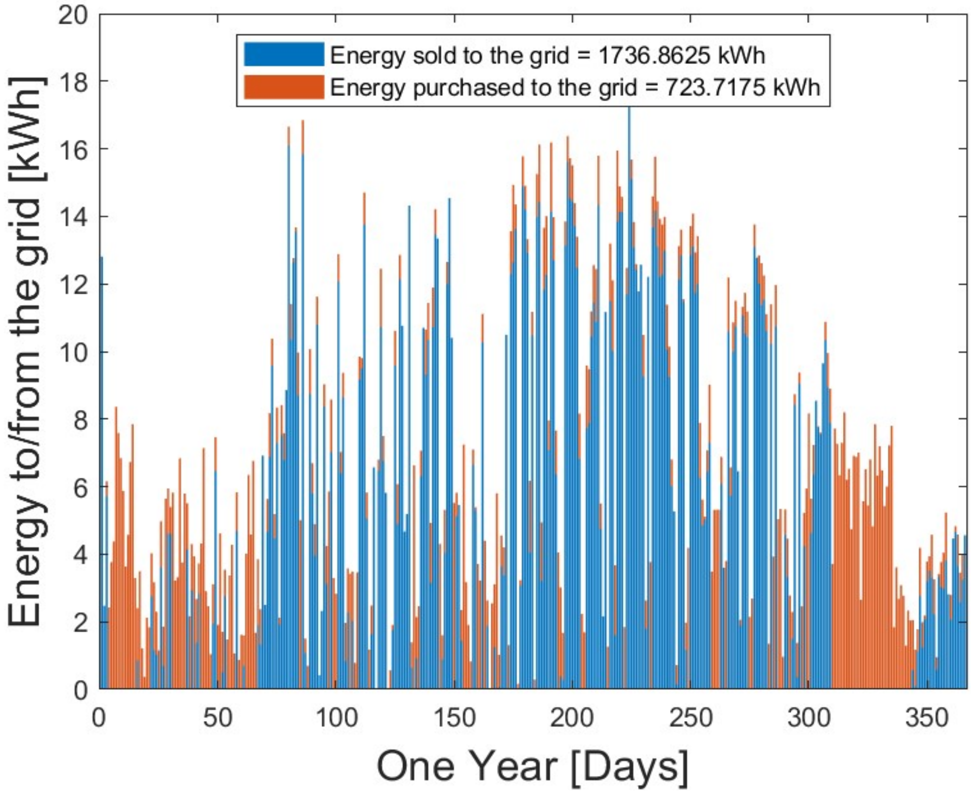

Figure 97 Annual graph showing the interaction of the generation system with the national grid (in the case of a 4 kWp PV system and a 4.5 kWh battery), in red the electricity purchased, in blue the electricity sold.

Considering the following values, the self-sufficiency and self-consumption parameters can be calculated on an annual scale.

Table 11 Annual report of energies involved for the chosen sizing.

Energy	[kWh/year]
Sold	1736.9
Purchased	723.7
Produced by PV	4552.7
Load	3409.2
Accumulator Losses	134.7

The loss data have been obtained assuming an accumulator efficiency of 90%. The analysis shows the following values:

Self-sufficiency = 78.77%

Self-consumption = 58.99%

Comparing these values with those prior to the installation of the storage system and with a PV system of 1.4 kWp shows an increase of 158.43% for the first factor (previous value of self-sufficiency = 30.48%) and a decrease of 9.51% for the second one (previous value of self-consumption = 65.19%). A graph of the interaction of the domestic system with the grid in the absence of the accumulator is shown below.

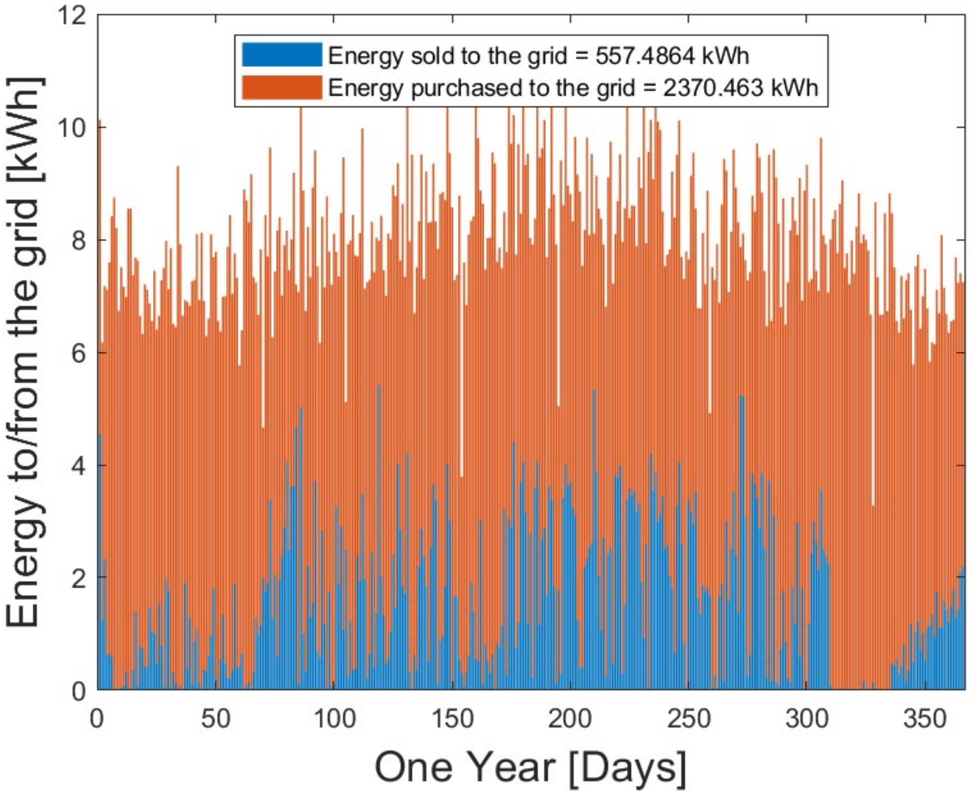

Figure 98 Annual graph showing the interaction of the generation system with the national grid (in the case of a 1.4 kWp PV system and in absence of storage), in red the electricity purchased, in blue the electricity sold.

The increase in self-sufficiency is due to the inclusion of the storage. This component has the function of increasing self-sufficiency even during the non-production hours of the PV system.

The decrease in self-consumption is due to the different purpose of the sizing chosen in the two systems. In the system with storage, the size of the PV array needs to be increased in order to recharge the batteries during the entire year. In the system without storage the instantaneous production must be maximised, which results in a smaller PV system size and reduces the amount of energy sold to the grid, thus increasing self-consumption.

8.3 SC sizing

After the dimensioning of the total storage capacity, it is necessary to analyse the size of the individual components of the hybrid system. The study focuses on the correlation between the size of the SC array and the reduction in the number of cycles completed by the battery. This reduction occurs because the priority use of SCs makes it possible to meet small power peaks without interrupting the battery recharging cycle by discharging it. This means that, in addition to a reduction in the number of annual cycles, it is possible to have longer and more complete cycles, thus ensuring less deterioration of the system.

The total capacities of the SCs assumed in the various simulations and the relative charge/discharge cycles performed by the battery are shown below. In order to optimise the system from an economic point of view, it is also necessary to take into account the increase in price caused by the introduction of the SC. By inserting the SC, there is also a reduction in the battery capacity and therefore its price, but this reduction has been neglected because it is insignificant compared to the overall increase [86].

Table 12 Data derived from simulations for sizing the SC, the cycles completed by the battery and the cost of the SC are taken into account. The prices are taken from the price list of "MAXWELL TECHNOLOGIES" [86].

SC Capacity [Wh]	SC Price [$]	N° of cycles - SC	N° of cycles - Battery	Reduction in Battery cycles [%]
0.0	-	-	1420	0
2.1	120	1420	1286	10.4
18.0	500	1420	912	35.8
27.0	750	1420	731	48.5
30.4	920	1420	706	50.3
34.4	980	1420	672	52.7
36.5	1100	1420	642	54.8
54.0	1350	1420	580	59.2
69.0	N/A	1420	532	62.5
96.0	N/A	1420	511	64.0

It can be seen that, after a sudden reduction in battery cycles as the SC capacity increases, there is an asymptotic trend towards a minimum number of cycles. This minimum number of cycles is due to day/night phases and large variations in producibility due to atmospheric factors. The size of the SC must be chosen correctly, as oversizing would not bring any benefits and would result in a considerable increase in economic expenditure.

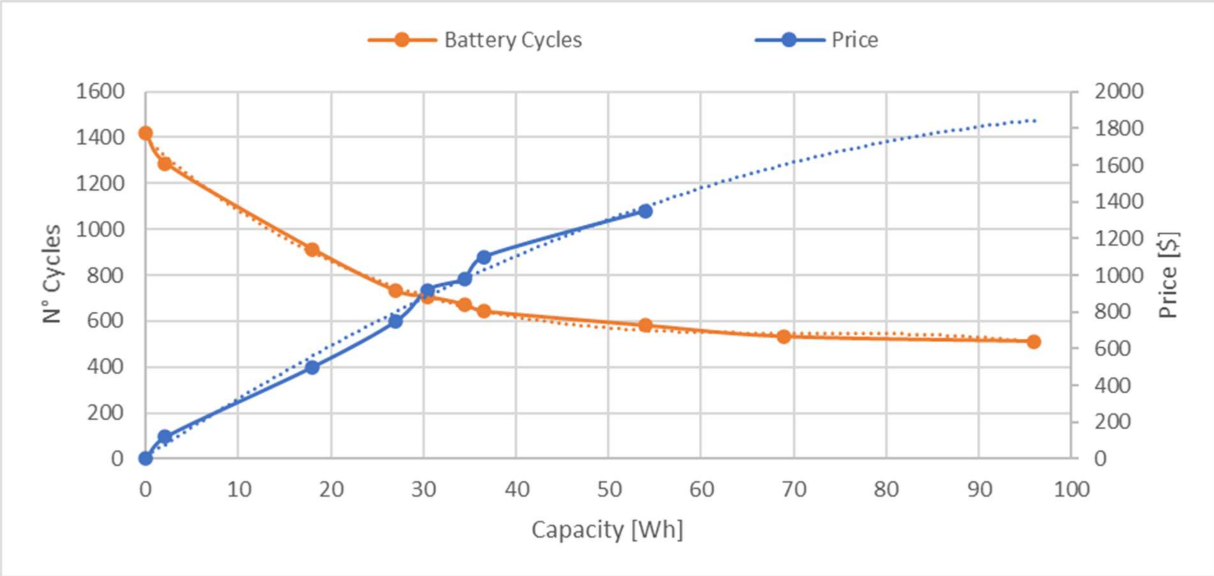

Figure 99 Diagram showing the decrease in the number of cycles for the battery in the hybrid accumulator and the increase in price due to the inclusion of the SC.

Considering the reduction of battery wear and the economic factor, it is acceptable to use an SC with a capacity of 36.5 Wh. This will result in a 54.8% reduction in the number of battery cycles.

8.4 Analysis of MATLAB code

This chapter examines the main points and programming logic that was adopted during the simulation. The full code can be found in the *Appendix A*.

8.4.1 Data initialisation

In the first part of the programme, it is necessary to initialise the various variables previously defined. By modifying these variables, the entire simulation can be affected by changing the boundary conditions.

```
TOT_Storage = 4.5e3;        %[Wh] Total installed storage capacity
TOT_SC = 36.5;              %[Wh] SC installed storage capacity

TOT_PV = 4;                 %[kWp] Total installed PV power

EffBa = 0.95;               % Battery efficiency for charge and discharge phases considered
                            separately
EffSC = 0.99;               % SC efficiency for charge and discharge phases considered
                            separately

ProbWor = [0.4 0.3 0.2 0.1]; % Probability assigned for each working day
ProbHol = [0.9 0.1];        % Probabilità di ogni gg festivo

Kmonths = 0.3;              % Variation in consumption between summer and winter (30%)
```

The battery size for the hybrid system is calculated consequently, as the difference between the total storage capacity and that of the SC. For the capacity of the conventional accumulator, consisting only of batteries, the total storage value is considered. The efficiencies of the two different types of storage are also defined in order to take into account the losses due to the storage of electrical energy in systems which do not have ideally reversible behaviour. The last variable is used to take into account a supplement for the summer months, which is necessary to consider the energy consumption of the air conditioning system. This Gaussian consumption trend also makes it possible to guarantee better use of the energy produced, which will have a peak generation in summer too.

The next step is to load the annual production values and the six consumption curves onto two different matrices.

```
Production = readmatrix('Production.xlsx','Range','C19:C8802')*TOT_PV;
LoadMatrix = [readmatrix('Load.xlsx','Range','B2:E145')
              readmatrix('Load.xlsx','Range','W2:X145')];
```

8.4.2 Energy management

All the days of a year are analysed by means of two concatenated "for" cycles and each day is subdivided into 10 min time slots.

Within the first cycle, the load curve that will characterise the study of the energies involved is assigned by generating a random value. This curve is then chosen from the appropriate matrix, depending on if the day is a working day or a holiday. In the same cycle, using the following equation for linear interpolation, a vector is also generated showing the powers produced by the PV system divided into 10 min time steps.

```
DailyProduction = [DailyProduction(1:end-1); linspace(Production(Hour), Production(Hour+1),
                  1/6+1)'];    %"Hour" is the position of the production value to be used.
```

Having obtained the power absorbed by the domestic load and the power generated by the PV system, it is possible to obtain the net power for the time period in examination and the relative energy by multiplying it with 1/6.

The energy obtained in this way can be positive or negative, indicating an excess or deficit, respectively, in production. In the first case the energy is stored, in the second case the accumulators are discharged. The logical process followed is to give priority to the SC, thus exploiting its high discharge/charge power and capacity to undergo a large number of cycles without degrading. The logical process followed is schematised below:

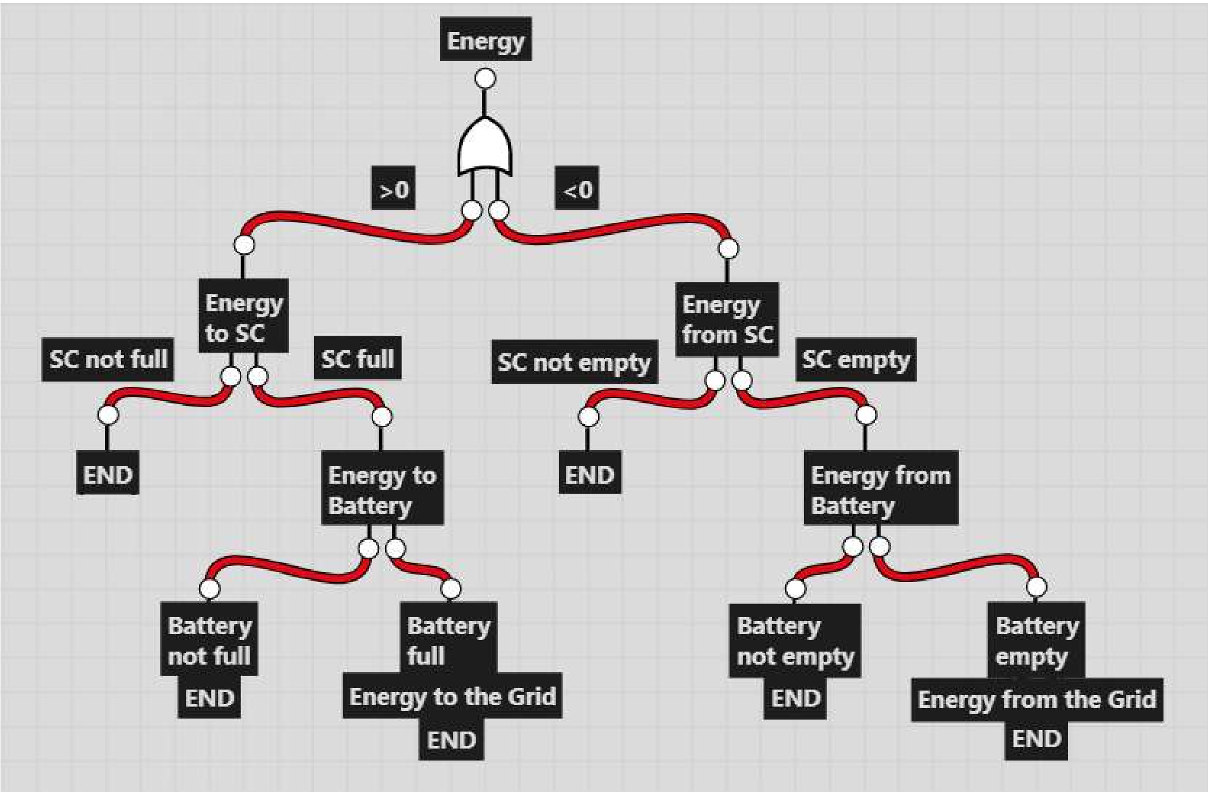

Figure 100 Logic diagram of the charging and discharging process of the hybrid accumulator.

Several parameters were taken into account during each charge and discharge cycle:

- **Losses due to efficiencies:** the efficiencies of the systems were taken into account during the charging and discharging of the accumulators. These losses were deducted from the net usable energy and stored for future consideration.
- **Number of cycles:** the number of charging and discharging cycles performed by the different systems was counted using a counter. A cycle is defined as the transition of the battery state from "in charging" to "in discharging".
- **Cycle duration:** the duration of each cycle was measured, *i.e.* the actual duration net of the phases of sale and purchase of power from the grid. These durations were taken separately for the cycles of the SC, the battery and the traditional storage system.
- **SOC:** at the end of the most internal "for" cycle, *i.e.* at the end of the analysis of each 10 min time step, the SOC values of the SC, the battery and the conventional storage system were saved.

8.4.3 Leakage analysis

As the hybrid system is made up of two different components with different efficiencies, its overall efficiency is different from that of a conventional battery. To this end, the energy lost during the charge and discharge phases has been taken into account.

At each charging and discharging stage of the storage system, the net energy exchanged has been reduced by a fraction due to the non-ideal behaviour of the accumulators. An example of an equation adopted with this intention is given below.

For charging:

*SC = SC + Energy*EffSC;*
LostSC = Lost(SC + Energy(1-EffSC);*

For discharging:

SC = SC - Energy/EffSC;
LostSC = LostSC + Energy(1/EffSC - 1);*

8.5 Results

The following simulations were carried out with the optimal values previously calculated in the component dimensioning section; they are shown below for completeness:

Table 13 Values considered during the following simulations.

Installed PV power [kWp]	4
Total capacity [kWh]	4.5
SC capacity [Wh]	36.5
Annual load [kWh]	3,409

8.5.1 Comparison of cycle numbers and SOC

The aim of this simulation was to validate the effectiveness of using hybrid storage systems to reduce stress and wear on the primary battery. One major source of battery degradation is cyclical use caused by repetitive charging and discharging processes. Often these cycles are very short and due to temporary consumption peaks or sudden climatic changes, which momentarily lead to zero or reduced PV production. In these circumstances, the SC operates in the hybrid system. Thanks to its considerable resistance to usage cycles and high charge/discharge power, it is able to compensate for the short energy fluctuations without causing the battery to have to intervene and start a new cycle.

The simulation therefore consists of two analyses, the first carried out on a hybrid system and the second on a traditional system with the same total storage capacity as the first. In this way, the two systems under analysis are subjected to the same external conditions and allow a careful comparison and contrast between the two behaviours. This first analysis focuses on the SOC of the individual components, analysed on an annual basis and the relative number of cycles completed. In the first analysis, the behaviour of the conventional accumulator is observed.

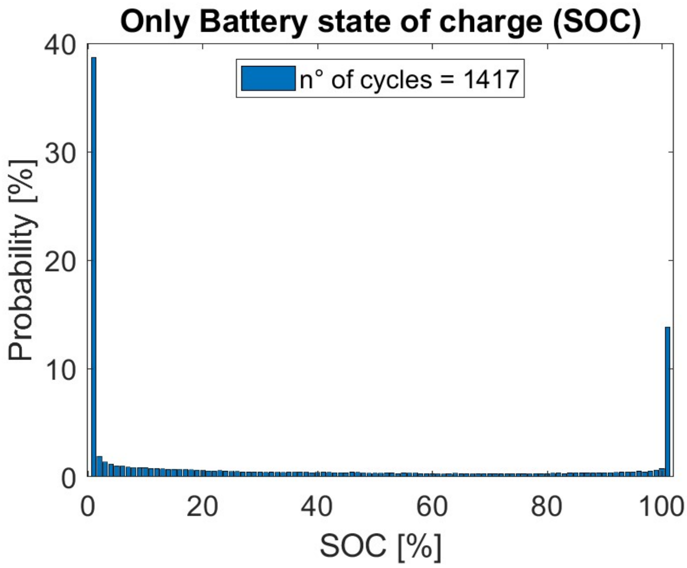

Figure 101 Number of cycles and SOC distribution resulting from the simulation with the conventional battery.

The number of cycles completed in one year is 1417, the battery is discharged about 40% of the time and charged less than 15% of the time. A full charge means a phase in which current is sold to the grid, while a total discharge means a period of energy deficit and therefore purchase from the grid. The period of deficit is due to a dimensioning based on the need to reduce dependence on the grid and not to cancel it, these periods of total discharge are mostly at night and therefore related to low energy deficit. The same graphs showing the hybrid system analysed in its individual parts are shown below.

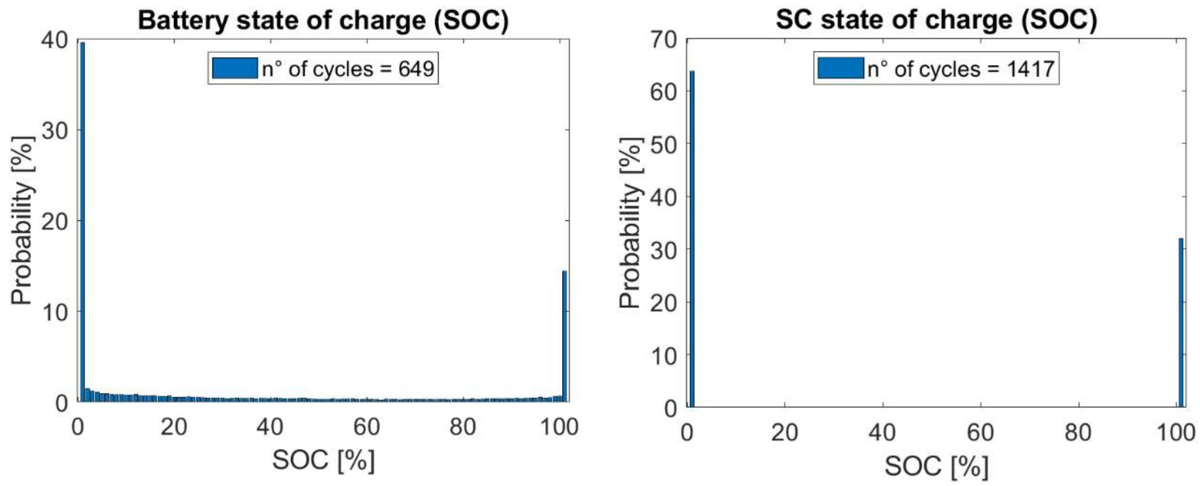

Figure 102 Number of cycles and SOC distribution resulting from the simulation for the individual parts of the hybrid battery. (left) Battery graph, (right) SC graph.

Analysing the graphs, the following considerations can be made:

- The number of cycles carried out by the SC are equal to those undergone by the accumulator in the case of battery alone. This is due to the fact that the SC does not affect the distribution of the load peaks and the production trend. It acts as a filter between the domestic network and the battery, mitigating the deteriorating factors. The conditions seen by the SC are therefore the same as those experienced by the accumulator in the previous simulation, resulting in the same amount of charge/discharge cycles.
- The filter function, performed by the SC, can be seen in the significant reduction in battery cycles. This implementation has reduced the number of battery cycles by 55% and significantly extended battery life.
- The use of the hybrid battery does not significantly affect the SOC distribution of the battery.
- The SC, due to its considerably low capacity, fluctuates between SOCs of 100% during daytime charging and 0% during battery discharge. This is why there is a clear preponderance of these states over the overall distribution.

8.5.2 Comparison of cycle lengths

In addition to the number of cycles, one of the main causes of battery degradation is the length of the operating cycles. Short cycles may represent large power exchanges, partial and not complete usage cycles. The difference between the cycle duration of a conventional and a hybrid battery was analysed. In both cases, only the moments of real battery activity were counted; the phases of buying and selling power from and to the grid are not included in the following analysis as they do not represent real use of the storage system.

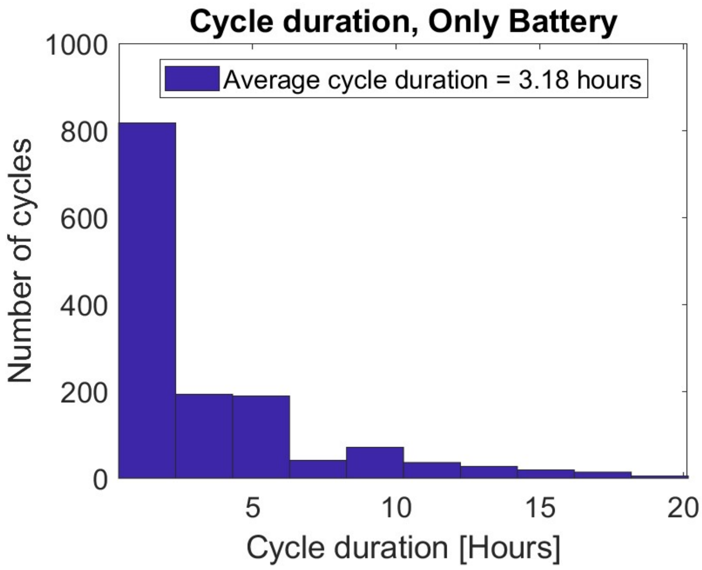

Figure 103 Cycle length distribution and average duration resulting from the simulation with the conventional battery.

In the case of the battery alone, there is an average duration of 3.18 h with a considerable concentration of cycles in the first band (0-2.5 h).

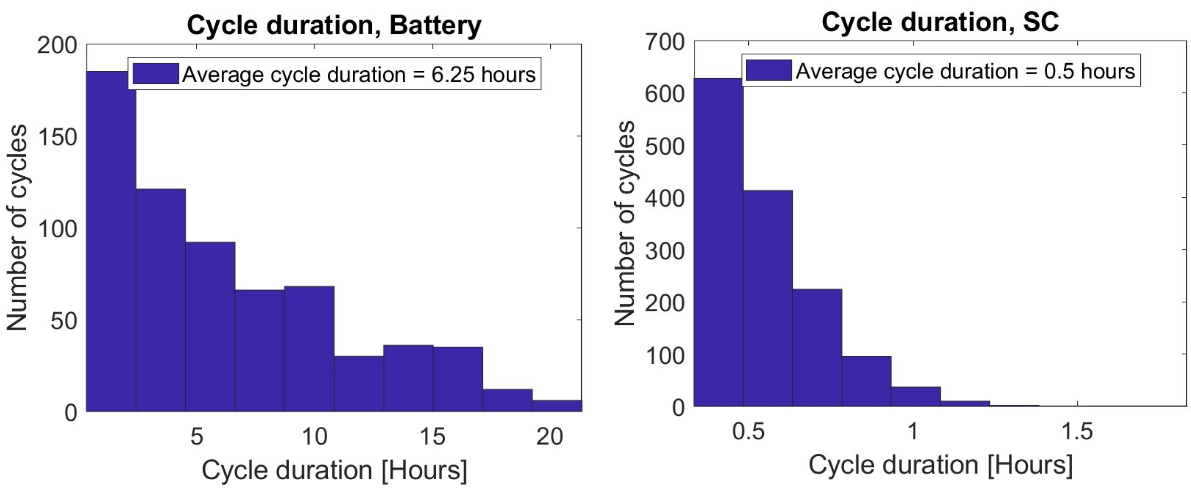

Figure 104 Cycle length distribution and average duration resulting from the simulation for the individual parts of the hybrid battery. (left) Battery graph, (right) SC graph.

By analysing the graphs of the hybrid system, the following considerations can be made:

- The average runtime of the battery is significantly increased, with an average time almost double the previous one.
- The distribution of cycle durations is more equal, with a decrease of more than 4-fold in the number of cycles with durations between 0 and 2.5 h.
- In the SC case, it can be seen that it is able to perform at its best, working with an average cycle time of half an hour. It is also necessary to take into account the different time scale. If the SC graph were compared with that of the batteries, the values would fall entirely within the first range (0-2.5 h).

8.5.3 Comparison of lost energies

SCs differ from batteries both in the number of cycles they can support and in their overall operating efficiency. SCs are characterised by a higher ratio of discharge energy to energy input during charging, which leads to energy savings. The losses generated by the traditional system and those related to the hybrid system were then analysed. The results are available in the graph below.

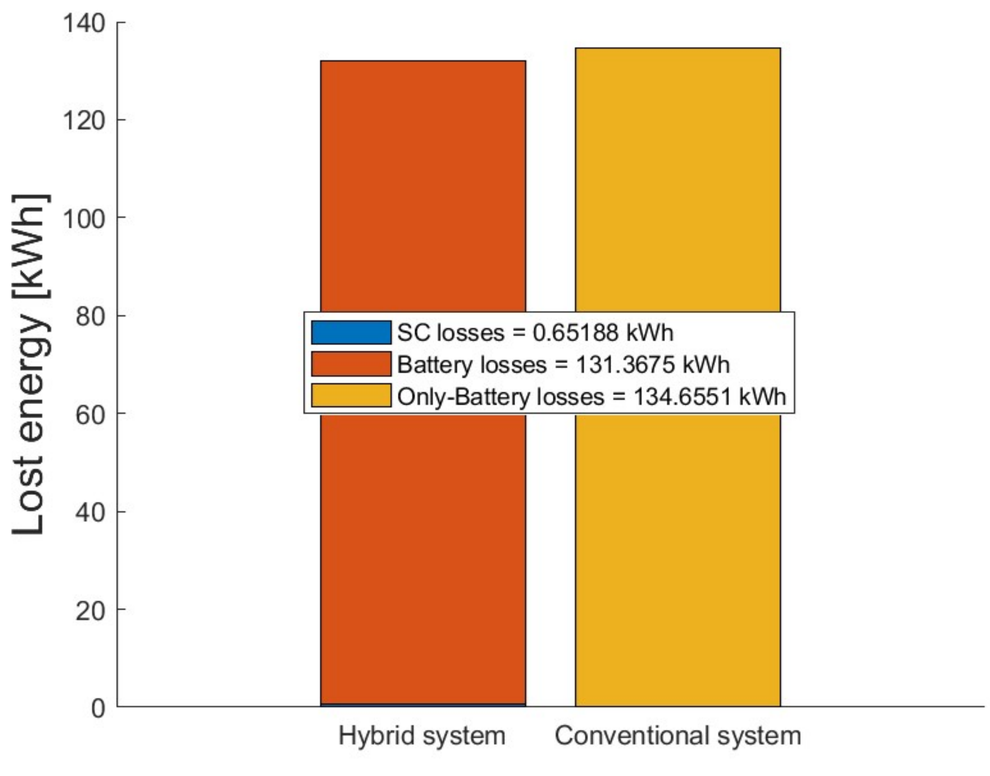

Figure 105 Total losses due to hybrid accumulator vs. conventional battery.

Because of the low energy flowing through the SC, the related gain is also very small. There is therefore an increase in overall efficiency of 1.96%, but since it is very small it does not by itself justify the expense of buying a SC.

8.5.4 Analysis of daily trends

In this sub-section, a selection of days of the simulation has been analysed, focusing on the boundary conditions and the corresponding system response.

- *Normal production day with consumption peaks*

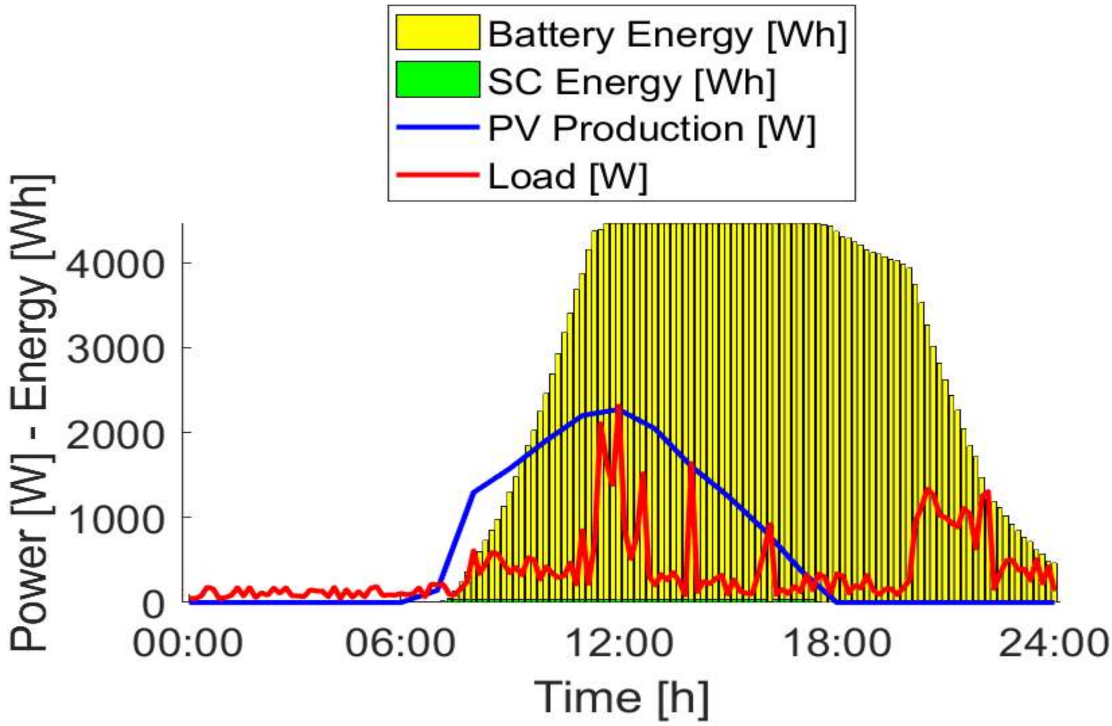

Figure 106 Graph of a typical day with three load peaks.

On the day under analysis, a typical PV production curve can be seen, without any particular deficits due to weather conditions. The storage system, initially unloaded due to the high consumption of the previous day, was able to reach full charge at 11:30, from that moment until 17:40, the power was fed and sold into the national grid. Three consumption peaks, exceeding PV production, can be observed at 12:00, 14:00 and 16:10, respectively. In all cases, it was not necessary to use the battery as the SC was able to manage them completely. An overview of the intervention implemented by the SCs is shown in Figure 107.

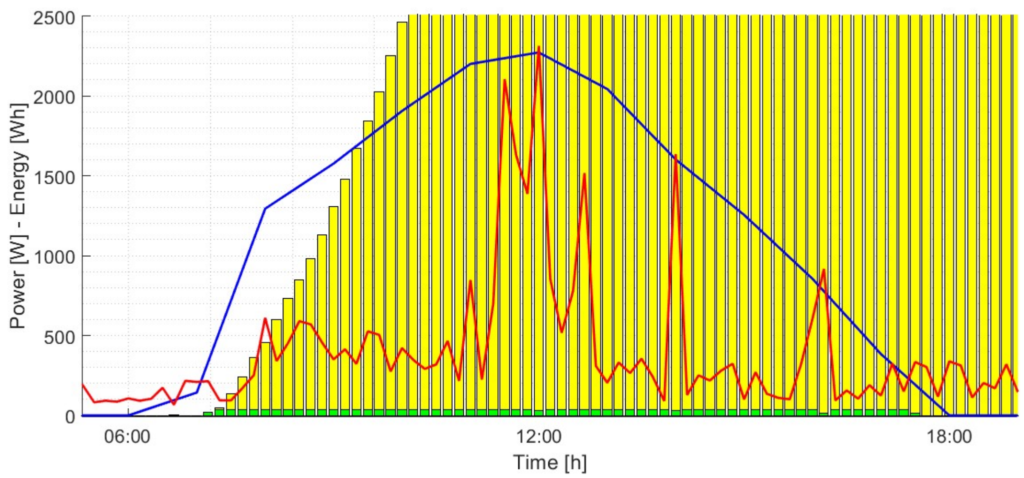

Figure 107 Magnification showing SC response to daily system variations.

- *Day marked by a drop in production in the late morning*

The SC intervention is not only useful in the case of load peaks, but can also be useful when, due to unfavourable weather conditions, there is a temporary production deficit. On the day under analysis, there was a drop in production in the late morning at the same time as two increases in consumption. Again, excess consumption was managed by the SC.

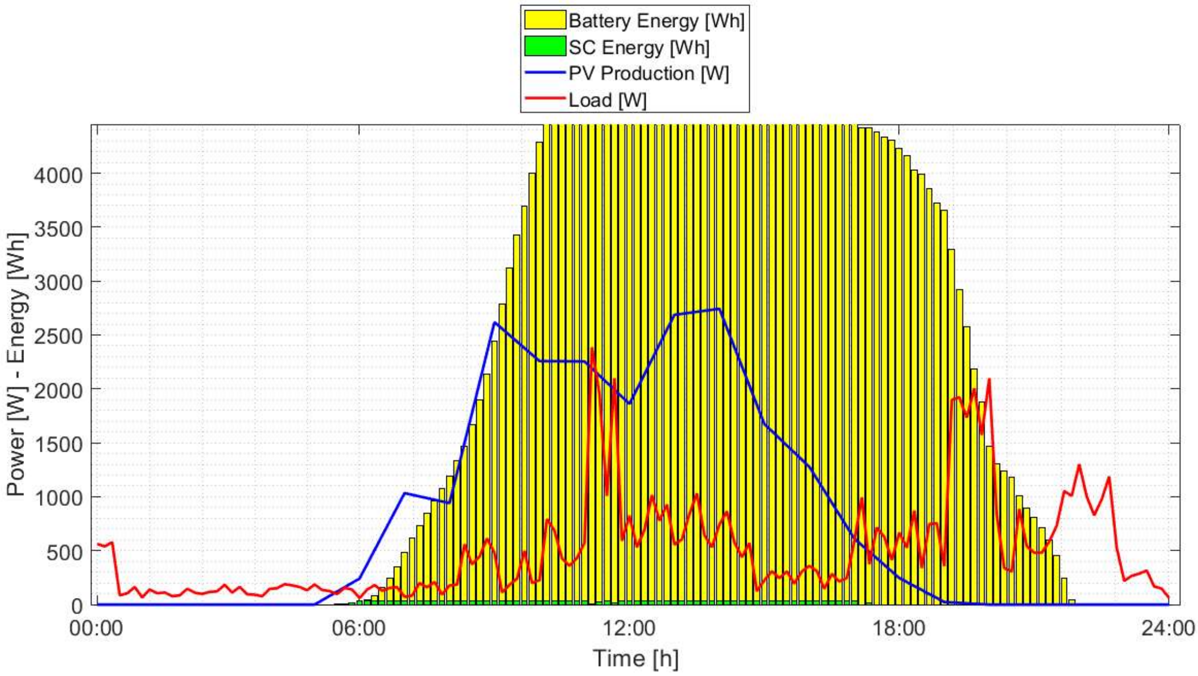

Figure 108 Daily graph characterised by a load peak coinciding with a reduction in PV production.

At 17:00, a new SC intervention can also be observed, but this time the operation was opposite to the previous ones. In the first peak there was a complete discharge of the SC, with the consequent start of the battery discharge phase. With the decrease in consumption, compared to PV production, there was no start of a new charging phase because, thanks to its filter function, the SC stored that excess energy and used it again shortly afterwards.

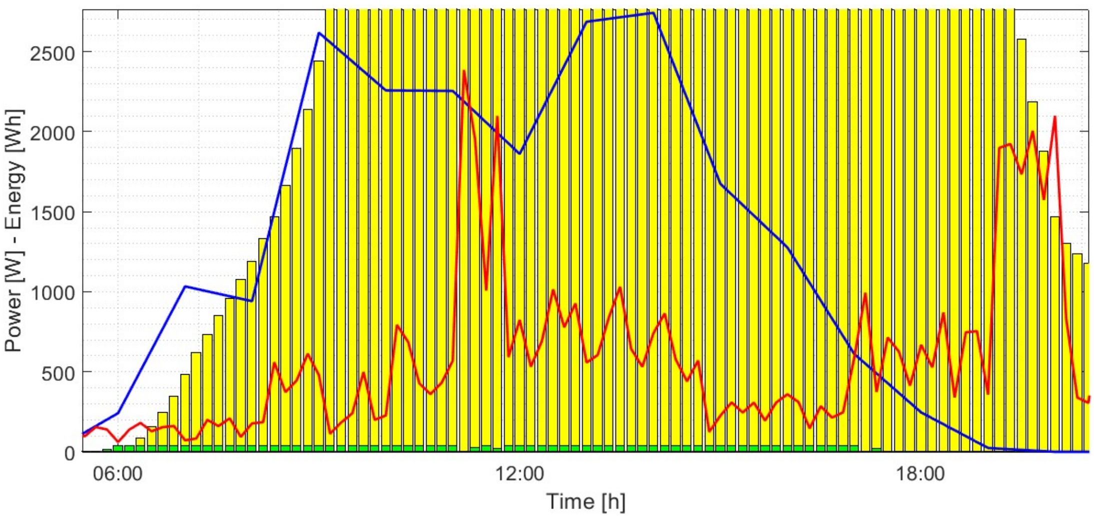

Figure 109 Magnification showing SC response to daily system variations.

This ensured the continuity of the battery discharge cycle without causing it to be interrupted and a new cycle to begin.

9 Conclusions

The study examined the main technologies currently under analysis regarding the dynamics of integration between PV panels and batteries. Particular interest was given to the future of SCs in this sector and the role they could play. Two main areas of interest were identified for SCs: in small devices directly integrated with PV cells or inserted into a hybrid accumulator to serve as filters and compensate sudden power variations. In the first case, the great versatility and resistance of SCs has made them a valid alternative to batteries for powering small portable devices or *in situ* analysis modules developed to withstand bad weather and numerous charge/discharge cycles. In the second case, however, due to the high costs, it is not convenient to use a storage system made entirely of SCs, which would also not be justified by the modest powers normally involved in a PV system. The function of SCs is therefore to act as a filter to support the main battery storage.

The second field of applicability has also been analysed using a MATLAB simulation to investigate the degradation process undergone by a battery with and without the presence of a supporting SC. The results obtained are consistent with what has been learned from the analysis of the previous publications. The insertion of SCs, if correctly sized, makes it possible to guarantee an improvement in the operating conditions of the system. The flattening of peak loads and the reduction in the number of cycles are valid reasons to invest in a hybrid storage system. The results have shown that a hybrid storage system extends the life of the batteries and reduces possible future maintenance and replacement costs. The analysis of the SC sizing showed that its capacity should be about 1⁄120 of the total capacity. In the case under analysis the total cost of the system increases by 1000 €, compared to a starting price of 5800 € for the battery pack (price referred to a battery pack 'Soltaro AIO2 5 kW / 5 kWh' with net usable energy of 4.5 kWh [87]). This battery pack is guaranteed to have a lifetime of at least ten years. The adoption of a hybrid storage system can therefore be considered if the increase in the useful life of the installation is at least 1⁄6 of the initial one, an improvement proportional to the increase in costs.

To validate the results of this analysis, by measuring the real increase in the useful life of the batteries, it is appropriate to carry out tests with a pilot plant, comparing and implementing the results obtained with the experimental ones. The test plant should verify the actual operation of the hybrid accumulator as well as the changes made to the dynamics of the powers managed and the amount of decrease in depletion recorded.

10 Appendix A

```
close all
clear
clc

%% DATA

TOT_Storage = 4.5e3;          % [Wh] Total installed storage capacity
TOT_SC = 36.5;                % [Wh] SC installed storage capacity

TOT_PV = 4;                   % [kWp] Total installed PV power

EffBa = 0.95;                 % Battery efficiency for charge and discharge phases considered
                              separately
EffSC = 0.99;                 % SC efficiency for charge and discharge phases considered
                              separately

CumProbL = [0.4 0.7 0.9 1];   % Cumulative probability assigned for each working day
CumProbF = [0.9 1];           % Cumulative probability assigned for each holiday
Kmonths = 0.3;                % Consumption variation between summer and winter
Kreduction = -0.3;            % Reduction to be applied to values in Excel

DayPrint = 124;               % Day to print


%% LOADING

Production = readmatrix('Production.xlsx','Sheet','Production','Range','C19:C8802')*TOT_PV;
                                                                        % [W]
LoadMatrix = [readmatrix('Load.xlsx','Sheet','Load','Range','B2:E145')
              readmatrix('Load.xlsx','Sheet','Load','Range','W2:X145')];        % [W]
LoadMatrix = LoadMatrix - LoadMatrix*Kreduction;

%% CALCULATION

DAY= 366;                     % Total days
Working = 5;                  % Working days in a week
Holiday = 7 - Working;        % Holidays in a week

TypeDay = 1;                  % If <= Working is a working day otherwise it is a holiday
tt = 6;                       % To define timesteps of 10min in linear interpolation
Hour = 0;                     % Indicates which time unit I am analysing

TOT_Battery = TOT_Storage - TOT_SC;         % [Wh] HybridBattery installed storage capacity

Battery = 0.1* TOT_Storage;         % Initial HybridBattery charge value for the first day
SC = 0;                             % Initial SC charge value for the first day
OnlyBat = 0.1*TOT_Storage;          % Initial OnlyBattery charge value for the first day

Grid = zeros(2,DAY);          % Sold in column 1
                              % Purchased in column 2
Lost = zeros(3,1);            % Losses related to SC in column 1
```

```
                                % Losses related to HybridBattery in column 2
                                % Losses related to OnlyBattery in column 3

Slot = zeros(3,1);              % Load time slots
MonthlySlot = zeros(3,12);
AverageLoad = zeros(24*tt,1);
LoadDay = zeros(24*tt,4);
ProdDay = zeros(24*tt,3);
MonthlyBat = zeros(24*tt,3);

SOCB = zeros(101,1);            % State of charge HybridBattery
SOCOB = zeros(101,1);           % State of charge OnlyBattery
SOCS = zeros(101,1);            % State of charge SC

CyclesBa = 1;                   % HybridBattery charge/discharge cycles
CyclesSC = 1;                   % SC charge/discharge cycles
StatusBa = 1;                   % 1 = discharging; 0 = loading
StatusSC = 1;                   % 1 = discharging; 0 = loading

CyclesOB = 1;                   % OnlyBattery charge/discharge cycles
StatusOB = 1;                   % 1 = discharging; 0 = loading

TimeSC = zeros;                 % Cycle time SC
TimeBa = zeros;                 % Cycle time HybridBattery
TimeOB = zeros;                 % Cycle time OnlyBattery

for day=1:DAY

  % I decide what day I am analysing and what load I have

  Choice = rand;
  if TypeDay <= Working

    if Choice<CumProbL(1)              % I choose load condition Working
      DayChosen = 1;
    elseif Choice<CumProbL(2)
      DayChosen = 2;
    elseif Choice<CumProbL(3)
      DayChosen = 3;
    else
      DayChosen = 4;
    end

  else

    if Choice<CumProbF(1)              % I choose load condition Holiday
      DayChosen = 5;
    else
      DayChosen = 6;
    end

    if TypeDay == Working + Holiday          % If the week is over, repeat
      TypeDay = 0;
    end
  end
```

```
TypeDay = TypeDay + 1;

% Split the production into the desired time slots

DailyProduction = zeros(6,1);          % Between midnight and 1am I have no production
Hour = Hour + 1;
for TenMinutes=1:23          % Linear interpolation of hourly production to get the different time
                             bands
   if Production(Hour) == 0 && Production(Hour+1) == 0
      DailyProduction = [DailyProduction; zeros(6,1)];
   else
   DailyProduction = [DailyProduction(1:end-1); linspace(Production(Hour),
   Production(Hour+1), tt+1)'];
   end
   Hour = Hour + 1;
end

if day==DayPrint       % I print the chart of the predetermined day
   figure
   hold on
   BatDay=zeros(1,24*tt);
   SCDay=zeros(1,24*tt);
end

% COMPARISON OF PRODUCTION WITH LOAD

for TenMinutes=1:(24*tt)

   Load = LoadMatrix(TenMinutes,DayChosen)+LoadMatrix(TenMinutes,DayChosen)*(rand-1/2);
   Load = Load - LoadMatrix(TenMinutes,DayChosen)*Kmonths*abs(2*(day-1)/(DAY-1)-1);
   AverageLoad(TenMinutes) = AverageLoad(TenMinutes) + Load;

   if TenMinutes<7*tt || TenMinutes>=23*tt || TypeDay == 1
      Slot(3) = Slot(3) + Load/tt;
   elseif TenMinutes<8*tt || TenMinutes>=19*tt || TypeDay == 7
      Slot(2) = Slot(2) + Load/tt;
   else
      Slot(1) = Slot(1) + Load/tt;
   end

   if TenMinutes>=StartDay*tt && TenMinutes<=EndDay*tt
      DayNight(1,1) = DayNight(1,1) + Load/tt;
   else
      DayNight(2,1) = DayNight(2,1) + Load/tt;
   end

   % Calculating the difference between production and consumption
   Energy = (DailyProduction(TenMinutes) - Load)/tt;

   if TenMinutes>=StartDay*tt && TenMinutes<=EndDay*tt
      DayNight(1,2) = DayNight(1,2) - Energy;
   else
      DayNight(2,2) = DayNight(2,2) - Energy;
   end
```

```
if Energy>0        % I HAVE TO CHARGE THE ACCUMULATOR

  if StatusSC == 1               % If it was discharging before
    StatusSC = 0;                % Now it is charging
    CyclesSC = CyclesSC + 1;     % A new cycle has begun
    TimeSC(CyclesSC) = 1;        % Initialise new cycle time
  else
    if SC ~= TOT_SC      % I increase the counter that marks the duration time of the cycles
      TimeSC(CyclesSC) = TimeSC(CyclesSC) + 1;
    end
  end

  SC = SC + Energy*EffSC;
  Lost(1) = Lost(1) + Energy*(1-EffSC);

  if SC>TOT_SC

    if StatusBa == 1               % If it was discharging before
      StatusBa = 0;                % Now it is charging
      CyclesBa = CyclesBa + 1;     % A new cycle has begun
      TimeBa(CyclesBa) = 1;        % Initialise new cycle time
    else
      if Battery ~= TOT_Battery            % I increase the counter that marks the duration time
                                           of the cycles
        TimeBa(CyclesBa) = TimeBa(CyclesBa) + 1;
      end
    end

    Battery = Battery + (SC - TOT_SC)*EffBa/EffSC;
    Lost(1) = Lost(1) - (SC - TOT_SC)/EffSC*(1-EffSC);
    Lost(2) = Lost(2) + (SC - TOT_SC)/EffSC*(1-EffBa);

    if Battery>TOT_Battery                        % I have to sell
      Grid(1,day) = Grid(1,day) + (Battery - TOT_Battery)/EffBa;
      Lost(2) = Lost(2) - (Battery - TOT_Battery)/EffBa*(1-EffBa);
      Battery = TOT_Battery;

    end
    SC = TOT_SC;
  end

  % OnlyBattery

  if StatusOB == 1               % If it was discharging before
    StatusOB = 0;                % Now it is charging
    CyclesOB = CyclesOB + 1;     % A new cycle has begun
    TimeOB(CyclesOB) = 1;        % Initialise new cycle time
  else
    if OnlyBat ~= TOT_Storage  % I increase the counter that marks the duration time of the
                               cycles
      TimeOB(CyclesOB) = TimeOB(CyclesOB) + 1;
    end
  end

  OnlyBat = OnlyBat + Energy*EffBa;
```

```
    Lost(3) = Lost(3) + Energy*(1-EffBa);

    if OnlyBat > TOT_Storage
      Lost(3) = Lost(3) - (OnlyBat - TOT_Storage)/EffBa*(1-EffBa);
      OnlyBat = TOT_Storage;
    end

  elseif Energy<0     % I HAVE TO DISCHARGE THE ACCUMULATOR

    if StatusSC == 0                 % If it was charging before
      StatusSC = 1;                  % Now it is discharging
    end

    if SC ~= 0             % I increase the counter that marks the duration time of the cycles
      TimeSC(CyclesSC) = TimeSC(CyclesSC) + 1;
    end

    SC = SC + Energy/EffSC;
    Lost(1) = Lost(1) + Energy - Energy/EffSC;

    if SC<0

      if StatusBa == 0               % If it was charging before
        StatusBa = 1;                % Now it is discharging
      end

      if Battery ~= 0      % I increase the counter that marks the duration time of the cycles
        TimeBa(CyclesBa) = TimeBa(CyclesBa) + 1;
      end

      Battery = Battery + SC*EffSC/EffBa;
      Lost(1) = Lost(1) - SC*EffSC + SC;
      Lost(2) = Lost(2) + SC*EffSC - SC*EffSC/EffBa;

      if Battery<0                   % I have to buy
        Grid(2,day) = Grid(2,day) - Battery*EffBa;
        Lost(2) = Lost(2) - Battery*EffBa + Battery;
        Battery = 0;
      end
      SC = 0;
    end

    % OnlyBattery

    if StatusOB == 0                 % If it was charging before
      StatusOB = 1;                  % Now it is discharging
    end

    if OnlyBat ~= 0        % I increase the counter that marks the duration time of the cycles
      TimeOB(CyclesOB) = TimeOB(CyclesOB) + 1;
    end

    OnlyBat = OnlyBat + Energy/EffBa;
    Lost(3) = Lost(3) + Energy - Energy/EffBa;
```

```
    if OnlyBat < 0
      Lost(3) = Lost(3) - OnlyBat*EffBa + OnlyBat;
      OnlyBat = 0;
    end
  end

  SOCB(round(Battery/TOT_Battery*100) + 1) = SOCB(round(Battery/TOT_Battery*100) + 1) +
  1;
  SOCS(round(SC/TOT_SC*100) + 1) = SOCS(round(SC/TOT_SC*100) + 1) + 1;
  SOCOB(round(OnlyBat/TOT_Storage*100) + 1) = SOCOB(round(OnlyBat/TOT_Storage*100)
  + 1) + 1;

  if day==DayPrint          % I print the chart of the predetermined day
    BatDay(TenMinutes) = Battery;
    SCDay(TenMinutes) = SC;
    LoadDay(TenMinutes,1) = Load;
  end


  % For the average load of a month
  if day>31+29 && day<=31+29+31                                    % March
    LoadDay(TenMinutes,2) = LoadDay(TenMinutes,2) + Load;
    MonthlyBat(TenMinutes,1) = MonthlyBat(TenMinutes,1) + OnlyBat;
    if TenMinutes==1
      ProdDay(1:end,1) = ProdDay(1:end,1) + DailyProduction;
    end
  elseif day>30+31+30+31+29+31 && day<=31+30+31+30+31+29+31        % July
    LoadDay(TenMinutes,3) = LoadDay(TenMinutes,3) + Load;
    MonthlyBat(TenMinutes,2) = MonthlyBat(TenMinutes,2) + OnlyBat;
    if TenMinutes==1
      ProdDay(1:end,2) = ProdDay(1:end,2) + DailyProduction;
    end
  elseif day>30+31+30+31+31+30+31+30+31+29+31                      % December
    LoadDay(TenMinutes,4) = LoadDay(TenMinutes,4) + Load;
    MonthlyBat(TenMinutes,3) = MonthlyBat(TenMinutes,3) + OnlyBat;
    if TenMinutes==1
      ProdDay(1:end,3) = ProdDay(1:end,3) + DailyProduction;
    end
  end
end

if day==DayPrint            % I print the chart of the predetermined day
  bar(BatDay,'y');
  bar(SCDay,'g');
  plot((1:24*tt),DailyProduction,'b','linewidth',2);
  plot((1:24*tt),LoadDay(1:end,1),'r','linewidth',2);
  hold off
  xticks([1 36 72 108 144])
  xticklabels({'00:00','06:00','12:00','18:00','24:00'})
  legend('Battery Energy [Wh]','SC Energy [Wh]','PV Production [W]','Load
   [W]','Location','northoutside');
  xlabel('Time [h]','fontsize',16)
  ylabel('Power [W] - Energy [Wh]','fontsize',16)
  set(gca,'fontsize',16)
  print -dpng GG
```

```
    grid minor
    box on
  end

% Time slots by month

  if day==31
    MonthlySlot(1,1) = Slot(1);
    MonthlySlot(2,1) = Slot(2);
    MonthlySlot(3,1) = Slot(3);
  elseif day==29+31
    MonthlySlot(1,2) = Slot(1) - MonthlySlot(1,1);
    MonthlySlot(2,2) = Slot(2) - MonthlySlot(2,1);
    MonthlySlot(3,2) = Slot(3) - MonthlySlot(3,1);
  elseif day==31+29+31
    MonthlySlot(1,3) = Slot(1) - sum(MonthlySlot(1,1:2));
    MonthlySlot(2,3) = Slot(2) - sum(MonthlySlot(2,1:2));
    MonthlySlot(3,3) = Slot(3) - sum(MonthlySlot(3,1:2));
  elseif day==30+31+29+31
    MonthlySlot(1,4) = Slot(1) - sum(MonthlySlot(1,1:3));
    MonthlySlot(2,4) = Slot(2) - sum(MonthlySlot(2,1:3));
    MonthlySlot(3,4) = Slot(3) - sum(MonthlySlot(3,1:3));
  elseif day==31+30+31+29+31
    MonthlySlot(1,5) = Slot(1) - sum(MonthlySlot(1,1:4));
    MonthlySlot(2,5) = Slot(2) - sum(MonthlySlot(2,1:4));
    MonthlySlot(3,5) = Slot(3) - sum(MonthlySlot(3,1:4));
  elseif day==30+31+30+31+29+31
    MonthlySlot(1,6) = Slot(1) - sum(MonthlySlot(1,1:5));
    MonthlySlot(2,6) = Slot(2) - sum(MonthlySlot(2,1:5));
    MonthlySlot(3,6) = Slot(3) - sum(MonthlySlot(3,1:5));
  elseif day==31+30+31+30+31+29+31
    MonthlySlot(1,7) = Slot(1) - sum(MonthlySlot(1,1:6));
    MonthlySlot(2,7) = Slot(2) - sum(MonthlySlot(2,1:6));
    MonthlySlot(3,7) = Slot(3) - sum(MonthlySlot(3,1:6));
  elseif day==31+31+30+31+30+31+29+31
    MonthlySlot(1,8) = Slot(1) - sum(MonthlySlot(1,1:7));
    MonthlySlot(2,8) = Slot(2) - sum(MonthlySlot(2,1:7));
    MonthlySlot(3,8) = Slot(3) - sum(MonthlySlot(3,1:7));
  elseif day==30+31+31+30+31+30+31+29+31
    MonthlySlot(1,9) = Slot(1) - sum(MonthlySlot(1,1:8));
    MonthlySlot(2,9) = Slot(2) - sum(MonthlySlot(2,1:8));
    MonthlySlot(3,9) = Slot(3) - sum(MonthlySlot(3,1:8));
  elseif day==31+30+31+31+30+31+30+31+29+31
    MonthlySlot(1,10) = Slot(1) - sum(MonthlySlot(1,1:9));
    MonthlySlot(2,10) = Slot(2) - sum(MonthlySlot(2,1:9));
    MonthlySlot(3,10) = Slot(3) - sum(MonthlySlot(3,1:9));
  elseif day==30+31+30+31+31+30+31+30+31+29+31
    MonthlySlot(1,11) = Slot(1) - sum(MonthlySlot(1,1:10));
    MonthlySlot(2,11) = Slot(2) - sum(MonthlySlot(2,1:10));
    MonthlySlot(3,11) = Slot(3) - sum(MonthlySlot(3,1:10));
  elseif day==31+30+31+30+31+31+30+31+30+31+29+31
    MonthlySlot(1,12) = Slot(1) - sum(MonthlySlot(1,1:11));
    MonthlySlot(2,12) = Slot(2) - sum(MonthlySlot(2,1:11));
    MonthlySlot(3,12) = Slot(3) - sum(MonthlySlot(3,1:11));
```

```
    end
end

AverageLoad = round(AverageLoad/DAY);
LoadDay(1:end,2:end) = LoadDay(1:end,2:end)/31;
ProdDay(1:end,1:end) = ProdDay(1:end,1:end)/31;
MonthlyBat(1:end,1:end) = MonthlyBat(1:end,1:end)/31;

% March sizing
figure
hold on
plot((1:24*tt),ProdDay(1:end,1),'b','linewidth',2);
plot((1:24*tt),LoadDay(1:end,2),'r','linewidth',2);
plot((1:24*tt),MonthlyBat(1:end,1),'y','linewidth',2);
LoadDay(1,2) = 0;
LoadDay(end,2) = 0;
MonthlyBat(1,1) = 0;
MonthlyBat(end,1) = 0;
patch((1:24*tt),LoadDay(1:end,2),'r');
patch((1:24*tt),ProdDay(1:end,1),'b');
patch((1:24*tt),MonthlyBat(1:end,1),'y');
alpha(0.2);
hold off
legend('PV Production [W]','Load [W]','Battery Energy [Wh]','Location','southoutside');
xlabel('Time [h]','fontsize',16)
title('March')
set(gca,'fontsize',16)
ylabel('Power [W] - Energy [Wh]','fontsize',14)
print -dpng March
grid minor
box on

% July sizing
figure
hold on
plot((1:24*tt),ProdDay(1:end,2),'b','linewidth',2);
plot((1:24*tt),LoadDay(1:end,3),'r','linewidth',2);
plot((1:24*tt),MonthlyBat(1:end,2),'y','linewidth',2);
LoadDay(1,3) = 0;
LoadDay(end,3) = 0;
MonthlyBat(1,2) = 0;
MonthlyBat(end,2) = 0;
patch((1:24*tt),LoadDay(1:end,3),'r');
patch((1:24*tt),ProdDay(1:end,2),'b');
patch((1:24*tt),MonthlyBat(1:end,2),'y');
alpha(0.2);
hold off
legend('PV Production [W]','Load [W]','Battery Energy [Wh]','Location','southoutside');
xlabel('Time [h]','fontsize',16)
title('July')
set(gca,'fontsize',16)
ylabel('Power [W] - Energy [Wh]','fontsize',14)
print -dpng July
grid minor
box on
```

```
% December sizing
figure
hold on
plot((1:24*tt),ProdDay(1:end,3),'b','linewidth',2);
plot((1:24*tt),LoadDay(1:end,4),'r','linewidth',2);
plot((1:24*tt),MonthlyBat(1:end,3),'y','linewidth',2);
LoadDay(1,4) = 0;
LoadDay(end,4) = 0;
MonthlyBat(1,3) = 0;
MonthlyBat(end,3) = 0;
patch((1:24*tt),LoadDay(1:end,4),'r');
patch((1:24*tt),ProdDay(1:end,3),'b');
patch((1:24*tt),MonthlyBat(1:end,3),'y');
alpha(0.2);
hold off
legend('PV Production [W]','Load [W]','Battery Energy [Wh]','Location','southoutside');
xlabel('Time [h]','fontsize',16)
title('December')
set(gca,'fontsize',16)
ylabel('Power [W] - Energy [Wh]','fontsize',14)
print -dpng December
grid minor
box on

% HybridBattery state of charge (SOC)
figure
bar(SOCB/Hour/tt*100);
title('Battery state of charge (SOC)');
leg=(['n° of cycles = ' num2str(CyclesBa)]);
legend(leg,'Location','north');
xlabel('SOC [%]','fontsize',16)
ylabel('Probability [%]','fontsize',16)
set(gca,'fontsize',16)
print -dpng SOCBattery
grid minor
box on

% SC state of charge (SOC)'
figure
bar(SOCS/Hour/tt*100);
title('SC state of charge (SOC)');
leg=(['n° of cycles = ' num2str(CyclesSC)]);
legend(leg,'Location','north');
xlabel('SOC [%]','fontsize',16)
ylabel('Probability [%]','fontsize',16)
set(gca,'fontsize',16)
print -dpng SOCSC
grid minor
box on

% OnlyBattery state of charge (SOC)
figure
bar(SOCOB/Hour/tt*100);
title('Only Battery state of charge (SOC)');
leg=(['n° of cycles = ' num2str(CyclesOB)]);
```

```
legend(leg,'Location','north');
xlabel('SOC [%]','fontsize',16)
ylabel('Probability [%]','fontsize',16)
set(gca,'fontsize',16)
print -dpng SOCOB
grid minor
box on

% Cycle duration, SC
figure
hist(TimeSC/tt);
xlim([min(TimeSC/tt) max(TimeSC/tt)])
title('Cycle duration, SC');
legend(['Average cycle duration = ' num2str(round(mean(TimeSC/tt),2)) ' hours'],'Location','north');
xlabel('Cycle duration [Hours]','fontsize',16)
ylabel('Number of cycles','fontsize',16)
set(gca,'fontsize',16)
print -dpng TimeSC
grid minor
box on

% Cycle duration, HybridBattery
figure
hist(TimeBa/tt);
xlim([min(TimeBa/tt) max(TimeBa/tt)])
title('Cycle duration, Battery');
legend(['Average cycle duration = ' num2str(round(mean(TimeBa/tt),2)) ' hours'],'Location','north');
xlabel('Cycle duration [Hours]','fontsize',16)
ylabel('Number of cycles','fontsize',16)
set(gca,'fontsize',16)
print -dpng TimeBa
grid minor
box on

% Cycle duration, OnlyBattery
figure
hist(TimeOB/tt);
xlim([min(TimeOB/tt) max(TimeOB/tt)])
title('Cycle duration, Only Battery');
legend(['Average cycle duration = ' num2str(round(mean(TimeOB/tt),2)) ' hours'],'Location','north');
xlabel('Cycle duration [Hours]','fontsize',16)
ylabel('Number of cycles','fontsize',16)
set(gca,'fontsize',16)
print -dpng TimeOB
grid minor
box on

% Use of the Grid
figure
bar(Grid'/1e3,'stacked')
xlabel('One Year [Days]','fontsize',16)
ylabel('Energy to/from the grid [kWh]','fontsize',16)
leg1=(['Energy sold to the grid = ' num2str(sum(Grid(1,1:end))/1e3) ' kWh']);
leg2=(['Energy purchased to the grid = ' num2str(sum(Grid(2,1:end))/1e3) ' kWh']);
legend(leg1,leg2,'Location','north');
```

```
print -dpng Grid
grid minor
box on

% Time zones
figure
hold on
bar(1, Slot(1)'/1e3, 'r')
bar(2, Slot(2)'/1e3, 'y')
bar(3, Slot(3)'/1e3, 'g')
hold off
xticks([1 2 3])
xticklabels({'F1','F2','F3'})
xlabel('Time zones','fontsize',16)
ylabel('Total active energy [kWh]','fontsize',16)
tit=(['Energy consumed = ' num2str(sum(Slot/1e3)) ' kWh']);
title(tit);
print -dpng TimeZones
grid minor
box on

% Time zones, months
figure
hold on
bar(MonthlySlot'/1e3,'stacked')
hold off
xticks([1 2 3 4 5 6 7 8 9 10 11 12])
xticklabels({'Jan.','Feb.','Mar.','Apr.','May','June','July','Aug.','Sept.','Oct.','Nov.','Dec.'})
xlabel('Months','fontsize',16)
ylabel('Total active energy [kWh]','fontsize',16)
legend('F1','F2','F3','Location','eastoutside');
print -dpng TimeZonesMonths
grid minor
box on

% Leakage
figure
hold on
bar(1, Lost(1:2)'/1e3, 'stacked')
bar(2, Lost(3)'/1e3)
hold off
xticks([1 2])
xticklabels({'Hybrid system','Conventional system'})
ylabel('Lost energy [kWh]','fontsize',16)
leg1=(['SC losses = ' num2str(Lost(1)/1e3) ' kWh']);
leg2=(['Battery losses = ' num2str(Lost(2)/1e3) ' kWh']);
leg3=(['Only-Battery losses = ' num2str(Lost(3)/1e3) ' kWh']);
legend(leg1,leg2,leg3,'Location','best');
print -dpng Leakage
grid minor
box on
```

1 bp p.l.c.
Statistical Review of World Energy
(2020) Bp, pp. 1-68.
Link:https://www.bp.com/content/dam/bp/businesssites/en/global/corporate/pdfs/energy-economics/statistical-review/bp-stats-review-2020-full-report.pdf

2 Reddy, K.G., Deepak, T.G., Anjusree, G.S., Thomas, S., Vadukumpully, S., Subramanian, K.R.V., Nair, S.V., Nair, A.S.
On global energy scenario, dye-sensitized solar cells and the promise of nanotechnology
(2014) Physical Chemistry Chemical Physics, 16 (15), pp. 6838-6858.
DOI: 10.1039/c3cp55448a

3 A. E. Becquerel
CR Acad. Sci. Paris
(1839), 9, 14.

4 Kuang, Yinghuan & Di Vece, Marcel & Rath, J.K. & van Dijk, Lourens & Schropp
(2013). Elongated nanostructures for radial junction solar cells. Reports on progress in physics. Physical Society (Great Britain). 76. 106502. 10.1088/0034-4885/76/10/106502.

5 Coiante D.,
Fotovoltaico di prima generazione: il punto.
(2013)

6 Liu, M., Johnston, M.B., Snaith, H.J.
Efficient planar heterojunction perovskite solar cells by vapour deposition
(2013) Nature, 501 (7467), pp. 395-398. Cited 5276 times.
DOI: 10.1038/nature12509

7 Klaus Mueller
This image is a cutout of an image by Klaus Mueller
https://commons.wikimedia.org/wiki/File:Comparison_solar_cell_poly-Si_vs_mono-Si.png

8 Kalogirou, S.
McEvoy's handbook of photovoltaics: Fundamentals and applications
(2017) McEvoy's Handbook of Photovoltaics: Fundamentals and Applications, pp. 1-1340.

9 Green, M.A., Emery, K., Hishikawa, Y., Warta, W., Dunlop, E.D.
Solar cell efficiency tables (Version 45)
(2015) Progress in Photovoltaics: Research and Applications, 23 (1), pp. 1-9.
DOI: 10.1002/pip.2573

10 Cdang
released under cc-by-sa-3.0,2.5,2.0,1.0, GFDL
https://commons.wikimedia.org/wiki/File:Schematic_of_allotropic_forms_of_silcon_horizontal_plain.svg

11 Acevedo-Luna, A., Bernal-Correa, R., Montes-Monsalve, J., Morales-Acevedo, A.
Design of thin film solar cells based on a unified simple analytical model
(2017) Journal of Applied Research and Technology, 15 (6), pp. 599-608.
DOI: 10.1016/j.jart.2017.08.002

12 Snaith, H.J.
Perovskites: The emergence of a new era for low-cost, high-efficiency solar cells

(2013) Journal of Physical Chemistry Letters, 4 (21), pp. 3623-3630.
DOI: 10.1021/jz4020162

13 Leonid Leiva
Paul Scherrer Institute, Memory effect now also found in lithium-ion batteries, su phys.org, 15 aprile 2013.

14 Yamamura, Tomoo Wu, Xiongwei Sato, Isamu
TOHOKU UNIVERSITY (Sendai-shi, JP)
https://www.freepatentsonline.com/9419279.html

15 EW Staff
(November 2018)
https://www.electronicsweekly.com/news/design/will-supercapacitors-supersede-batteries-2018-11/

16 Gurung, A., & Qiao, Q.
Solar Charging Batteries: Advances, Challenges, and Opportunities.
(2018). Joule, 2(7), 1217–1230.
DOI:10.1016/j.joule.2018.04.006

17 Gibson, T.L., Kelly, N.A.
Solar photovoltaic charging of lithium-ion batteries
(2010) Journal of Power Sources, 195 (12), pp. 3928-3932.
DOI: 10.1016/j.jpowsour.2009.12.082

18 Kelly, N.A.
Direct solar photovoltaic charging of a high voltage nickel metal hydride traction battery
(2012) Journal of Power Sources, 209, pp. 105-119.
DOI: 10.1016/j.jpowsour.2012.02.106

19 Gurung, A., Chen, K., Khan, R., Abdulkarim, S.S., Varnekar, G., Pathak, R., Naderi, R., Qiao, Q.
Highly Efficient Perovskite Solar Cell Photocharging of Lithium Ion Battery Using DC–DC Booster
(2017) Advanced Energy Materials, 7 (11).
DOI: 10.1002/aenm.201602105

20 Khataee, A., Azevedo, J., Dias, P., Ivanou, D., Dražević, E., Bentien, A., Mendes, A.
Integrated design of hematite and dye-sensitized solar cell for unbiased solar charging of an organic-inorganic redox flow battery
(2019) Nano Energy, 62, pp. 832-843.
DOI: 10.1016/j.nanoen.2019.06.001

21 Guo, W., Xue, X., Wang, S., Lin, C., Wang, Z.L.
An integrated power pack of dye-sensitized solar cell and Li battery based on double-sided TiO 2 nanotube arrays
(2012) Nano Letters, 12 (5), pp. 2520-2523.
DOI: 10.1021/nl3007159

22 Chakrapani, V., Rusli, F., Filler, M.A., Kohl, P.A.
A combined photovoltaic and Li ion battery device for continuous energy harvesting and storage
(2012) Journal of Power Sources, 216, pp. 84-88.
DOI: 10.1016/j.jpowsour.2012.05.048

23 Xu, J., Chen, Y., Dai, L.
Efficiently photo-charging lithium-ion battery by perovskite solar cell
(2015) Nature Communications, 6, art. no. 8103, .
DOI: 10.1038/ncomms9103

24 Nagai, H., Suzuki, T., Takahashi, Y., Sato, M.
Photovoltaic lithium-ion battery fabricated by molecular precursor method
(2016) Functional Materials Letters, 9 (3), art. no. 1650046, .
DOI: 10.1142/S1793604716500466

25 Agbo, S.N., Merdzhanova, T., Yu, S., Tempel, H., Kungl, H., Eichel, R.-A., Rau, U., Astakhov, O.
Photoelectrochemical application of thin-film silicon triple-junction solar cell in batteries
(2016) Physica Status Solidi (A) Applications and Materials Science, 213 (7), pp. 1926-1931.
DOI: 10.1002/pssa.201532918

26 Ogaryov, V.A., Rudoy, V.M., Dementyeva, O.V.
Metal nanoparticles and quantum dots as photosensitizers of solar cell batteries
(2016) Inorganic Materials: Applied Research, 7 (4), pp. 509-516.
DOI: 10.1134/S2075113316040237

27 Xia, X., Ku, Z., Zhou, D., Zhong, Y., Zhang, Y., Wang, Y., Huang, M.J., Tu, J., Fan, H.J.
Perovskite solar cell powered electrochromic batteries for smart windows
(2016) Materials Horizons, 3 (6), pp. 588-595.
DOI: 10.1039/c6mh00159a

28 Vega-Garita, V., Hanif, A., Narayan, N., Ramirez-Elizondo, L., Bauer, P.
Selecting a suitable battery technology for the photovoltaic battery integrated module
(2019) Journal of Power Sources, 438, art. no. 227011, .
DOI: 10.1016/j.jpowsour.2019.227011

29 Yuan, Y., Lu, Y., Jia, B.-E., Tang, H., Chen, L., Zeng, Y.-J., Hou, Y., Zhang, Q., He, Q., Jiao, L., Leng, J., Ye, Z., Lu, J.
Integrated System of Solar Cells with Hierarchical NiCo2O4 Battery-Supercapacitor Hybrid Devices for Self-Driving Light-Emitting Diodes
(2019) Nano-Micro Letters, 11 (1), art. no. 42, .
DOI: 10.1007/s40820-019-0274-0

30 Weng, G.-M., Kong, J., Wang, H., Karpovich, C., Lipton, J., Antonio, F., Fishman, Z.S., Wang, H., Yuan, W., Taylor, A.D.
A highly efficient perovskite photovoltaic-aqueous Li/Na-ion battery system
(2020) Energy Storage Materials, 24, pp. 557-564.
DOI: 10.1016/j.ensm.2019.06.032

31 Di, Y., Jia, S., Yan, X., Liang, J., Hu, S.
Available photo-charging integrated device constructed with dye-sensitized solar cells and lithium-ion battery
(2020) New Journal of Chemistry, 44 (3), pp. 791-796.
DOI: 10.1039/c9nj05367k

32 Thounthong, P., Chunkag, V., Sethakul, P., Sikkabut, S., Pierfederici, S., Davat, B.
Energy management of fuel cell/solar cell/supercapacitor hybrid power source
(2011) Journal of Power Sources, 196 (1), pp. 313-324.
DOI: 10.1016/j.jpowsour.2010.01.051

33 Meekhun, D., Boitier, V., Dilhac, J.-M., Petibon, S., Alonso, C., Estibals, B.
Buck converter design for photovoltaic generators with supercapacitor energy storage
(2011) Renewable Energy and Power Quality Journal, 1 (9), art. no. 422, pp. 682-685.
DOI: 10.24084/repqj09.422

34 Yuan, Y., MacHmoum, M., Bourguet, S., Amelon, N.

A novelty control strategy for the photovoltaic supercapacitor and battery hybrids storage system
(2011) Advanced Materials Research, 301-303, pp. 1522-1527.
DOI: 10.4028/www.scientific.net/AMR.301-303.1522

35 Thounthong, P., Luksanasakul, A., Koseeyaporn, P., Davat, B.
Intelligent model-based control of a standalone photovoltaic/fuel cell power plant with supercapacitor energy storage
(2013) IEEE Transactions on Sustainable Energy, 4 (1), art. no. 6317213, pp. 240-249.
DOI: 10.1109/TSTE.2012.2214794

36 Benyahia, N., Denoun, H., Zaouia, M., Tamalouzt, S., Bouheraoua, M., Benamrouche, N., Rekioua, T., Haddad, S.
Characterization and control of supercapacitors bank for stand-alone photovoltaic energy
(2013) Energy Procedia, 42, pp. 539-548.
DOI: 10.1016/j.egypro.2013.11.055

37 Guerrero, M.A., Romero, E., Miñambres, V., Milanés, M.I.
Supercapacitor energy storage system for attenuating and conditioning power from photovoltaic generation plants
(2013) International Conference-Workshop Compatibility in Power Electronics , CPE, art. no. 6601141, pp. 126-131.
DOI: 10.1109/CPE.2013.6601141

38 Worku, M.Y., Abido, M.A., Iravani, R.
Power fluctuation minimization in grid connected photovoltaic using supercapacitor energy storage system
(2016) Journal of Renewable and Sustainable Energy, 8 (1), art. no. 013501, .
DOI: 10.1063/1.4942547

39 Sikkabut, S., Mungporn, P., Ekkaravarodome, C., Bizon, N., Tricoli, P., Nahid-Mobarakeh, B., Pierfederici, S., Davat, B., Thounthong, P.
Control of high-energy high-power densities storage devices by Li-ion battery and supercapacitor for fuel cell/photovoltaic hybrid power plant for autonomous system applications
(2016) IEEE Transactions on Industry Applications, 52 (5), art. no. 7492168, pp. 4395-4407.
DOI: 10.1109/TIA.2016.2581138

40 Fahmi, M.I., Rajkumar, R., Wong, Y.W., Chong, L.W., Arelhi, R., Isa, D.
The effectiveness of new solar photovoltaic system with supercapacitor for rural areas
(2016) International Journal of Renewable Energy Development, 5 (3), pp. 249-257.
DOI: 10.14710/ijred.5.3.249-257

41 Cabrane, Z., Ouassaid, M., Maaroufi, M.
Analysis and evaluation of battery-supercapacitor hybrid energy storage system for photovoltaic installation
(2016) International Journal of Hydrogen Energy, 41 (45), pp. 20897-20907.
DOI: 10.1016/j.ijhydene.2016.06.141

42 Yin, C., Wu, H., Locment, F., Sechilariu, M.
Energy management of DC microgrid based on photovoltaic combined with diesel generator and supercapacitor
(2017) Energy Conversion and Management, 132, pp. 14-27.
DOI: 10.1016/j.enconman.2016.11.018

43 Cabrane, Z., Ouassaid, M., Maaroufi, M.
Battery and supercapacitor for photovoltaic energy storage: A fuzzy logic management
(2017) IET Renewable Power Generation, 11 (8), pp. 1157-1165.
DOI: 10.1049/iet-rpg.2016.0455

44 Miñambres-Marcos, V.M., Guerrero-Martínez, M.Á., Barrero-González, F., Milanés-Montero, M.I.
A grid connected photovoltaic inverter with battery-supercapacitor hybrid energy storage
(2017) Sensors (Switzerland), 17 (8), art. no. 1856, .
DOI: 10.3390/s17081856

45 Cabrane, Z., Ouassaid, M., Maaroufi, M.
Management and control of the integration of supercapacitor in photovoltaic energy storage
(2017) International Conference on Green Energy and Conversion Systems, GECS 2017, art. no. 8066128, .
DOI: 10.1109/GECS.2017.8066128

46 Wang, L., Vo, Q.-S., Prokhorov, A.V.
Stability Improvement of a Multimachine Power System Connected With a Large-Scale Hybrid Wind-Photovoltaic Farm Using a Supercapacitor
(2018) IEEE Transactions on Industry Applications, 54 (1), art. no. 8031031, pp. 50-60.
DOI: 10.1109/TIA.2017.2751004

47 Barbosa, V., Nogueira, T., Carati, E., Felgueiras, C.
Supercapacitor in battery charges of photovoltaic panel: Analysis of the technical feasibility
(2018) Energy Procedia, 153, pp. 80-85.
DOI: 10.1016/j.egypro.2018.10.019

48 Ciccarelli, F., Di Noia, L.P., Rizzo, R.
Integration of photovoltaic plants and supercapacitors in tramway power systems
(2018) Energies, 11 (2), art. no. 410, .
DOI: 10.3390/en11020410

49 Shchur, I., Kulwas, D., Wielgosz, R.
Combination of distributed MPPT and distributed supercapacitor energy storage based on cascaded converter in photovoltaic installation
(2018) 2018 IEEE 3rd International Conference on Intelligent Energy and Power Systems, IEPS 2018 - Proceedings, 2018-January, art. no. 8559513, pp. 139-144.
DOI: 10.1109/IEPS.2018.8559513

50 Vargas, U., Lazaroiu, G.C., Tironi, E., Ramirez, A.
Harmonic modeling and simulation of a stand-alone photovoltaic-battery-supercapacitor hybrid system
(2019) International Journal of Electrical Power and Energy Systems, 105, pp. 70-78.
DOI: 10.1016/j.ijepes.2018.08.004

51 Perdana, Y.S., Muyeen, S.M., Al-Durra, A., Morales-Paredes, H.K., Simoes, M.G.
Direct connection of supercapacitor-battery hybrid storage system to the grid-tied photovoltaic system
(2019) IEEE Transactions on Sustainable Energy, 10 (3), art. no. 8452994, pp. 1370-1379.
DOI: 10.1109/TSTE.2018.2868073

52 Kong, L., Yu, J., Cai, G.
Modeling, control and simulation of a photovoltaic /hydrogen/ supercapacitor hybrid power generation system for grid-connected applications
(2019) International Journal of Hydrogen Energy, 44 (46), pp. 25129-25144.
DOI: 10.1016/j.ijhydene.2019.05.097

53 Kamel, A.A., Rezk, H., Abdelkareem, M.A.
Enhancing the operation of fuel cell-photovoltaic-battery-supercapacitor renewable system through a hybrid energy management strategy
(2020) International Journal of Hydrogen Energy, .

DOI: 10.1016/j.ijhydene.2020.06.052

54 Guo, K., Dong, Y., Fu, J.
Charging Strategy of Supercapacitor in Photovoltaic Power Generation System
(2020) Journal of Physics: Conference Series, 1449 (1), art. no. 012014, .
DOI: 10.1088/1742-6596/1449/1/012014

55 Jaszczur, M., Hassan, Q.
An optimisation and sizing of photovoltaic system with supercapacitor for improving self-consumption
(2020) Applied Energy, 279, art. no. 115776, .
DOI: 10.1016/j.apenergy.2020.115776

56 Kim, Y., Chang, N., Wang, Y., Pedram, M.
Maximum power transfer tracking for a photovoltaic-supercapacitor energy system
(2010) Proceedings of the International Symposium on Low Power Electronics and Design, pp. 307-312.
DOI: 10.1145/1840845.1840909

57 Li, J., Chen, Y., Liu, Y.
Research on a stand-alone photovoltaic system with a supercapacitor as the energy storage device
(2012) Energy Procedia, 16 (PART C), pp. 1693-1700.
DOI: 10.1016/j.egypro.2012.01.262

58 Ongaro, F., Saggini, S., Mattavelli, P.
Li-Ion battery-supercapacitor hybrid storage system for a long lifetime, photovoltaic-based wireless sensor network
(2012) IEEE Transactions on Power Electronics, 27 (9), art. no. 6158609, pp. 3944-3952.
DOI: 10.1109/TPEL.2012.2189022

59 Liu, Z., Yang, X., Yang, S., McCann, J.
Efficiency-aware: Maximizing energy utilization for sensor nodes using photovoltaic-supercapacitor energy systems
(2013) International Journal of Distributed Sensor Networks, 2013, art. no. 627963, .
DOI: 10.1155/2013/627963

60 Bagheri, N., Aghaei, A., Ghotbi, M.Y., Marzbanrad, E., Vlachopoulos, N., Häggman, L., Wang, M., Boschloo, G., Hagfeldt, A., Skunik-Nuckowska, M., Kulesza, P.J.
Combination of asymmetric supercapacitor utilizing activated carbon and nickel oxide with cobalt polypyridyl-based dye-sensitized solar cell
(2014) Electrochimica Acta, 143, pp. 390-397.
DOI: 10.1016/j.electacta.2014.07.125

61 Zhang, Z., Chen, X., Chen, P., Guan, G., Qiu, L., Lin, H., Yang, Z., Bai, W., Luo, Y., Peng, H.
Integrated polymer solar cell and electrochemical supercapacitor in a flexible and stable fiber format
(2014) Advanced Materials, 26 (3), pp. 466-470.
DOI: 10.1002/adma.201302951

62 Westover, A.S., Share, K., Carter, R., Cohn, A.P., Oakes, L., Pint, C.L.
Direct integration of a supercapacitor into the backside of a silicon photovoltaic device
(2014) Applied Physics Letters, 104 (21), art. no. 213905, .
DOI: 10.1063/1.4880211

63 Xu, X., Li, S., Zhang, H., Shen, Y., Zakeeruddin, S.M., Graetzel, M., Cheng, Y.-B., Wang, M.
A power pack based on organometallic perovskite solar cell and supercapacitor
(2015) ACS Nano, 9 (2), pp. 1782-1787.
DOI: 10.1021/nn506651m

64 Selvam, S., Balamuralitharan, B., Karthick, S.N., Savariraj, A.D., Hemalatha, K.V., Kim, S.-K., Kim, H.-J.
Novel high-temperature supercapacitor combined dye sensitized solar cell from a sulfated ß-cyclodextrin/PVP/MnCO3 composite
(2015) Journal of Materials Chemistry A, 3 (19), pp. 10225-10232.
DOI: 10.1039/c5ta01792k

65 Xu, J., Ku, Z., Zhang, Y., Chao, D., Fan, H.J.
Integrated Photo-Supercapacitor Based on PEDOT Modified Printable Perovskite Solar Cell
(2016) Advanced Materials Technologies, 1 (5), art. no. 1600074, .
DOI: 10.1002/admt.201600074

66 Wen, Z., Yeh, M.-H., Guo, H., Wang, J., Zi, Y., Xu, W., Deng, J., Zhu, L., Wang, X., Hu, C., Zhu, L., Sun, X., Wang, Z.L.
Self-powered textile for Wearable electronics by hybridizing fiber-shaped nanogenerators, solar cells, and supercapacitors
(2016) Science Advances, 2 (10), art. no. 1600097, .
DOI: 10.1126/sciadv.1600097

67 Kim, J., Lee, S.M., Hwang, Y.-H., Lee, S., Park, B., Jang, J.-H., Lee, K.
A highly efficient self-power pack system integrating supercapacitors and photovoltaics with an area-saving monolithic architecture
(2017) Journal of Materials Chemistry A, 5 (5), pp. 1906-1912.
DOI: 10.1039/C6TA09117B

68 Scalia, A., Bella, F., Lamberti, A., Bianco, S., Gerbaldi, C., Tresso, E., Pirri, C.F.
A flexible and portable powerpack by solid-state supercapacitor and dye-sensitized solar cell integration
(2017) Journal of Power Sources, 359, pp. 311-321.
DOI: 10.1016/j.jpowsour.2017.05.072

69 Sun, Y., Yan, X.
Recent Advances in Dual-Functional Devices Integrating Solar Cells and Supercapacitors
(2017) Solar RRL, 1 (3-4), art. no. 1700002, .
DOI: 10.1002/solr.201700002

70 Muralee Gopi, C.V.V., Ravi, S., Rao, S.S., Eswar Reddy, A., Kim, H.-J.
Carbon nanotube/metal-sulfide composite flexible electrodes for high-performance quantum dot-sensitized solar cells and supercapacitors
(2017) Scientific Reports, 7, art. no. 46519, .
DOI: 10.1038/srep46519

71 Liu, Z., Zhong, Y., Sun, B., Liu, X., Han, J., Shi, T., Tang, Z., Liao, G.
Novel Integration of Perovskite Solar Cell and Supercapacitor Based on Carbon Electrode for Hybridizing Energy Conversion and Storage
(2017) ACS Applied Materials and Interfaces, 9 (27), pp. 22361-22368.
DOI: 10.1021/acsami.7b01471

72 Liu, R., Wang, J., Sun, T., Wang, M., Wu, C., Zou, H., Song, T., Zhang, X., Lee, S.-T., Wang, Z.L., Sun, B.
Silicon Nanowire/Polymer Hybrid Solar Cell-Supercapacitor: A Self-Charging Power Unit with a Total Efficiency of 10.5%
(2017) Nano Letters, 17 (7), pp. 4240-4247.
DOI: 10.1021/acs.nanolett.7b01154

73 Dong, P., Rodrigues, M.-T.F., Zhang, J., Borges, R.S., Kalaga, K., Reddy, A.L.M., Silva, G.G., Ajayan, P.M., Lou, J.

A flexible solar cell/supercapacitor integrated energy device
(2017) Nano Energy, 42, pp. 181-186.
DOI: 10.1016/j.nanoen.2017.10.035

74 Ng, C.H., Lim, H.N., Hayase, S., Zainal, Z., Shafie, S., Lee, H.W., Huang, N.M.
Cesium Lead Halide Inorganic-Based Perovskite-Sensitized Solar Cell for Photo-Supercapacitor Application under High Humidity Condition
(2018) ACS Applied Energy Materials, 1 (2), pp. 692-699.
DOI: 10.1021/acsaem.7b00103

75 Liu, H., Li, M., Kaner, R.B., Chen, S., Pei, Q.
Monolithically Integrated Self-Charging Power Pack Consisting of a Silicon Nanowire Array/Conductive Polymer Hybrid Solar Cell and a Laser-Scribed Graphene Supercapacitor
(2018) ACS Applied Materials and Interfaces, 10 (18), pp. 15609-15615.
DOI: 10.1021/acsami.8b00014

76 Yun, J., Song, C., Lee, H., Park, H., Jeong, Y.R., Kim, J.W., Jin, S.W., Oh, S.Y., Sun, L., Zi, G., Ha, J.S.
Stretchable array of high-performance micro-supercapacitors charged with solar cells for wireless powering of an integrated strain sensor
(2018) Nano Energy, 49, pp. 644-654.
DOI: 10.1016/j.nanoen.2018.05.017

77 Kalasina, S., Phattharasupakun, N., Maihom, T., Promarak, V., Sudyoadsuk, T., Limtrakul, J., Sawangphruk, M.
Novel Hybrid Energy Conversion and Storage Cell with Photovoltaic and Supercapacitor Effects in Ionic Liquid Electrolyte
(2018) Scientific Reports, 8 (1), art. no. 12192, .
DOI: 10.1038/s41598-018-30707-z

78 Yuan, Y., Lu, Y., Jia, B.-E., Tang, H., Chen, L., Zeng, Y.-J., Hou, Y., Zhang, Q., He, Q., Jiao, L., Leng, J., Ye, Z., Lu, J.
Integrated System of Solar Cells with Hierarchical NiCo2O4 Battery-Supercapacitor Hybrid Devices for Self-Driving Light-Emitting Diodes
(2019) Nano-Micro Letters, 11 (1), art. no. 42, .
DOI: 10.1007/s40820-019-0274-0

79 Chuang, W.-C., Lee, C.-Y., Wu, T.-L., Ho, C.-T., Kang, Y.-Y., Lee, C.-H., Meen, T.-H.
Fabrication of integrated device comprising flexible dye-sensitized solar cell and graphene-doped supercapacitor
(2020) Sensors and Materials, 32 (6), pp. 2077-2087.
DOI: 10.18494/SAM.2020.2802

80 Orozco-Messana, J., Daly, R., Zanchetta-Chittka, I.F.
Cu2O–ZnO heterojunction solar cell coupled to a Ni(OH)2-rGO-PPy supercapacitor within a porous stoneware tile
(2020) Ceramics International, .
DOI: 10.1016/j.ceramint.2020.06.229

81 Yue, X., Kiely, J., Gibson, D., Drakakis, E.M.
Charge-Based Supercapacitor Storage Estimation for Indoor Sub-mW Photovoltaic Energy Harvesting Powered Wireless Sensor Nodes
(2020) IEEE Transactions on Industrial Electronics, 67 (3), art. no. 8673773, pp. 2411-2421.
DOI: 10.1109/TIE.2019.2896321

82 Qin, L., Jiang, J., Tao, Q., Wang, C., Persson, I., Fahlman, M., Persson, P.O.A., Hou, L., Rosen, J., Zhang, F.

A flexible semitransparent photovoltaic supercapacitor based on water-processed MXene electrodes
(2020) Journal of Materials Chemistry A, 8 (11), pp. 5467-5475.
DOI: 10.1039/d0ta00687d

83 Liu, R., Takakuwa, M., Li, A., Inoue, D., Hashizume, D., Yu, K., Umezu, S., Fukuda, K., Someya, T.
An Efficient Ultra-Flexible Photo-Charging System Integrating Organic Photovoltaics and Supercapacitors
(2020) Advanced Energy Materials, 10 (20), art. no. 2000523, .
DOI: 10.1002/aenm.202000523

84 https://www.ovoenergy.com/guides/energy-guides/how-much-electricity-does-a-home-use.html

85 https://www.smart-energy.ag/en/pv-storage-systems/#projects_widget-5-0-0-smartenergy-dc

86 https://www.maxwell.com/

87 https://www.solarquotes.com.au/battery-storage/comparison-table/